Investigation into the Role of ELF5 during the Initiation and Development of Cutaneous Squamous Cell Carcinoma

HETAL JASHVANTBHAI PATEL
N0955111

A thesis submitted in partial fulfilment of the requirements of Nottingham Trent University for the degree of the Doctor of Philosophy.

JUNE 2025

DECLARATION

ACKNOWLEDGEMENTS

This research work represents the completion of a long and transformative journey made possible through the support, guidance and encouragement of many exceptional individuals.

I am profoundly grateful to my primary supervisor Dr. Mohammed Ahmed, for his steadfast support, insightful advice and patience all of which have played a crucial role in shaping both my research and professional growth. I would also like to sincerely thank my co-supervisors, Dr. Amanda Coutts and Dr. Alan Hargreaves for their thoughtful feedback, invaluable suggestions and consistent encouragement throughout the course of my PhD.

To my lab members Max, Maryam and Chandra thank you for your camaraderie, insightful discussions and for making the lab a place of learning and laughter. I am grateful to Biola for her technical support and for always being willing to help when challenges arose.

To everyone in my department - thank you for your kindness, insight and for fostering an environment of learning and support. And to my incredible IBRC members Sri Nithya, Suraj, Maria Pia, Laura, Melanie, Bishr, Mahesh, Ozde, Komal and Shiv - thank you for being my sounding boards, my motivation and my joy. I would also like to thank Preeti for her warmth, the many comforting get-togethers at her place. A special thank you to my dear friend Sri Nithya for holding me through the hardest moments with unmatched grace and care. Big thanks to my incredible friend Eruchi for saving me with those last-minute thesis fixes you're a lifesaver!

I am particularly obliged to Dr. Shreyasi Chatterjee and Dr. Keeley Brookes, whose words of encouragement during my low phases reminded me of my worth and capabilities.

To my dearest friend Jasmine, who has stood by me for the past 15 years and still counting - you have been my constant, my confidante and my chosen family. Thank you.

I am indebted to my family for their absolute love and unwavering faith in me. To my dearest mother Mrs. Simaben and my amazing father Mr. Jashvantbhai your sacrifices, prayers and encouragement are the foundation of my achievements. Your love and emotional support have made an immeasurable difference. To my sister Bijal and brother-in-law Mayank, thank you for your constant reassurance and support. To my brother Arjun and his partner Grachel and to my youngest brother Ketan, thank you for being my pillars of joy and sanity. Ketan, your late-night TED talks and philosophical musings and Twinkle, your warmth and that unforgettable Paris trip! Thank you both for your love.

I want to sincerely thank all my teachers from my early school days to university for the knowledge, encouragement and values you've instilled in me over the years. Each of you in your own way has helped shape my thinking, nurtured my curiosity and inspired me to keep moving forward, even when things felt uncertain.

I am also deeply grateful to God, who has walked beside me every step of this journey. Through moments of doubt, joy, frustration and growth, your presence has been my quiet strength, my comfort and my guide. This journey would not have been possible without your constant presence and grace.

And to my ancestors, whose strength and spirit walk with me still, Thank you.

This work is a tribute not only to academic perseverance but to the love, kindness and strength of every soul who has walked beside me.

HARE KRISHNA!

"In layers like skin, I shed, I healed, I grew, each challenge a wound, each finding a scar of strength. What began in the lab became a quiet transformation-this thesis, evidence to regeneration, both cellular and soul."

Table of Contents

LIST OF FIGURES

LIST OF TABLES

ABBREVIATIONS

Abbreviation	Full Form
A431	Human epidermoid carcinoma cell line
ABEs	Adenine Base Editors
ACTB	Actin Beta
aFGF	Acidic Fibroblast Growth Factor
AK	Actinic Keratosis
APC	Adenomatous Polyposis Coli
APS	Ammonium Persulphate
BCA	Bicinchoninic Acid
bFGF	Beta Fibroblast Growth Factor
BMPs	Bone Morphogenetic Factors
BS	Binding Site
BSA	Bovine Serum Albumin
CAFs	Cancer Associated Fibroblasts
CaMKII	Calmodulin dependent Kinase II
Cas9	CRISPR Associated Protein 9
CBEs	Cytosine Base Editors
CCNB1	Cyclin B1
CCNB2	Cyclin B2
CCND1	Cyclin D1
CCND2	Cyclin D2
CCNE1	Cyclin E1
CDK1	Cyclin-Dependent Kinase 1
CDK16	Cyclin-Dependent Kinase 16
CHIP-seq	Chromatin Immunoprecipitation
CK1	Casin Kinase 1
CNV	Copy Number Variation
CRISPR	Clustered Regularly Interspaced Short Palindromic Repeats
crRNA	CRISPR Associated RNA
CSC	Chondroitin Sulphate Sodium Salt
cSCC	Cutaneous Squamous Cell Carcinoma
DAG	Diacylglycerol
DAPI	4′,6-Diamidino-2-Phenylindole
dCas9	Dead (nuclease-deficient) CRISPR-associated protein 9
DMEM	Dulbecco’s Modified Eagle Medium
DMEM/F12	Dulbecco’s Modified Eagle Medium: Nutrient Mixture F-12
dNTPs	Deoxynucleotide Triphosphates
DP	Dermal Papilla
dPBS	Dulbecco's Phosphate-Buffered Saline
DPX	Distyrene Plasticizer Xylene

DSBs	Double Strand Breaks
dT	Deoxythymidine
DVL	Dishevelled
ECM	Extracellular Matrix
EDTA	Ethylenediaminetetraacetic Acid
EGF	Epidermal Growth Factor
EGFR	Epidermal Growth Factor Receptor
ELF5	E74 Like Factor 5
EMT	Epithelial Mesenchymal Transition
Epo	Erothropietin
ESE	Epithelium Specific ETS
ETS	E-Twenty-Six
FACS	Fluorescent Activated Cell Sorter
FBS	Fetal Bovine Serum
FCS	Fetal Calf Serum
FGFRs	Fibroblast Growth Factor Receptors
FGFs	Fibroblast Growth Factors
FLI-1	Friend Leukemia 1
F-MuLV	Friend Murine Leukaemia Virus
FZDR	Frizzled Receptors
GATA-3	GATA Binding Protein 3
gDNA	Genomic DNA
GFP	Green Fluorescent Protein
GO	Gene Ontology
GSK-3β	Glycogen Synthase Kinase 3β
HaCaT	Human adult immortalized keratinocyte cell line
HDR	Homology Directed Repair
HPA Axis	Hypothalamic Pituitary Adrenal Axis
IFE	Interfollicular Epidermis
IP3	Inositol 1, 4,5-triphosphate
IRS	Inner Root Sheath
KRT1	Cytokeratin 1
KRT16	Cytokeratin 16
LCs	Langerhans Cells
Lgr5	Leucine rich-G-protein coupled Receptor 5
MgCl2	Magnesium Chloride
MMC	Mitomycin C
MOI	Multiplicity Of Infection
MSCs	Mesenchymal Stem Cells
NB Site	Non-Binding Site
NBT	Nitroblue Tetrazolium Chloride
NEAA	Non-Essential Amino Acid
NEB	New England Biolabs

NGS	Normal Goat Serum
NHEJ	Non-Homologous End Joining
NMSC	Non-Melanoma Skin Cancer
OCT	Optimal Cutting Temperature compound
OPMD	Oral Potentially Malignant Disorders
PAM	Protospacer Adjacent Motif
PCA	Principal Component Assay
PCP	Planar Cell Polarity
PEs	Prime Editors
PIP2	Phosphatidylinositol 4,5-biphosphate
PKC	Protein Kinase C
PLC	Phospholipase C
PLCγ	Phospholipase C Gamma
Pr1	Prolactin Receptor 1
RB	Retinoblastoma Protein
RFP	Red Fluorescent Protein
SCC	Squamous Cell Carcinoma
SCC-9	Squamous Cell Carcinoma cell line-9
SCs	Stem Cells
SDS	Sodium Dodecyl Sulphate
SEM	Standard Error Mean
sgRNA	Single Guide RNA
SMAD	SMA- and MAD-related proteins
TA	Transit-Amplifying
TALENs	Transcription Activator Like Effector Nucleases
TEWL	Transepidermal Water Loss
tracrRNA	Transactivating RNA
UVR	Ultraviolet Rays
ZFNs	Zinc Finger Nucleases
α-SMA	Alpha Smooth Muscle Actin

PUBLICATIONS

- **Patel H.J,** Pickup M. E, Lawal M.A, Khadka C and Ahmed M.I. Interplay of ELF5, GATA-3 and FLI-1 Regulate Malignant Transformation of Keratinocytes (under review).

- Hu, A., Pickup, M.E., Lawal, M.A., **Patel, H.J**. and Ahmed, M.I., 2025. The involvement of Elf5 in regulating keratinocyte proliferation and differentiation processes in skin. *PloS one*, *20*(1), p.e0316134.

- Pickup, M.E., Hu, A., **Patel, H.J.** and Ahmed, M.I., 2023. MicroRNA-148a controls epidermal and hair follicle stem/progenitor cells by modulating the activities of ROCK1 and ELF5. *Journal of Investigative Dermatology*, *143*(3), pp.480-491.

CONFERENCES AND PRESENTATIONS ATTENDED DURING PHD

1. British Society of Investigative Dermatology (BSID)-Conference
   Awarded Travel Grant - London, April 2025
   Organised by: British Society of Investigative Dermatology

2. European Society of Dermatology Research (ESDR)-Conference
   Poster Presenter – Lisbon, Portugal, September 2024
   Organised by: European Society of Dermatology Research

3. SHIMR Seminars (Centre for Systems Health and Integrated Metabolic Research)
   Oral Presentation – Nottingham, February 2025
   Organised by: Nottingham Trent University

4. SHIMR Symposium (Centre for Systems Health and Integrated Metabolic Research)
   Poster Presentation – July 2024
   Awarded 3rd Place
   Organised by: Nottingham Trent University (NTU)
5. STAR Conference
   Oral Presentation – Nottingham, June 2022
   Organised by: Nottingham Trent University

ABSTRACT

Cutaneous squamous cell carcinoma (cSCC), the second most prevalent epithelial cancer, originates from epidermal keratinocytes. ELF5 (E74-like factor 5) a transcription factor from epithelium specific Members of the ETS transcription factor subfamily are critical for maintaining epithelial development, tissue homeostasis, and preventing epithelial-derived cancers. Malignant transformation of keratinocytes involves the disruption of the progenitor differentiation program causing keratinocytes to fail to complete the differentiation process, leading to dysplastic epithelium and precancerous cells in skin. However, the precise mechanisms that causes the failure of keratinocytes to differentiate completely is not well understood. This study highlights a novel tumour-suppressive function of ELF5 in keratinocytes. We observed high levels of ELF5 expression in normal human skin, particularly within both basal and suprabasal layers, whereas its expression was notably diminished in cSCC biopsy samples. Using CRISPR-Cas9-mediated gene knockout, alongside transcriptomic and proteomic analyses, we demonstrated that loss of ELF5 in non-tumorigenic keratinocytes (HaCaT cells) compromises their ability to differentiate and enhances their migratory, invasive, and tumorigenic potential in vitro. While overexpression of ELF5 leads to inhibition of cell migration and proliferation in keratinocytes and in skin cancer cell lines (A431 and SCC-9), *in vitro*. Further analysis using RNA transcriptomics has uncovered that GATA-3 and FLI-1 are key molecular targets of ELF5 in keratinocytes. ELF5 regulation of both GATA-3 and FLI-1 is required to maintain the balance between healthy keratinocytes (proliferation/differentiation) and to prevent precancerous cell formation (tumourigenicity). Our findings suggest that ELF5 serves a critical role in safeguarding keratinocytes against malignant transformation and may act as a suppressor of skin tumour development. Uncovering the molecular pathways regulated by ELF5 will offer important insights, with potential applications in developing future

therapeutic strategies for cSCC and in improving outcomes for individuals with precancerous skin lesions.

CHAPTER

1.0 INTRODUCTION

1.1THE HUMAN SKIN

As an essential organ and one of the most expansive in the human anatomy, the skin is the body's largest organ, covering approximately 1.5 to 2.0 square meters and accounting for around 15% of an adult's total body weight (Proksch et al., 2008).

1.1.1 THE FUNCTIONAL ROLES OF SKIN

The human skin serves as a multifunctional organ essential to overall physiological health and survival. Its primary role is as a barrier, protecting internal organs from physical injury, microbial invasion, chemical exposure, and dehydration. The outermost layer of the epidermis, called stratum corneum is composed of corneocytes embedded in a lipid matrix, forming a selectively permeable shield that regulates transepidermal water loss (TEWL) and blocks pathogen entry (Elias, 2005). In addition to mechanical defence, the skin hosts a complex immune surveillance system involving Langerhans cells, keratinocytes, dermal dendritic cells, and resident memory T cells, which detect and respond to antigens, facilitating both innate and adaptive immune responses (Pasparakis et al., 2014).

Beyond protection, the skin plays a pivotal role in thermoregulation, sensory perception, metabolic activity, and endocrine function. Thermoregulation is achieved through eccrine sweat glands and cutaneous blood flow modulation, which help maintain internal temperature during environmental extremes (Flouris, 2011). Skin is densely innervated with mechanoreceptors, nociceptors, and thermoreceptors that detect touch, pain, pressure, and temperature, relaying this information to the central nervous system for sensory processing (Proksch et al., 2008). Furthermore, the skin contributes to vitamin D synthesis, initiated when ultraviolet B (UVB) radiation converts 7-dehydrocholesterol in the epidermis to pre-vitamin D3, essential for calcium homeostasis and immune regulation (Holick, 2007). A study also have highlight the skin's neuroendocrine functions, where it acts as a peripheral analog to the

hypothalamic-pituitary-adrenal (HPA) axis, producing hormones like cortisol and regulating local and systemic stress responses (Slominski et al., 2000). Together, these functions underscore the skin's critical role not merely as a passive barrier but as an active participant in immune, endocrine, and neurophysiological processes.

1.1.2 SKIN HOMEOSTASIS

Skin homeostasis refers to the dynamic balance that maintains the skin's structural integrity, physiological functions, and capacity to respond to environmental and internal stimuli. This balance is orchestrated through a tightly regulated interplay of cellular proliferation, differentiation, apoptosis, immune regulation, barrier function, and microbiome stability. The epidermis, for example, undergoes continuous renewal through basal keratinocyte proliferation and upward migration, culminating in the formation of the stratum corneum, which is essential for barrier maintenance (Fuchs, 2007). Disruption of this renewal process, either through genetic mutations or environmental insults, can impair skin barrier function and lead to diseases such as psoriasis or atopic dermatitis (Segre, 2006). Additionally, the skin's immune system, including Langerhans cells and resident memory T cells, plays a vital role in preserving homeostasis by detecting pathogens while avoiding overactive immune responses that could cause chronic inflammation (Pasparakis et al., 2014). Furthermore, a study by Byrd and colleagues emphasize the role of the skin microbiome in maintaining homeostasis, with microbial dysbiosis linked to inflammatory disorders and impaired skin healing (Byrd et al., 2018). Maintaining skin homeostasis is thus critical for protecting the body from external threats, regulating immune tolerance, and ensuring overall dermatological health.

1.1.3 FACTORS AFFECTING SKIN HOMEOSTASIS

Skin homeostasis refers to the dynamic balance that maintains the structure, function, and integrity of the skin. This complex equilibrium is regulated by a variety of intrinsic and extrinsic factors that affect cellular proliferation, differentiation, immune responses, barrier integrity, and the skin microbiome. Intrinsic factors include age, genetics, hormonal levels, and immune status. Aging, for example, reduces fibroblast function and collagen production, leading to thinning of the dermis and impaired repair mechanisms (Farage et al., 2008). Genetic mutations in skin barrier proteins like filaggrin are linked to conditions such as atopic dermatitis, indicating a key genetic role in homeostatic regulation (Palmer et al., 2006). Hormones, particularly sex hormones and glucocorticoids, influence sebaceous gland activity, epidermal turnover, and immune surveillance, thus affecting skin's resilience and repair (Slominski et al., 2012).

Extrinsic factors such as ultraviolet (UV) radiation, pollution, diet, microbiome alterations, and mechanical stress also disrupt skin homeostasis. UV radiation is a major environmental stressor that induces DNA damage, oxidative stress, and inflammatory responses, which can lead to photoaging and carcinogenesis (Rittié & Fisher, 2002). Environmental pollutants like polycyclic aromatic hydrocarbons have been shown to trigger oxidative damage and impair skin barrier function (Vierkötter & Krutmann, 2012). Diets rich in antioxidants and essential fatty acids can support epidermal barrier integrity and reduce inflammation (Boelsma et al., 2003). Additionally, the skin microbiome plays an essential role in maintaining barrier homeostasis and modulating immune responses. Dysbiosis of this microbial community is associated with inflammatory skin conditions such as acne, psoriasis, and eczema (Byrd et al., 2018). Collectively, these factors interact in complex ways, and disturbances in any of them can shift the skin away from homeostasis, resulting in various pathological states.

1.1.4 FORMATION OF SKIN BARRIER

During prenatal development, it is thought that both the anatomical and functional traits of the cutaneous barrier are essential for skin barrier formation (Holbrook, 1979). By around 34 weeks of gestation, prominent dermal-epidermal ridges begin to form, and it is believed that at this stage, the fetal skin barrier is sufficiently developed to serve a protective function (Vujevich and Mancini, 2004; Segre, 2003). Although the skin barrier properties in newborns and infants are fairly well understood, the stratum corneum during the first two weeks after birth has not yet reached full hydration (Kishi et al., 2012). During this early stage, the infant's stratum corneum is approximately 30% thinner than in adults, while the epidermis is slightly thicker at around 35 μm, eventually thinning with age to about 25 μm (Boireau-Adamezyk et al., 2014). Within couple years of after birth, the skin typically establishes a fully functional water barrier along with stable thermoregulatory and growth-supportive properties (Stamatas et al., 2011). Upon birth, exposure to maternal and environmental factors leads to rapid colonization of the infant’s skin by a range of pathogens (Kong and Segre, 2017; Capone et al., 2011). This early microbial colonization is believed to be critical not only for immune system maturation but also for fostering immune tolerance (Scharschmidt, 2017). The interaction between cutaneous microbes and the host is thought to have guided the evolution of innate and adaptive immune responses in the skin, with the skin microbiota playing a key role in maintaining barrier integrity and function (Grice and Segre, 2011).

1.1.5 SKIN EPITHELIUM IN EMBRYO

Subsequent to the process of gastrulation, neuroectoderm- a single layer will appear on the surface of the embryo which will lead to the formation of the layer of epidermis and nervous system. The Wnt signalling pathway plays a pivotal role by suppressing the ectoderm's ability to respond to fibroblast growth factors (FGFs). In situations where FGF signalling is absent, the ectoderm instead expresses bone morphogenetic proteins (BMPs), which steer it toward an

epidermal fate. Conversely, neural identity is established when Wnt signals are lacking, allowing the ectoderm to respond to FGFs. These FGFs, in turn, inhibit BMP signalling by delivering antagonistic cues (Fuchs, 2007) (Figure 1). The embryonic epidermis formed through this interplay initially consists of a single layer of multipotent epithelial cells. This layer is covered by a transient protective sheet of tightly packed, squamous cells resembling endoderm, known as the periderm. The periderm is eventually shed once the underlying epidermis begins to stratify and differentiate (Boneko & Merker, 1988).

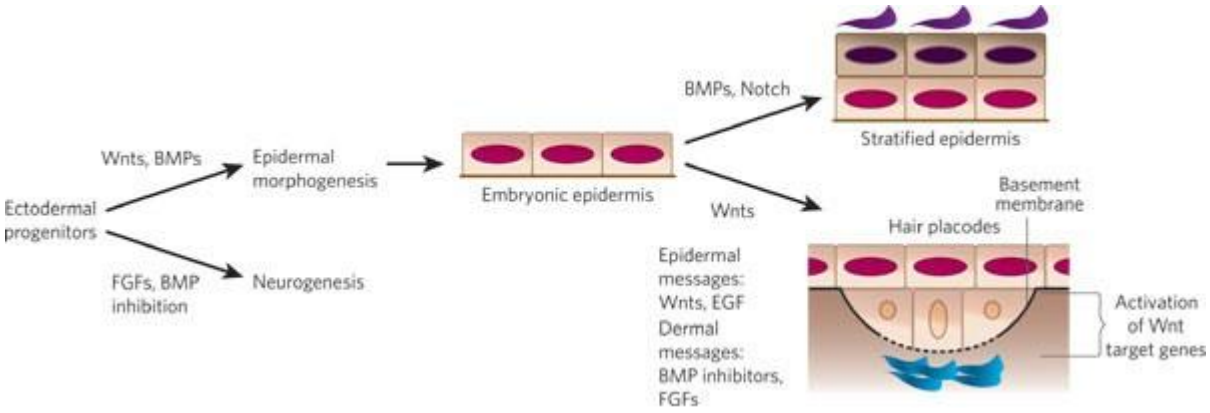

Figure 1.1: Molecular signalling in epidermal development.

A schematic depiction of key molecular pathways orchestrating epidermal morphogenesis. In absence of Wnt signalling pathways, Ectodermal progenitors interact with FGFs leading to a downregulation of BMP signalling and advancing towards the process of neurogenesis. However, in presence of Wnt signalling it hinders the activity of ectodermal progenitors to respond to FGFs and permits the activation of BMP signalling pathways and facilitate the epidermal morphogenesis. As the development process continues, the single -layered stratified epidermis begins to express Wnt proteins. If the cells fail to respond Wnt signals, it will commit to epidermal identity via BMP, epidermal growth factor (EFG) and NOTCH signalling pathways. The basement membrane provides structural support, while epidermal-derived signals such as Wnts and EGF, along with dermal factors like BMP inhibitors and FGFs, influence differentiation and tissue patterning. Hair placode formation is regulated by BMP inhibition and FGF signalling, contributing to follicular development. Additionally, activation of Wnt target genes refines epidermal architecture, ensuring proper tissue function (Fuchs, 2007).

1.1.6 SKIN STRUCTURES AND LAYERS

The human skin is architecturally complex, comprising several layers, each with specialized roles that contribute to the organ's overall functionality. Primarily, our skin is divided in three levels namely epidermis, dermis and hypodermis. Epidermis being the outmost provides protective barrier for the underlying skin tissues. The middle layers called as dermis consists of different structures such as blood vessels, sweat glands and hair follicles. The extreme subcutaneous layer also known as hypodermis acts as an insulating layer due to presence of adipose tissues (Figure 1.2) (Hofmann et al., 2023).

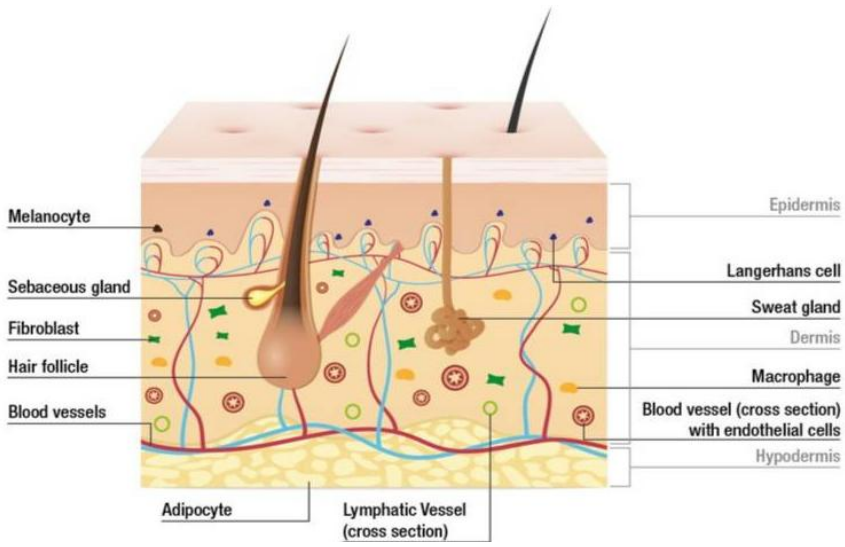

Figure 1.2: Structural details of human skin.

This image demonstrates the structural organization of human skin, highlighting its primary layers- epidermis, dermis and hypodermis- along with key cellular and glandular components. The epidermis is the topmost layer, providing a protective barrier and containing melanocytes, which produce melanin for pigmentation and UV protection and Langerhans cells which serve as antigen-presenting immune cells. Beneath lies the dermis, a connective tissue-rich layer housing fibroblasts (produces collagen and elastin), hair follicles, sebaceous glands (secretes sebum to lubricate skin and hair), sweat glands (involved in thermoregulation, blood vessels (for nutrient supply and heat exchange), and lymphatic

vessels (for immune cell trafficking and fluid drainage). The composition of hypodermis is of mainly adipose tissue, where they store energy and insulate the body, and macrophages contribute to immune defense and tissue homeostasis. This layered architecture reflects the skin's multifunctional roles in protection, sensation, immunity and homeostasis (Hofmann et al., 2023).

1.1.6.1 HYPODERMIS

The hypodermis, the innermost layer of the skin, contains a diverse population of cells, including adipocytes, pre-adipocytes, adipose-derived stem cells, fibroblasts, pericytes, macrophages, T-cells, and erythrocytes, all embedded within a stromal vascular network interwoven with nerves, muscles, and hair follicles (Trevor et al., 2020). This layer functions as a major site for long-term energy storage and contributes to thermal insulation, while also playing a crucial role in anchoring the skin to fundamental tissues namely muscles as well as bones (Mancuso and Bouchard, 2019).

The hypodermis is predominantly composed of loose connective tissue, which, contingent upon its anatomical location, can develop gliding layers or substantial deposits of adipose tissue that serve to insulate and safeguard the dermal layers. This particular tissue type is notably enriched in proteoglycans and glycosaminoglycans, which possess the capacity to attract fluid into the extracellular matrix, thereby imparting mucous-like characteristics to the tissue (Wong, et al., 2016). The cellular constituents of the hypodermis include fibroblasts, adipocytes, and macrophages, each playing a critical role in the maintenance of adipocyte homeostasis during states of obesity (Guimberteau, et al., 2010), potentially linked to processes of tissue remodelling (Stienstra, et al., 2014) and may additionally promote thermogenic activity of adipose tissue in response to cold exposure and physical exercise (Fjeldborg, et al., 2014 ; Lee and Tontonoz, 2014). The adipocytes are organized into discrete lobules, interspersed with fibrous septa and a robust vascular and lymphatic supply. The hypodermis plays an important role in the regulation of adipose homeostasis and is particularly abundant in G protein-coupled

receptors that modulate lipolysis, as well as the secretion of adiponectin and leptin (Amisten, et al., 2015).

1.1.6.2 DERMIS

In Embryo, dermis exhibits a highly cellular composition, and by the second month of development, the subcutis and dermis are indistinguishable from one another. Fibrillar components begin to emerge shortly thereafter, with organized bundles of collagen fibers becoming apparent by the conclusion of the third month (McGrath, 2023). Progressively, the papillary and reticular layers become differentiated, and by the fifth month, connective tissue sheaths are established around the hair follicles. The presence of elastic fibres is first noted at 22 weeks of gestation. Under the dermis lies a more loosely arranged tissue, depicted by the formation of adipose islands in specific locations. During the embryonic period of 6 to 14 weeks, three distinct types of cells have been identified within the dermis including macrophages, granule secretory cell which can be mast cell or melanoblast and stellate cells (Sergi, 2020). Between the 14th and 21st weeks, fibroblasts are observed to be abundant and functionally active, with individual identification of melanoblasts, pericytes, Merkel cells, perineurial cells and mast cells being possible. Additionally, different cell type of bone marrow origin may serve as a precursor to both the histiocytes and Langerhans' cell (Hu et al., 2018).

Depending upon the location, the thickness of dermis can fluctuate between 2 mm and 6 mm (Wong et al., 2016,). By supplying the oxygenated blood to the epidermis and removes waste products from the epidermis, it regulates blood supply via thermoregulation (Zeng et al., 2017). Dermis safeguards the body injuries by retaining the significant amount of body’s water. Diverse nature of dermis consists of blood vessels, nerve endings, glands and hair follicles. A predominant cell types- dermal fibroblast are responsible for secreting proteins of the extracellular matrix (ECM) into the intercellular space where collagen and elastin provide

flexibility and strength to the skin, while proteoglycans like hyaluronic acid contribute to tissue hydration and viscosity (Reihsner et al., 1995). Fibronectin plays a pivotal role in wound healing and is involved in cell adhesion, growth, migration, and cell differentiation (Chermnykh et al., 2018,). Mesenchymal stem cells (MSCs) and adipocytes are also found along with few immune cell populations due to the presence of blood vessels (Gaur et al., 2017).

Further the dermis is separated by two different layers known as stratum papillae and stratum reticulare. The former possesses a porous structure consists of loosely woven collagen fibre bundles, connective tissue and extracellular matrix. Due to vascularization, it forms projections extending to epidermis to allow exchange with dermis. Such distinct structures provide with distinct fingerprints- such as on palms of the hand or soles of the feet. The stratum papillare contains numerous nerve endings responsible for the transmission of tactile sensations, vibrations, or heat (Zeng et al., 2017.). The lower layer, the stratum reticulare, contains tightly interconnected elastic and collagen fibres that confer firmness, extensibility, and elasticity to the dermis. It possesses hair roots, lymphatic and blood vessels, nerves, sebaceous glands and sweat glands (Barbieri et al., 2014; Weng et al., 2020).

1.1.6.3 EPIDERMIS

Being the outermost layer, the epidermis creates a useful barrier against microbes, pollutants and dehydration (Wertz ,2013). The sustenance of the epidermis is facilitated through the diffusion of intercellular fluids derived from the dermal vasculature (Menon et al., 2009). The epidermis primarily constitutes layers of keratinocytes, while also encompassing non-epithelial cell types, such as melanocytes, Langerhans cells and Merkel cells. Melanocytes are responsible for the synthesis of melanin, a skin pigment that absorbs UV radiation and determines skin colour, are in the basal layer (Cichorek et al., 2013). Merkel cells, acting as

sensory receptors in the skin, are found in or near the basal layer (Abraham and Mathew, 2019). Langerhans cells, the antigen presenting immune cells of the epidermis, are most abundant in the stratum spinosum. The epidermis doesn't have any blood or lymph vessels, which strictly relies on diffusion from the underlying dermis for nutrient delivery, oxygenation and waste removal (Shpichka et al., 2019).

Keratinocytes, which originate from the ectodermal layer during embryogenesis, are the predominant cell type found within the epidermis are responsible for forming the protective barrier of the skin. Due to the migration of keratinocytes from the basal layer towards the skin surface, they undergo structural modifications and produce keratins, fibrous proteins that contribute to the strength and waterproofing of the skin (Zhang and Michniak-Kohn, 2012; Hill et al., 2015). The formation of stratum corneum takes place when there is a cellular turnover process and accumulation of keratin along with lipids, subsequently undergo terminal differentiation. Keratinocytes carry out various functions like they exhibit proliferation to facilitate wound healing, transport water and urea via aquaporins, assimilate melanin from melanocytes, regulate water permeability, and engage in innate and adaptive immunity through the secretion of antimicrobial peptides and the involvement of Langerhans cells, respectively (Horst et al., 2019).

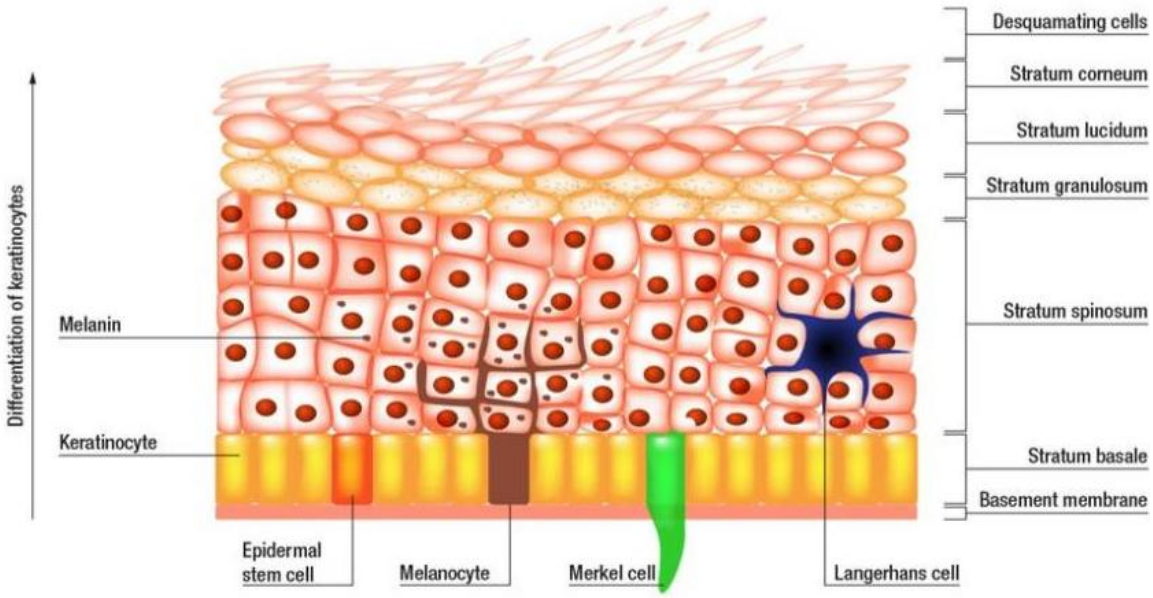

Figure 1.3: Epidermal structure in detail.

The diagram illustrates the detailed organization of the human epidermis, highlighting its stratified layers, cellular components and differentiation pathways. The epidermis is composed of five distinct layers arranged from superficial to deep, the stratum corneum, consisting of enucleated, flattened , desquamating corneocytes hat form the skin's outermost barrier, the stratum lucidum (prominent in thick skin), a translucent layer of dead keratinocytes, the stratum granulosum, where keratinocytes accumulate keratohyalin granules and initiate terminal differentiation, the stratum spinosum, characterised by desmosome-rich keratocytes with spiny appearance and the stratum basale, a single layer of the proliferative epidermal stem cells and early keratinocytes anchored in basement membrane. This basal layer also contains melanocytes, which synthesise and transfer melanin to keratinocyte for pigmentation, Merkel cells which are mechanosensory cells involve in touch perception and Langerhans cells immune cells responsible for antigen processing. Keratinocyte differentiation progress upward from the basal layer, with cells undergoing sequential morphological and biochemical changes culminating in corneocyte formation and eventual desquamation (Hoffman et al., 2023).

By physiological aspects, maintenance of the homeostasis is subjected to particular metabolic or gene transcription regulation by skin due to its protective mechanisms (Cibrian et al., 2020). The process of maturation occurs when keratinocytes derived from epidermal stem cells (SCs) are firmly attached to the basal membrane of the innermost layer of the skin, known as the "stratum basale". Here the epidermal stem cells continuously generate transit-amplifying (TA) daughter cells, which rapidly divide until they undergo differentiation and stop proliferating (Rousselle et al., 2019). Throughout this process of maturation, TA cells migrate towards the surface of the skin and undergo gradual transformations in terms of their physical appearance, organelle structure, and cytoskeletal organization. These changes ultimately lead to the development of sublayers that are visually and functionally distinct from one another (Houben et al., 2007). At each distinct stage these keratinocytes produce specific types of keratins, which provide structural support and play a major role in cell viability, as well as signalling pathways associated with protein synthesis, cell growth, and cell differentiation. Mostly basal keratinocytes predominantly express keratins 5 and 14 filaments, which serve to firmly anchor keratinocytes to the basement membrane (Srivastava et al., 2025). As the process of maturation progresses, the expression of cytokeratin's 5 and 14 is downregulated and ultimately changed by the expression of cytokeratin's 1 and 10. Keratin 15 (KRT15) is a type I intermediate filament protein normally expressed in basal epidermal keratinocytes. These cells are pushed into the interfollicular basal layer, and the hair follicle bulge places packed with stem and progenitor cells. Because KRT15 stays in this basal compartment, scientists rely on it as a marker for epidermal stem cell populations that hold real long-term regenerative power (Lyle et al., 1998; Morris et al., 2004). When keratinocytes remain undifferentiated, they keep expressing KRT15, but as they start to differentiate and move upward, KRT15 fades out. At the same time, differentiation markers like KRT1, KRT10, involucrin, and filaggrin shows increase expression. (Waseem & Lane, 1990; Jensen & Watt, 2006). In addition, the maturation

process is accompanied by the expression of other structural proteins, such as loricrin, involucrin, profilaggrin, and trichohyalin (Yousef, Alhajj and Sharma, 2017). Finally, keratinocytes differentiate into corneocytes, which are characterized by the absence of a nucleus and are densely packed with cytokeratin's 1 and 10. These corneocytes are enclosed by a robust polymer structure known as the cornified cell envelope, which consists of both lipid and protein components. The protein component is composed of loricrin and involucrin, which are cross-linked by transglutaminase enzymes, as well as small proline-rich proteins, late envelope proteins, and filaggrin (Tong et al., 2006; Jackson et al., 2005). The lipid component of the envelope comprises ceramides, omega-hydroxy-fatty acids and omega-acylated-hydroxy-ceramides, which are covalently attached to the protein layer (Elias, 2014). Together, these components form a hydrophilic barrier that effectively prevents fluid loss and provides protection against microbes (Nemes and Steinert, 1999). Almost eighty percent of corneocytes comprises cytokeratin, whose filaments are organized into disulfide cross-linked macrofibres under the influence of filaggrin (Pockney and Lane 2007). This protein is synthesized as a precursor known as pro-filaggrin, which is liberated from the keratohyalin granules located within the granular layer. The convoluted interstice among the stacked corneocytes is occupied by "mortar" lipids, which are secreted into the intercellular space via the lamellar body secretory system of the granular layer, thereby forming an intercellular lipid membrane bilayer consisting of three classes of lipids: ceramides, cholesterol, and free fatty acids in an equimolar ratio (Coderch et al., 2003) (Figure 1.4). The employment of a water-soluble tracer injected into the dermis has demonstrated an upward movement of water occurring between the epidermal cells; however, outflow is obstructed at the interface of stratum corneum or stratum granulosum. Beyond this juncture, water is lost in vapour form, although it remains entrapped within the corneocytes, plasticizing the keratin. Consequently, the lipids retain moisture while simultaneously facilitating transepidermal water loss (Pappas, 2009). The cornified cell

envelope is synthesized through the cross-linking of the proteins loricrin and involucrin, which are also produced from the keratohyalin granules, following the action of calcium-dependent epidermal transglutaminase (Yoneda et al., 1992). The stratum corneum additionally encompasses a variety of lipolytic and proteolytic enzymes that are engaged in the processing of probarrier lipids, mediating the desquamation of corneocytes, and the degradation of profilaggrin into filaggrin, which is subsequently broken down into a composite of amino acids collectively referred to as the NMF, or Natural Moisturizing Factor, which serves to plasticize keratin (Robinson et al., 2010).

It is imperative to note that keratinocytes do not function in isolation. The signalling pathways governing the growth and differentiation of the skin through mitotic spindle orientation necessitate molecular interactions among diverse cellular entities (Murolama and Yechler, 2012). This collective assembly is designated as an interactome, which imparts polarity to the cells, thereby ensuring proper cellular orientation (Boneta, 2010). The hair shaft measures approximately one-tenth of a millimetre in width and possesses a minute weight of only a few millionths of a gram. This intricately organized and segmented structure emerges from a significant stem cell reservoir located in the outer root sheath beneath the sebaceous gland, referred to as the follicular bulge (Blainpain et al., 2004). Within this niche, the 7-transmembrane receptor, leucine-rich G-protein coupled receptor 5 (Lgr5), serves as a defining marker of the Wnt-regulated adult stem cell population. Expression mapping has additionally identified Lgr6+ epithelial stem cells, which are closely homologous to Lgr5, situated in a Wnt-independent niche within the adult skin just superior to the bulge, specifically in the isthmus region of the hair follicle (Snippert et al., 2010). Under physiological conditions, these follicular stem cells and their progeny are primarily responsible for the regeneration of the hair follicle, the isthmus, and the sebaceous gland (Ito et al., 2005; Leushacke and Barker, 2012). The basal layer of the epidermis contains the interfollicular epidermis (IFE), which give rise to

transient progenitors that generate epidermal proliferative units, while the maintenance of sebaceous gland cells is facilitated by progenitors situated above the bulge that express the Blimp1 protein (Telerman et al., 2017). Conversely, in instances of skin injury, the follicular cells are actively mobilized to generate all the cellular lineages of the skin, including the IFE a process that necessitates intricate epithelial-mesenchymal interactions (Fuchs, 2009).

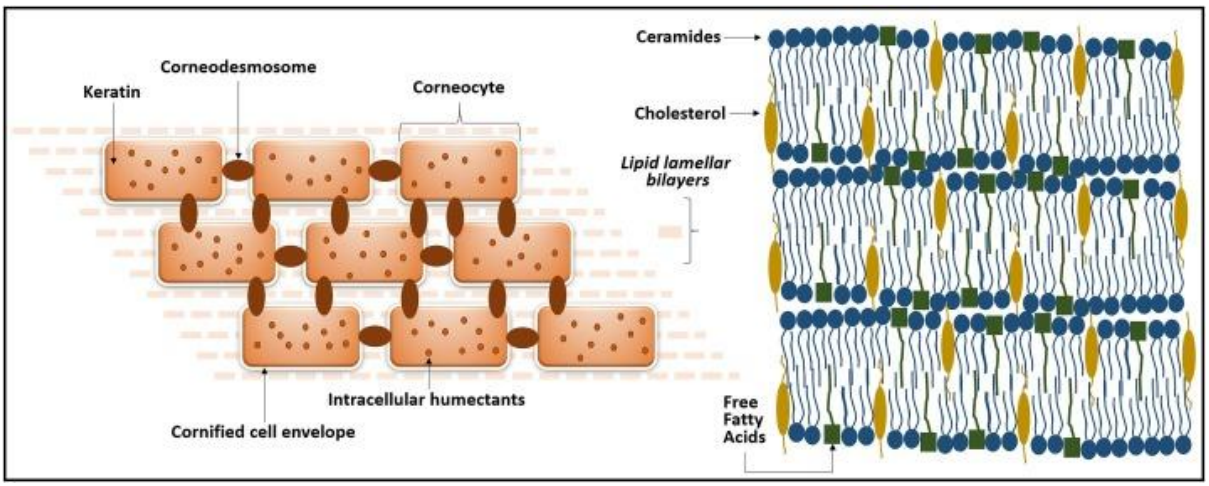

Figure 1.4: Structural organization- illustrating the Brick-and-Mortar hypothesis.

The diagram is a representation of the brick-and-mortar hypothesis of the stratum corneum, illustrating the structural organization and key components that maintain skin barrier function. The picture on left shows corneocytes, depicted as brick-like flattened cells within a continuous extracellular lipid matrix ("mortar"). These corneocytes are densely packed with keratin filaments and intracellular humectants, which help retain water. Adjacent corneocytes are connected via corneodesmosomes, specialised adhesive structures that maintain cohesion within the stratum corneum and regulate desquamation. The picture on right shows the organisation of the intercellular lipid matrix layer, consisting of free fatty acids, cholesterol and ceramides, which together form lamellar bilayers. This lipid arrangement is critical for maintaining epidermal permeability barrier integrity, preventing trans epidermal water loss, and defending against environmental insults (Nemes & Steinert, 1999).

To carry out various physiological processes in the body, cell to cell coordination is critically required. These cellular processes in the skin are orchestrated by molecular pathway signals.

Number of morphogenetic pathways play essential roles in development and regulation. Any disturbances in this finely tuned homeostatic process can result in skin diseases such as cancers.

To fully understand the epithelial cell behaviour and skin tumorigenesis, it is essential to consider the interplay of core signalling pathways that govern cellular processes. Among these, the Wnt, BMP (Bone Morphogenetic Protein), and FGF (Fibroblast Growth Factor) pathways represent three fundamental and highly conserved systems. While Wnt signalling is critical for maintaining stem cell populations and promoting epidermal proliferation (Lim and Nusse, 2013). BMP signalling primarily influences cellular differentiation and acts as a context-dependent modulator of growth (Botchkarev, 2003). Meanwhile, the FGF pathway contributes to tissue repair, angiogenesis, and morphogenesis (Werner and Grose, 2003). Though distinct in their mechanisms, these pathways are intricately interconnected and often converge at the level of transcriptional regulation modulating common downstream targets and cross regulating each other's activity. Their integration within this study provides a comprehensive framework for exploring how upstream signalling dynamics shape transcription factor activity and contribute to the molecular underpinnings of skin homeostasis and squamous cell carcinoma development.

1.1.7 Wnt SIGNALLING IN SKIN

Wnt signalling plays a critical role in the development of the skin. For process of formation of the epidermis, this pathway specifies the embryonic ectoderm which leads to the formation of skin epithelium and initiates the production of keratins by inhibiting the fibroblast growth factor signalling (Wilson et al., 2001). Moreover, Wnt signalling is essential for the development of skin appendages, specifically HFs. This involves communication between the epidermis and dermis, resulting in the formation of epidermal placodes at regular intervals on the skin. It is proposed that dermally derived Wnt ligands serve as the initial signal for placode

formation (DasGupta and Fuchs, 1999; Zhang et al., 2009). Subsequently, Wnt/β-catenin signalling is activated in the epidermis in response to this signal, promoting the fate of the placodes (Zhang et al., 2009). Furthermore, this signalling pathway is also necessary for communication with the underlying mesenchymal cells, leading to the formation of dermal condensates and the subsequent development of dermal papillae (Huelsken et al., 2001; Zhang et al., 2009). The importance of Wnt/β-catenin signalling in HF development is further highlighted by the absence of placode formation when the Wnt/β-catenin-specific inhibitor, DKK, is ectopically expressed in the basal cells of developing murine epidermis (Andl et al., 2002).

In the development and maintenance of skin tissue, Wnt signalling plays an important role and is essential for regulating the proliferation, differentiation, and organization of skin cells (Clevers 2006). During embryonic development, it is critical for the homeostasis of sebaceous glands and hair follicles (Nusse and Clevers 2017). The stem cells which are responsible for the continuous renewal of the epidermis located in the basal layer of the interfollicular epidermis and the bulge region of hair follicles are regulated by Wnt signals by maintaining the self-renewal capacity of these stem cells and direct their differentiation into specific epidermal cell lineages (Veltri et al., 2018; Lim and Nusse, 2013). It also shows involvement in the regulation of hair follicle cycling. It controls the transition between the resting (telogen) and growth (anagen) phases of the hair cycle. Activation of Wnt signalling in the dermal papilla, a specialized mesenchymal structure at the base of hair follicles, is critical for initiating the anagen phase and promoting hair shaft elongation (Widelitz, 2008; Mater et al., 2003). Wnt signalling plays a key role in cutaneous wound healing. The pathway is activated in response to skin injury and regulates various aspects of the healing process, including inflammation, cell migration, and tissue regeneration. To repair the damaged tissue, Wnt signalling also promotes the mobilization of stem cells to the wound site (Houschyar et al., 2019; Whyte et al., 2013).

In the interfollicular epidermis (IFE), the Wnt pathway plays a complex role. In murine skin, it was considered that Wnt/β-catenin regulates the fate of epidermal stem cells (SCs) towards a hair follicle lineage, rather than affecting their self-renewal properties (Andl et al., 2002; Beronja et al., 2013; Gat et al., 1998; Huelsken et al., 2001). However, the lineage tracing studies conducted on the murine plantar epidermis have discovered a population of Axin2þ basal cells that represent IFE SCs, continuously producing keratinocytes. These Axin2þ cells themselves serve as the source of Wnt ligands in the IFE, where the suprabasal layers of the epidermis contain a high level of secreted Wnt inhibitors, creating a gradient that confines autocrine Wnt signalling to the basal layer (Lim et al., 2013). In essence, this leads to spatial self-organization within the epidermis (Clevers et al., 2014). Additional studies have been demonstrated that β-catenin is essential for epidermal proliferation and SC maintenance *in vivo* the IFE (Choi et al., 2013; Jensen et al., 2009) as well as the Wnt/β-catenin pathway also sustains human IFE SC population is in vitro (Zhu and Watt, 1999). Under homeostatic conditions in murine IFE if the Wnt/β-catenin signalling is reduced it inhibits proliferation process however it is not necessary for extended inflammatory-induced hyper proliferation and maintenance of the IFE (Choi et al., 2013). However, the abnormal regulation of Wnt/β-catenin signalling in humans during wound healing causes epidermal thickening and keratinocyte proliferation during keloid scarring (Chua et al., 2011).

Rho GTPases are key mediators of Wnt signalling, particularly in the noncanonical pathways. These small GTPases regulate cytoskeletal dynamics and cell migration, which are critical for the morphogenesis of skin appendages and the maintenance of tissue architecture (Schlessinger et al., 2009).

Depending upon β-catenin dependent and β-catenin independent, there are two classes- Wnt/β-catenin dependent pathway or canonical pathway (Figure 1.5) and Wnt/β-catenin-independent pathway or non-canonical pathway, which is further divide into two classes includes-

Wnt/planar cell polarity (PCP) and Wnt/calcium (Wnt/Ca +2) pathway (Figure 1.6). The canonical pathway primarily regulates cell proliferation process whereas non-canonical pathway regulates polarity and mobility of the cell (Amin and Vincan 2012; Gajos-Michniewicz and Czyz 2020).

Any disruption in the non-canonical pathways can be influencing cancer progression by affecting processes like invasion and metastasis (Zhang et al., 2022; Prgomet et al., 2015). Dysregulation of Wnt signalling is a common feature of skin cancers, including basal cell carcinoma and squamous cell carcinoma. Any mutations of Wnt signalling can result in uncontrolled proliferation of keratinocytes and the results in formation of malignant tumours (Lim and Nusse, 2013; Widelitz, 2008).

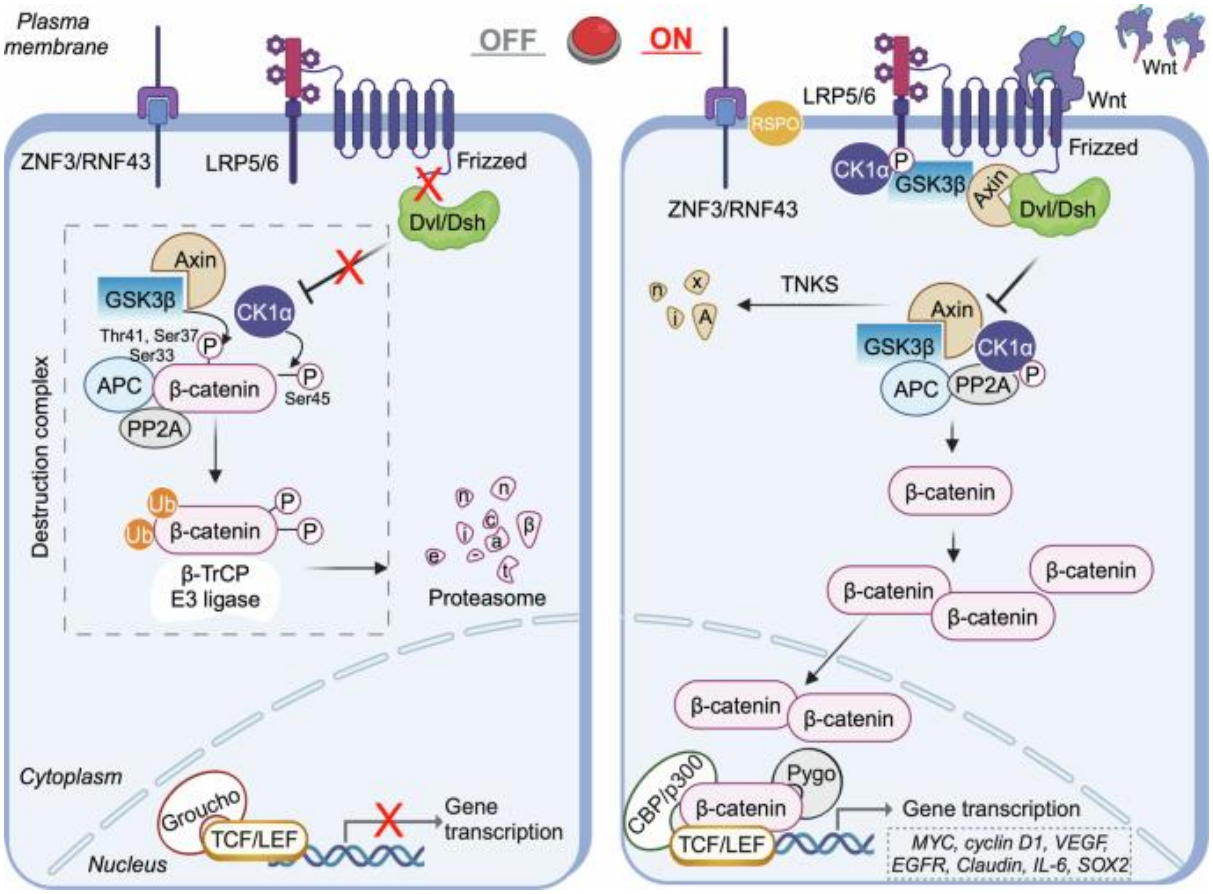

Figure 1.5 Canonical Wnt/β-catenin signalling pathway in the absence and presence of Wnt ligands.

(Left panel: Wnt OFF state) - In the absence of Wnt ligands, frizzled (Fzd) receptors and co-receptors LRP5/6 remain inactivated at the plasma membrane. In the cytoplasm, β-catenin is continuously targeted for degradation by the destruction complex, comprising Axin, APC, GSK3β, CK1α, and associated with E3 ubiquitin ligase activity. Phosphorylated β-catenin is ubiquitinated and degraded by the proteasome, preventing its nuclear accumulation. In the nucleus, transcriptional repressors such as Groucho remain bound to TCF/LEF transcription factors, thereby inhibiting Wnt target gene expression. (Right panel: Wnt ON state) – Upon Wnt ligand binding, Frizzled and LRP5/6 are activated, leading to recruitment of Dishevelled (Dvl/Dsh) and inhibition of the destruction complex. Membrane-associated E3 ligases RNF43/ZNRF3 are negatively regulated, allowing stabilization of Fzd receptors. Destruction complex components (Axin, APC) are sequestered or inhibited, and PP2A-mediated dephosphorylation further stabilizes β-catenin. Stabilized β-catenin accumulates in the cytoplasm, translocate into the nucleus, and binds to TCF/LEF, displacing Groucho and promoting transcription of Wnt target genes (Xue et al, 2025).

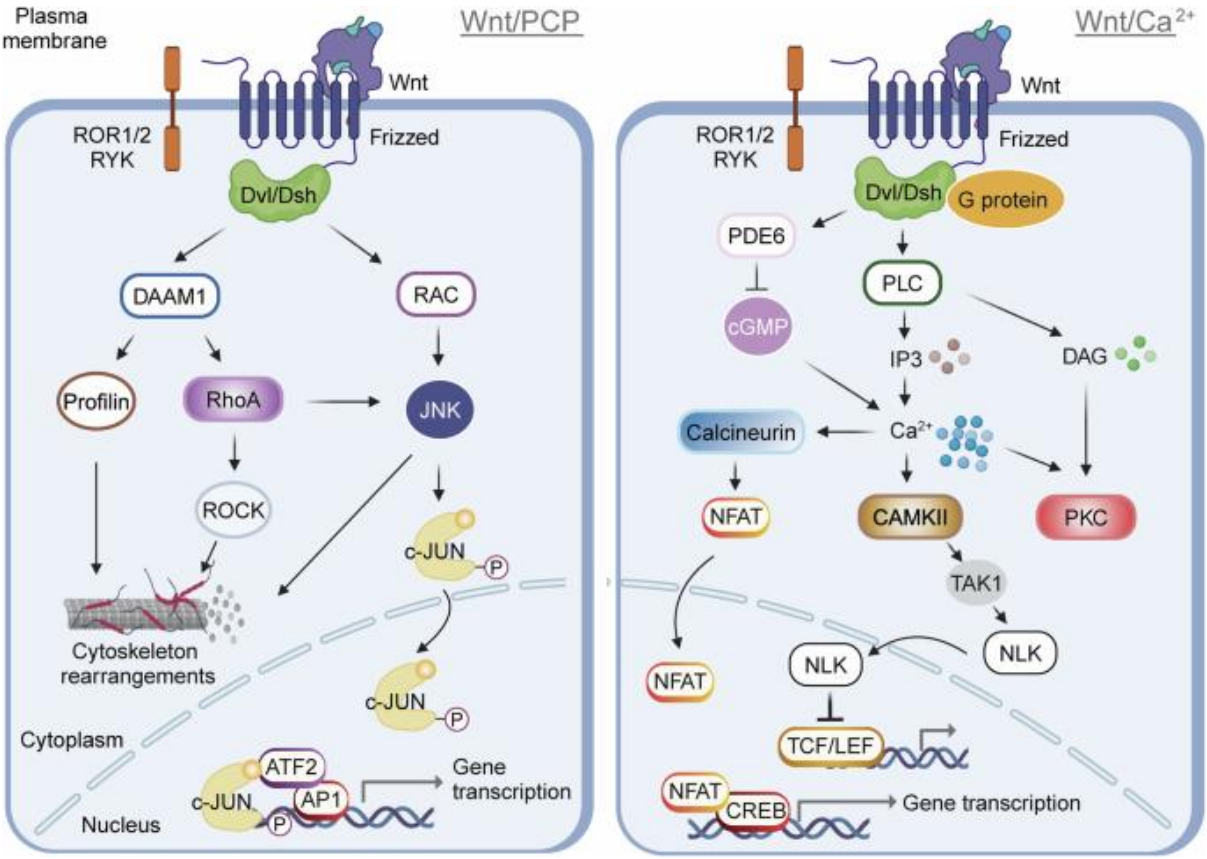

Figure 1.6: Wnt/Planer Cell Polarity (PCP) and Wnt/Ca^{2+} pathways.

The non-canonical Wnt signalling pathways operate independently of β-catenin. These pathways are typically activated by Wnt ligands, bind to Frizzled (FZD) receptors and co-receptors, such as Ror2 and Ryk. (Left panel: Wnt/PCP pathway) Ligand binding activates Dishevelled (DVL), leading to downstream signalling via Daam1, RhoA, Rac1, and JNK. Activation of JNK also influences gene expression indirectly through c-Jun and AP-1 transcription factors. (Right panel: Wnt/Ca^{2+} Pathway): Wnt ligands stimulate intracellular calcium release through phospholipase C (PLC) activation. Elevated cytoplasmic Ca^{2+} levels activate protein kinase C (PKC), calmodulin-dependent kinase II (CaMKII), and calcineurin, which modulates transcription via the CREB and NFAT transcription factors. (Xue et al, 2025)

1.1.8 FIBROBLAST GROWTH FACTORS IN SKIN

FGF (fibroblast growth factor) signalling constitutes a pivotal pathway integral to a multitude of biological processes, encompassing angiogenesis, developmental biology and cellular

migration. Fibroblast growth factor (FGF) signalling is integral to the biological functions of the skin. This is particularly evident in processes such as wound healing and cellular differentiation. The FGFs, which encompass acidic FGF (aFGF) and basic FGF (bFGF), are implicated in a multitude of dermal processes, ranging from the promotion of cellular proliferation to the modulation of myofibroblast activity. Empirical evidence has demonstrated that aFGF significantly expedites the healing of dermal wounds in rodent models, facilitating angiogenesis and granulation tissue formation while refraining from inducing dermal contraction (Mellin et al., 1992). Conversely, the action of bFGF is linked with a diminution in alpha-smooth muscle actin (α-SMA) expression within myofibroblasts, a factor that is pivotal for wound contraction, thus fostering a more advantageous environment for healing (Ishiguro et al., 2009). FGFs are known to stimulate the proliferation of skin-derived cellular entities, such as keratinocytes and fibroblasts, which are vital for the repair of the skin (Thomas 1987). Mutations in FGFR3 within the skin context result in mild hyperplasia but do not appear to incite tumorigenesis, indicating a multifaceted role in skin homeostasis and differentiation (Duperret et al., 2015). The FGF signalling pathway involves ligand-mediated activation of FGFRs and subsequent signal transduction via canonical pathways. The RAS/MAPK and PI3K/AKT pathways are central to the regulation of cellular processes like differentiation, migration and proliferation.

This signalling cascade functions through the intricate interactions between FGFs and their cognate receptors (FGFRs), thereby modulating both normative physiological activities and pathological states, including malignancies. FGF signalling serves as a potent pro-angiogenic agent, facilitating neovascularization within tumours. The inhibition of the FGF/FGFR axis has been recognized as a promising therapeutic approach to mitigate tumour progression and metastasis (Ronca et al., 2015). FGF plays a critical role in modulating cellular adhesion characteristics, thereby affecting cellular interactions and differentiation during developmental

processes, while also acting as a chemoattractant that directs cellular migration throughout organogenesis (Bae et al., 2012).

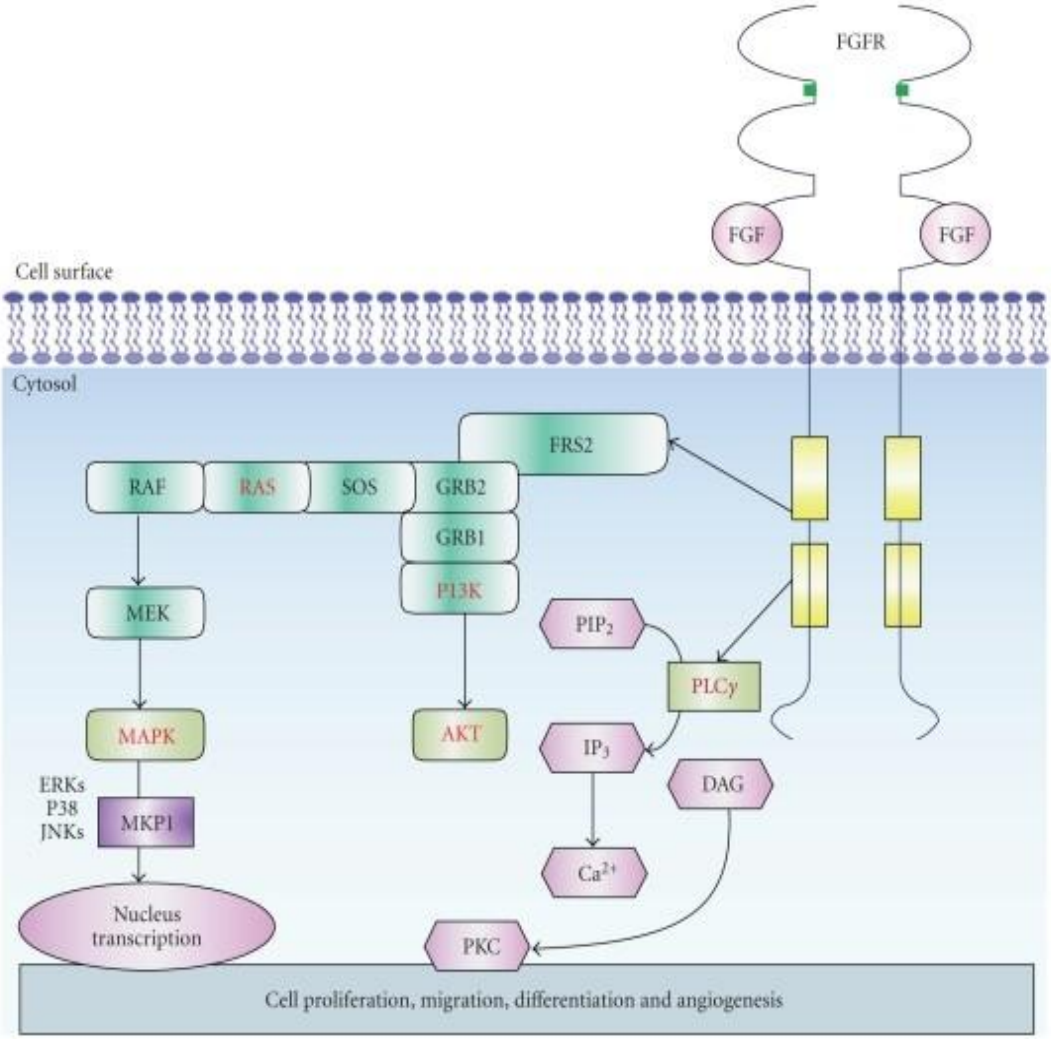

Figure 1.7: Fibroblast Growth Factor (FGF) signalling pathway.

Schematic diagram of Fibroblast Growth Factor where it initiates with the tyrosine phosphorylation of the adaptor protein FRS2, which facilitates the assembly of a signalling complex comprising GRB2, SHP2, and GAB1. This complex subsequently activates both the PI3K–AKT and RAS–MAPK signalling cascades. In the PLCγ branch of the pathway, activated phospholipase C gamma (PLCγ) catalyzes the hydrolysis of phosphatidylinositol 4,5-bisphosphate (PIP2), producing inositol 1,4,5-trisphosphate (IP3) and diacylglycerol (DAG), which together contribute to the activation of protein kinase C (PKC) (Yun et al., 2010).

1.1.9 BONE MORPHOGENETIC PROTEIN IN SKIN

BMP (Bone morphogenetic proteins) play a major role in skin development which includes epidermal stratification, hair follicle morphogenesis, and the regulation of stem cells. Epidermal stratification is an intricate process that includes the proliferation of basal progenitors and their differentiation into intermediate and post-mitotic cells. BMP signalling has been implicated in this process, particularly through its interaction with other signalling pathways. For instance, in mammalian skin, BMP signalling interacts with FGF signalling to regulate epidermal stratification. BMP4, produced in the dermis, activates FGF7 and FGF10 signalling, which in turn promotes the proliferation of basal progenitor cells. This BMP-FGF axis is necessary for the foundation of the spinous layer, a critical step in epidermal stratification (Zhu et al., 2014). BMP7 has been recognized as a major factor in the differentiation of human epidermal Langerhans cells (LCs), promoting their proliferation and maturation through selective signalling pathways (Yasmin et al., 2013). For instance, the expression of BMP7 in the epidermis contrasts with TGF-ß1, which inhibits LCs, suggests a regulatory balance essential for skin immune function (Yasmin et al., 2013). BMP signalling in the dermis has non-cell autonomous effects on the epidermis. For example, dermal BMP4 promotes the activation of FGF signalling, which feeds back to regulate basal progenitor cells. This crosstalk between dermal and epidermal compartments highlights the importance of BMP signalling in coordinating tissue development (Zhu et al., 2014). While, Wnt signalling is traditionally associated with epidermal stratification, BMP signalling modulates this process by interacting with Wnt pathways. For example, BMP signalling can influence the Wnt target genes expression. BMP signalling is central to this process, influencing both the formation and cycling of hair follicles. This signalling is essential for the hair follicle-inductive properties of dermal papilla (DP) cells. BMPs maintain the signature characteristics of DP cells and their ability to instruct epithelial progenitors during hair follicle formation. Loss of BMP signalling

in DP cells results in the failure to generate hair follicles in vivo (Rendl et al., 2008). It also regulates the size of hair follicles by modulating cell cycle-associated genes. For example, BMP signalling inhibits the proliferation of hair matrix cells by upregulating p27Kip1, a cyclin-dependent kinase inhibitor. Overexpression of BMP antagonists, such as noggin, leads to enlarged hair follicles due to increased cell proliferation (Sharov et al., 2006). BMP signalling participates in regulating the hair follicle cycle. Cyclic expression of BMP4 and BMP2 in the dermis creates alternating phases of refractory and competent states for hair regeneration. Overexpression of BMP4 can inhibit hair regeneration by maintaining the refractory phase (Plikus et al., 2008). It is also needed for the differentiation of the inner root sheath and hair shaft. Mutations in BMPR-IA, a key BMP receptor, result in impaired differentiation and hair follicle morphogenesis. This emphasizes the importance of BMP signalling in regulation of cell fate decisions during the development of hair follicle (Kwan et al., 2004; Andl et al., 2004). Skin stem cells, particularly residing in the bulge of hair follicle, are tightly regulated by BMP signalling. BMP signalling is critical for maintaining the quiescent state of follicle stem cells. Loss of BMP signalling leads to premature activation of these cells, resulting in expanded niche compartments and aberrant differentiation (Kobielak et al., 2007). The interaction of BMP signalling with Wnt signalling regulates the stem cell behaviour. For instance, BMP signalling can enhance β-catenin stabilization in the niche, promoting hair cycle activation. However, sustained BMP signalling can also block activation and promote premature differentiation, underscoring the need for precise regulation (Kobielak et al., 2007). BMP signalling has been implicated in skin tumorigenesis, particularly in the context of squamous cell carcinoma (SCC). By acting as a tumour suppressor, BMP signalling regulates apoptosis and cell cycle arrest. Loss of Smad4, a key mediator of BMP signalling, leads to increased proliferation and tumorigenesis in the skin (Qiao et al., 2006). BMP signalling relates with the PTEN-AKT pathway to regulate tumour formation. Loss of BMP signalling

can lead to activation of AKT, promoting cell proliferation and survival, which contributes to SCC development (Qiao et al., 2006). Mutations in BMPR-IA signalling can lead to the formation of hair follicle tumours. This signifies the reputation of BMP signalling in preserving the balance between proliferation and differentiation in the skin (Kwan et al., 2004; Andl et al., 2004). The fundamental components of BMP signalling pathway which underpins many of the regulatory mechanisms, particularly in the context of cutaneous epithelial differentiation or tumour suppression via SMAD signalling in figure 1.8 (Wang et al., 2014).

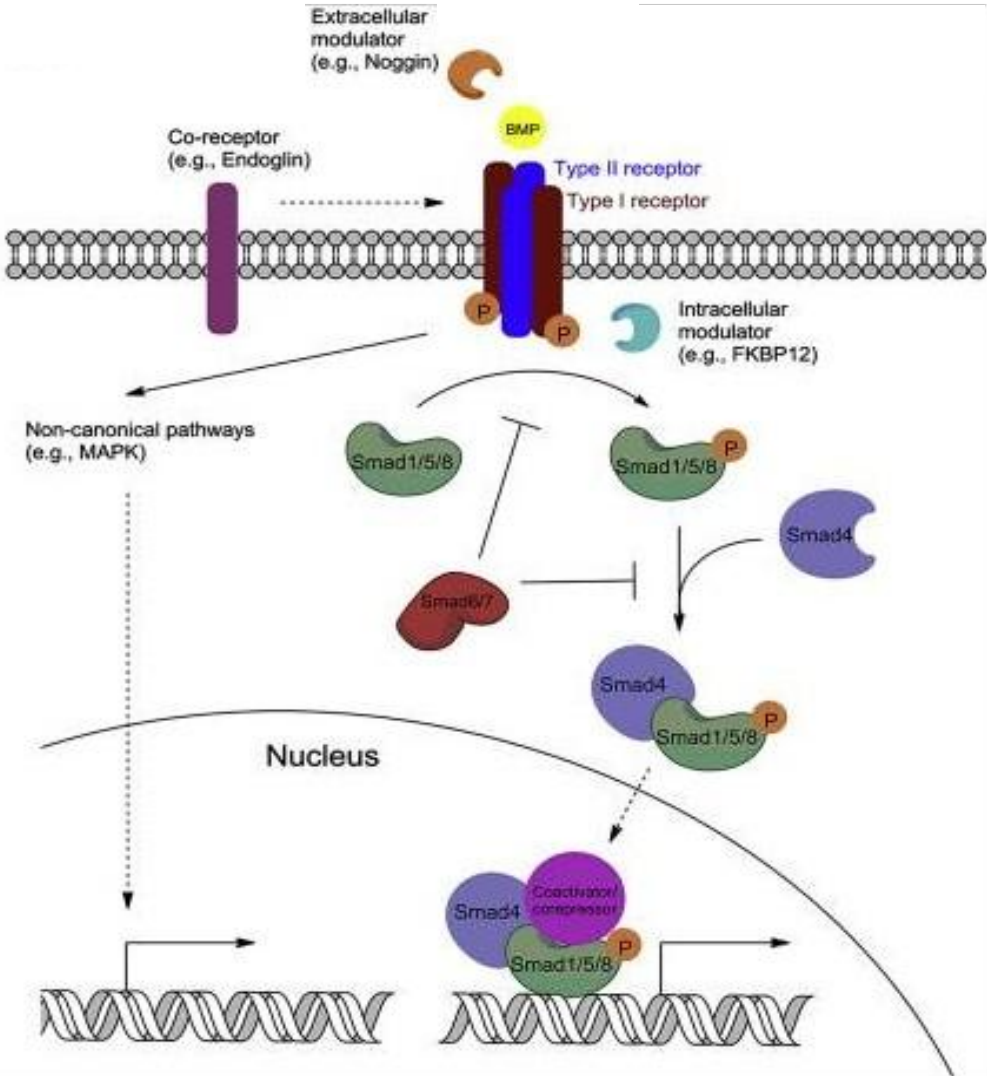

Figure 1.8: Bone Morphogenetic Protein (BMP) Signalling Pathway.

Schematic representation of the BMP signalling pathway, including extracellular and intracellular regulation, canonical SMAD signalling, and non-canonical branches. Extracellularly, BMP ligands are regulated by secreted antagonists such as Noggin, which binds directly to BMPs and prevents their interaction with surface receptors. Upon ligand availability, BMPs bind to a receptor complex composed of type I and type II BMP receptors, with type II receptors phosphorylating and activating type I receptors upon ligand-induced dimerization. Co-receptors assist in stabilizing this interaction and enhancing signal specificity. Intracellularly, in the resting state, FKBP12 binds to type I receptors, acting as an inhibitor to prevent ligand-independent activation. Upon BMP binding and FKBP12 displacement, activated type I receptors phosphorylate receptor-regulated SMADs (SMAD1, SMAD5, SMAD8), which then form complexes with the common mediator SMAD4. These complexes translocate into the nucleus, where they regulate transcription of BMP-responsive genes. In parallel, non-canonical BMP signalling can also be activated, leading to the engagement of alternative pathways such as MAPK, PI3K/AKT, or JNK, contributing to diverse cellular responses including cytoskeletal remodelling, survival, and proliferation (Wang et al., 2014).

Given its multifaceted roles in protection, sensory perception, and systemic regulation, the skin is not only vital to physiological well-being but also uniquely exposed and vulnerable to a broad spectrum of pathological conditions. Despite its resilience, disturbances in skin homeostasis produced by environmental, immunological, genetical or microbial factors can indicate to a range of abnormalities, including inflammatory skin disorders, chronic disorders, and cutaneous malignancies. Among these, cutaneous squamous cell carcinoma (cSCC) stands out as the one of the most common forms of skin cancer, occurring from keratinocytes of the epidermis and often driven by cumulative UV radiation exposure and impaired immune surveillance. As a condition with both high prevalence and potential for metastasis, cSCC represents a substantial public health concern and will be the central focus of this investigation.

1.2 CUTANEOUS SQUAMOUS CELL CARCINOMA (cSCC)

Squamous cell carcinoma (SCC) is the second most common form of non-melanoma skin cancer (NMSC) globally, accounting for approximately 20–25% of the over 5.4 million NMSC cases diagnosed each year. Although comprehensive global cancer registries often exclude NMSC due to high incidence and generally low mortality, it is projected that over 65,000 deaths occur worldwide yearly as a result of these cancers, with SCC contributing significantly due to its metastatic potential (Skin Cancer Foundation, 2024). In the United States, SCC incidence is alarmingly high, with approximately 1.8 million new cases diagnosed annually, and over 15,000 deaths reported every year, making it a substantial public health concern (Siegel et al., 2024). The burden is disproportionately higher in males, with a male-to-female ratio of nearly 2:1, largely attributed to greater occupational sun exposure and lifestyle factors. Similarly, in the United Kingdom, an estimated 150,000–200,000 cases of SCC are managed annually, with around 700 associated deaths, though these numbers are likely underestimated due to underreporting and limitations in national cancer registration systems. As in the U.S., SCC in the U.K. shows a male predominance, particularly in individuals over the age of 60 (Cancer Research UK, 2024). These epidemiological patterns underscore the growing need for improved surveillance and targeted prevention strategies, especially in high-risk populations. The incidence of CSCC has experienced a notable increase, ranging from 50% to 300%, over the course of the past three decades (Brouham et al., 2014). Projections indicate that by the year 2030, European countries will witness a doubling in the occurrence of CSCC (Leiter et al., 2017).

The increased rate of squamous cell carcinoma (SCC) in men related to women is attributed to a combination of behavioural, environmental, and biological factors. One of the most prominent contributors is greater cumulative exposure to ultraviolet (UV) radiation, as men are

more frequently employed in outdoor occupations such as construction, agriculture, and manual labour, and are generally less likely to use sun protection measures like sunscreen or protective clothing (Linares et al., 2015). Beyond behavioural aspects, hormonal and immunological differences also play a critical role. Estrogen, which is more prevalent in females, has been shown to exert shielding effects against UV-induced DNA damage and promote more efficient skin repair, potentially reducing the risk of malignant transformation (Guerra and Piera-Velazquez, 2018). Additionally, females tend to mount stronger immune responses, which enhance immune surveillance and the clearance of atypical or precancerous cells (Klein and Flanagan, 2016). In contrast, males are more prone to delayed medical consultations, resulting in later-stage diagnoses and worse outcomes. Together, these factors contribute to a man-to-woman ratio of approximately 2:1 in SCC incidence, highlighting the importance of sex-specific prevention and screening strategies in mitigating the public health burden of this disease.

Geographical variability is evident among the populations impacted, exhibiting an elevated independent risk for individuals inhabiting areas characterized by high to medium ultraviolet radiation exposure, in contrast to individuals residing in locales with low UVR exposure (Qureshi et al., 2008). Within diverse ethnic cohorts, cutaneous squamous cell carcinoma (cSCC) is predominantly observed in individuals of European descent, followed in prevalence by those of Asian, Latin, and African heritages. Amongst patients who have undertaken solid-organ transplantation, cSCC manifests most frequently in individuals of Latin American lineage within the demographic of non-European ethnicities (Dusendang et al., 2022). In individuals of African descent, cSCC occurrences in areas of the body not subjected to sun exposure are comparatively more prevalent, underscoring the influence of non-UVR-related determinants such as infections and environmental carcinogens in the etiology of the disease (Nadhan et al., 2019). It has been established that individuals of Caucasian ancestry possess a

7% to 11% probability of developing cutaneous squamous cell carcinoma at some juncture in their lives (Miller et al., 1994). This probability is further stratified by sex, with males experiencing a risk range of 9% to 14% and females encountering a risk range of 4% to 9% (Alam et al., 2001).

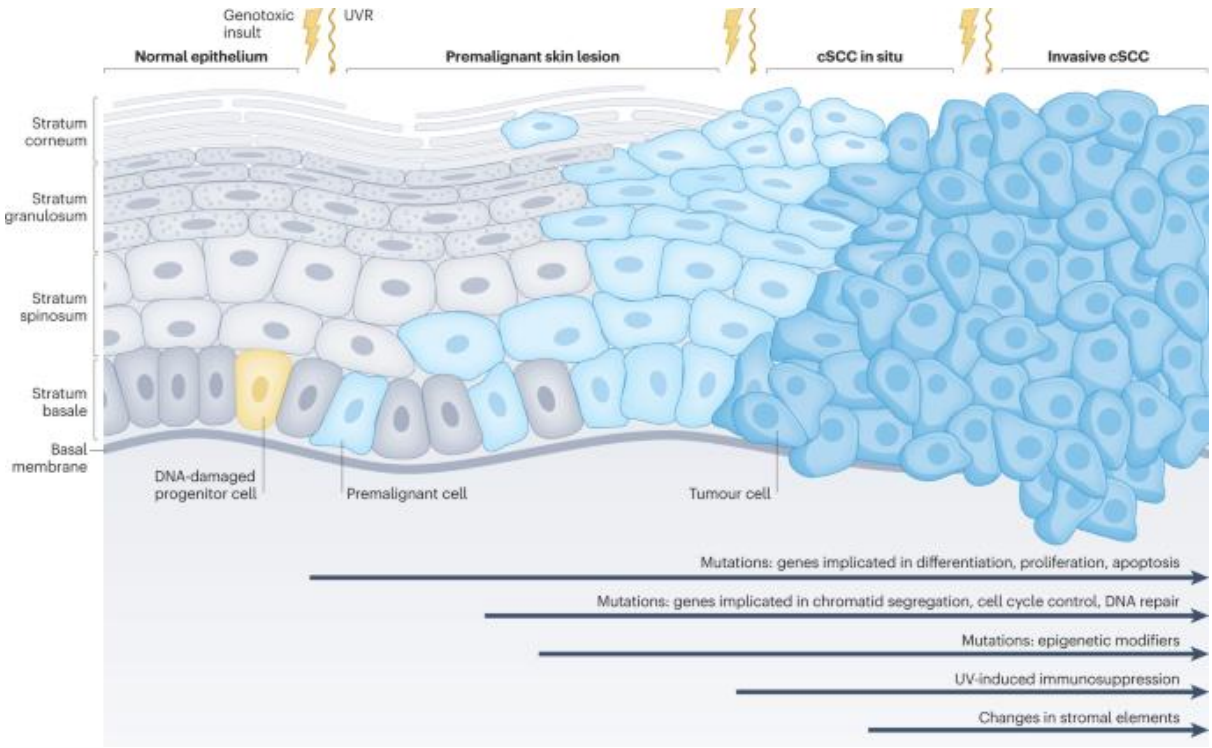

Figure 1.9: **A stagewise progression of cSCC from normal epidermis to invasive carcinoma.**

This schematic illustrates the multistep development of cSCC, transitioning from normal epithelium through premalignant lesions (e.g., actinic keratosis), to cSCC in situ, and ultimately invasive cSCC, shown from left to right across five epidermal layers. Ultraviolet radiation (UVR) and other genotoxic insults target epidermal progenitor cells in the basal layer, inducing DNA damage and initiating carcinogenesis. In early stages, DNA-damaged basal cells exhibit aberrant proliferation and give rise to premalignant cells, with early mutations in genes regulating differentiation, apoptosis, and proliferation. As transformation progresses, tumour cells accumulate additional alterations, including mutations in genes involved in chromatin remodelling, DNA repair, epigenetic regulation, and cell cycle control, promoting clonal expansion and architectural disruption. In situ cSCC is marked by full-

thickness atypia without dermal invasion, while invasive cSCC breaches the basement membrane and infiltrates underlying dermis. Additional tumour-promoting factors illustrated include UV-induced immunosuppression and stromal remodelling, both of which contribute to tumour progression and invasion. Cellular morphology visibly shifts across stages, with increasing nuclear atypia, pleomorphism, and architectural disorganization reflective of malignancy. (Winge et al., 2023).

cSCC occurs from the malignant proliferation of epidermal keratinocytes. As shown in Figure 1.9 (Winge et al., 2023), the development of cSCC involves distinct stages characterized by cumulative genetic and epigenetic alterations. These stages provide a context for evaluating the role of transcriptional regulators such as ELF5 in the transition from pre-malignant to malignant phenotypes. Various risk factors, both environmental and constitutional, contribute to its development. Fair skin, male sex, older age, immunosuppression, and a prior history of actinic keratosis (AK) are recognized as significant environmental risk factors. Among these, prolonged sun exposure stands as the most influential and deep-rooted factor linked to cSCC (Que et al., 2018; Gloster et al., 2006, Garcovich et al., 2017). AK is regarded as a precursor lesion that holds the potential to progress into an invasive cSCC, thereby establishing itself as the most substantial predictive factor for cSCC occurrence (Werner et al., 2013). Several molecular pathways have been involved in the development of cutaneous squamous cell cancer (cSCC) (Figure 1.9). Early events in cSCC include the most important ecological risk factor ultraviolet induced (UVR) mutations in the P53 gene, leading to genomic instability with occurrence rates ranging from 54% to 95% (Ziegler et al., 1994). Subsequent genetic changes occur in other suppressor genes, such as NOTCH and CDKN2A, as well as in oncogenes, such as RAS (South et al., 2014; Pierceall et al., 1991). The skin is directly impacted by UV radiation, where prolonged exposure to sunlight negatively affects keratinocytes, leading to a decline in the functional capacity of the skin tissue and co-operating the bodily homeostasis of the skin (Brand et al., 2018). Unnecessary exposure to UV rays can result in necrosis of certain

epidermal cells. The loss of membrane integrity in these damaged cells enables the release of cellular contents into the surrounding environment. Adjacent healthy keratinocytes absorb these liberated molecules, containing double-stranded RNA, which subsequently activates toll-like receptor 3 within their endosomes. This initiates a series of events that promote lipid-related processes and inflammation (Bernard et al., 2012; Borkowski and Gallo, 2014). When UVB radiation is directed towards naturally transformed aneuploid immortal keratinocyte cell line cells, it leads to the release of mitochondria and nuclear-damaged DNA, triggering the activation of cyclic guanosine monophosphate-adenosine monophosphate synthase/protein stimulator of interferon genes DNA sensor, which in turn induces an innate immune response (Li et al., 2021). The accumulation of mutations affects various signalling pathways, including, PI3K/AKT/mTOR and NF-kB, MAPK, which contribute to the overexpression of the epidermal growth factor receptor (EGFR) (Canueto et al., 2017; Toll et al., 2010). Additionally, epigenetic changes may also occur (Murao et al., 2006).

1.2.1 MOLECULAR MECHANISMS OF CUTANEOUS SQUAMOUS CELL CARCINOMA

cSCC cancer is known for its high mutation rate among human cancers (Pickering et al., 2014; Li et al., 2015). An innate understanding of the molecular mechanisms underlying cSCC could potentially lead to improved treatment strategies for this disease. UVR-induced mutagenesis leads to specific C-T and CC-TT dipyrimidine transitions, enabling tumour cells to evade apoptosis and promote the expansion of p53 mutant keratinocytes (Wikonkal et al., 1999). The importance of p53 in ultraviolet B-induced carcinogenesis has been confirmed in $p53^{-/-}$ mice, which exhibit increased susceptibility to the development of AK lesions and cSCCs following exposure to ultraviolet B (UVB) (Berg et al., 1996; Li et al., 1998). Furthermore, multiple studies have identified p53 mutations in cSCC cell lines (Hassan et al., 2019, Inman et al.,

2018). The CDKN2A gene encodes two alternative proteins, p16INK4a and p14ARF. Inactivation of the CDKN2A locus can occur through loss of heterozygosity, point mutations, and promoter hypermethylation (Brown et al., 2004). The loss of function of either p14ARF or p16INK4a can result in uncontrolled cell cycle and unrestricted cell growth, affecting p53 and pRB pathways (Serrano et al., 1993; Stott et al., 1998).

Moreover, loss of function mutations in NOTCH1 and NOTCH2 are observed in above 75% of cSCCs (Wang et al., 2011). *In vivo* studies in mice with *Notch1* deletion, an early mutation in cSCC, demonstrate the skin tumours development and enabling of chemically induced skin carcinogenesis (Nicolas et al., 2003; Proweller et al., 2006). The Notch1 gene is directly regulated by p53, and the disruption of Notch1 in keratinocytes affects the balance between differentiation and growth (Lefort et al., 2007; Lefort et al., 2004). The upregulation of the Wnt/β-catenin pathway, which might result from loss of Notch1 function, promotes skin tumour development and is partially dependent on p21WAP/Cip1 (Nicolas et al., 2003, Devgan et al., 2005). Studies on Notch1-deficient mouse skin reveal an increase in fibroplasia, angiogenesis, and inflammation, highlighting the significance of the stromal microenvironment in cSCC development (Demehri et al., 2009). Loss of the *NOTCH1* gene may have collaborative effects with Ras-activation in the transformation of keratinocytes (South et al., 2014; Lefort et al., 2007).

EGFR overexpression is prevalent in cSCC and is linked to the attainment of more destructive phenotype and a bleak diagnosis (Canueto et al., 2017; Shimizu et al., 2001). EGFR belongs to the ErbB family of tyrosine kinase receptors. They ae responsible for the transmitting a growth-inducing signal to cells that are stimulated by an appropriate EGFR ligand. The binding of the ligand with EGFR results in a conformational alteration that allows the formation of a homodimer with another EGFR or a heterodimer with another member of the ErbB family,

both of which lead to activation (Wieduwilt et al., 2008). The pathways affected by the activation of EGFR include PLC-gamma/PKC, PI3K/AKT/mTOR and RAS-RAF-MEK-MAPK. Also, NF-kB and STAT can be activated (Oda et al., 2005). All of these pathways are regularly modified in tumours, including cSCC (Jost et al., 2000), and trigger increased migration, proliferation, survival, altered differentiation and resistance to apoptosis.

The epigenetic events play significant roles in cSCC and AK (Rodriguez-Paredes et al., 2018). cSCC involves the hypermethylation of various promoter genes, such p14ARF and p16INK4a as well as RB1, MGMT, CDH1, and RASSF1. The involvement of these genes has been observed in DNA repair, epithelial adhesion, cell cycle regulation and signal transduction, while hypermethylation of CpG islands in the promoter regions leads to transcriptional silencing (Murao et al., 2006). MicroRNAs also play a crucial role; some act as oncogenes and others as tumour suppressors (Garcia-Sancha et al., 2019), and some are regulated by epigenetic factors.

Lastly, the tumour microenvironment shows a vital part in the carcinogenesis of cSCC (Dotto et al., 1988), gaining more attention as its relevance in tumour development has become evident (Hanahan and Coussens, 2012; Junttila de Sauvage, 2013). Inflammation is one of the key components of the tumour microenvironment (Junttila de Sauvage, 2013), which can act as a tumour promoter (Grivennikov et al., 2010; Wong et al., 2013). The absence of an inflammatory response is relevant to tumour progression (Thommen, 2018). The studies have shown that the cSCC tumour microenvironment is enriched in cancer-associated fibroblasts (CAFs) (Sasaki et al., 2018) and tumour-associated macrophages (Moussai et al., 2011). Tumour stromal cells are associated in metastasis, invasion, tumour progression, and chemotherapy response (Chan et al., 2018; Bernat-Peguera, 2019).

1.3 TRANSCRIPTIONAL REGULATORS OF SKIN DEVELOPMENT

Transcription factors are proteins that play a pivotal role in the regulation of transcriptional processes during the development of skin. Typically, they possess a domain for DNA binding and a regulatory domain, which serves to either enhance or suppress transcription. The looping of DNA can facilitate interactions between these regulatory domains and the transcription complex, thereby leading to either the promotion or inhibition of transcriptional activity. Numerous families of transcription factors exist, categorized according to the nature of their DNA-binding domains, such as the homeodomain or zinc-finger domain (Fulton et al., 2009). Predominantly, these factors are localized within the nucleus, although certain transcription factors reside in the cytoplasm until activated, at which point they translocate to the nucleus. Activation frequently transpires in response to intracellular signalling mechanisms (Figure 1.10). A specific category of transcription factors, known as the nuclear receptor family, is directly activated by lipophilic signalling molecules, including retinoic acid or glucocorticoids. Each distinct type of DNA-binding domain within a protein corresponds to a specific target sequence in the DNA, generally comprising 20 nucleotides or fewer. The activation domains of transcription factors are often considered by an elevated concentration of acidic amino acids, forming what is referred to as an ‘acid blob’, which facilitates the assembly of the general transcription complex. Transcription factors exhibit a preferential binding affinity for specific DNA sequences that may exceed 1,000-fold relative to non-target sequences (Damante et al., 1994). Given that transcription factors can impede the DNA-binding sites of proteins (for instance, lac, the classical lambda and trp repressors (Ptashne, 2011), the capacity to bind to specific DNA sequences is frequently regarded as an indicator of the potential to regulate transcription. Many transcription factors function as “master regulators” and “selector genes,” exerting regulatory influence over cellular processes that determine cell identity and developmental patterns (Lee & Young, 2013), while also modulating specific pathways,

including immune responses (Singh et al., 2014). Certain transcription factors engage histone acetylases, which modify chromatin structure by neutralizing amino groups on histones through acetylation, thereby facilitating the accessibility of other proteins to the DNA. Although transcription factors are conventionally classified as activators or repressors of transcription, their functionality is also context-dependent, with the presence of other factors occasionally enabling an activator to behave as a repressor, or vice versa. In experimental settings, transcription factors can induce cellular differentiation (Fong & Tapscott, 2013) and can also promote trans-differentiation and de-differentiation processes (Takahashi & Yamanaka, 2016). A comprehensive functional understanding of these proteins necessitates an in-depth knowledge of the DNA sequences they associate with. The binding specificities of transcription factors are often encapsulated in the concept of "motifs"models that delineate the set of related, short sequences that a given transcription factor preferentially binds, which can subsequently be employed using screen longer sequences like, promoters to pinpoint potential binding sites. The DNA-binding motif identification is frequently regarded as the preliminary stage in the thorough investigation of a transcription factor's function, as elucidating potential binding sites opens avenues for further analytical exploration.

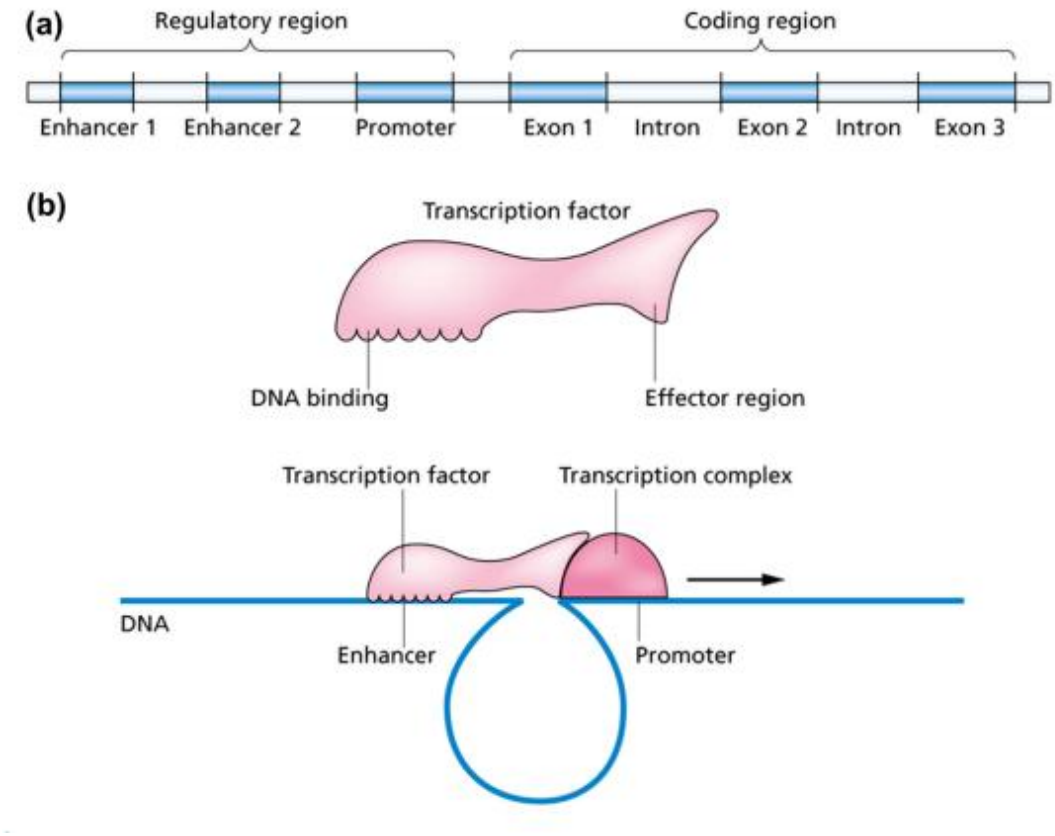

Figure 1.10: Structure and Regulation of a typical gene.

A. *Structure of typical gene- This panel illustrates the organization of a eukaryotic gene, highlighting its regulatory and coding regions. The regulatory region, located upstream of the coding region, includes two enhancers 1 and 2 and a promoter. The coding region consists of Exons 1,2 and 3, which are segments of DNA that will be transcribed and translated into protein, and introns, which are non-coding sequences that will be spliced out of the mature mRNA before translation.* ***B.*** *Operation of transcription factor. This panel demonstrates the working by which a transcription factor controls gene expression A transcription factor, shown in pink, contains two key functional domains: the DNA binding domain which permits the transcription factor to specifically fix to an enhancer sequence on the DNA and the effector region interacts with the transcription complex, which includes RNA polymerase and other proteins, to activate transcription. The DNA is depicted looping to bring the enhancer-bound transcription factor into close proximity with the promoter- bound transcription complex, facilitating the activation of gene expression. An arrow indicates the direction of transcription, starting from the*

promoter and proceeding downstream through the coding region. This looping mechanism illustrates how distant regulatory elements like enhancers can influence gene expression by interacting with the promoter through protein-protein interactions mediated by transcription factors (Slack and Dale, 2021).

Among the various transcription factors that govern epithelial cell fate and differentiation, ELF5 (E74-like factor 5) has emerged as a critical controller of epithelial lineage specification. Being the member of the E-twenty-six (ETS) transcription factor family, ELF5 is predominantly articulated in epithelial tissues and plays crucial roles in maintaining tissue homeostasis, especially in organs such as the salivary gland, lung, and mammary gland (Oakes et al., 2008). It functions by modulating the expression of genes involved in differentiation, immune signalling and cell proliferation. Notably, ELF5 has been associated in the regulation of epithelial mesenchymal transition (EMT) and has shown situation-dependent roles in cancer-acting either as an oncogene tumour suppressor relying on tissue type and molecular environment (Kalyuga et al., 2012). Although its functions have been extensively explored in breast and prostate cancers, its precise role in cutaneous epithelial biology and squamous cell carcinoma remains less defined, making it a compelling target for further investigation.

1.3.1 ELF5-(E74 LIKE TRANSCRIPTION FACTOR)

The Ets family is considered large as it comprises of 26 distinct members that possess diverse spatial-temporal and tissue-specific expression patterns, some of which may overlap (Sharrocks, 2001). Ets proteins function as transcriptional activators as well as repressors, thereby regulating the genes expression. This regulatory mechanism is acquired via the binding of such proteins to their specific recognition sites in the regulatory regions of target genes. This binding is facilitated by an 85 amino acid segment known as the ETS domain, which is a conserved DNA binding domain that serves as a distinctive motif for this family. Furthermore, the Ets family of proteins can be further categorized based on the similarities in the sequence

of the ETS domain, as well as the presence of other conserved domains, such as the Pointed domain, which plays a role in protein-protein interactions. In certain cases, there can be similarities within a specific subfamily of Ets proteins in terms of molecular functions, biological functions and expression profiles, as exemplified by the Epithelium Specific Ets (ESE) subfamily. This Ets domain recognizes core elements of GGAA/T present in promoter/enhancer regions of downstream target genes. There are multiple studies which indicate that Ets factors regulates the embryonic development, cellular proliferation, differentiation, haematopoiesis, apoptosis, angiogenesis and oncogenesis (Sementchenko & Watson, 2000). Transcription factors that belong to the Ets family have a significant role in the process of normal growth and development primarily by influencing various cellular processes, such as morphogenesis, proliferation, and differentiation (Sharrocks et al., 1997).

In addition, ESE transcription factors are categorized within a subset of the Ets family. These transcription factors share a high degree of sequence similarity and are predominantly expressed in epithelial cells across a variety of tissues and organs (Feldman et al., 2003). The ESE (epithelial-specific Ets) family primarily includes three key members: ESE-1 (also known as Elf3 in mice), ESE-2 (Elf5), and ESE-3 (Ehf) (Bochert et al., 1998; Choi et al., 1998; Oettgen et al., 1997; Oettgen et al., 1999; Zhou et al., 1998). Even though PDEF (Prostate-Derived Ets Factor), another epithelial-expressed transcription factor within the Ets family, is often grouped with the ESE proteins, notable differences in the amino acid composition of its ETS domain suggest it is not closely related to this subgroup (Oettgen et al., 2000). Considerable advancements have been made in understanding the biological functions of the ESE subfamily. Research involving cell lines and genetically modified animal models has shown that ESE factors are vital regulators of epithelial cell development and differentiation (Neve et al., 1998; Ng et al., 2002; Yoshida et al., 2000). The prevalence of epithelial cells across various organs and tissues, along with their status as a major cell population, suggests potential novel sites for

the expression of ESE proteins and the existence of yet-to-be-discovered unique functions. Although research into the biological roles of ESE proteins in different epithelial cell types and their downstream targets is still in its early stages, the mechanisms governing their cell-type-specific expression remain poorly understood. This gap in knowledge is particularly important, as abnormal regulation of critical transcription factors such as members of the Ets family can interfere with normal epithelial cell differentiation and is commonly linked to the development of cancers originating from epithelial tissues (Sharrocks, 2001).

The expression of Elf5 in various mouse tissues is not widespread but rather limited to a specific subset of organs that have a substantial presence of epithelial cells. These organs primarily consist of glandular or secretory tissues, such as the kidney, salivary gland, and mammary gland (Lapinskas et al., 2004). The Ahmed group has shown that miR-148a can regulate stem/progenitor cell population in skin and hair in part by regulating Elf5 expression (Pickup et al., 2023). Furthermore, we have identified Elf5 as a novel transcriptional regulator in skin and HF development/regeneration (Hu et al., 2024,). Additionally, Elf5 is predominantly related with the differentiated state of keratinocytes (Oettgen et al., 1999; Tummala & Sinha, 2006).

1.3.2 ELF5-MEDIATED TRANSCRIPTION REGULATION

Elf5 has been identified as a key regulator of cell fate decisions in stem and progenitor cells, influencing the expression of target genes such as *Gata3* and components of the BMP and Notch signalling pathways (Piggin et al., 2016; Grassmeyer et al., 2017; Chakrabarti et al., 2012), which are central to controlling cell proliferation and differentiation during epithelial tissue development, including in organs like the kidney (Grassmeyer et al., 2017) and mammary gland (Chakrabarti et al., 2012; Ahmed et al., 2016). Notably, Elf5 expression is highly restricted to the extraembryonic ectoderm, an essential structure for mammalian placental development and embryonic survival within the uterus (Donnison et al., 2005).

Studies involving complete loss of Elf5 in mice have clearly demonstrated that homozygous knockout embryos die at an early embryonic stage, accompanied by defects in extraembryonic ectoderm formation (Donnison et al., 2005; Zhou et al., 2005). Importantly, Elf5 expression is significantly upregulated during pregnancy and is localized to luminal epithelial cells of the mammary gland. Female mice heterozygous for Elf5 exhibit strain-dependent abnormalities in mammary alveolar development (Zhou et al., 2005). Additionally, Elf5 functions as a key regulator of mammary stem cells (SCs) and acts as a suppressor of epithelial-to-mesenchymal transition (EMT) and metastasis in breast cancer (Chakrabarti et al., 2012). Overexpression of Elf5 in mammary epithelial cells lacking the prolactin receptor (PrlR) has been shown to rescue defects in alveolar development (Harris et al., 2006). Collectively, these findings underscore Elf5's pivotal role in epithelial development and highlight its integration within major signalling pathways that govern cellular differentiation and morphogenesis.

Given the emerging importance of transcription factors like ELF5 in regulating epithelial identity and potentially modulating tumorigenic processes in squamous cell carcinoma, functional studies are essential to unravel their precise roles. Traditional gene expression studies often fall short in delineating gene function with precision and specificity. In this context, the advent of CRISPR-Cas9 genome editing technology has revolutionized functional genomics by enabling targeted, efficient, and heritable gene modifications. CRISPR provides a powerful platform to investigate gene function by allowing loss-of-function or gain-of-function experiments with high accuracy. By leveraging this system, the current study employs CRISPR to dissect the role of ELF5 in cutaneous epithelial cells, offering novel insights into its involvement in cellular pathways that may contribute to squamous cell carcinoma development or suppression. This approach not only enhances the mechanistic understanding of ELF5 but also exemplifies the utility of CRISPR as a tool in cancer biology research.

1.4 CLUSTERED REGULARLY INTERSPACED SHORT PALINDROMIC REPEATS (CRISPR)

Gene editing is an advanced biotechnology that enables precise modifications to the genome, including insertions, deletions, or single-base changes (Jiang et al., 2020). The development of gene-editing tools has progressed through three major generations: the first utilized zinc-finger nucleases (ZFNs), followed by the second generation featuring transcription activator-like effector nucleases (TALENs), and most recently, the widely adopted third generation involves CRISPR (clustered regularly interspaced short palindromic repeats) in combination with the Cas9 (CRISPR-associated protein 9) enzyme (Gaj et al., 2023). Unlike ZFNs and TALENs, which rely on engineered proteins to recognize specific DNA sequences, CRISPR-Cas9 uses a short, customizable guide RNA to direct the Cas9 enzyme to specific genomic sites, greatly improving editing precision and expanding the range of gene-editing applications (Hsu et al., 2014). The native Cas9 enzyme functions by creating double-strand breaks (DSBs) in DNA, which are subsequently repaired by the cell through homology-directed repair (HDR) or nonhomologous end joining (NHEJ) (Wu et al., 2025; Fu et al., 2021; Ran et al., 2013). While disrupting a single harmful gene may be effective in some cases, this approach alone is insufficient for addressing complex diseases involving multiple genetic factors (Landrum et al., 2016). To enhance the functionality of Cas9, researchers have investigated its structural and biochemical properties, leading to the development of modified versions such as catalytically inactive Cas9 (dCas9). By fusing dCas9 with regulatory domains like transcriptional activators (e.g., VP64) or repressors (e.g., KRAB), scientists can modulate gene expression with high specificity without inducing DNA cleavage. Figure 1.11 presents a schematic of widely used dCas9-based gene regulation systems (Li et al., 2023). Additional innovations include engineering Cas9 for single-base editing via cytosine base editors (CBEs), adenine base editors (ABEs), and prime editors (PEs). These adaptations provide Cas9 with

new capabilities, allowing it to precisely regulate gene function and edit the genome without introducing double-strand breaks.

The CRISPR/Cas protein family is systematically categorized into two distinct classes predicated upon genomic and protein structural properties, with the extensively characterized protein Cas9 classified within the Class II CRISPR/Cas systems (Haft et al., 2005; Makarova, 2011). Class I is characterized by a substantial Cas9 protein complex that facilitates the cleavage of DNA strands, whereas Class II is defined by the necessity of merely a singular cleavage protein. Cas9 is notably identified by the presence of two ribonuclease structural domains: a RuvC-like nuclease domain located proximally to the amino terminus and the HNH nuclease domain positioned centrally within the protein, both of which are intrinsically capable of cleaving DNA strands (Nishimashu et al., 2014). Of significant importance, protospacer sequences are not assimilated arbitrarily from external sources; rather, they are invariably associated with a guanine-rich sequence referred to as protospacer-adjacent motifs (PAMs) (Deveau et al., 2008). Subsequent research has elucidated that PAM sequences are instrumental in the acquisition of the spacer region, wherein the Cas proteins perform cleavage (Hsu et al., 2014; Doudna & Charpentier, 2014; Wright et al, 2016). The CRISPR/Cas9 system is a key element of adaptive immunity in archaea and bacteria, where it functions to eliminate invading genetic material such as plasmids and bacteriophages (Barrangou et al., 2007). Within the bacterial genome, the CRISPR locus contains segments of foreign DNA acquired during previous infections or external exposures. Upon subsequent invasions, this locus is transcribed into a long precursor RNA, which is processed into shorter guide RNAs by the CRISPR-associated (Cas) protein complex. These guide RNAs, together with Cas proteins, recognize and cleave foreign DNA sequences referred to as protospacers that match the stored spacer sequences.

A critical requirement for this recognition is the presence of a short DNA sequence known as the protospacer adjacent motif (PAM), which varies in length and sequence among bacterial species (Makarova et al., 2015). The PAM ensures that only foreign DNA is targeted, preventing accidental cleavage of the host's own CRISPR sequences. CRISPR/Cas systems are classified into five major types, each with distinct evolutionary origins and mechanisms of action (Makarova et al., 2015). Under natural conditions, activation of the Cas9 nuclease requires two distinct RNA molecules: the CRISPR RNA (crRNA), which contains the guide sequence derived from the viral DNA, and the trans-activating crRNA (tracrRNA), which assists in crRNA processing and Cas9 activity (Wright et al., 2016). For genome-editing applications, these two RNAs are often fused into a single synthetic molecule called a single-guide RNA (sgRNA). This chimeric RNA consists of a 19-20 nucleotide region complementary to the DNA target and incorporates both crRNA and tracrRNA functionalities, typically ranging from 100 to 250 base pairs in length.

For Cas9 to effectively bind and cleave DNA, a three-nucleotide PAM sequence (NGG) must be located immediately downstream of the target site on the 3′ end. Once bound to the matching DNA sequence, the Cas9-sgRNA complex introduces a double-strand break precisely three nucleotides upstream of the PAM site, resulting in blunt-ended DNA cleavage (Wright et al., 2016).

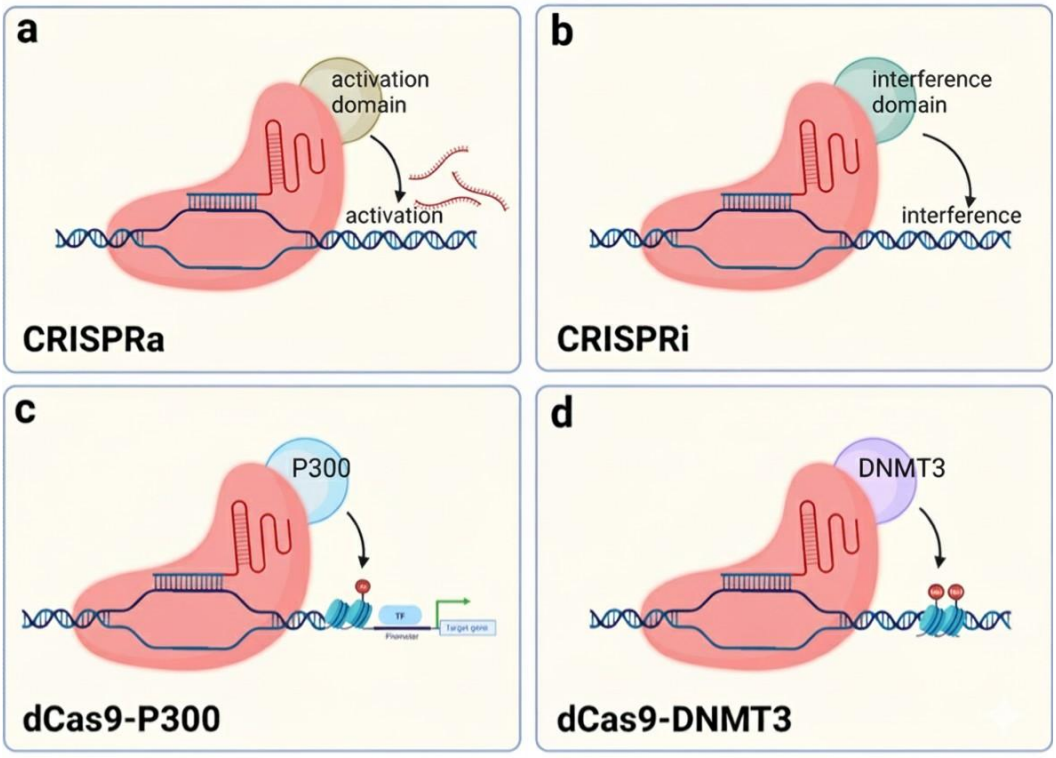

Figure 1.11: Schematic diagram of dCas9-based tools to regulate expression.

A. *CRISPR activation (CRISPRa): dCas9 is fused to a transcriptional activation domain (e.g., VP64, p65, or VPR), enabling recruitment of the transcriptional machinery to promoter or enhancer regions, thereby inducing upregulation of target gene expression.* ***B.*** *CRISPR interference (CRISPRi): dCas9 is coupled with a repressor domain (e.g., KRAB), which suppresses transcription by obstructing RNA polymerase binding or recruiting chromatin-modifying complexes, resulting in gene silencing without DNA cleavage.* ***C****. dCas9-p300: A fusion of dCas9 with the histone acetyltransferase domain of p300, enabling epigenetic activation of gene expression by promoting histone acetylation at target loci, particularly at enhancers or promoters.* ***D.*** *dCas9-DNMT3: A construct linking dCas9 to DNA methyltransferase 3A (DNMT3A), which facilitates site-specific DNA methylation, leading to transcriptional repression through epigenetic gene silencing mechanisms. Together, these tools enable precise, programmable, and locus-specific control of gene expression, either through direct transcriptional modulation or epigenetic modification, without introducing DNA breaks (Li et al., 2023).*

Building on the investigation of ELF5 using CRISPR, two key molecular targets-GATA-3 and FLI-1 were identified as being significantly affected by its modulation. Their altered expression highlights potential downstream effects of ELF5 activity in keratinocytes and supports a broader regulatory role relevant to squamous cell carcinoma. Including these targets in the study provides deeper insight into the transcriptional networks influenced by ELF5 and strengthens the functional link between transcription factor dynamics and skin cancer progression.

1.5 GATA-3

GATA-3 is a member of the GATA family of zinc finger transcription factors, which comprises six proteins (GATA-1 through GATA-6). These factors are named for their ability to recognize and bind the specific DNA sequence "GATA" found in the promoter or enhancer regions of target genes. GATA-3 is categorized as a type II GATA factor and is primarily expressed in epithelial and hematopoietic tissues (Patient & McGhee, 2002).

GATA-3 was initially discovered through a screen targeting GATA transcription factors within the T cell lineage (Ho et al., 1991). It is expressed in both hematopoietic and non-hematopoietic tissues and plays a crucial role in early T cell development, particularly in the differentiation of the Th2 subset of T cells (Ho, I-Cheng Tai and Pai, 2009). Beyond the immune system, GATA-3 is also essential for the development of multiple organ systems in both humans and mice. Notably, it is a key regulator in the formation and maintenance of the mammary epithelium, where it stands out as the most abundantly expressed transcription factor in the luminal epithelial cells of the mammary ductal system (Asselin-Labat et al., 2007; Kouros-Mehr et al., 2006). During development, GATA-3 plays a critical role in branching morphogenesis and the differentiation of luminal epithelial cells. In adult mice, conditional deletion of GATA-3 leads to the loss of luminal cell identity, along with increased cellular proliferation, decreased adhesion, and reduced apoptosis. Additionally, GATA-3 contributes

to the regulation of noradrenaline levels during development by upregulating the enzyme dopamine β-hydroxylase (Lim et al., 2000), and in the kidney, it helps prevent the formation of ectopic metanephric ducts (Grote et al., 2008).

GATA-3 is also essential for skin and hair follicle development. In the epidermis, epithelial cells differentiate in an upward trajectory to form distinct hair follicle lineages such as the medulla, cortex, cuticle, and the inner root sheath (IRS) (Fuchs, 2007). GATA-3 specifically promotes the differentiation of IRS cells, and targeted disruption of the *Gata3* allele via lacZ knock-in leads to an accumulation of IRS precursors and a deficiency in fully differentiated IRS cells (Kaufman et al., 2003). Conditional knockout mice lacking GATA-3 show delayed hair growth, disorganized follicular structure, and abnormal epidermal differentiation. These mice also display dry, fragile skin, which compromises the epidermal barrier, and exhibit increased proliferation of basal epidermal cells, despite lacking fur (de Guzman Strong et al., 2006; Kurek et al., 2007).

In the context of breast cancer, GATA-3 expression is strongly associated with estrogen receptor (ER) positivity in both cancer cell lines and primary tumours (Hoch et al., 1999). Low or absent GATA-3 expression is linked to poorer prognosis, including shorter survival, more aggressive histological features, lymph node involvement, larger tumour size, absence of progesterone receptor expression, and overexpression of HER2/ERBB2, a marker of aggressive breast cancer (Mehra et al., 2005).

1.6 FRIEND LEUKAEMIA (FLI-1)

Friend leukaemia integration 1 (FLI-1) is a significant member of the ETS family of transcription factors and is classified as a proto-oncogene due to its aberrant activation being linked to the development of erythroleukemia (Wang et al., 2018). In humans and mice, the *FLI1* gene is located on chromosome 11q23 and chromosome 9, respectively. It encodes two

protein isoforms p51 (452 amino acids) and p48 (419 amino acids) (Truong and Ben-David, 2000). The human *FLI1* gene spans approximately 120 kb and contains nine exons (Selleri et al., 1994). Under physiological conditions, FLI-1 functions as a regulator of haematopoiesis and angiogenesis, with particularly high expression levels found in hematopoietic stem cells and vascular endothelial cells (Zhao et al., 2018; Mazzotta et al., 2021; Hemida and Holah, 2022). It plays a regulatory role in the expression of several essential genes, including GATA-1, GATA-2, FOG-1, VEGF, SCA-1, and RUNX1, which are involved in blood cell differentiation and vascular function (Vecchiarelli-Federico et al., 2017).

FLI-1 is also active in lymphocyte development, with its expression significantly increasing in prethymic T-cell progenitors and continuing through T-cell maturation (Li et al., 2015). Overexpression of FLI-1 suppresses genes involved in erythroid differentiation, thereby hindering red blood cell maturation (Vecchiarelli-Federico et al., 2017). In endothelial cells, it upregulates GATA-2, Flk-1, and LMO2, while activating p53, which in turn suppresses Bcl-2, a key anti-apoptotic protein ultimately promoting apoptosis (De Val and Black, 2009).

In the context of cancer, FLI-1 is involved in several critical processes, including cell growth, proliferation, differentiation, and apoptosis, through its binding to promoter or enhancer regions of specific genes (Sakurai et al., 2007; Li et al., 2013). Given its diverse roles in tumour initiation, progression, and prognosis, FLI-1 is considered a biomarker and a promising therapeutic target (Wang et al., 2021). Its expression has been detected in a range of solid tumours and hematologic malignancies, such as breast cancer, Merkel cell carcinoma, small cell lung cancer, squamous cell carcinoma, bladder cancer, non-Hodgkin's lymphoma, olfactory neuroblastoma, Ewing sarcoma, erythroleukemia, and multiple myeloma (Harkness and McCluggage, 2020; Stephen et al., 2021; Yan et al., 2018).

In breast cancer, FLI-1 has shown a dual role. While some evidence suggests its upregulation suppresses tumour growth, invasion, and metastasis, supported by findings that FLI-1-deficient mice are more susceptible to breast tumour development (Scheiber et al., 2014), other studies indicate an oncogenic role, where FLI-1 overexpression enhances the proliferation and metastatic capacity of breast cancer cells (Stephen et al., 2021; Chen et al., 2018). These contrasting findings suggest that FLI-1 may function as both a tumour suppressor and proto-oncogene in a context-dependent manner.

1.7 AIM

ELF5 is predominantly expressed in epithelial cells and functions as a key transcriptional regulator of cell fate in stem and progenitor cells. It exerts its effects by modulating critical signalling pathways such as BMP and Notch (Metzger, Stahlman and Shannon, 2008; Piggin et al., 2016; Grassmeyer et al., 2017; Wei et al., 2012), which are essential for controlling cell proliferation and differentiation during the development of epithelial tissues, including the kidney (Grassmeyer et al., 2017), mammary gland (Ahmed et al., 2016), and lung (Metzger, Stahlman & Shannon, 2008). In the skin, our findings demonstrate that Elf5 is a direct target of miR-148a and plays a vital role in regulating stem/progenitor cell behaviour. Additionally, Elf5 is required for the proper growth and maturation of keratinocytes in mouse models (Pickup et al., 2023; Hu et al., 2025).

In various epithelial cancers, ELF5 has been associated in the regulation of genes involved in cell growth, differentiation, programmed cell death, and the suppression of metastasis (Piggin et al., 2016; Chakrabarti et al., 2012; Singh et al., 2020; Yao et al., 2015), supporting its act as a tumour suppressor across multiple cancer types. Nevertheless, the potential protective role of ELF5 in the initiation and progression of cutaneous squamous cell carcinoma (cSCC) has not yet been established.

The aim was to identify ELF5 role as a potential anti-tumour suppressor role in preventing malignant transformation of keratinocyte and development.

HYPOTHESIS:

ELF5 acts as a tumour suppressive transcription factor in keratinocytes by regulating key genes and signalling pathways that control proliferation, differentiation and stem/progenitor cell behaviour. Loss or downregulation of ELF5 disrupts these processes and promotes the initiation and progression of cutaneous squamous cell carcinoma (cSCC).

OBJECTIVES:

1. To characterise the expression pattern and relevance of ELF5 in normal and malignant keratinocytes.
2. To determine the functional impact of ELF5 in regulating key keratinocyte behaviours (migration, proliferation and differentiation) associated with tumour initiation and progression.
3. To identify and validate novel transcriptional gene targets and regulatory pathways controlled by ELF5 in keratinocytes.
4. To evaluate the functional impact of ELF5 *via* gene targets in regulating keratinocyte behaviour (migration, proliferation and differentiation) and tumourigenicity potential after loss of ELF5.

CHAPTER

2.0 METHODS

2.1 HUMAN TISSUE

Biopsy samples of healthy human skin and cutaneous squamous cell carcinoma (cSCC) were collected from donors aged 42 to 78 years who were undergoing either facial cosmetic surgery or lesion excision. All tissue samples were obtained with informed written consent, in compliance with the principles outlined in the Declaration of Helsinki, and with approval from relevant ethics committees in accordance with Human Tissue Act regulations from Nottingham Trent University. Human skin tissues were analysed to ensure that experimental findings derived from in vitro models were biologically relevant. The use of human tissue enables validation of ELF5 and target gene expression within native epidermal architecture and disease context, which is essential for translational relevance in cSCC research (Rittié & Fisher, 2015; Pickup et al., 2023).

2.2 IMMUNOHISTOCHEMISTRY (IHC)

Immunohistochemistry was employed to localise protein expression within specific epidermal layers and tumour regions while preserving tissue architecture (Taylor & Levenson, 2006). Human skin cryosections, 10 µm thick, were fixed using 4% paraformaldehyde for 10 minutes at room temperature. After fixation, sections were rinsed and blocked for 1 hour at room temperature in a blocking solution containing 0.2% Triton X-100 in PBS, 5% fetal calf serum, 2% bovine serum albumin, and 10% normal goat and/or donkey serum (Merck, UK). Samples were then incubated overnight at 4 °C with primary antibodies targeting ELF5 and KRT1 (Appendix Table 7.4). The following day, the sections were incubated for 1 hour at room temperature with appropriate Alexa Fluor 488 (green) or Alexa Fluor A555 (red) secondary antibodies (Appendix Table 7.4). All antibody incubation steps were followed by washes in 0.2% Triton X-100/PBS.

For paraffin-embedded cSCC tissue sections of10 µm fixed in 10% formalin, samples were first deparaffinized and then rehydrated through sequential treatments with Histoclear II (3 × 5 minutes), followed by descending ethanol gradients: 100% ethanol (2 × 10 minutes), 95% ethanol (2 × 10 minutes), 70% ethanol (2 × 10 minutes), and 50% ethanol (2 × 10 minutes), and finally rinsed in deionized water (2 × 5 minutes) at room temperature. Antigen retrieval was performed by boiling the sections in Tris-EDTA buffer (pH 9.0) for 1 hour. After cooling to room temperature (approximately 1 hour), slides were washed with TBST (3 × 5 minutes), treated with 0.1% Triton X-100 in TBS for 10 minutes, and again washed in TBST (3 × 5 minutes). Blocking was performed using a solution of 0.2% Triton X-100/PBS, 5% fetal bovine serum, 2% bovine serum albumin, and 10% normal goat or donkey serum for 1 hour at room temperature. Sections were then incubated overnight at 4 °C with primary antibodies against ELF5 and Cytokeratin 1 (KRT1) (Appendix Table 7.4). The next day, slides were treated with corresponding Alexa Fluor 488 or Alexa Fluor A555 secondary antibodies for 1 hour at room temperature. Each incubation step was followed by washes with 0.2% Triton X-100/PBS. Finally, the tissue sections were mounted with DAPI-containing medium for nuclear staining, and images were acquired using the Leica THUNDER Imager 3D Cell Culture system (Leica, Germany).

2.3 TISSUE CULTURE

2.3.1 CELL CULTURE

In vitro culture of keratinocytes provided a controlled system to study ELF5 function in proliferation, differentiation, and tumour-associated behaviours. Cell culture models are widely used to dissect molecular mechanisms underlying epithelial homeostasis and carcinogenesis (Freshney, 2010). Under sterile handling techniques, cell culture experiments were performed in a laminar flow hood. Cell culture of immortalised human keratinocytes (HaCaT; 300493, 2B Scientific), A431 (CRL-1555, ATCC) were cultured in complete growth media DMEM

(Fisher UK) and SCC-9 (89062003-1VL, Merck, UK) were cultured in DMEM-F12 (Fisher UK) respectively. The medium was supplemented with 10% heat-inactivated fetal bovine serum (Fisher, UK), 100 U/ml penicillin, 100 µg/ml streptomycin, and 2 mM L-glutamine (all from Fisher, UK), along with hydrocortisone and sodium pyruvate for SCC-9 cells and maintained in a humidified incubator at 37 °C with 5% CO_2.

2.3.2 MAINTENANCE AND PASSAGING OF CELLS

Once the cultures reached approximately 70-80% confluency, the culture medium was carefully aspirated to ensure minimal disturbance to the cell monolayer.; the cells underwent a single wash with pre-warmed dPBS to eliminate any residual media components and were subsequently passaged via trypsinization employing 0.25 % Trypsin-EDTA for a duration of 10 minutes at 37°C. For deactivation of 0.25 % Trypsin-EDTA 4 mL of complete growth media were added. The cell suspension was centrifuged at 300 × g for 5 minutes, after which the resulting pellet was resuspended in fresh complete growth medium. The cells were then seeded according to the specific requirements of the experiment.

2.3.3 CELL COUNTING

Following the steps of trypsinization and centrifugation, the cells were resuspended in fresh culture media and 20 ul of cell suspension media was mixed with 20 ul Tryphan blue stain. The cell count was determined utilizing a cell counting chamber -hemacytometer, 10ul of mixture was added to the slide and placed into automated cell counter (BioRad- TC20) and the viable cells were considered for the experimental requirements, employing the following equation—

Cells/mL= Average cell count x 10^4 x dilution factor

$$\text{Volume of cells (mL)} = \frac{\text{Required cell number}}{\text{Cell concentration}}$$

2.3.4 CRYOPRESERVATION

For preservation purposes, cells were cultured and collected in T75 flasks as previously described, then centrifuged at 300 × g for 5 minutes to form a pellet. The pellets were subsequently resuspended in either 1 mL or 500 µL of Cryo-SFM (Merck, UK), transferred into cryovials, and initially stored at -80°C. Working cell stocks were kept at -80°C, while vials intended for long-term storage were pre-cooled at -80°C before being transferred to liquid nitrogen for extended preservation.

2.3.5 MYCOPLASMA SCREENING

Mycoplasma contamination was routinely assessed using the EZ-PCR Mycoplasma Test Kit (Sartorius, #20-700 20), following the manufacturer's instructions to ensure experimental validity, as mycoplasma contamination can alter gene expression, metabolism, and cell-cycle progression, leading to unreliable results (Young et al., 2010). To begin, 1 mL of culture medium was centrifuged at 300 × g for 5 minutes to eliminate cellular debris. The supernatant was then transferred to a sterile tube and centrifuged at 15,000 × g for 10 minutes to pellet any mycoplasma. The resulting pellet was resuspended in 50 µL of buffer solution, heated at 95°C for 3 minutes, and then stored at -20°C until further analysis.

For PCR setup, the reaction mixture included 2 µL of the sample, 2 µL of internal control primer mix, 0.5 µL of internal control DNA template, 4 µL of reaction mix, and was topped up with nuclease-free water to a final volume of 20 µL. PCR amplification was carried out along with positive and negative controls, using the thermal cycling conditions specified in Table 1.

Table 1. Mycoplasma test amplification cycle:

Cycles	Temperature (°C)	Time (s)
1x	94	60
35x	94	30
	60	120
	72	60
1x	94	30
	60	120
	72	300

A 2% (w/v) agarose gel was prepared using 100 mL of TAE buffer (containing 2 M Tris-HCl at pH 8.0, 1 M acetic acid, and 50 mM EDTA) and supplemented with 5 µL of SYBR™ Safe dye (Fisher, UK) for DNA visualization. PCR products were loaded onto the gel along with a 100 bp DNA ladder, and electrophoresis was carried out at 100 V for 45 minutes. DNA bands were subsequently visualized using the iBright Imager (Model A32752). An illustrative result from the experiment is shown below. (Figure 2.1).

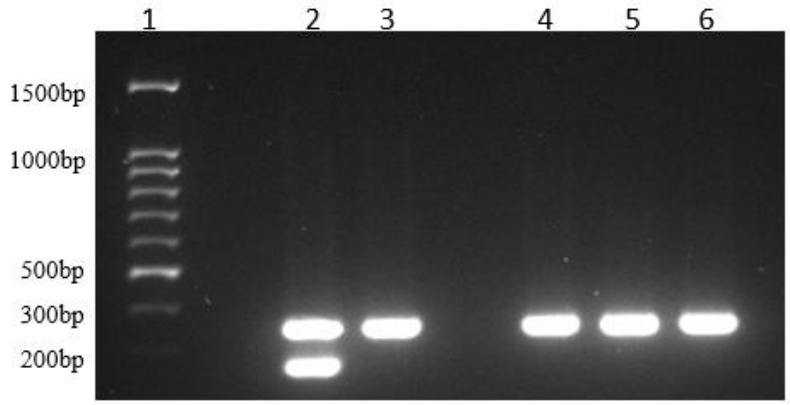

Figure 2.1: Mycoplasma screening.

HaCaT cells (lane 4), A431 cells (lane 5), SCC-9 cells (lane 6), and the negative control (lane 3) all display a single band at approximately 357 bp, corresponding to the amplification of the internal DNA template. In contrast, the positive control (lane 2) shows an additional band at ~250 bp, indicating the

presence of mycoplasma DNA. A DirectLoad™ 100 bp DNA ladder (Merck, UK) was used as a molecular size reference.

2.4 IMMUNOCYTOCHEMISTRY (ICC)

For immunocytochemistry, cells were seeded onto coverslips placed in 6-well plates. Once cultures reached 70–80% confluency, the culture medium was removed, and cells were fixed with 4% paraformaldehyde for 10 minutes at room temperature. After fixation, cells were rinsed with wash buffer (0.2% Triton X-100 in PBS) and then treated with a permeabilization buffer of the same composition for 15 minutes at room temperature. A blocking solution containing 0.2% Triton X-100 in PBS, 5% fetal calf serum, 2% bovine serum albumin, and 10% normal goat and/or donkey serum (Merck, UK) was added to each well and incubated for 1 hour at room temperature. This was followed by two brief rinses and two 5-minute washes with wash buffer. Cells were then incubated overnight at 4°C with primary antibodies against ELF5 (Appendix Table 7.4). On the following day, cells were incubated for 1 hour at room temperature with the appropriate Alexa Fluor A488-conjugated secondary antibodies (Appendix Table 7.4). Each antibody incubation step was followed by washes using 0.2% Triton X-100/PBS. Finally, cells were counterstained with DAPI-containing mounting medium, and imaging was performed using the Leica THUNDER Imager 3D Cell Culture system (Leica).

2.5 TRANSIENT TRANSFECTION OF CELLS

Transient transfection enabled short-term modulation of ELF5, GATA3, and FLI1 expression to assess immediate functional effects without permanent genomic alteration. This approach is widely used for mechanistic studies of transcriptional regulation (Kim & Eberwine, 2010). HaCaT, A431, and SCC-9 cell lines were maintained as outlined previously (Methods 2.3.1). Cells were transfected with either a control plasmid (pEGFP-N1, CloneTech, UK) or an Elf5 overexpression plasmid (pElf5-OE, RG231905, Insight Biotechnology, UK).

Transfections were performed using Lipofectamine 3000 (Fisher, UK) prepared in reduced-serum OPTI-MEM medium. Lipofectamine and OPTI-MEM were first mixed in a separate tube and incubated at room temperature for 5 minutes. This mixture was then combined with the OPTI-MEM containing the control or Elf5 plasmid, followed by an additional 15-minute incubation at room temperature before being applied to the cells. Cells were transfected in reduced-serum OPTI-MEM, with the transfection volume adjusted according to the plate format used (as detailed in Table 2). After initial incubation, the culture medium was removed, and cells were washed three times with dPBS. The transfection mixture was then added dropwise onto the cells and incubated for 4 hours. Following this incubation, the transfection solution was removed, cells were again rinsed with dPBS, and fresh complete growth medium was added. The cells were then cultured for an additional 48 hours, after which they were harvested for downstream analyses.

Table 2. Different size culture plates describing different volumes used for cell transfection

Plate Type	Lipofectamine 3000 (µl)	Plasmid (µg) pELF5 and pControl	OptiMEM (µl)
96 well	0.2	0.1	100
6 well	5	2.5	750
60 mm dish	10	5	1000

2.6 CALCIUM INDUCED KERATINOCYTE DIFFERENTIATION

Calcium-induced differentiation was used to model epidermal stratification in vitro. Elevation of extracellular calcium is a well-established method to induce keratinocyte differentiation and assess lineage commitment (Hennings et al., 1980; Watt, 1989). To induce calcium-mediated keratinocyte differentiation, the following cell lines were used: HaCaT CRISPR-Cas9-SC Control, HaCaT CRISPR-Cas9-SC ELF5-KO, HaCaT CRISPR-Cas9-SC KO + GATA3, and HaCaT CRISPR-Cas9-SC KO + Control RFP+. These cells were cultured in complete DMEM growth medium (Fisher, UK) supplemented with 10% chelated fetal bovine serum, 100 U/mL penicillin, 100 µg/mL streptomycin, and 2 mM L-glutamine (all from Fisher, UK), under

humidified conditions at 37°C with 5% CO_2. Cells were plated in triplicate in 6-well plates and incubated for three time points: 24, 48, and 72 hours. Differentiation was induced using a standard calcium-switch method, where media were supplemented with either low calcium (0.05 mM) or high calcium (1.8 mM) concentrations. Samples were harvested at each time point- 24 h, 48 h, and 72 and subsequently processed for further analysis.

2.7 TAQMAN ASSAY COPY NUMBER VARIATION ASSAY

TaqMan copy number assays were employed to quantify ELF5 genomic copy number due to their high specificity, sensitivity, and reproducibility for detecting gene dosage changes (Livak & Schmittgen, 2001). TaqMan Copy Number Assays was performed using TaqMan MGB probe kit (ThermoFisher, UK) following manufacturer instructions to determine copy number of ELF5 in HaCaT cell line. Genomic DNA (gDNA) was used as a target template for copy number assay. The kit consists of Mastermix (2X), TaqMan CNV (20X)-ELF5, TaqMan CNV reference (2X). A PCR reaction was created using copy number reference assays and copy number assays by gently vortexing and centrifuged briefly before plating in 96 well standard plate. The samples were plated in quadruplicates. gDNA (5 ng/ul) was added to each well in plates. The following are the details assigned targets, detectors, reporters (Table 3) to samples prior thermal cycling and the following are the thermal cycling conditions to run the plate on PCR instrument (Table 4). The results were exported for analysis to Copy Caller™ software. The result so obtained is shown in Figure 2.2

Table 3. List of assigned targets for copy number assay

Instrument	Detector name	Target name	Reporter	Quencher
FOR COPY NUMBER ASSAY				
QuantStudio 3 and 5 Real Time PCR systems	NA	User defined	FAM dye	MGB-NFQ
FOR COPY NUMBER REFERENCE ASSAY				
QuantStudio 3 and 5 Real Time PCR systems	NA	User defined	VIC dye	TAMRA probe

Table 4. Thermal cycle conditions for copy number assay

Step	Temperature	Time	Cycles
Initial denature/Enzyme activation	95°C	10 minutes	1
Denature	95°C	15 seconds	40
Anneal/Extend	60°C	60 seconds	

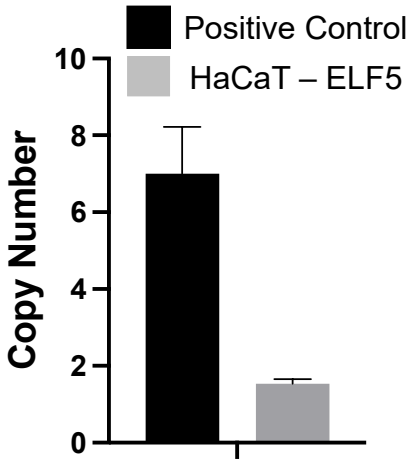

Figure 2.2: Copy Number Assay.

RT-qPCR determination for copy number in healthy keratinocytes HaCaT shows 2 copies of ELF5 alleles. n=3 technical experimental repeats.

2.8. LENTIVIRAL TRANSDUCTION

Lentiviral transduction was used to achieve stable gene delivery in keratinocytes, which are otherwise difficult to transfect efficiently. This method enables long-term gene modulation and is widely applied in functional genomic studies (Naldini, 2015).

2.8.1 PROPAGATION AND PASSAGING OF HEK293 CELLS

HEK293T cells were initially seeded in T75 flasks, and after 48 hours, when the cultures reached approximately 90% confluency, the cells were split and replated into 60 mm dishes at a density of 2.5×10^6 cells per plate in 14 mL of complete HEK293T medium. On the following day, the culture medium was replaced in preparation for transfection. HEK293T cells were maintained in DMEM (ThermoFisher, UK) supplemented with 10% heat-inactivated fetal bovine serum, 1% L-glutamine, and 5% non-essential amino acids (Fisher, UK), under standard conditions of 37°C and 5% CO_2, in line with previously established protocols (Pickup et al., 2023; Hu et al., 2025).

2.8.2 LENTIVIRAL-VIRUS PRODUCTION

For transfection, 1.5 mL of reduced serum OPTI-MEM media, 5 µg of lenti-plasmid with 6 µg packaging plasmid were pipetted and mixed gently, then 33 µL of TurboFectin transfection reagent was added to the diluted DNA at a confluence of 40 %, HEK293T cells were co-transfected with either DharmaconTM All-in-one system SMARTvector Non-targeting hCMV-TurboGFP (CRISPR-Cas9 Control, Horizon, UK), DharmaconTM All-in-one system SMARTvector Human Lentiviral shRNA ELF5 (CRISPR-Cas9 ELF5-KO, Horizon, UK), GATA-3 Lenti-ORF (Insight Biotechnology, UK), SMARTvector Human Lentiviral shRNA FLI-1 (Horizon, UK), along with a packaging plasmid, utilizing the TransLentiviral packaging kit (TLP5913, Horizon, UK) pipetted gently and incubate at room temperature for 15 minutes. The transfection solution was added dropwise directly to each well containing complete

growing media. The transfection mixture was gently swirled over the cells to ensure even distribution and then incubated at 37°C in a 5% CO_2 atmosphere. After 12–18 hours, the transfection medium was removed and replaced with fresh complete growth medium. Approximately 24 hours after the media change, the first batch of viral supernatant was collected from the culture dishes and stored at +4°C. Around 10 mL of fresh complete medium was then added to each dish.

A second batch of viral supernatant was collected 48 hours later, combined with the first batch, and used for lentiviral particle concentration. To concentrate the virus, 80 µg/mL polybrene (Fisher, UK) and 80 µg/mL chondroitin sulfate C (Merck, UK) were added. The pooled viral supernatants were then passed through a 0.45 µm filter to eliminate any cellular debris. The filtered solution was incubated for 16–20 hours on a shaker at 4°C, followed by centrifugation at 10,000 × g for 30 minutes at 4°C. The resulting lentiviral pellets were resuspended in 1/100th of the original volume using complete medium and stored at –80°C for future use.

2.8.3 QUANTIFICATION OF LENTIVIRAL-VIRUS

Lentiviral particle titration was carried out using a qPCR Lentivirus Titration Kit (NBS Biologicals, UK), following the manufacturer's instructions. To determine the viral particle concentration, the ABM qPCR Lentivirus Titre Kit (ABM, LV900) was used. Quantification was performed via RT-qPCR, employing the provided standard DNA to construct a standard curve for accurate titre calculation. The qPCR reaction mix included 1 µL of ROX reference dye and BlasTaq 2x qPCR Titre Master Mix. Serial dilutions of the test viral particles were prepared in dPBS, with dilution ratios of neat (undiluted), 1:10, 1:100, 1:1000, and 1:10,000. Standard control dilutions were generated by serially diluting 5 µL of standard control DNA into 45 µL of nuclease-free water at each step. The reaction setup and qPCR cycling conditions were applied as detailed in Table 5.

Table 5. Thermal cycle conditions for Lentiviral Titration

Steps	Temperature (°C)	Duration	Cycles
Enzyme Activation	95	3 mins	1
Denaturation	95	15 seconds	35
Annealing/Extension	60	1 min	

To generate the logarithmic regression curve, the Ct values obtained from the standard dilutions were plotted against their corresponding viral titres, resulting in a regression line. The titres of unknown viral samples were then determined by interpolating their Ct values onto the standard curve, using the equation: y = m 1n (x) + b, where *m* represents the slope of the curve, *y* is the Ct value, and *b* is the y-intercept.

2.8.4 ANTIBIOTIC KILL CURVE

Antibiotic kill curves were performed to determine the minimal concentration required for efficient selection of transduced cells while minimising cytotoxicity, ensuring consistent selection pressure (Davies & Davies, 2010). To determine the optimal concentration of the antibiotic an antibiotic kill curve was generated. Lentiviral sgRNA vectors of Edit-R All-in-one with the puromycin resistance gene enable cells to resist the effects of puromycin post-transduction. The optimal concentration range of puromycin for eliminating non-transduced cells was selected between 0 µg/mL to 10 µg/mL according to manufacturer's protocol. The HaCaT cells were cultured as described above (Methods 2.3.1) and seeded in 96 well plates, after 24 hours the selected antibiotic media was added to each well with chosen concentrations to each corresponding well. The antibiotic media was replaced every 2 days until the antibiotic kills all the non-transduced cells. After 9 days a lowest concentration of 0.5 µg/mL was selected due to its efficacy in killing cells for HaCaT. The antibiotic kill curve obtained is shown in Figure 2.3.

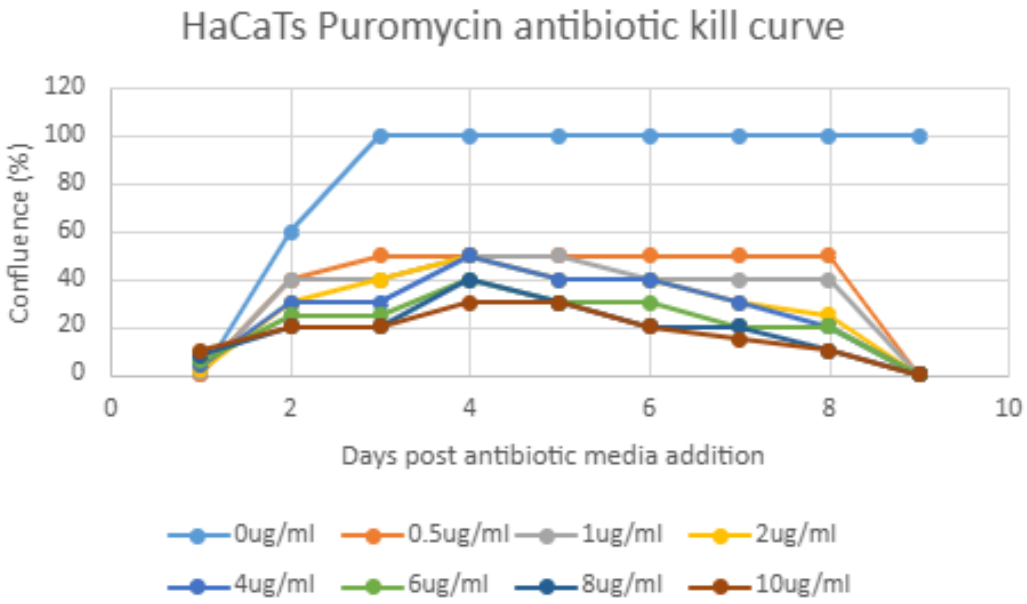

Figure 2.3: Puromycin kill curve for HaCaT cells over time.

HaCaT cells were treated with varying concentrations of puromycin (0-10 µg/mL), and cell confluence (%) was monitored over several days. A dose- and time-dependent decline in confluence was observed, with higher puromycin concentrations leading to more rapid and complete cell death. This analysis was used to determine the minimum puromycin concentration required to effectively eliminate non-resistant HaCaT cells. n=3 technical experiment groups per time point

2.8.5 CELL TRANSDUCTION FOR CRISPR-MEDIATED KERATINOCYTES

CRISPR-Cas9 mediated gene knockout was used to investigate the functional consequences of ELF5 loss in keratinocytes. This approach enables precise gene disruption and is widely used for studying gene function in epithelial systems (Doudna & Charpentier, 2014). HaCaT cells were maintained in DMEM supplemented with 10% fetal calf serum (FCS) and 2% penicillin/streptomycin and cultured at 37°C in a 5% CO_2 incubator. For CRISPR/Cas9-mediated gene editing, cells were transduced with either a CRISPR-Cas9 Control Lentivirus or a CRISPR-Cas9 ELF5-KO Lentivirus. Transduction was performed using a defined Multiplicity of Infection (MOI), calculated using the formula: MOI = viral titre x virus volume/Total cell number. HaCaT cells were infected at an MOI of 20, using a viral titre of 5.7

× 10^6 per mL. Cells were cultured as previously described (Methods 2.3.1) and plated in triplicate. The next day, cells were exposed to transduction media, consisting of the appropriate virus, serum-free growth medium, and polybrene (8 µg/mL), and incubated for 4–6 hours to facilitate infection. After incubation transduction media was removed, cells were washed with PBS to remove debris and replaced with complete growth media. The cells were cultured for 48 hours, and corresponding antibiotic was added to the cells for the selection. The concentration of puromycin 0.5µg/ml antibiotic used for HaCaT cell lines used and expanded for further experiments.5 × 10^4 transduced cells were serially diluted from which single cell-derived clones were isolated and further expanded. To assess CRISPR/Cas-induced mutations, the genomic region encompassing the gRNA binding site was amplified via PCR using primers supplied by Horizon, UK. The resulting PCR products were cloned using the Zero Blunt Cloning Kit (Fisher, UK), and approximately 10 individual clones were sequenced to identify the mutation site. Successful knockouts were further validated through RT-qPCR and Western blot analysis. Successful knockouts are now known as HaCaT CRISPR-ELF5-KO and their corresponding control cell line, HaCaT CRISPR-Cas9-Control. Plasmids details are summarised in (Appendix table 7.7).

2.9 GROWTH CURVE ASSAY

Growth curve assays were used to quantify cell proliferation dynamics over time following ELF5 modulation. This method provides direct insight into changes in growth kinetics associated with tumour-suppressive or oncogenic functions (Hafner et al., 2016). To assess if there were any effects on the growth potential of HaCaT cells after CRISPR-Cas9-mediated knockout of ELF5, a growth curve was performed. The cells were grown as described above (Methods 2.3.1), trpsyinized and counted, about 5 x 10^3 cells were seeded per six well. The cells were trypsynized and counted at 50 hours and 100 hours. Data from *n*=3 experimental

repeats per group were analysed and statistical analysis was performed using unpaired student's *t*-test.

2.10 TOTAL RNA EXTRACTION PROTOCOL

High-quality RNA extraction was essential for accurate transcriptomic and gene expression analyses. The selected method ensures efficient recovery of intact RNA suitable for downstream qPCR and RNA-seq applications (Rio et al., 2010). For total RNA extraction, the culture medium was first removed from each well, and 1 mL of TRIzol reagent was added. Cells were lysed using a cell scraper, and the lysates were transferred into fresh Eppendorf tubes, then mixed thoroughly by pipetting and vortexing. The tubes were left to incubate at room temperature for 2-3 minutes, followed by centrifugation at 12,000 × g for 15 minutes. The clear aqueous upper phase was carefully transferred into a new tube, avoiding the white DNA interface layer. To precipitate RNA, 0.5 mL of isopropanol was added for every 1 mL of TRIzol used, along with 2 µL of GlycoBlue, and the mixture was vortexed for 10 seconds. The tubes were incubated for 10 minutes at room temperature, then centrifuged at 12,000 × g for 10 minutes at 4°C. The supernatant was discarded, leaving a small blue RNA pellet, which was washed with 1 mL of 75% ethanol (per 1 mL TRIzol). The solution was briefly vortexed, then centrifuged at 7,500 × g for 5 minutes at 4°C. The supernatant was discarded, and the pellet was air-dried for 5 minutes. The RNA pellet was then resuspended in 10 µL of RNase-free water per 1 mm of pellet diameter. For DNase treatment, 0.1× the RNA volume of 10× DNase buffer and 1 µL of DNase I were added, mixed by gentle flicking, and incubated at 37°C for 30 minutes. Following this, DNase inactivation reagent equal to 0.1× the original RNA volume was added and mixed thoroughly. The mixture was incubated at room temperature for 2 minutes, with mixing every 30 seconds, then centrifuged at 10,000 × g for 1.5 minutes. The resulting RNA-containing supernatant was transferred into a fresh tube. RNA concentrations

were measured using a Nanodrop spectrophotometer (ThermoFisher), and samples were stored at -80°C for future use.

2.10.2 ZYMO RNA MINI KIT

Cells were seeded into 6-well plates prior to transfection, and treatments were carried out as required. For RNA isolation, cell pellets were resuspended in 1 mL of TRIzol reagent, and RNA was extracted using the Direct-Zol RNA MiniPrep Kit (Zymo, Cambridge Biosciences, R2050), following the manufacturer's protocol. To begin, an equal volume of 100% ethanol was added to the TRIzol sample and mixed thoroughly. This TRIzol-ethanol mixture was then applied to a Zymo-Spin IIC column and centrifuged at 16,000 × g for 30 seconds, after which the flow-through was discarded. Next, 400 µL of RNA wash buffer was added to the column, followed by another centrifugation at 16,000 × g for 30 seconds, and the flow-through was again discarded. DNase treatment was carried out by combining 5 µL of DNase I with 75 µL of DNA digestion buffer and applying the mixture directly to the column matrix. The column was then incubated at room temperature for 15 minutes to digest contaminating DNA while retaining RNA on the column. Following digestion, 400 µL of RNA PreWash buffer was added, and the column was centrifuged again at 16,000 × g for 30 seconds; this step was repeated to ensure thorough washing. RNA quality and concentration were assessed using a NanoDrop™ spectrophotometer, and RNA integrity was verified by evaluating the 28S and 18S rRNA bands on a 1% (w/v) agarose gel (Schroder et al., 2006). An illustrative gel image showing intact RNA is provided in Figure 2.4. RNA samples were stored at -80°C for subsequent use.

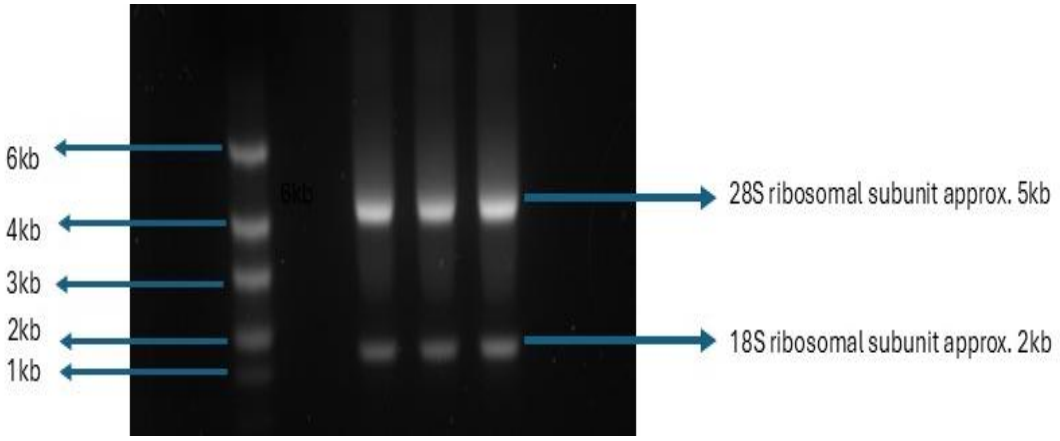

Figure 2.4: Gel Electrophoresis of RNA integrity check.

A 1% TAE agarose gel containing SYBR Safe dye was used to analyze 800 ng of RNA per sample. Two distinct bands corresponding to the 28S (~5 kb) and 18S (~2 kb) ribosomal RNA subunits indicate intact RNA. A RiboRuler High Range RNA Ladder was included as a molecular size reference. Gel was visualized using the iBright imaging system.

2.10.3. TOTAL RNA EXTRACTION FORM PARAFFIN TISSUE

RNA Extraction was performed in three different steps: 1) Deparaffinization, 2) Tissue Digestion and 3) Total RNA purification. During the deparaffinization step, excess paraffin wax was excised from the sample and subsequently transferred into a new tube. To the sample, 400 µl of deparaffinization solution was administered and incubated at 55 °C for 1 minute following brief vortexing. The samples were then subjected to centrifugation at 16,000 g for 30 seconds. The following mixture was added to the samples as shown in table 6.

Table 6. Reagents mixture added to the paraffinized tissue

DNase/RNase-Free water	95 ul
2X Digestion Buffer	95 ul
Proteinase K	10 ul

The samples were first incubated at 55 °C for 2 hours to allow for enzymatic digestion, followed by a 15-minute incubation at 65 °C to complete the process. Total RNA purification was then carried out. For tissue samples, 600 µL of RNA lysis buffer was added and mixed

thoroughly. The lysates were centrifuged at 16,000 × g for 1 minute to remove insoluble debris, and the supernatant was transferred into a nuclease-free tube.

An equal volume of ethanol was added to the supernatant, mixed well, and the mixture was loaded onto a Zymo-Spin™ IICR Column placed in a fresh collection tube. The column was centrifuged at 16,000 × g for 30 seconds, and the flow-through was discarded. To wash the bound RNA, 400 µL of RNA wash buffer was added to the column, followed by centrifugation at 16,000 × g for 30 seconds, and the flow-through was removed.

Next, a DNase I treatment was carried out by preparing a solution of 5 µL DNase I and 75 µL DNA digestion buffer, which was applied directly to the column matrix. The column was incubated at room temperature for 15 minutes. After digestion, 400 µL of RNA prep buffer was added and centrifuged at 16,000 × g for 30 seconds, discarding the flow-through. This was followed by a wash step with 700 µL of RNA wash buffer, centrifugation, and disposal of the flow-through. An additional 400 µL of RNA wash buffer was then added, and the column was centrifuged for 1 minute to ensure complete removal of wash buffer. Finally, the column was carefully transferred to a clean, nuclease-free tube, and 50 µL of DNase/RNase-free water was added directly to the matrix. After a final centrifugation, the purified RNA samples were stored at -80 °C until further use.

2.21 RNA-SEQUENCING ANALYSIS

HaCaT-SC Control and HaCaT-SC-KO cells were cultured, transfected, and RNA was extracted using the Zymo Direct-zol RNA Kit. The RNA samples were submitted to Novogene (Cambridge, UK) for sequencing, which was performed using the Human mRNA Sequencing (WOBI) platform on the NovaSeq X Plus Series (PE150). The resulting sequencing data were uploaded to the Galaxy web platform, and analysis was conducted using the public server at https://usegalaxy.org/, following previously described methods (Baker et

al., 2016; Pickup et al., 2023; Hu et al., 2025). Sequencing reads were aligned to the human reference genome (hg38). Genes that showed no statistically significant change ($P > 0.05$) or had an expression fold change of less than 1.5 were excluded from further analysis. Gene ontology enrichment and heatmap visualizations were generated using tools available on the Galaxy platform, in line with previously established protocols (Pickup et al., 2023). The RNA sequencing data that support the findings of this study are openly available in Gene Expression Omnibus Datasets at https://www.ncbi.nlm.nih.gov/gds, reference number: GSE295801. For Galaxy analysis all tools and versions have been listed in table appendix 7.10.

2.10.4 RT-qPCR ANALYSIS

2.10.4.1 CDNA SYNTHESIS

The cDNA synthesis procedure involved the preparation of specific reaction mixtures. The reaction mixture for cDNA synthesis included 2 µL of 5× cDNA synthesis mix (containing oligo(dT), random hexamer primers, 15 mM $MgCl_2$, and 5 mM dNTPs), 0.5 µL of reverse transcriptase, 100 ng of total RNA, and DNase/RNase-free water, bringing the final volume to 10 µL. The cDNA synthesis was performed using a T-100 thermal cycler, with incubation at 42°C for 30 minutes to allow reverse transcription, followed by 85°C for 10 minutes to inactivate the enzyme. After the reaction, the cDNA samples were diluted with nuclease-free water and stored at -20°C for future use.

2.10.4.2 QUANTITATIVE REAL TIME PCR (RT-qPCR)

Total RNA was extracted using the Zymo Direct-zol RNA Kit (Cambridge Biosciences, UK), following the procedure outlined in Method Section 2.8.2. For gene expression analysis, 100 ng of total RNA was reverse transcribed into cDNA using the qPCRBIO cDNA Synthesis Kit (PCR Biosystems, UK). Quantitative PCR was carried out on the QuantStudio5 Real-Time

PCR System (ThermoFisher, UK) using the qPCRBIO SyGreen mix (PCR Biosystems, UK) under the following cycling conditions: initial denaturation at 95°C for 2 minutes, followed by 40 cycles of denaturation at 95°C for 5 seconds, and annealing/extension for 30 seconds at primer-specific temperatures. RT-qPCR primers (Appendix Table 7.5) were designed using Primer3 (https://primer3.ut.ee/), and validated through both the UCSC Genome Browser (https://genome.ucsc.edu/) and NCBI Primer-BLAST (https://www.ncbi.nlm.nih.gov/tools/primer-blast/). Stock primers were initially resuspended in nuclease-free water at 100 µM and further diluted to a 10 µM working concentration.

Gene expression levels were calculated using the ΔΔCt method, with normalization to the human ACTIN (ACTB) gene. Data from triplicate samples were averaged, and the standard error of the mean (± SEM) was calculated. Statistical significance was determined using an unpaired Student's t-test.

2.11 PROTEIN EXTRACTION

Protein extraction enabled quantitative and qualitative assessment of ELF5 and downstream signalling components. This approach is essential for validating transcriptional findings at the protein level (Kurien & Scofield, 2015). Cells were seeded in 6-well plates, transfected, and cultured as detailed previously (Methods 2.3.1) prior to collection. Whole-cell protein lysates were prepared using RIPA lysis buffer (containing 50 mM Tris-HCl, 1% NP-40, 0.25% sodium deoxycholate, 150 mM NaCl, and 1 mM EDTA; pH 7.4) supplemented with cOmplete ULTRA Protease Inhibitor Cocktail (Merck, UK). Lysates were kept on ice for 1 hour, with vortexing for 1 minute every 5 minutes, followed by centrifugation at maximum speed for 20 minutes. The supernatants were collected, and samples were transferred to fresh Eppendorf tubes for further analysis.

2.11.1 PROTEIN QUANTIFICATION

Protein quantification was performed using the Micro BCA Protein Assay Kit (Fisher, UK) following the manufacturer's protocol. Bovine Serum Albumin (BSA) at a concentration of 10 mg/mL was used to prepare a standard curve, with serial dilutions ranging from 10 mg/mL to 0.08 mg/mL, including a blank. All standards were prepared in equal volumes with RIPA buffer. Protein lysates were diluted at 1:2, 1:4, and 1:10 ratios in RIPA buffer and added to a 96-well flat-bottom plate. For the working reagent, 100 µL of reagent MA, 96 µL of reagent MB, and 4 µL of reagent MC were mixed to prepare a 200 µL reaction volume, which was added in triplicate to each well containing test samples. The plate was then covered with foil and incubated at 37°C for 2 hours. After incubation, absorbance was measured at 562 nm using a CLARIOstar plate reader. A standard curve was generated by plotting the absorbance values of the known BSA concentrations, and a line of best fit was established. The protein concentrations of the unknown samples were determined by interpolating their absorbance values against the standard curve. An example is shown (Figure 2.5).

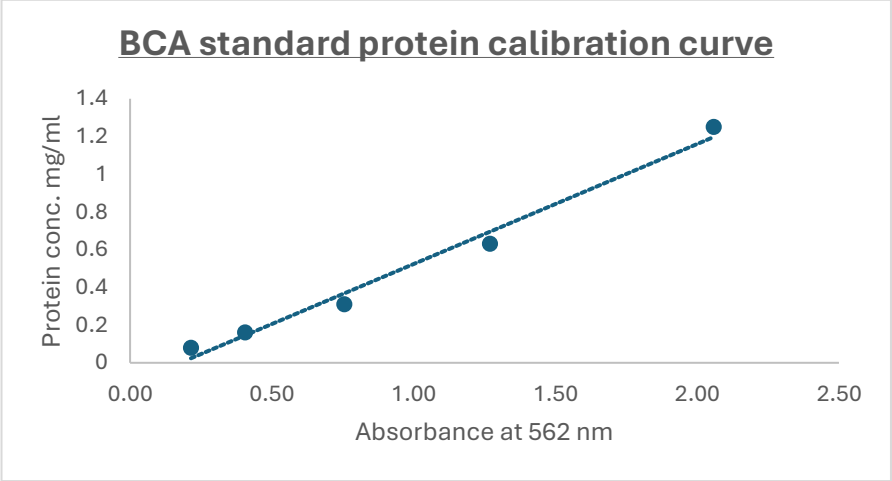

Figure 2.5: Example of a BCA calibration curve.

The schematic graph demonstrates the known protein concentrations ranging from 2.5 mg/mL to 0.08 mg/mL were plotted against their corresponding absorbance values at 562 nm. A best-fit line was

generated from this standard curve and used to calculate the protein concentrations of the unknown test samples by interpolation.

2.11.2 WESTERN BLOTTING

Western blotting was used to detect and quantify specific proteins, allowing validation of ELF5 expression and pathway modulation. This technique remains a gold standard for protein analysis in molecular biology (Mahmood & Yang, 2012). SDS-PAGE gels were prepared at concentrations ranging from 10% to 12%, depending on the molecular weight of the protein being analyzed, using the Mini-PROTEAN® Electrophoresis System (BioRad, #1658003FC). The gels consisted of two layers: a resolving gel for protein separation and a stacking gel to concentrate the proteins before separation. For instance, to prepare a 10% resolving gel (1 mm thick), the following components were mixed: 4.9 mL of distilled water, 4 mL of 30% acrylamide, 3 mL of 4× lower buffer (1.5 M Tris-base, 0.4% SDS, pH 8.8), 75 µL APS, and 10 µL TEMED (Fisher, UK). The gel was left to polymerize for 30 minutes at room temperature.

The 4% stacking gel was prepared using 3.075 mL of distilled water, 0.65 mL of 30% acrylamide, 1.25 mL of 4× upper buffer (0.5 M Tris-base, 0.4% SDS, pH 6.8), 25 µL APS, and 5 µL TEMED (Fisher, UK), poured on top of the polymerized resolving gel, followed by insertion of a comb. The stacking gel was also allowed to polymerize for 30 minutes. After setting, the comb was removed, and the gel was placed in the electrophoresis chamber filled with 1× running buffer (25 mM Tris-base, 192 mM glycine, 3.5 mM SDS, pH 7.4).

Protein samples were prepared by adding 5 µL of 4× sample buffer (0.25 M Tris-HCl, 0.28 M SDS, 40% glycerol), 0.5 µL of 2-mercaptoethanol, and topped up with RIPA buffer to a total volume of 20 µL. The samples were then denatured at 98°C for 10 minutes before loading into the gel. Electrophoresis was conducted using a Mini-PROTEAN® Tetra Cell and PowerPac™

system (BioRad, #1658001FC) at 120 V for 90 minutes at room temperature in 1× running buffer.

Protein transfer was carried out using the wet transfer method. The transfer sandwich was assembled from the positive to negative electrode as follows: two 2.5 mm thick filter papers, a 0.45 µm nitrocellulose membrane (Bio-Rad, UK), the SDS-PAGE gel, followed by two additional filter papers. A roller was used to eliminate any air bubbles between layers. The transfer stack was placed into a cold transfer buffer (0.192 M glycine, 25 mM Tris-base, 20% methanol), surrounded by ice, and transferred at 90 V for 90 minutes.

Following transfer, membranes were stained with Ponceau S (prepared in 5% acetic acid, 0.1% Ponceau S) to confirm successful protein transfer (Refer Figure 2.6). After de-staining, membranes were cut when appropriate, based on the molecular weights of the target proteins. Membranes were then incubated overnight at 4°C on a rocker with primary antibodies diluted in 5% (w/v) skimmed milk in 0.1% Tween-20 in TBS. Following primary antibody incubation, membranes were washed five times for 5 minutes each in 0.1% Tween-20 in TBS to remove excess antibodies.

Next, membranes were incubated with secondary antibodies diluted in 1% skimmed milk in 0.1% Tween-20 in TBS for 60 minutes at room temperature on a rocker. Details of all antibodies and their working dilutions are listed in Appendix Table 7.4. After secondary incubation, membranes were washed three times in 0.1% Tween-20 in TBS, followed by a final rinse in distilled water to remove any remaining detergent.

Protein detection was performed using the SuperSignal West Pico PLUS Chemiluminescence Kit. Equal volumes (500 µL each) of the luminol/enhancer solution and the stable peroxide solution were mixed and applied to the membranes for 5 minutes. Signal detection was carried out using the iBright FL1000 GelDoc Imager, and images were captured accordingly.

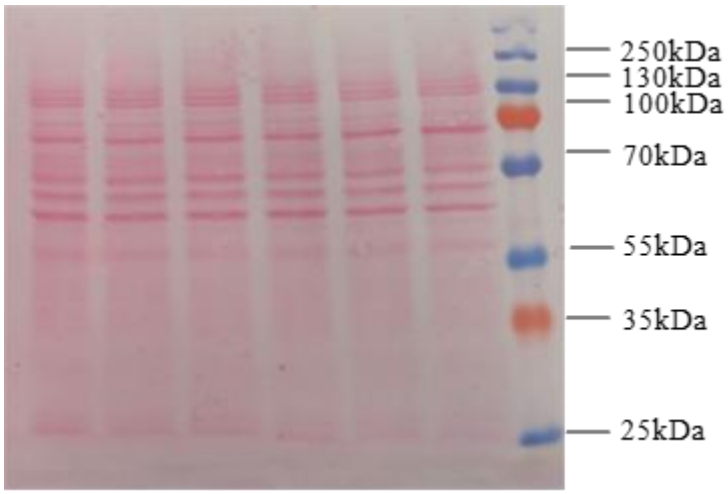

Figure 2.6: Ponceau S-stained membrane following protein transfer.

The illustrative image of the membrane displays protein bands of varying molecular weights, visualized after SDS-PAGE and transfer to a PVDF/nitrocellulose membrane. The distinct banding pattern confirms efficient protein transfer and equal loading across lanes. This staining serves as a loading and transfer control prior to immunodetection steps.

2.11.3 STRIPPING

If reprobing was necessary following signal detection, membranes were first washed in 0.1% Tween-20 in TBS for 5 minutes. They were then treated with stripping buffer (containing 200 mM glycine and 1% SDS [v/v], adjusted to pH 2.5 with HCl) for 5 minutes, repeated twice to remove the bound antibodies. After stripping, membranes were re-blocked with 5% milk and subsequently incubated with a new primary antibody for reprobing.

2.12 gDNA ISOLATION

Genomic DNA (gDNA) was extracted using the Zymo Quick-DNA Miniprep Plus Kit (D40685). Cells were first trypsinized and pelleted by centrifugation at 500 × g for 5 minutes. After discarding the supernatant, the cell pellet was resuspended in 400 µL of Genomic Lysis Buffer, briefly vortexed, and left to incubate at room temperature for 10 minutes. The lysate

was then loaded onto a Zymo-Spin column placed in a collection tube and centrifuged at ≥10,000 × g for 1 minute. The column was transferred to a clean collection tube, and 200 µL of DNA Pre-Wash Buffer was added, followed by another centrifugation at ≥10,000 × g for 1 minute. Next, 500 µL of gDNA Wash Buffer was added to the column and spun again for 1 minute at ≥10,000 × g. The column was then placed into a fresh microcentrifuge tube, and ≥10 µL of DNA Elution Buffer was added directly to the membrane. After a 2-5 minute incubation at room temperature, the tube was centrifuged to elute the DNA. The concentration and purity of the extracted DNA were assessed using a NanoDrop spectrophotometer, and samples were stored at 4°C until further use.

2.13 FLOW CYTOMETRY

The principle of the cell-cycle assay is based on the quantitative measurement of cellular DNA content to determine the distribution of cells across different phases of the cell cycle. As DNA content changes predictably during cell-cycle progression, cells in G0/G1 contain a diploid (2N) amount of DNA, cells in S phase show intermediate DNA content due to DNA synthesis, and cells in G2/M contain a tetraploid (4N) amount of DNA prior to mitosis (Kim and Sederstrom, 2015). In this assay, fixed cells are stained with a DNA-intercalating fluorescent dye such as propidium iodide (PI), which binds stoichiometrically to DNA. The fluorescence intensity recorded by flow cytometry is directly proportional to DNA content, enabling generation of DNA-content histograms that distinguish G0/G1, S, and G2/M populations. This approach allows quantitative assessment of how experimental conditions such as ELF5 modulation affect cell-cycle progression and cellular proliferation dynamics (Darzynkiewicz et al., 1992; Pozarowski & Darzynkiewicz, 2004; Ormerod, 2008).

To carry out cell cycle analysis, CRISPR-edited HaCaT cell lines including CRISPR-ELF5 knockout, CRISPR control, as well as cancer cell lines A431 and SCC-9 along with HaCaT cells transiently transfected with the pELF5 overexpression plasmid (pELF5-OE), were

cultured according to the procedure outlined in Methods 2.3.1. Cells were seeded in 60 mm dishes in triplicate and treated as needed prior to collection for flow cytometry analysis. Cells were harvested by trypsinization, and the growth medium was collected along with the cells. The suspensions were centrifuged at 300 × g for 5 minutes at 4°C, and the resulting pellets were placed on ice. Cells were then washed and fixed in 70% ethanol diluted in dPBS and incubated at –20°C for 30 minutes. Following fixation, cells were treated with RNase A (100 µg/mL) for 30 minutes at 37°C, then stained with Propidium Iodide (20 µg/mL; ThermoFisher, UK) for 30 minutes at 4°C. Cell cycle distribution was assessed using flow cytometry on a Cytek Aurora system (Cytek, UK). For each sample, 10,000 events were recorded and analyzed using Beckman Coulter Kaluza Analysis Software (Beckman Coulter, UK), as described in previous studies (Pickup et al., 2023; Hu et al., 2025).

2.14 SCRATCH ASSAY

The scratch assay was used to assess collective cell migration in vitro, modelling wound repair and tumour-associated migratory behaviour in keratinocytes (Liang et al., 2007). HaCaT, A431 and SCC-9 including CRISPR edited and GFP+/RFP+ sorted cell lines for HaCaT, A431 and SCC-9 cell lines as well as HaCaT, A431 and SCC-9 overexpression with pELF5 and Control plasmids were cultured as described above (Methods 2.3.1) in Incucyte® Imagelock 96-well Microplate (Sartorius ,BA-04856,) 50,000 cells were seeded in triplicates 24 hours prior to scratch. Two hours before the scratched was induced the wells were supplemented with mitomycin C (final concentration of 10 µM, Fisher UK). The scratch was set by using a Incucyte® Woundmaker Tool (Sartorius, 4563). Then the cells were transferred to the Incucyte® Live-Cell Imager (Sartorius) were Phase/GFP/RFP contrast images were taken with a 10 × air objective every 30 minutes to 120 minutes for a total of 72 hours. Analysis of the scratch closing was done using Incucyte® Base Analysis Software (Sartorius).

2.15 MOLECULAR CLONING

Molecular cloning was performed to generate expression and reporter constructs required for functional and transcriptional analyses. This technique enables precise manipulation of genetic elements (Green & Sambrook, 2012). For the purpose of generating plasmids that integrate GATA-3 and FLI-1 binding sites on promoter region, both forward and reverse primers, which contained KpnI-XhoI restriction sequences (Table 7), were employed to amplify the promoter segments corresponding to GATA-3 and FLI-1 from the genomic DNA of HaCaT cells. Genomic DNA from HaCaT was extracted utilizing the Zymo-gDNA extraction kit (Methods 2.12). PCR promoter fragments from human genomic DNA using Phusion High-Fidelity PCR Master Mix (Fisher, UK) were amplified using the following primers: pGATA-3-Luc: 5'-ttttggtaccGGTTGGGGTCGGTGCAGA-3' and 5'-aaaactcgagACGCTCAGTGTAGACGGAC-3' and pFLI-1-Luc: 5'-ttttggtaccCGCCTCAGGAAAAGCAAAGA-3' and 5'-aaaactcgagAAGAGCTAGCCGGGAACAAT. The PCR products synthesized using the Phusion Flash High-Fidelity PCR Master mix (F548S, ThermoFisher). The amplified PCR products were subsequently ligated into the pGL3-Basic plasmid via the Zero Blunt cloning kit (K270020, ThermoFisher). Primers were meticulously designed flanking the GATA-3 and FLI-1 binding as well as non-binding sites of ELF5, utilizing the tools delineated in (Methods 2.17). The restriction enzymes XhoI and KpnI were incorporated into the forward and reverse primers, respectively, to facilitate cloning between these specific sites in the pGL3-Basic plasmid. The composition of the PCR reaction mixture was as follows: 10 µl of 2X Phusion Flash PCR master mix, 1 µl (0.5 µM) forward primer, 1 µl (0.5 µM) reverse primer, 50 ng gDNA, and sufficient H_2O to reach a total volume of 20 µl. The PCR underwent cycling conditions (Table 7) that were predicted using an online tool to ascertain the gradient annealing temperature.

Table 7. Thermal cycle conditions for cloning plasmids

Steps	Temperature (°C)	Duration	Cycles
Initial Denaturation	98	10 seconds	1
Denaturation	98	1 seconds	30
Annealing	X	5 seconds	
Extension	72	15 seconds	
Final extension	72	1 minute	1

Subsequently, the PCR mix was subjected to electrophoresis on a 1 % TAE gel, and the band of interest was visualized utilizing SybrSafe on a transilluminator (Methods 2.15.3). The sizes of the PCR products pertaining to GATA-3 and FLI-1 (Table 17) were extracted from the gel employing the Nucleospin gel and PCR clean-up kit (740609.50, Machery-Nagel) as specified in (Methods 2.15.4).

2.15.1 LUCIFERASE PLASMID CLONING

Luciferase reporter constructs were generated to investigate direct transcriptional regulation by ELF5 and its downstream targets. Reporter assays are a standard method for validating promoter activity (Brasier & Ron, 1992). The PCR products containing the GATA-3 and FLI-1 binding sites, alongside the non-binding sites, were integrated into the PGL3-Basic plasmid through a sophisticated procedure. Initially, the PGL3-Basic plasmid was linearized via double digestion with KpnI and XhoI to create ‘sticky ends’ at both the 5’ and 3’ termini of the plasmid.

2.15.2 DOUBLE DIGESTION OF PGL3 BASIC PLASMID

For the double digestion using KpnI and XhoI restriction enzymes, the following reaction mixture was prepared: 1 µg of plasmid DNA, 2 µL of NEB Cutsmart buffer, 2 µL of BSA, 0.5 µL (10 units) of KpnI, 0.5 µL (10 units) of XhoI, and nuclease-free water to bring the final volume to 25 µL. The reaction was gently mixed by flicking and incubated at 37°C for 1 hour,

followed by a 20-minute incubation at 65°C to inactivate the enzymes. The digested PGL3-Basic plasmid was then analyzed by 1% TAE agarose gel electrophoresis containing SYBR Safe dye (as described in Methods 2.15.3). The desired DNA band was excised from the gel and purified following the procedure outlined in (Methods 2.15.4).

PCR amplification was carried out using the Phusion Flash High-Fidelity PCR Master Mix, which produces blunt-ended products. However, adding sequence overhangs to generate sticky ends can significantly improve cloning efficiency into the PGL3-Basic plasmid. The blunt-ended PCR products were first cloned into the PCR-Blunt plasmid using the Zero Blunt PCR Cloning Kit (K270020, ThermoFisher), employing a 10:1 molar ratio of insert to vector.

The ligation reaction included the following components: 1 µL (25 ng) of PCR-Blunt plasmid, the appropriate volume of PCR product insert (as specified in Table 9), 2 µL of 5× ExpressLink T4 DNA ligase buffer, 1 µL of ExpressLink T4 DNA ligase (5 U/µL), and nuclease-free water to a final volume of 10 µL. The amount of PCR product required for ligation was calculated using the following formula:

$$x \text{ ng insert} = \frac{(10)\,(y \text{ bp PCR product})\,(25 \text{ ng linearized pCR®-Blunt})}{(3500 \text{ bp pCR®-Blunt})}$$

Table 8. Plasmid vector concentration and size of PCR product

Sample Name	Concentration (ng/ul)	Size of PCR insert
FLI1-BS1	6.03	137 bp
FLI1-BS2	8.50	136 bp
FLI1-NB	12.05	117 bp
GATA3-BS1	14.24	162 bp

GATA3-BS2	41.09	162 bp
GATA3-BS3	27.55	158 bp
GATA3-NB	46.53	241 bp

The reaction mixture was incubated at ambient temperature for a duration of 15 minutes. The ligated PCR-blunt vector in conjunction with the PCR insert was subsequently cloned into DH5α competent E. coli (Methods 2.15.5), extracted, and quantified. The purified plasmid underwent double digestion utilizing KpnI and XhoI restriction enzymes, as delineated in prior sections. The digested plasmids were subjected to electrophoresis on a 1 % TAE agarose gel, and the PCR products were extracted from the gel as specified in (Methods 2.15.3).

Both the pGL3-Basic plasmid and the PCR product inserts possess sequence overhangs, which significantly enhance the efficiency of ligation. The double-digested PCR products in conjunction with the pGL3-basic plasmid were ligated utilizing T4 DNA ligase. A molar ratio of 5:1 for the PCR insert to the pGL3 plasmid was employed as shown in Table 18. The ensuing reaction mixture consisted of 2 µl of T4 DNA ligase buffer (10X), 50 ng of the pGL3 vector, 1 µl of T4 DNA ligase, with the volume of H2O adjusted to achieve a total of 20 µl.

Table 9. Plasmid inserts names with required molar ratio and PCR inserts sizes.

Insert name	Required Molar ratio (5:1)(ng)	Size of PCR inserts
FLI1-BS1	7.9	137 bp
FLI1-BS2	7.9	136 bp
FLI1-NB	6.8	117 bp
GATA3-BS1	9.4	162 bp
GATA3-BS2	9.4	162 bp
GATA3-BS3	9.1	158 bp
GATA3-NB	14	241 bp

The reaction mixture was subjected to incubation at 16°C overnight, followed by a temperature elevation to 65°C for a duration of 10 minutes. The next step is to carry out a bacterial transformation for these ligated plasmids (Methods 2.15.5). The bacterial mixture was added to the prepared agar plated with 100 mg/mL of Ampicillin and set for incubation at 37°C overnight. Following day, post incubation, single colonies were picked up and expanded further for DNA extraction by using a Nucleospin plasmid mini kit. A double digestion was performed for these purified plasmids with KpnI and XhoI. A gel electrophoresis was performed with these double digested plasmids (Methods 2.15.3) to verify the incorporation of the PCR product into the pGL3-Basic plasmid (Figure 2.7).

2.15.3 AGAROSE GEL ELECTROPHORESIS

According to the DNA sizes, the samples were separated using gel electrophoresis. 1-2% Agarose was diluted in 200 mL TAE buffer. The solution was warmed up in microwave for 2-3 minutes or until the agarose dissolved fully. The agarose solution was kept aside to cool, 5 µl SybrSafe was added to the solution. To the electrophoresis apparatus containing 15 wel comb, the gel mixture was added. Once the gel was solidified, by removing the comb the gel was transferred to electrophoresis tank which contains TAE buffer. DNA marker of size 100-1500 bp (PCRBIO ladder IV) and DNA samples were loaded into the wells. The samples were run for about 50-60 minutes at 100 V. The samples in the gel were visualised under iBright nucleic acid gel visualiser.

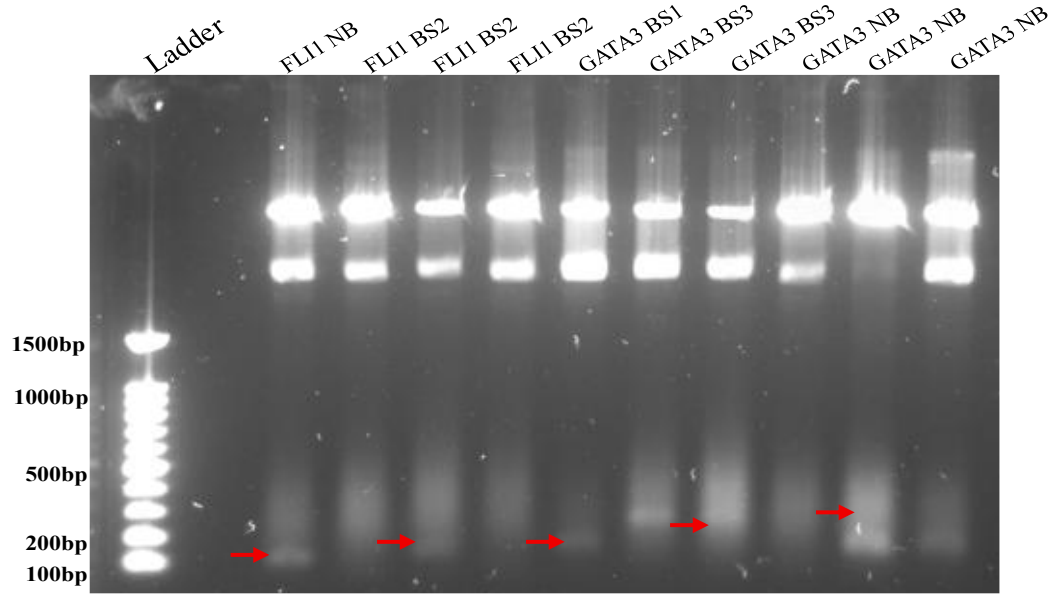

Figure 2.7: Agarose gel electrophoresis of plasmid DNA samples following cloning.

Gel image shows plasmid DNA bands of varying sizes corresponding to different constructs. Samples containing constructs were resolved on a 1% agarose gel stained with SyBr Safe and visualized under UV light. Distinct bands represent successfully cloned plasmids, with fragment sizes consistent with expected insert lengths. From left to right- ladder with 100 bp. FLI-1 non-binding site (NB) with 117 bp, FLI-1 binding site 2(BS2) with 136 bp, GATA-3 binding site 1(BS1) with 162 bp, GATA-3 binding site 3(BS3) with 158 bp and GATA-3 non-binding site (NB) with 241 bp (marked with red arrows) were extracted from the gel.

2.15.4 NUCLEOSPIN GEL AND PCR CLEAN-UP

DNA samples were extracted from agarose gel by Nucleopsin Gel & PCR Clean-up kit. Using a sterile scalpel, DNA fragments were carefully excised from the agarose gel, ensuring the removal of any excess gel. The gel slices were weighed and transferred to clean microcentrifuge tubes. For gels containing less than 2% agarose, 200 µL of NTI buffer was added per 100 mg of gel. If the gel concentration exceeded 2%, the volume of NTI buffer was doubled accordingly. The samples were then incubated at 50°C for 5-10 minutes, with gentle vortexing every 2-3 minutes, until the gel pieces were completely dissolved. Following

dissolution, the Nucleospin Gel and PCR Clean-Up column was placed into a 2 mL collection tube, and up to 700 µL of the sample was loaded into the column. The columns were centrifuged at 11,000 × g for 30 seconds, and the flow-through was discarded. This loading and centrifugation step was repeated until all of the sample had passed through the column. To wash the silica membrane, 700 µL of NT3 buffer was added to the column and centrifuged again at 11,000 × g for 30 seconds. After discarding the flow-through, the column was returned to the collection tube and centrifuged for an additional minute at the same speed to ensure complete removal of residual wash buffer. To remove any remaining ethanol, the columns were incubated at 70°C for 2-5 minutes. For DNA elution, the columns were transferred into clean microcentrifuge tubes and 15-30 µL of NE buffer was added directly to the membrane. After a 1-minute incubation at room temperature, the columns were centrifuged at 11,000 × g for 1 minute. The eluted DNA was quantified using a NanoDrop spectrophotometer and stored at -20°C for future use.

2.15.5 BACTERIAL TRANSFORMATION

Bacterial transformation was used to propagate plasmid constructs efficiently, providing high-yield DNA for downstream applications (Sambrook & Russell, 2001). For bacterial transformation, defrosting of *E. coli* DH5α competent bacteria (Fisher, UK) was carried out on ice for 15 minutes. In a clean tube, 50 µL of competent bacteria was aliquoted and about 5 ng of purified plasmid was added. This mixture was kept on ice for 20 minutes. To facilitate the entry of bacteria into the plasmid, firstly the tube containing mixture was incubated at 42ºC for 45 seconds and next to recover from the heat shock, the tube was transferred on ice again for 2 minutes. Further, to this tube, a sterile SOC media about 450 µL was added and left for incubation at 37ºC for 1 hour. The LB plates prepared previously were pre-warmed and the mixture of bacteria along with required antibiotics were seeded onto the plates. These plates were left for incubation overnight at 37ºC. Following day, after 16-18 hours, process of picking

up single colonies was carried out which were then added to the liquid culture with required antibiotics and left for incubation at 37ºC overnight followed by plasmid isolation. Colonies were observed only on plates containing the selected plasmid while negative control plates showed no growth, confirming successful selection (Figure 2.8).

2.15.5.1 PREPARATION OF LB AGAR PLATES

For preparation of LB-Agar plates, a mixture of LB-agar powder and distilled water was used after autoclaving. Followed by the addition of antibiotics that were resistant to the plasmids and prepared solution was poured to petri-dishes as required. The plated were set to solidify at room temperature. The solidified plates once ready kept at 4°C upside-down for storage. Prior using- the plates were pre-warmed for 30 minutes at 37°C.

2.15.5.2 BACTERIAL CULTURES

For preparation of bacterial cultures, a mixture of LB broth powder and distilled water was used after autoclaving. Post bacterial transformation, a single colony was picked up and transferred to 10 ml liquid LB broth culture containing selective antibiotics depending on the plasmids used. The liquid broth containing mixture was incubated overnight at 37°C and kept on shaker at 250 RPM. After 16-18 hours of incubation, bacterial stocks were prepared by mixture of 500 µL of bacterial culture and 500 µl of glycerol and were kept at -80ºC for long-term storage.

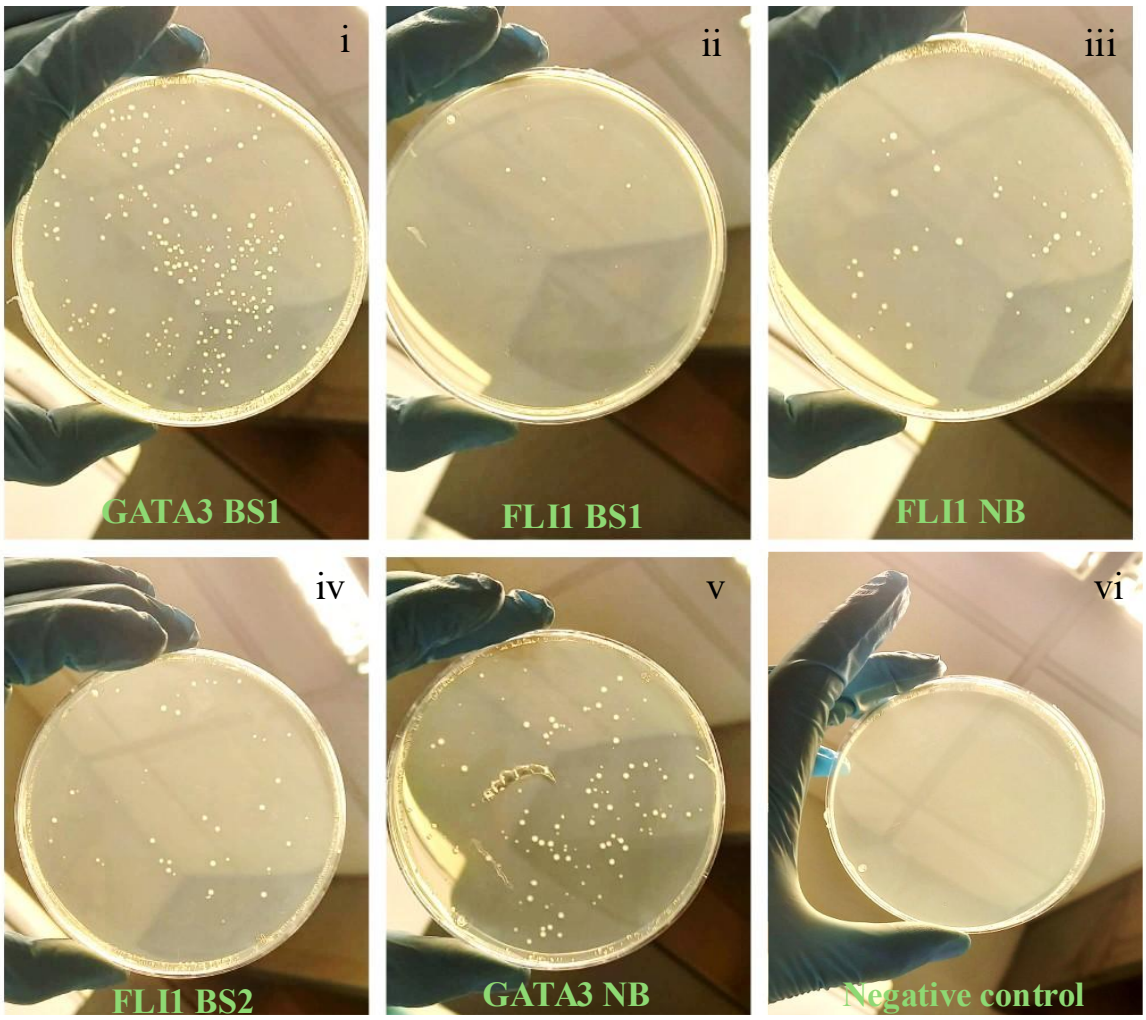

Figure 2.8: LB agar plates showing bacterial colony growth.

The illustrative images showing bacterial colony growth following plasmid transformation. The plate (i to v) successful colony growth on LB agar containing antibiotic, indicating transformation with the appropriate plasmid. The negative control plate (vi), containing LB agar with the same antibiotic but no plasmid, shows no colony growth, confirming the antibiotic selection efficacy and transformation specificity. Single colonies were picked and processed for mini and maxi preps.

2.16 PLASMID ISOLATION

2.16.1 MINI PREPS

The remaining bacterial culture was centrifuged at maximum speed for 10 minutes at room temperature to pellet the cells. Plasmid DNA was isolated from the bacterial pellet using the

Promega Miniprep Kit, following the manufacturer's protocol (Promega, UK). In brief, the bacterial pellets were resuspended in 100 µL of cell lysis buffer on ice by gently inverting the tubes three times. Subsequently, 350 µL of neutralization buffer was added, and the tubes were inverted six times until the mixture turned yellow, indicating neutralization. The lysates were then centrifuged at 1300 × g for 3 minutes, and the clear supernatant was transferred to spin columns for plasmid purification. Next, 200 µL of endotoxin removal buffer was added to each column, followed by centrifugation at 1300 × g for 15 seconds. This was followed by a wash step using 400 µL of column wash buffer, which was spun down at 1300 × g for 30 seconds. Finally, the plasmids were eluted using 30 µL of elution buffer, and the DNA concentration was determined using a NanoDrop™ spectrophotometer. The purified plasmid constructs were stored at -20°C until further use.

2.16.2 MAXI PREPS

For larger-scale plasmid preparation, 3-5 mL of bacterial culture was first incubated at 37°C for 8 hours with constant shaking and then used as a starter inoculum. This was transferred into LB broth in a conical flask and incubated overnight (16-18 hours) at 37°C on a bacterial shaker at 250 RPM. The following day, the bacterial culture was centrifuged at maximum speed for 5 minutes, and the supernatant was discarded. The resulting pellet was resuspended in 12 mL of cell resuspension solution. Next, 12 mL of cell lysis buffer was added, and the contents were gently mixed by inverting the tube 3-5 times, followed by a 3-minute incubation at room temperature. Then, 12 mL of neutralization solution was added, and the mixture was gently inverted 10–15 times to mix thoroughly. To clear the lysate, the tubes were centrifuged at 3900 RPM for 20 minutes at room temperature. For DNA purification, a column stack was assembled by placing a clearing column (blue) on top of the PureYield® Maxi Binding Column (white), and the entire setup was placed on a vacuum manifold. Approximately half of the cleared lysate was added to the blue clearing column, and maximum vacuum pressure was

applied to pass the liquid through both columns. This was repeated until the entire lysate was filtered. After filtration, the blue column was discarded. The white binding column was then washed with 5 mL of endotoxin removal wash, followed by 20 mL of column wash, both passed through using vacuum. The membrane was allowed to dry for 5 minutes under vacuum. The column was then removed from the manifold, and any residual ethanol was wiped from the exterior. For elution, the column was attached to an elutor vacuum device, with a fresh microcentrifuge tube positioned beneath. 1 mL of nuclease-free water was added to the column and allowed to pass through by applying vacuum for about 1 minute. Finally, the eluted plasmid DNA was quantified using a NanoDrop spectrophotometer, and the plasmid constructs were stored at -20°C until needed.

2.17 LUCIFERASE REPORTER ASSAY

Luciferase reporter assays were employed to assess transcriptional activity of ELF5-regulated promoters in a quantitative and sensitive manner (Promega Technical Manual; Alam & Cook, 1990). To create reporter constructs for GATA-3 and FLI-1, the -1 kb promoter regions of each gene were examined for putative ELF5 binding sites using Ciiider software (www.ciiider.org), as previously outlined by Gearing et al. (2019). The amplified PCR products (refer to Method 2.15) were purified and inserted into the pGL3-basic luciferase reporter vector (Promega, UK) at the KpnI and XhoI restriction sites (indicated by underlined sequences). For the reporter gene assay, HaCaT cells were seeded in 96-well plates at a density of 10^4 cells per well one day before transfection. Cells were co-transfected with either the pELF5-OE plasmid or the pCDN3 control vector (120 ng/well, Fisher, UK) along with reporter constructs either pFLI-1-Luc or pGATA-3-Luc (60 ng/well) using Lipofectamine 3000 (0.5 µl/well, Fisher, UK).

Forty-eight hours post-transfection, luciferase activity was assessed using the Dual-Glo Luciferase Assay System (Promega, UK), following the manufacturer's protocol and methods previously described (Mardaryev et al., 2011). Luminescence was recorded using the

CLARIOStar plate reader (BMG Labtech, Ortenberg, Germany). Data from five independent technical replicates were normalized against the activity of the pnull-Renilla construct (20 ng/well, Promega, UK). Final results were expressed as mean ± SEM, and statistical comparisons were made using an unpaired Student's t-test.

2.18 FLUORESCENT ACTIVATED CELL SORTING (FACS)

FACS was used to isolate keratinocyte subpopulations based on target gene expression, (Shapiro, 2005).

2.18.1 VIRAL TRANSDUCTION OF ELF5-KO CELL LINE WITH GATA-3 AND FLI-1 VIRUSES

Transduction was done using HaCaT ELF5-KO cell line: cells were infected a MOI of 20 for Control (7.8 x 10^5 viral titre/per ml), a MOI of 20 for GATA-3 overexpression (4.4 x 10^9 viral titre/per ml) and a MOI of 20 for shFLI-1 (2.06 x 10^7 viral titre/per ml) for 48 hours as described in (Methods 2.8.5). These cells were then prepared for FACs Melody sorting as described below.

Cells were transfected with corresponding fluorescent lentiviral virus as mentioned above in triplicates. After 10 days, the cells were confluent for splitting and trypsized and were resuspended into a single cell suspension and filtered using a 40 µm filter. The cells were centrifuged down at 300 x g for 10 minutes and resuspended in 1 mL of dPBS. Green Fluorescent Protein Positive (GFP+) and Red Fluorescent Protein Positive (RFP+) cells were sorted using a BD FACSMelody™ Cell Sorter (Beckman Coulter, UK) and data was analysed using BD FACSChorus™ Software (Beckman Coulter, UK). FACs sorted GFP+ and RFP+ cells were cultured under normal HaCaT growth conditions (Methods 2.3.1) and used for subsequent experimental analysis.

2.19 TRANSWELL ASSAY

Transwell assays were used to evaluate invasive capacity of keratinocytes, modelling tumour-associated invasion through extracellular matrix barriers (Boyden, 1962). Transwell assay was performed as described previously (Yang et al., 2021). CRISPR-Cas9 edited ELF5-control, ELF-KO as well as FACs isolated ELF5-KO-Control^{RFP+}, ELF5-KO-GATA-3-OE^{GFP+} and ELF5-KO-shFLI-1^{GFP+} cells were grown (Methods 2.3.1) and detached, resuspended in serum free DMEM media and total number of $2x10^5$ cells/ml cells were calculated and seeded to the upper chambers of Transwell equipment with 8-µm polycarbonate membrane filter (Corning, Inc.). The lower chambers were filled with DMEM containing 10% FBS and incubated overnight at 37°C. After incubation for 24 hours, the media from the upper chambers were removed and rinsed with dPBS. Next, migrated keratinocytes were stained with 0.5 % crystal violet for 15 minutes at room temperature and washed with dPBS 3 times and images were captured using an optical inverted microscope (magnification, x 100). The total number of average cell numbers were counted in ImageJ software. Data from n=3 per group were pooled and statistical analysis was performed using unpaired student's *t*-test.

2.20 SOFT AGAR ASSAY

Growth and survival of HaCaT cell variants was determined as described previously (O'Neill, et al., 1968, Kari, et al., 2006, Van Scoyk, et al., 2014). FACs GFP+ cells grown (Methods 2.3.1), the base agar (1.2%) and the top agar (0.6%) was prepared by 1.2 g agar-agar powder and 0.6 g agar-agar powder respectively to 100 mL milliQ water to sterile Schott bottles by dissolving completely in microwave and autoclaved. On the day of experiment the agar was dissolved in microwave for 2.5 minutes until completely dissolved and cool it at room temperature. The base agar was mix with DMEM media by gentle inversion; this will create 0.6% base agar mix. The agar-media mix was added to wells in quintuplicates. This will form base agar and kept aside in tissue culture hood for 15 minutes. A single cell solution was

generated with trypsized cells resuspended in media and counted. 1000 cells per 25 µl were added to 25 µl DMEM solution to top agar. This cell suspension was mixed with 0.6 % top agar and added on the base agar in each well. The top agar was set aside to set for 20 minutes at room temperature in tissue culture hood and topped it up with 100 µ l of complete media before placing the plates in the incubator for 28 days at 37°C, 5 % CO_2. The media was replaced every three days. Wells examined immediately after plating showed only single cells. Soft agar colonies were stained with NBT (nitroblue tetrazolium chloride solution, 1 mg/mL stock solution in 1 x dPBS) and incubated overnight at 37 °C. Once colonies are stained, images were taken by Thunder microscope (Leica, UK) and colonies counted using Image J (https://imagej.net/ij/) analysis software after 28 days in triplicates as done previously (Kari, et al., 2006).

2.22 STATISTICAL ANALYSIS

All statistical analyses were performed using GraphPad Prism version 9.0. Experiments were conducted using a minimum of three independent technical replicates. Technical replicates (e.g., triplicates run per RT-qPCR) were used where appropriate. Data are presented as the mean ± standard error of the mean (SEM) and individual data points are included in all graphs unless otherwise specified.

For normally distributed datasets, comparisons between two groups were performed using an unpaired, two-tailed student's t-test, which served as the primary statistical method in this study. Two-tailed tests were selected to allow detection of differences in either direction. Alternative statistical approaches, where required, are indicated in the corresponding figure legends.

Relative gene expression values were calculated using the $^{\Delta\Delta}$Ct method with *ACTIN* as the internal housekeeping gene. For luciferase assays, firefly luciferase signals were normalised to

pRenilla to account for transfection efficiency. Statistical significance was defined as follows: *p<0.05, **p<0.01, ***p<0.001. Exact p-values. Sample sizes (n) and statistical tests used are reported in the relevant figure legends.

CHAPTER
3.0 RESULTS

3.1 EXPRESSIONAL ANALYSIS OF ELF5

AIM: To determine the endogenous expression of ELF5 in: (i) healthy human tissue, (ii) cutaneous squamous cell carcinoma (cSCC) tissue, (iii) in healthy human keratinocytes and (iv) human cancerous cell lines.

3.1.1 EXPRESSIONAL ANALYSIS OF *ELF5* IN HEALTHY HUMAN AND CSCC SKIN TISSUES

To assess the expression profile of ELF5, quantitative reverse transcription PCR (RT-qPCR) was conducted to evaluate the relative fold change in ELF5 expression across both tissue types. The expression levels of *ELF5* in the cSCC tissues were decreased compared to healthy skin tissue, thereby showed downregulation of *ELF5* expression in skin cancer tissue compared to healthy tissue (Figure 3.1A).

To further assess the expression profile of ELF5, tissue specimens derived from both healthy human skin and malignant skin regions were analysed. We observed that a pronounced expression of ELF5 within the healthy human tissue was distributed throughout the epidermis: as observed in basal epidermis and suprabasal layers of epidermis. Also in healthy skin, *CYTOKERATIN 15* (KRT15) was strongly expressed in the basal layer of the interfollicular epidermis and in the outer root sheath of hair follicles (bright orange), consistent with its known role as a marker of epidermal stem cells (Figure 3.1B) whereas a complete lack of ELF5 expression was exhibited in the epidermis of cSCC tissue and ELF5 expression was absent from tumour lesions and cSCC tissue showed a significant reduction or complete loss of *CYTOKERATIN 15* (KRT15) staining (Figure 3.1C). This observation suggests a potential functional role of ELF5 in maintaining normal cellular activities, which appears to be disrupted during the process of skin carcinogenesis.

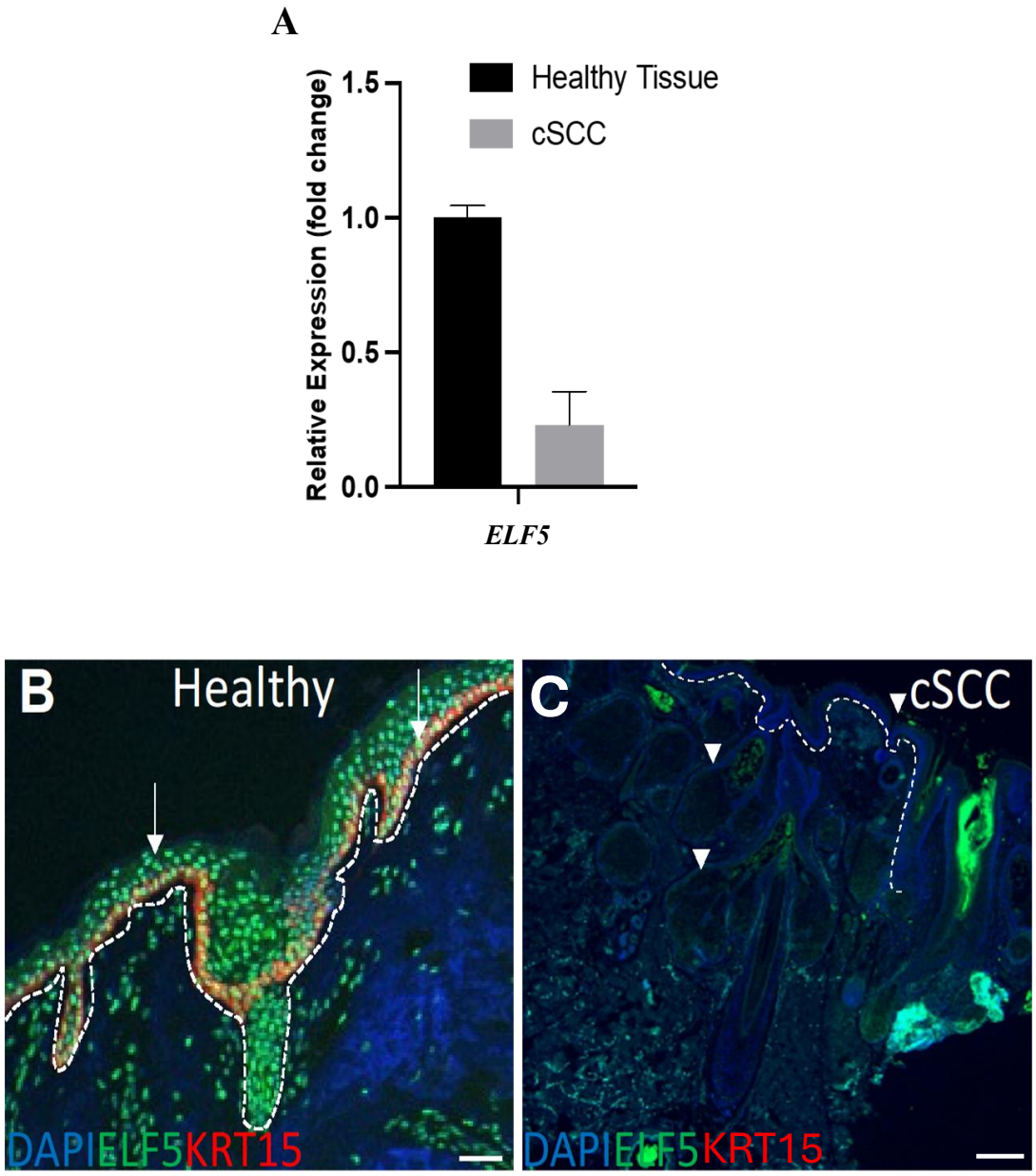

Figure 3.1: Expressional analysis of ELF5 in healthy human and cSCC skin samples.

A. *RT-qPCR depicts reduction in ELF5 expression analysed in cSCC tissues compared to healthy human tissue.* ***B***. *The healthy skin tissue shows abundant nuclear ELF5 expression in the epidermis (stratum basale and germinative layers, arrows) and shows strong KRT15 expression in basal cells* ***C.*** *In cSCC tissue, ELF5 expression is reduced in the epidermis and tumour lesions (arrowheads), KRT15 expression is markedly reduced or lost. Broken lines define epidermal-dermal border. Scale bar: 50µm.*

3.1.2 ENDOGENOUS EXPRESSION ANALYSIS OF ELF5 IN HEALTHY HUMAN KERATINOCYTES COMPARED TO HUMAN CANCEROUS CELL LINES

Next, to assess ELF5 expression levels in both healthy human keratinocytes and human cancerous cell lines, RT-qPCR was performed across four distinct cell lines including two cancerous cell lines; A431 (a squamous cell carcinoma cell line, epidermoid carcinoma) and SCC-9 (a squamous cell carcinoma cell line, tongue) and two healthy keratinocytes cells; HaCaT (a human keratinocyte cell line, which are spontaneously immortalized) and HPEK (a human primary epidermal keratinocytes).

HaCaT keratinocytes were selected as a model of non-tumorigenic, immortalised human epidermal cells that retain the capacity for calcium-induced differentiation and exhibit stable growth characteristics ((Boukamp *et al.*, 1988; Wilson, 2014; Colombo *et al.*, 2017). Their genetic stability and high transfection efficiency make then stable for CRISPR-mediated ELF5 knockout and functional assays. HaCaTs therefore provide a biologically relevant system for analysing ELF5-dependent regulation of keratinocyte proliferation, differentiation and early tumour associated behaviours.

Our data revealed a significantly, (**p<0.01, ***p<0.001) elevated expression of *ELF5* in the healthy cell lines relative to their cancerous counterparts (Figure 3.2A). This finding implies that ELF5 may show an essential function in sustaining normal cellular functions, which seems to be compromised in the malignant cells.

To further validate our RT-qPCR data, we performed western blot analysis. Our results demonstrated that healthy cell lines exhibited an elevated levels of ELF5 expression (HPEK - data not shown), while the cancerous cell lines showed a markedly reduced expression of ELF5 (Figure 3.2B). GAPDH served as a loading control to ensure uniform protein loading across all samples.

Subsequently, Immunocytochemistry was also performed to check the endogenous expression of ELF5 in healthy keratinocytes and both cancerous cell lines. As anticipated, HaCaT cells showed abundant expression of ELF5 *in vitro* (Figure 3.2Ci). The cancerous cell line A431 and SCC-9 showed reduced expression of ELF5 (Figure 3.2C ii & 3.2C iii) respectively.

These findings strongly indicate that ELF5 expression is significantly downregulated at the levels of mRNA and protein production in cancerous cell lines when compared to healthy counterparts.

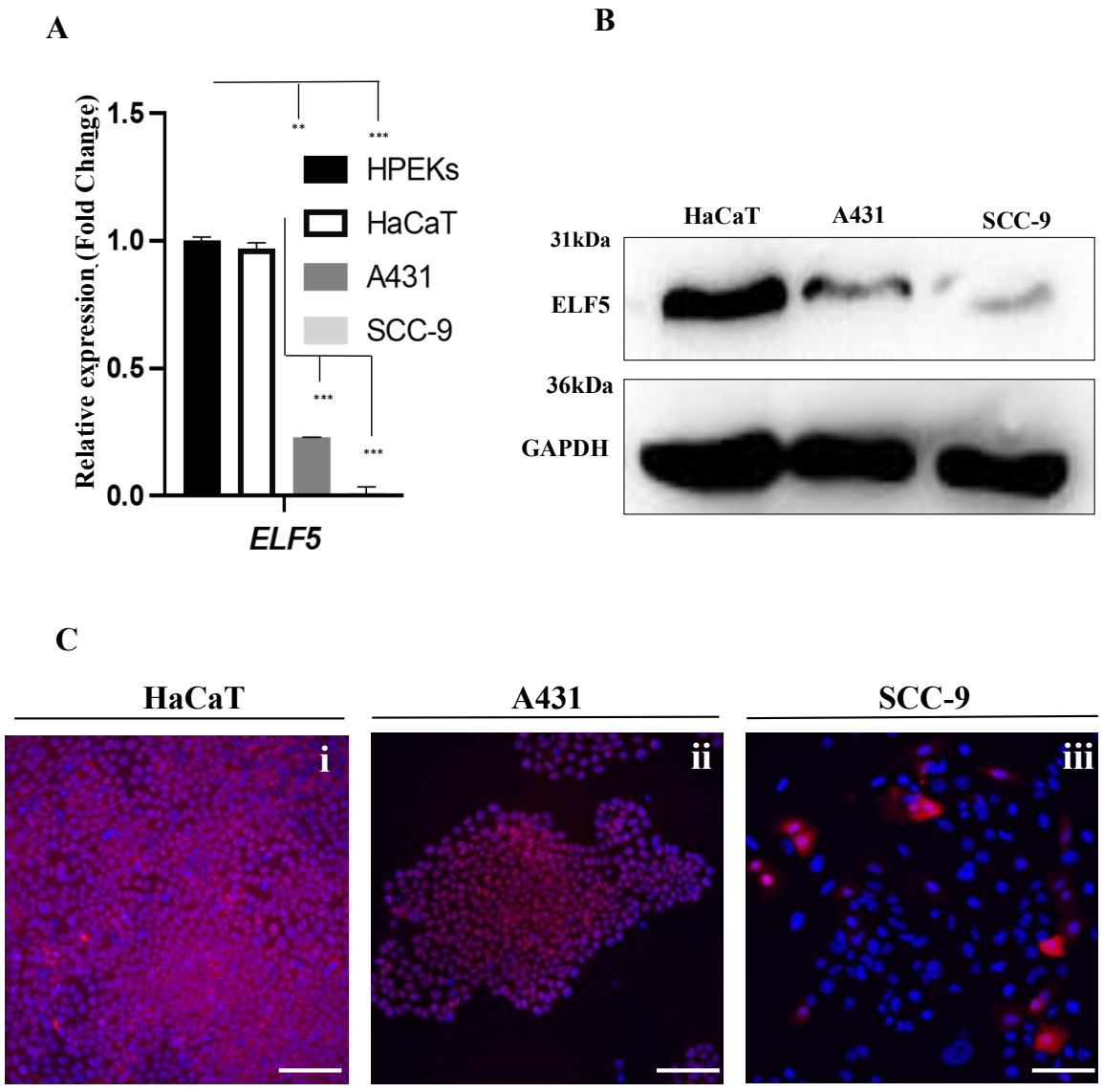

Figure 3.2: **Endogenous expression analysis of ELF5 in healthy human cell lines compared to human cancerous cell lines.**

A. *RT-qPCR analysis of ELF5 in primary human epidermal keratinocytes (HPEKs), normal human immortalized keratinocytes (HaCaT) and human squamous carcinoma cell lines (A431 and SCC-9), ELF5 expression is significantly reduce in both cancerous cell lines compared to both HPEK and HaCaT cell lines.* ***B.*** *Consistent with RT-qPCR data, protein analysis by western blotting shows abundant expression of ELF5 in normal human immortalized keratinocytes (HaCaT). Whereas in human squamous carcinoma cell lines (A431 and SCC-9) ELF5 expression is reduced.* ***C.*** *Immunohistochemistry micrograph shows abundant endogenous expression of ELF5 in (i) HaCaT and reduce expression in (ii) A431 and (iii) SCC-9 cancerous cell lines, Data are expressed as mean ± SEM values from three experimental repeats; **p < 0.01; ***p < 0.001. unpaired Student's t-test. WB Images are illustrative of n=3 technical repeats per treatment. Scale bar: 50µm.*

3.2. ELF5 MODULATION IN CELLULAR PROCESSES

AIM: To determine the role of ELF5 in both healthy and cancerous cell lines in controlling proliferation, differentiation and migratory properties after gain or loss of ELF5.

As expressional analysis of ELF5 in healthy human and cSCC skin tissues along with endogenous expression analysis of ELF5 in healthy vs cancerous cell lines (Figure 3.1 & 3.2) demonstrates that ELF5 expression is downregulated during keratinocyte transformation and malignancy. We therefore investigated the potential role of ELF5 on cellular processes after gain-or-loss of *ELF5* expression using CRISPR-Cas9 mediated gene knockouts and transient transfections experiments.

ELF5 knockout was performed exclusively in HaCaT cells because they provide a genetically stable, non-tumorigenic keratinocyte model with physiologically relevant ELF5 expression (Figure 3.2). In contrast, cancer derived cell lines used in this research study mainly A431 and SCC-9 exhibit extensive genomic instability, deregulated signalling and intrinsically low ELF5 levels (RNA and protein, Figure 3.2), making gene knockout technically challenging and

biologically uninformative. Eliminating ELF5 in these malignant backgrounds would not yield interpretable phenotypes, as ELF5 is already substantially downregulated and its regulatory networks are overridden by oncogenic mutations. HaCaTs therefore served as the most appropriate model to investigate the functional consequences of ELF5 loss and to examine early events in keratinocyte transformation, while cancer cell lines were used in complementary assays to assess ELF5 overexpression, target validation and phenotypic comparisons.

3.2.1 CRISPR-CAS9 MEDIATED KNOCKOUT (KO) OF *ELF5* IN HEALTHY HUMAN IMMORTALIZED KERATINOCYTES (HaCaT)

ELF5 knockout was performed exclusively in HaCaT cells because they provide a genetically stable, non-tumorigenic keratinocyte model with physiologically relevant ELF5 expression (Figure 3.2). In contrast, cancer derived cell lines used in this research study mainly A431 and SCC-9 exhibit extensive genomic instability, deregulated signalling and intrinsically low ELF5 levels (RNA and protein, Figure 3.2), making gene knockout technically challenging and biologically uninformative. Eliminating ELF5 in these malignant backgrounds would not yield interpretable phenotypes, as ELF5 is already substantially downregulated and its regulatory networks are overridden by oncogenic mutations. HaCaTs therefore served as the most appropriate model to investigate the functional consequences of ELF5 loss and to examine early events in keratinocyte transformation, while cancer cell lines were used in complementary assays to assess ELF5 overexpression, target validation and phenotypic comparisons.

To examine the role of ELF5 in human keratinocytes, stable knockout (KO) and corresponding control cell lines in healthy human immortalized keratinocytes (HaCaT) were established utilizing the CRISPR-Cas9 genome editing methodology (McKinley & Cheeseman, 2018). All the Edit-R All-in-one Lentiviral sgRNA positive vectors and non-targeting control vector (Appendix table 7.7) containing a human codon-optimized version of the *S. pyogenes* Cas9 gene with puromycin resistance marker (PuroR) were purchased from Horizon, UK.

Subsequent to transfection with guide RNA, single-cell clones those successfully proliferated underwent screening, and validation at both the transcriptional and translational levels was performed through quantitative real-time PCR and immunoblotting.

To ascertain the efficacy of CRISPR-mediated gene knockout of *ELF5* at the mRNA level, RT-qPCR was conducted on both HaCaT CRISPR-ELF5-KO (knockout) and HaCaT CRISPR control cell lines. Our analysis demonstrated a decrease in *ELF5* expression within the knockout cell line in comparison to the stable control cell lines as showed in clone 1(**p<0.01) (Figure 3.3A). These findings suggest that the CRISPR-Cas9 approach effectively disrupted ELF5 transcription, resulting in a considerable downregulation of mRNA expression.

To evaluate whether the noted decline at the ELF5 mRNA level corresponded with a reduction in protein expression, western blot analysis was carried out. The selected single cell clones (Clone 1 and clone 2) of HaCaT control and Knockout (KO) stable cell lines displayed elevated expression of ELF5 compared to a dramatic reduction of ELF5 protein respectively (Figure 3.3B). From this point, we used Clone 1 and its corresponding control for experimental purposes and will be known as ELF5-KO and ELF5-Control.

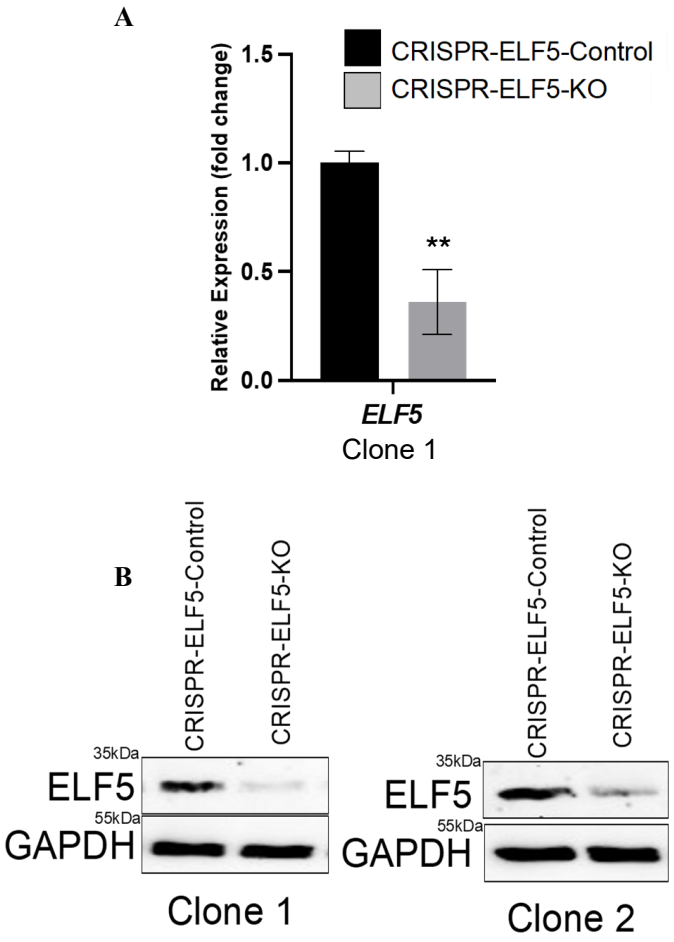

Figure 3.3: **Validation of CRISPR-Cas9 mediated knockout (KO) of ELF5.**

A. *RT-qPCR analysis in CRISPR-Cas9 mediated KO (knockout) of ELF5 in HaCaT cell line (CRISPR-ELF5-KO) via single cell cloning dilution technique show significantly reduced expression of ELF5 compared to corresponding CRISPR-Cas9 mediated control cell line in HaCaTs (CRISPR-Control) generated.* ***B.*** *Protein analysis by western blotting shows reduced expression of ELF5 in CRISPR-ELF5-KO cell lines (clone 1 & clone 2) compared to CRISPR-control cell lines. Data are expressed as mean ± SEM values from three experimental repeats; **p < 0.01; ***p < 0.001. unpaired Student's t-test. WB images are illustrative of n=3 technical repeats per treatment.*

3.2.2 TRANSIENTLY TRANSFECTED ELF5 IN HEALTHY HUMAN IMMORTALIZED KERATINOCYTES (HaCaT) AND HUMAN SQUAMOUS CARCINOMA CELL LINES- A431 & SCC-9

Next, ELF5 was overexpressed by transient transfection in all three cell lines- Healthy human keratinocytes (HaCaT), cancerous cell lines- A431 and SCC-9. To validate the transfection, RT-qPCR was performed. Our data revealed a significantly elevated expression of *ELF5* in HaCaT cells as well as in both cancerous cell lines- A431 and SCC-9 (**p<0.01, ***p<0.001), (Figure 3.4A) respectively. To further validate our RT-qPCR data, we performed western blot analysis, HaCaT cell line including the cancerous cell lines exhibited abundant expression of ELF5, compared to control cells (Figure 3.4B).

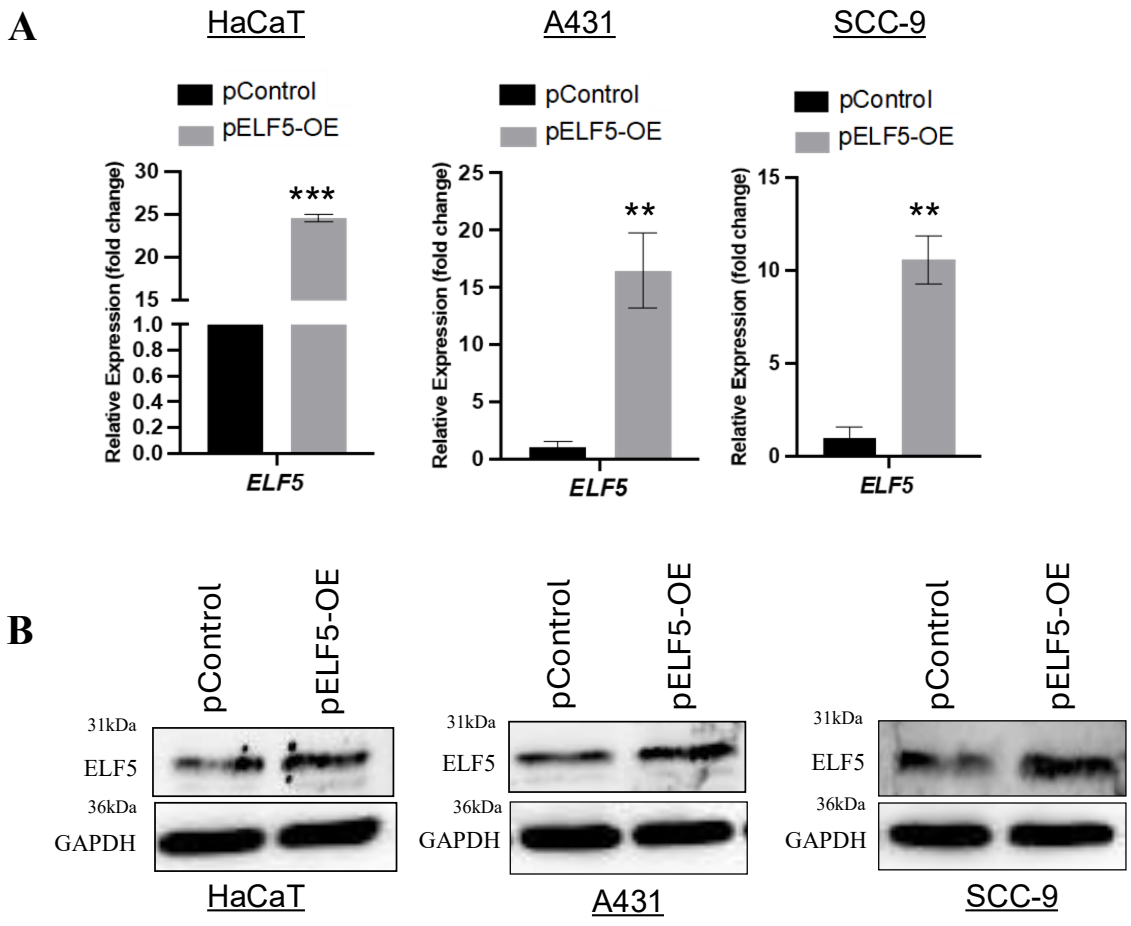

Figure 3.4: Expression of ELF5 in Transiently transfected Human keratinocytes and cancerous cell lines.

*__A__. RT-qPCR confirming the significant ELF5 expression in all three cell lines compared to controls. __B__. Western blot: successful overexpression of ELF5 (pELF5-OE) is observed in all cell lines compared to corresponding controls (pControl). Data are expressed as mean ± SEM values from three experimental repeats; **p < 0.01; ***p < 0.001. unpaired Student's t-test. WB Images are illustrative of n=3 technical repeats per treatment.*

3.2.3 CELL GROWTH CURVE AFTER LOSING ELF5 IN HaCaT CELLS

To assess if there were any impact on growth after loss of ELF5, total cell counts were measured over a period. Cells were counted at 50-hour and 100-hour post-seeding. As shown in Figure 3.5 both ELF5-control and ELF5-KO cells exhibited a progressive increase in total cell numbers over time. At the 50-hour and 100-hour time points, no statistically significant differences were observed between the ELF5-control and ELF5-KO groups. These findings indicate that loss of ELF5 in ELF5-KO does not significantly affect cell proliferation.

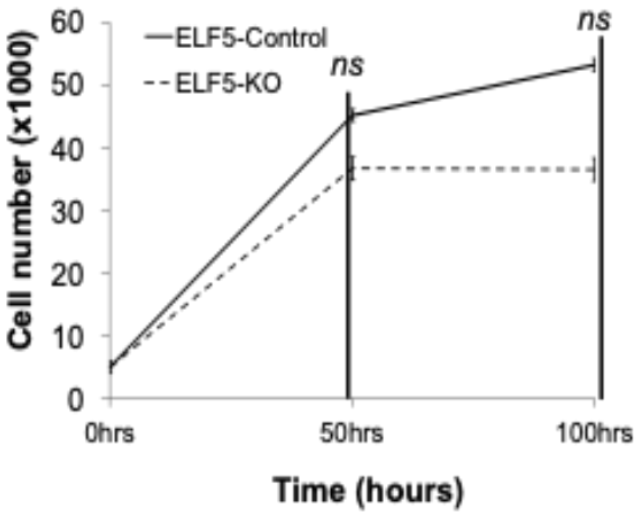

Figure 3.5: Cell growth curve for modified keratinocytes.

Total cell counts of ELF5-Control and ELF5-KO (knockout) cell line overtime. Cell proliferation was assessed at different time points. No statistically significant difference in cell counts was observed between ELF5-Control and ELF5-KO (knockout) cells at 50 hours and 100 hours. Data are expressed as mean SEM ± from n=3 independent experiments.

3.2.4 MODULATION OF ELF5 IMPACTS CELL PROLIFERATION

To assess the impact of ELF5 on cell cycle genes, RT-qPCR analysis was conducted. We observed that loss of ELF5 expression in ELF5-KO cells leads to significantly increase in expression of proliferation markers, especially *CYCLIN D2* (*CCND2), CYCLIN D1 (CCND1)* and *CYCLIN E1 (CCNE1)* (*p value <0.01; ***p value <0.001) (Figure 3.6A). In addition, we also performed RT-qPCR in transiently transfected HaCaT cells and data here revealed a significant (**p<0.01, ***p<0.001) downregulation of cell cycle markers namely; CYCLIN DEPENDENT *16 (CDK16*), *CYCLIN D1* (*CCND1*), *CYCLIN B1* (*CCNB1*), *CYCLIN D1* (*CCND1*), *CYCLIN B2* (*CCNB2*), *CYCLIN E1* (*CCNE1*) and *CYCLIN DEPENDENT KINASE* (*CDK1*) respectively (Figure 3.6B).

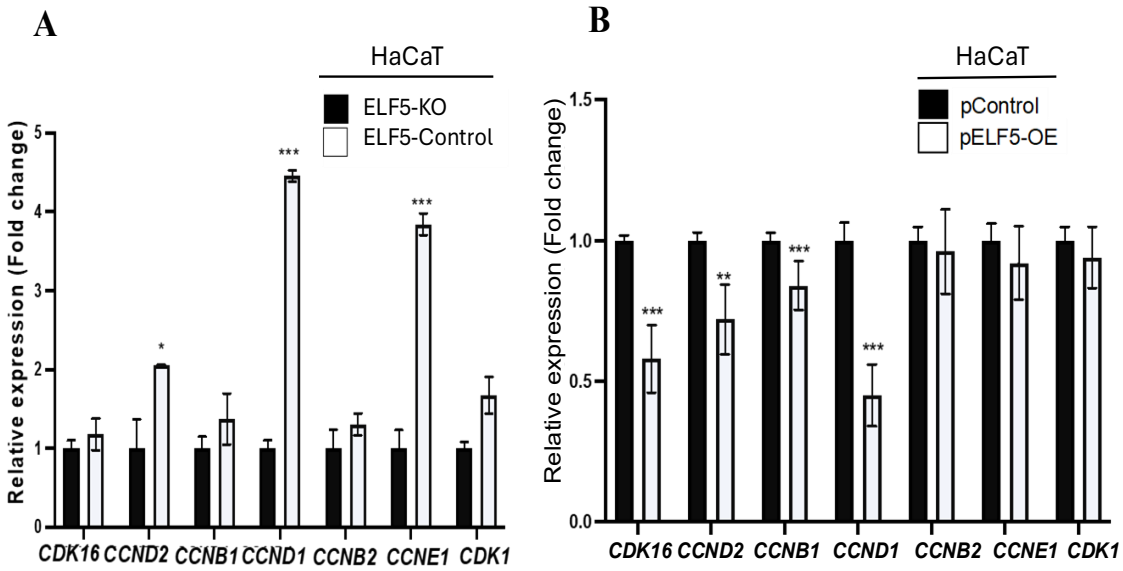

Figure 3.6: Modulation of ELF5 function impacts keratinocytes proliferation process in HaCaT cells.

(A–B) *RT-qPCR analysis of key cell cycle regulatory genes in keratinocytes following ELF5 modulation. Altered ELF5 expression, either through loss or overexpression, resulted in corresponding upregulation or downregulation of all assessed cell cycle genes. Data expressed as the mean ± SEM from n=3 technical replicates *p < 0.05, **p < 0.01, ***p < 0.001, unpaired Student's t-test.*

3.2.5 MODULATION OF ELF5 IMPACTS CELL PROLIFERATION IN CANCEROUS CELL LINES-A431 & SCC-9

As we observed that ELF5 does have an impact on the cellular processes of HaCaT cell, we went further to investigate if by transiently overexpressing *ELF5* in A431 and SCC-9 cell leads to see any impact proliferation abilities of these cells. *CDK16, CCND2, CCNB1, CCND1, CCNB2, CCNE1* and *CDK1* were significantly decreased (****p*<0.001) and showed reduced expression compared to control (Figure 3.7A). Additionally, in SCC-9 ELF5 overexpression leads to significant downregulation of *CDK16, CCND2*, *CCNB1* and, *CCND1* (Figure 3.7B). In both cases, overexpression of ELF5 led to significant downregulation of the majority of the proliferation markers compared to the controls suggesting an inhibition in cell growth.

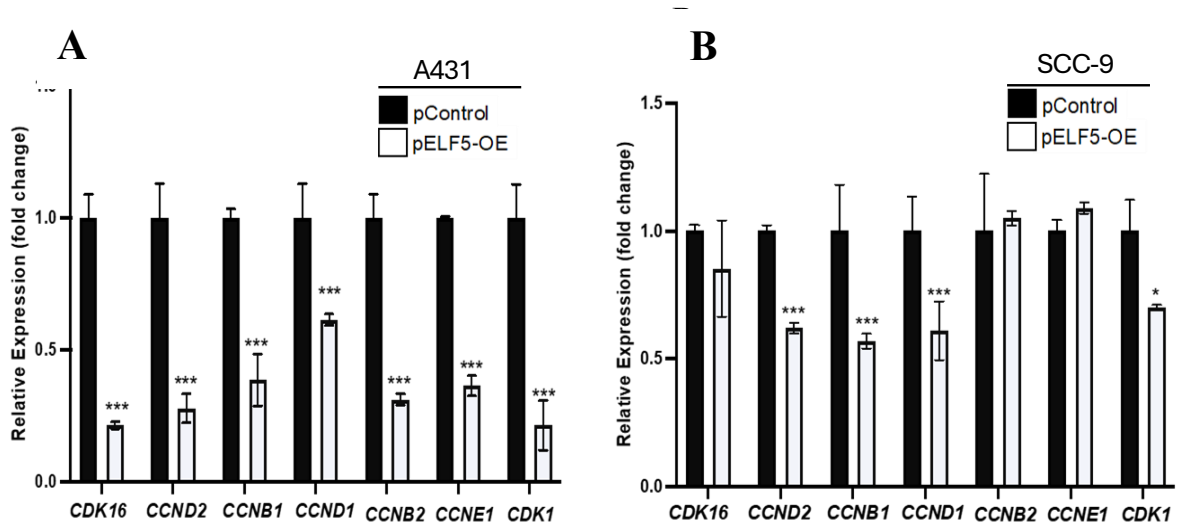

Figure 3.7: ELF5 overexpression impacts keratinocytes proliferation process in cancer cell lines A431 and SCC-9.

*(**A-B**) Quantitative RT-PCR profiling of cell cycle genes in A431 and SCC-9 showing pELF5-OE (overexpression) inhibits the upregulation in expression for all cell cycles markers with corresponding pControl cell lines. Data are reexpressed as ± SEM values from n=3 technical replicates. *p<0.01, **p<0.01, ***p<0.001 analysed by unpaired Student's t-test.*

3.2.6 MODULATION OF ELF5 EXPRESSION IN CELL CYCLE IN HaCaT CELLS

To further investigate ELF5's potential involvement in cell cycle regulation, flow cytometry analysis was performed using propidium iodide (PI) staining. The Figure 3.8 shows three histograms representing the cell cycle distribution of cells under three different experimental conditions: ELF5-Control, ELF5-KO and transiently overexpression of ELF5 in HaCaT cells (pELF5-OE). Flow cytometry with PI staining used to determine cell cycle phases. In control conditions, the distribution showed a relatively balanced cell cycle, with a significant portion of cells 27.3% in G0/G1 (resting or preparing for DNA replication), 13.98% in S phase (actively replicating DNA) and 13.23% in G2/M (preparing for or undergoing division). In ELF5-KO, compared to control there's a decrease in the G0/G1 phase (18% vs 27.3%) and a slight increase in the S phase (16% vs 13.98%). For pELF5-OE showed a dramatic increase in the G0/G1 phase (82% vs 27.3%) in ELF5-Control) and a sharp decrease in the G2/M phase (3% vs 13.23% in control).

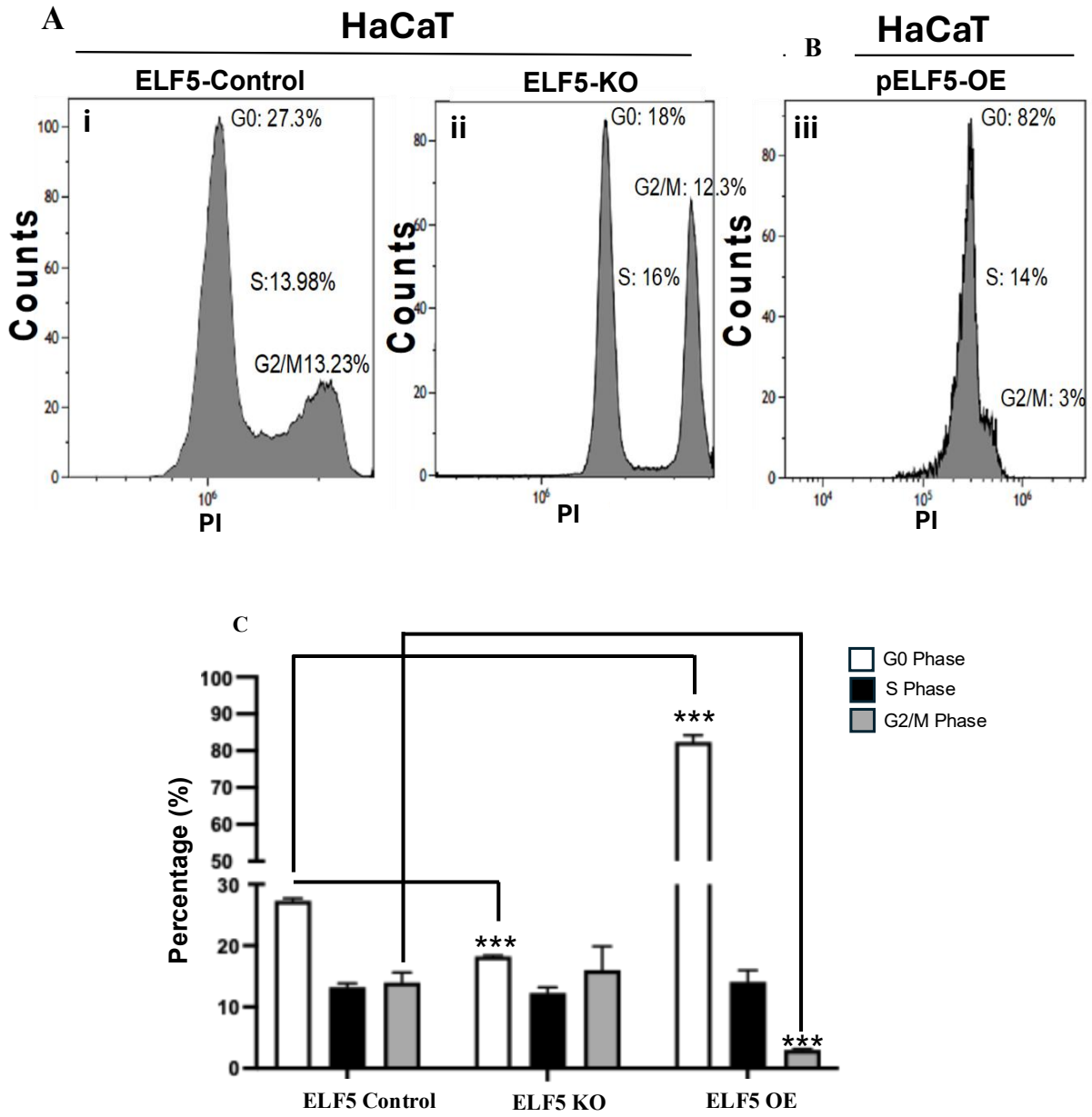

Figure 3.8: Modulation of ELF5 function impacts keratinocytes proliferation process in HaCaT cell line.

A. *Flow cytometric analysis of (i) ELF5-Control, (ii)ELF5- KO (knockout) and(iii) pELF5-OE (overexpression) by propidium iodide (PI) staining. In ELF5-KO suggests that loss of ELF5 may push more cells to S phase compared to ELF5-Control.* ***B.*** *In pELF5-OE, it causes a significant arrest or accumulation of cells in the G0/G1 phase, preventing them from progressing into S and G2/M phases compared to controls. Histograms shown are illustrative from a single experiment. Cell cycle stage distributions are expressed as mean values derived from three separate experiments n=3 technical repeats, each analysing 10,000 events.* ***C.*** *Bar graph showing the percentage of cells in G0/G1, S, and*

*G2/M phases following ELF5 modulation, determined by DNA-content flow cytometry.; data represent mean ± SEM, ***P < 0.001.*

3.2.7 MODULATION OF ELF5 IN CELL CYCLE IN CANCEROUS CELL LINES A431 & SCC-9

We wanted to determine if ELF5 overexpression had any impact on cell cycle distribution in both our cancer cell lines. Flow cytometry was performed using propidium Iodide (PI) staining. This analysis provided an understanding of ELF5 influence on cell cycle progression. In A431 control flow histograms most cells (84%) are in the G0/G1 phase, indicating a quiescent or early cell cycle profile. Only a small proportion are in S phase (8%) and G2/M (7%), reflecting limited proliferation under control conditions (Figure 3.9Ai). On contrary, there is a dramatic shift in cell cycle distribution in A431 overexpression, with a substantial decrease in G0/G1 population (to 37%) and a pronounced increase in S phase (29%) and G2/M phase (32%) populations suggesting active cycling in A431 cancer cell line (Figure 3.9Aii). On other hand, SCC-9 cell line shows moderate proliferative activity, with 68% of cells in G0/G1, and 23% in G2/M, suggesting ongoing mitotic activity. S phase remains low at 9% (Figure 3.9Bi). In overexpression state G/G1 population slightly decreases (to 58%), S phase increases significantly to 30%, while G2/M drops to 10%. This suggest that ELF5 overexpression blocks G2/M transition as indicated by the increased number of cells in S phase (Figure 3.9Bii).

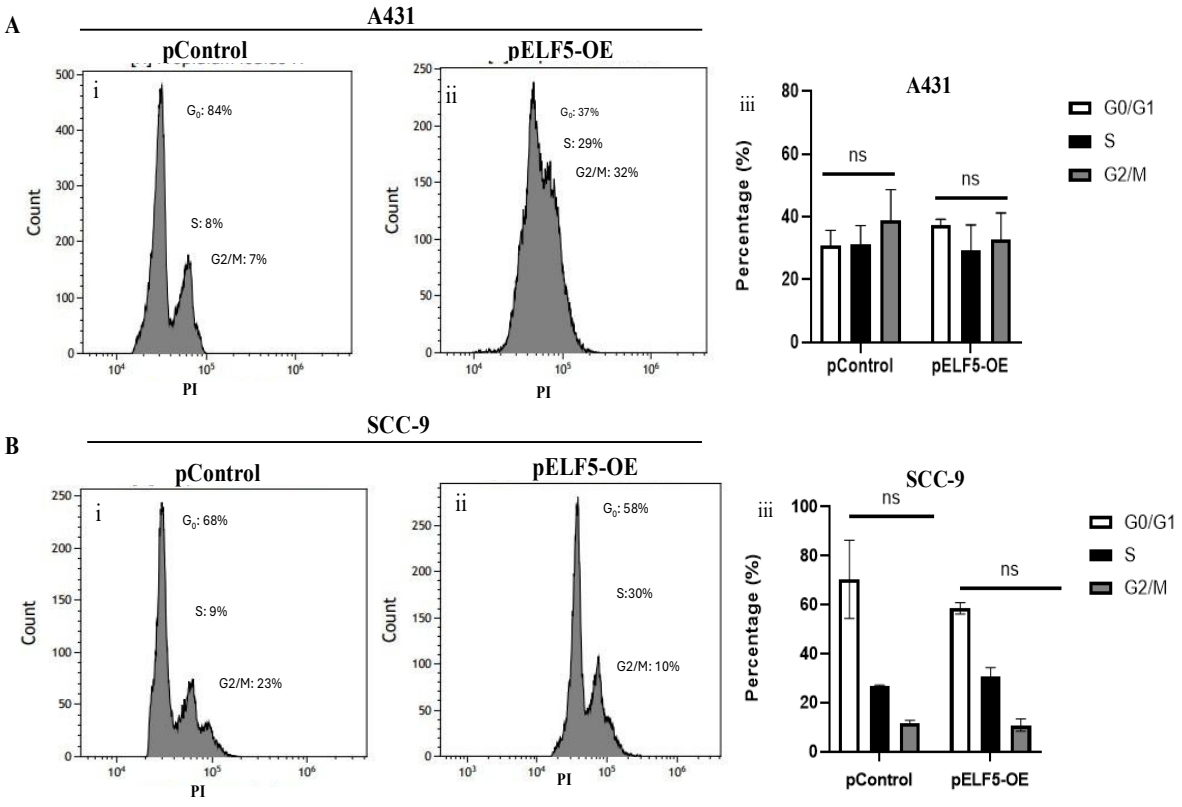

Figure 3.9: **ELF5 overexpression impacts proliferation process in cancer cell lines A431 and SCC-9.**

(A-B). *pELF5-OE (overexpression) alters cell cycle distribution in A431 cancer cell line.* ***(i-ii)*** *pELF5-OE led to a moderate decrease in G0/G1 phase and a marked increase in S phase, with a reduction in G2/M phase, suggesting enhanced S-phase entry but altered G2/M dynamics* ***(A-B iii)*** *Bar charts represents percentages of cells in G0/G1, S and G2/M phases are shown as mean ± SEM from three independent experiments where n=3 technical repeats. Statistical analysis showed all comparisons were non-significant (ns). Graphs shown are illustrative from a single experiment. Cell cycle stage distributions are expressed as mean values derived from three separate experiments, each analysing 10,000 events.*

3.2.8 MODULATION OF ELF5 IN CELL MIGRATION IN HaCaT CELLS

To check the migratory properties of HaCaT-ELF5-KO (knockout) and HaCaT pELF5-OE (overexpression), scratch assay was performed. The results showed significant increase in migration (*p<0.01) when ELF5 is loss compared to ELF5-Control (Figure 3.10A). Whereas

when we transiently overexpressed *ELF5* in HaCaT cells (pELF5-OE) we observed the opposite effect where cells showed significantly (***p<0.001) decreased migration compared to pControl (Figure 3.10B).

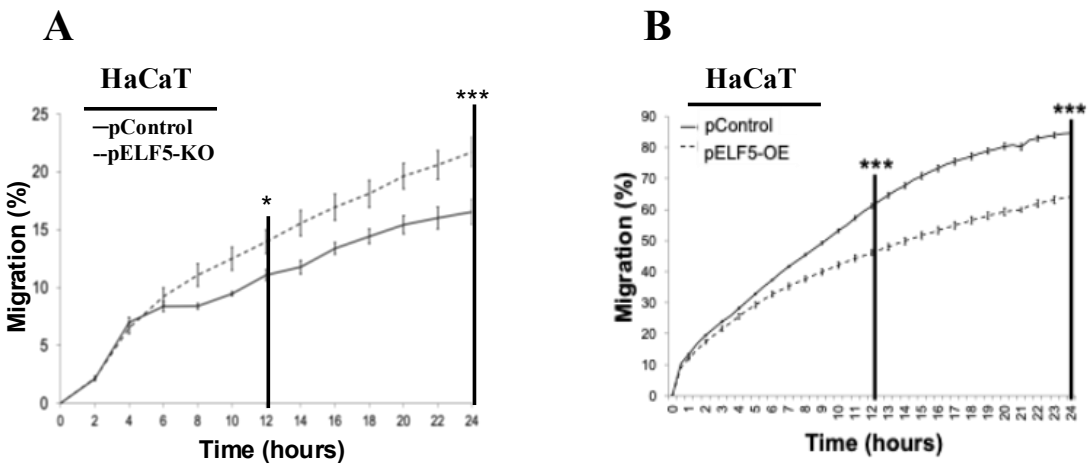

Figure 3.10: Modulation of ELF5 functions impacts migration process in HaCaT cell line.

A. *Using 2D Scratch assay analysis of ELF5-Control and ELF5-KO cell lines we observed the loss of ELF5 leads to significant increase migration ability of cells compared to its corresponding ELF5-Control cells.* ***B.*** *Scratch assay analysis in ELF5 overexpression (pELF5-OE) cells and control (pControl) cells shows a significant decrease in migration ability of cells compared to its corresponding pControl cells. Data reexpressed as n=5 scratches per group. *p<0.01, ***p<0.001; unpaired Student t-test.*

3.2.9 MODULATION OF ELF5 IN CELL MIGRATION IN CANCEROUS CELL LINES A431 & SCC-9

To check the migratory property in cancerous cell lines scratch assay was performed. Our data showed that after overexpression of ELF5 leads to a decrease in cell migration in A431 with no significance at 12 hours, but it shows significant at 24 hours (**p<0.001) (Figure 3.11A). Additionally, in SCC-9, expression of ELF5 cells showed a significant decrease in migration (***p<0.001) compared to control cells at 12- and 24-hours' time points (Figure 3.11B).

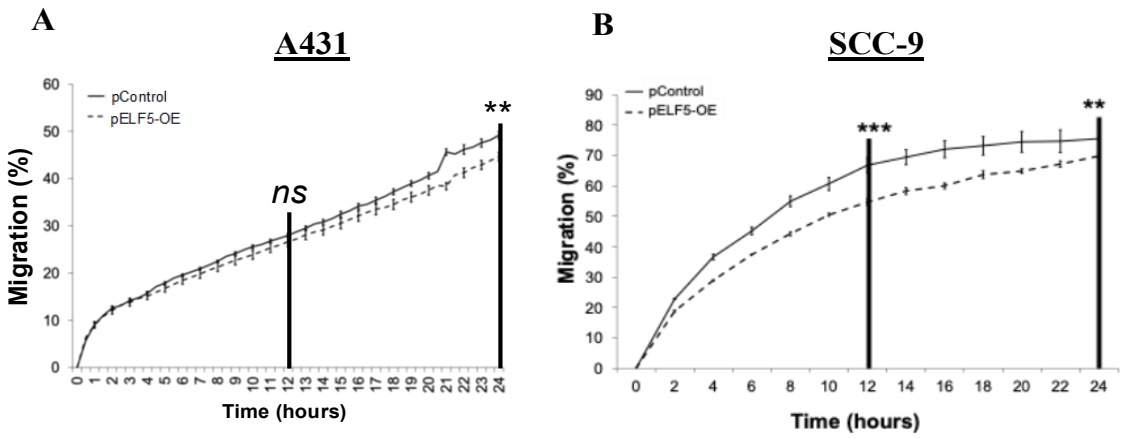

Figure 3. 11: ELF5 overexpression (OE) impacts migration in cancer cell lines A431 and SCC-9.

(A-B) *Using 2D Scratch assay analysis we observed that overexpression of ELF5 (pELF5-OE) in A431 and SCC-9 leads to reduced cell migration compared to corresponding controls (pControl). Data are expressed as n=5 scratches per group **p<0.01, ***p<0.001, ns-not significant; unpaired Student's t-test.*

3.2.10 LOSS OF ELF5 IMPACTS DIFFERENTIATION PROCESS IN HaCaT CELL LINE

Subsequently, we investigated the role of the ELF5 during keratinocyte differentiation in ELF5-KO and ELF5-Control cell lines using calcium-induced differentiation *in vitro* assay overtime as described previously (Pickup et al., 2023; Hu et al., 2025). Calcium-induced differentiation using low (0.05mM) or high (1.8mM) calcium concentrations. RT-qPCR analysis revealed that *ELF5* expression at 72 hours was significantly elevated(***p<0.001) along with differentiation markers *CYTOKERATIN 1* (*KRT1*), *CYTOKERATIN 10* (*KRT10*) and *INVOLUCRIN (Invol*) respectively (*p<0.05, ***p<0.005, Figure 3.12A) in ELF5-Control. On contrary, in ELF5-KO, *ELF5* and differentiation markers showed downregulation, which was not significant (Figure 3.12B).

Furthermore, we analysed by western blot, the expression of KRT1 and ELF5, in our ELF5-Control and ELF5-KO cells. In ELF5-Control cells, we observed that ELF5 protein levels elevated during in keratinocyte differentiated (high calcium) overtime. Additionally, KRT1 protein expression was elevated overtime (Figure 3.12C). However, in ELF5-KO, cells were unable to differentiate properly, as seen by low expression of ELF5 and KRT1 overtime (Figure 3.12D). This data confirms ELF5 has an important role in the differentiation process of keratinocytes.

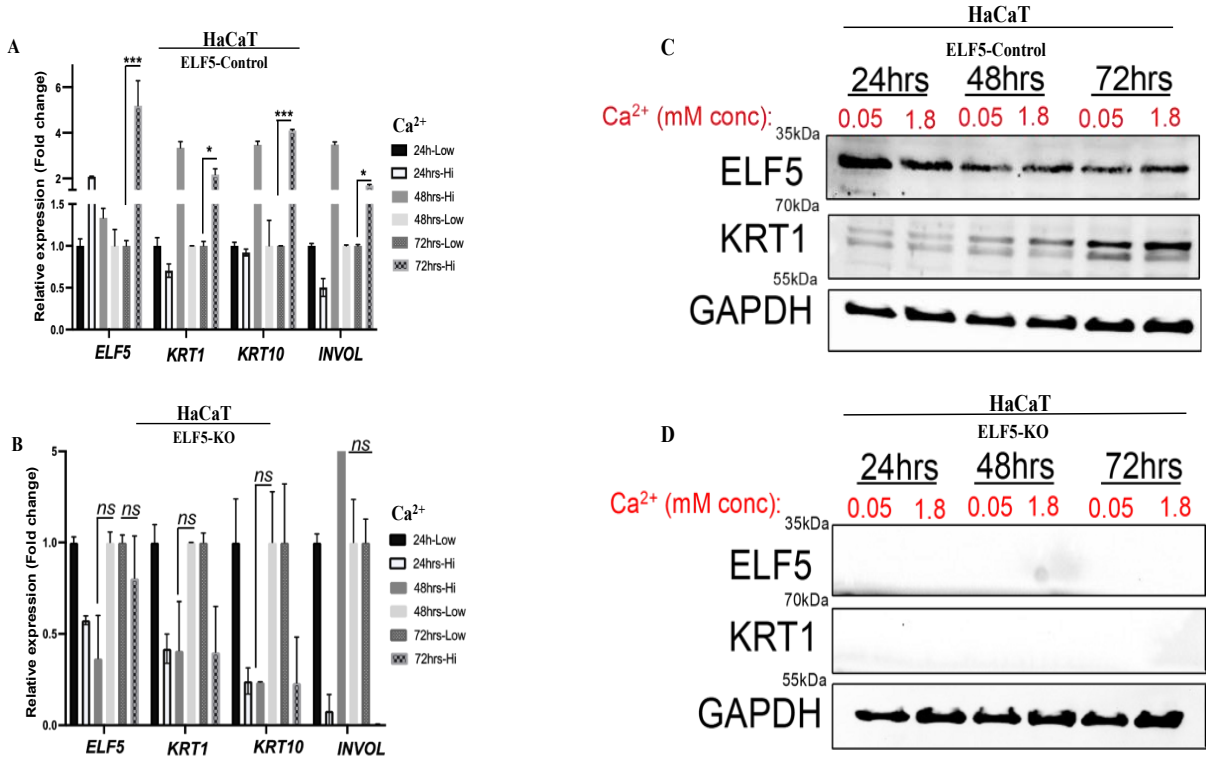

Figure 3.12: Loss of ELF5 function impacts differentiation process in HaCaT cell line.

(A-B) *RT-qPCR analysis during calcium ($Ca2^{+}$)-induced (low: 0.05 mM or high: 1.8 mM) keratinocyte differentiation in ELF5-knockout (ELF5-KO) (panel B) cells demonstrating that cells were unable to differentiate. While ELF5-Control cells were still able to differentiation as seen by increased expression of keratinocyte differentiation-associated markers Cytokeratin 1 (*KRT1*),* KRT10, *and INVOLUCRIN (*INVOL*) and* ELF5*, respectively (panel A). Data are expressed as mean ± SEM values from three*

*independent experiments. (**C-D**) Western blot analysis of ELF5 and Cytokeratin 1 (KRT1) during calcium-induced keratinocyte differentiation; consistent with RT-qPCR, ELF5 and KRT1 protein levels did not increase during calcium-induced differentiation of ELF5-KO cells (panel d) compared to ELF5-Controls cells overtime (panel C). Data shown are from a single illustrative experiment of n=3 experimental technical repeats. ns: not significant *p<0.05, ***p<0.001; unpaired Student's t-test.*

3.3. IDENTIFYING NOVEL TARGETS OF ELF5 IN HaCaT KERATINOCYTES

AIM: To identify and characterize novel transcriptional targets of the ELF5 in HaCaT keratinocytes through global gene expression profiling.

3.3.1 GLOBAL GENE EXPRESSION OF ELF5 IN KERATINOCYTES

The HaCaT keratinocytes that were transfected with either ELF5-KO (knockout) or ELF5-Controls were used for RNA-seq for the identification of the gene targets. Gene expression changes (both upregulation and downregulation) were visualized through a heat map and analysed for gene ontology using the Galaxy platform (https://usegalaxy.org/).The heat map depicts the changes following ELF5-KO and ELF5-Control. Green colour indicates higher expression, and red colour indicates lower expression of genes (Figure 3.13A). It is evident that there was a mix of both upregulated and downregulated genes. In gene ontology analysis we found that 595 genes were significantly differentially expressed with 179 genes being overexpressed and 416 genes being downregulated significantly (*p<0.01). Our Gene Ontology and differentially expressed gene analysis showed that majority of the genes that significantly changed belong to the “cell motility/migration,” “cell adhesion” and “cell differentiation” categories (Figure 3.13B).

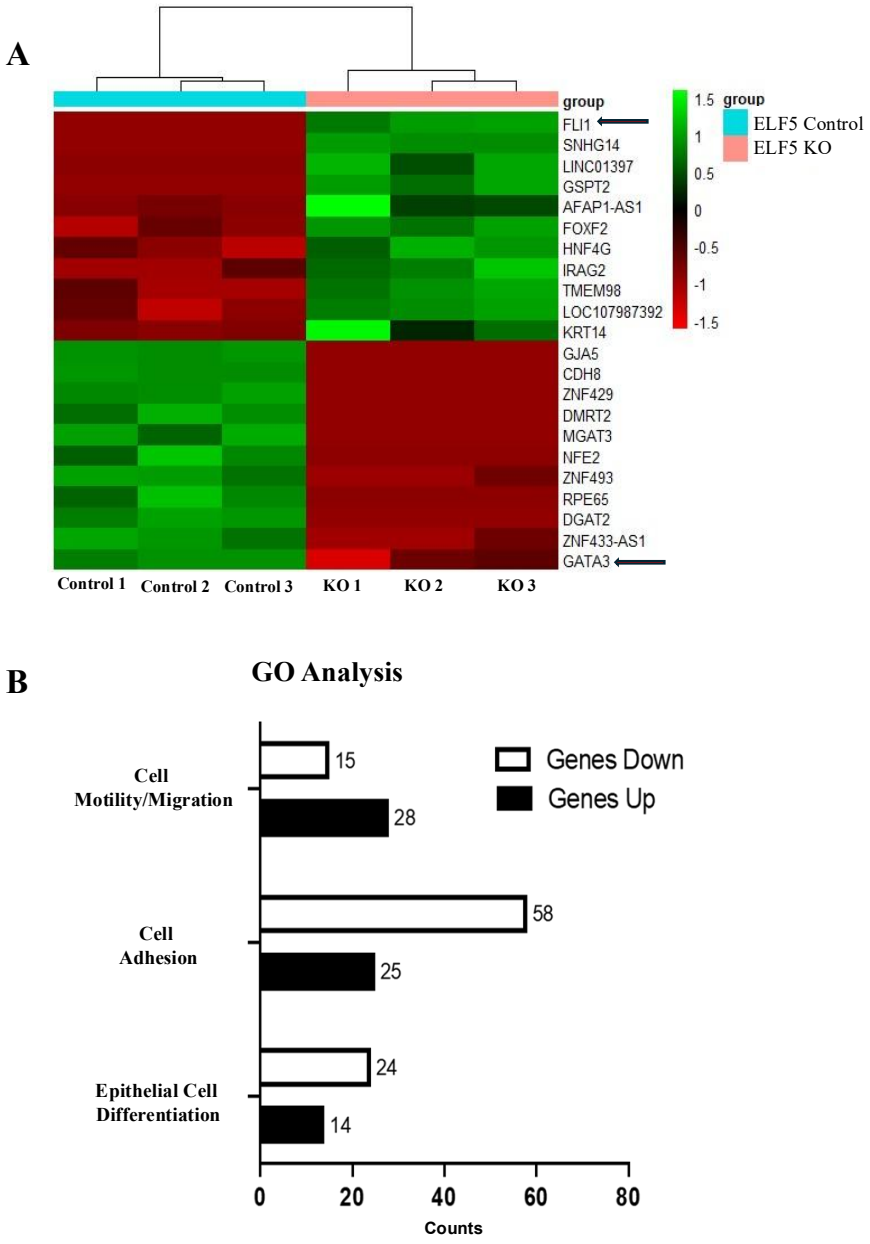

Figure 3.13: Global Gene Expression Analysis.

A. *Heatmap depicting significantly overexpressed and under expressed genes in ELF5-Controls compared to ELF5-KO samples. Red colour indicates reduction in gene expression and green indicates increase in gene expression compared to the average of all the samples.* ***B***. *Bar chart depicting the number of genes significantly up-down regulated using Gene Ontology (GO) pathways involved in cell differentiation, cell adhesion and cell migration/motility.*

3.3.2 DIFFERENTIAL GENE EXPRESSION ANALYSIS OF KERATINOCYTES AFTER LOSS OF ELF5

To normalise gene counts from RNA sequencing data of differentially expressed gene, Principal component assay (PCA) and volcano plot were generated (Figure 3.14A). In PCA plot, we observed 36.22% variance between ELF5-KO and ELF5-Control samples. The volcano plot complements the heatmap by showing genes that have statistically significant expression changes. volcano plot also confirmed large fold change which are statistically significant (*p<0.05) are caused by ELF5-Control compared to ELF5-KO samples. Genes that were not significant were excluded from further analyses (Figure 3.14B). Table 10 shows the most significantly upregulated and downregulated genes from RNA-seq analysis. The complete dataset, including gene identifiers, log2 fold change, adjusted P values (FDR), and expression counts, is provided as a separate Excel file submitted alongside this thesis. The file name is **Appendix table 7.11 full DEG list.xlsx**

Following the identification of target genes, GATA-3 and FLI-1 were selected as of GATA-3 is expressed in human keratinocytes and is crucial for keratinocyte differentiation and SC lineage determination for a healthy epidermal barrier (Zeitvogel et al., 2017). While in cancer, GATA-3 expression is decreased with cutaneous SCC progression (Solus et al., 2016). Other studies have shown that GATA-3 expression is associated with either survival advantage or disadvantage depending on the cancer type (Yang et al., 2021). In contrast, FLI-1 is a widely known oncogene contributing to various malignancies (Ben-David et al., 2022) and has no known role in keratinocytes or cSCC formation.

3.3.2.1 PATHWAY-LEVEL INTERPRETATION OF RNA-SEQ DATA FOLLOWING ELF5 LOSS

Signalling pathways were integrated into the RNA-seq narrative through a pathway-informed analysis of gene expression changes following ELF5 loss. Differentially expressed genes were examined using gene ontology and pathway enrichment analyses (Figure 3.13B), enabling transcriptomic alterations to be interpreted within the context of key signalling pathways outlined in the introduction, namely BMP, WNT, and FGF.

This analysis showed a significant downregulation of genes involved in epithelial differentiation and keratinocyte maturation, consistent with transcriptional programs associated with BMP-regulated differentiation. Conversely, upregulated gene sets were enriched for processes related to cell-cycle regulation and proliferation, which are commonly linked to WNT-associated proliferative programs (Figure 3.6, 3.8). The expression of canonical FGF ligands and receptors remained largely unchanged, enrichment of downstream transcriptional regulators indicated altered interpretation of FGF-dependent lineage cues at the transcriptional level.

A

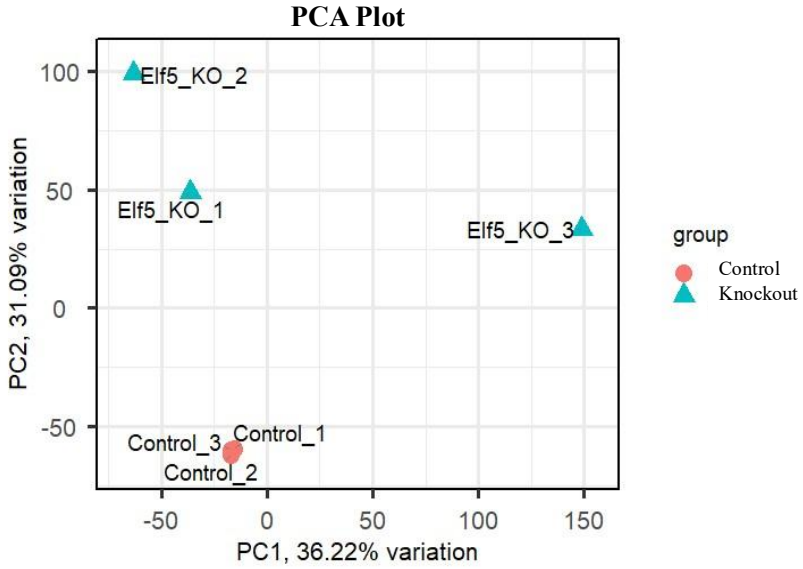

B

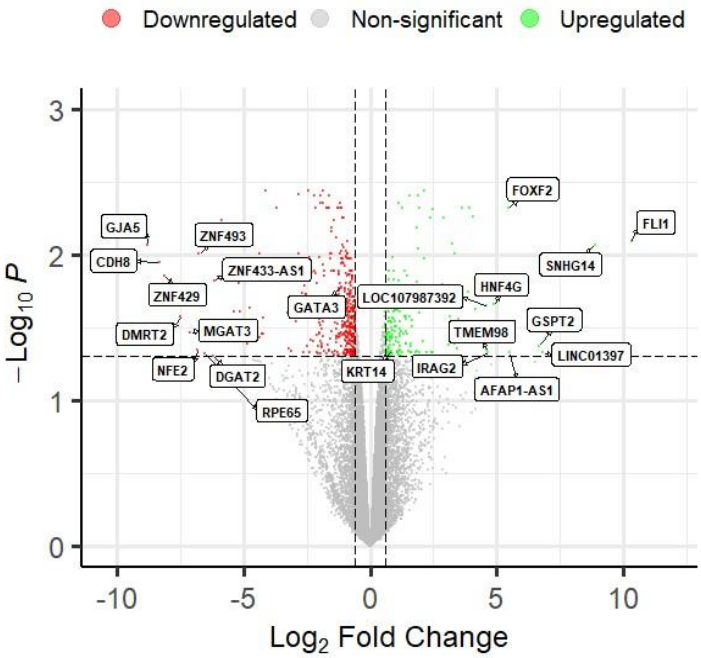

C

Table 10. *List of selected ELF5 gene targets*

Gene Name	Adjusted p value	Fold change
GATA-3	0.01968596	0.44895541
FLI-1	0.01669124	1277.48079

Figure 3.14: Global Gene Expression.

A. *PCA component analysis (PCA) depicting variance between ELF5-Control versus ELF5-KO (knockout) for principal component (PC) 1 and 2.* ***B***. *Volcano plot of differentially expressed genes between ELF5-Control versus ELF5-KO (knockout). Green coloured point are significantly upregulated genes; red coloured points are significantly downregulated genes.* ***C.*** *Table depicting GATA-3 and FLI-1 as the one of most significantly upregulated and downregulated genes.*

3.3.3 VALIDATION OF SELECTED TARGET GENES FROM RNA-SEQUENCING ANALYSIS

To validate the selected target genes, RT-qPCR was performed for ELF5-Control compared to ELF5-KO. *FLI-1* showed significantly higher expression (***$p<0.001$) in ELF5-KO samples and decreased expression in ELF5-Control samples suggesting upregulation due to loss of *ELF5*. While on the other hand *GATA3* shows significantly reduced in expression (Figure 3.15A) suggesting downregulation was due to loss of ELF5 knockout condition. Western blotting confirmed our RT-qPCR findings showing increased expression of FLI-1 in ELF5-KO and reduced GATA-3 expression in ELF5-KO compared to their corresponding ELF5-controls, respectively (Figure 3.15B).

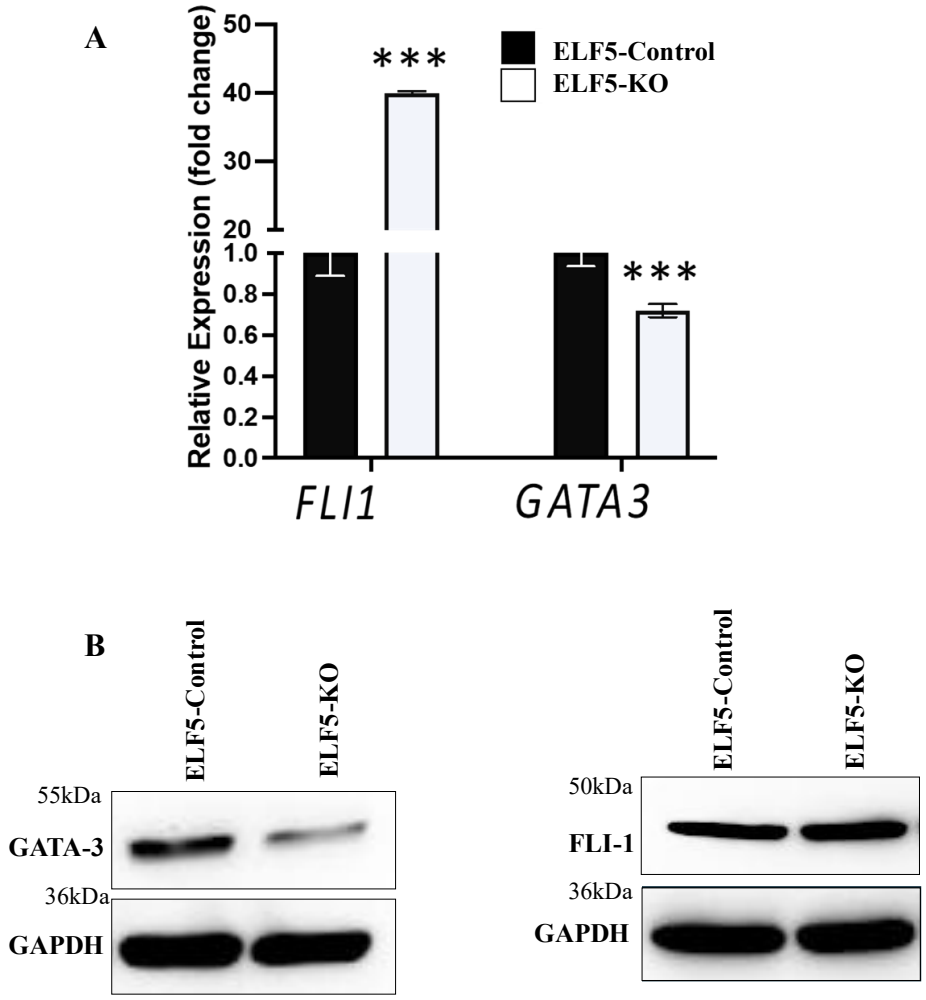

Figure 3.15: RNA sequencing target genes validation.

A. *Gene targets identified through RNA-sequencing were validated via RT-qPCR analysis GATA-3 and FLI-1 in ELF5-Control and ELF5-KO cells. Consistent with our RNA sequencing data, loss of ELF5 leads to an increase in the expression of FLI-1 and decrease in expression for GATA-3 compared to ELF5-Control cells, respectively. Data are expressed as mean ± SEM values from three independent experiments.* ***B****. Western blot analysis: consistent with our RT-qPCR, loss of ELF5 activity leads to an increase and/or a decrease in protein levels of FLI-1 and GATA-3, respectively. Data shown are from a single illustrative experiment from n=3 technical replicates. SEM ± values, ***p<0.005).*

3.3.4 FLI-1 AND GATA-3 EXPRESSION ANALYSIS IN HEALTHY SKIN TISSUE *VS* CSCC TISSUE

To assess if GATA-3 and FLI-1 expression was deregulated in healthy skin tissue compared to cSCC tissue, we performed RT-qPCR analysis using total RNA extracted from healthy human skin and cSCC tissue and we observed that FLI-1 expression was elevated in cSCC tissue compared to healthy skin tissue, whereas GATA-3 expression was reduced in cSCC tissue compared to healthy tissue(Figure 3.16).

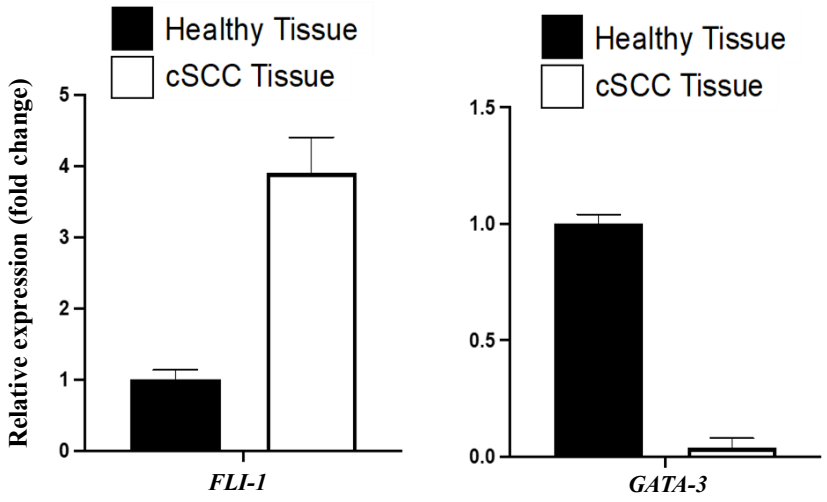

Figure 3.16: Expressional analysis of FLI-1 and GATA-3 in healthy human and cSCC skin samples.

RT-qPCR analysis of FLI-1 and GATA-3 in healthy human tissue compared to cSCC tissue biopsies showed that FLI-1 expression is elevated in cSCC tissue compared to healthy human tissue, conversely, GATA-3 is substantially reduced in cSSC tissue compared to healthy human tissue. n=2 biological samples per tissue.

3.3.5 IDENTIFICATION IF GATA-3 AND FLI-1 ARE DIRECT TARGETS OF ELF5

In addition, we utilized transiently overexpressed *ELF5* (pELF5-OE) in HaCaT cells and via RT-qPCR we observed a significant reduction in expression of *FLI-1* (***$p<0.001$) compared to control cells (pControl). While *GATA-3* expression was also significantly reduced after

ELF5 overexpression compared to control cells (***p<0.001) (Figure 3.17A). Furthermore, protein analysis after ELF5 overexpression in HaCaT cells also results in reduced protein levels of FLI-1 and GATA-3 compared to control cells (Figure 3.17B).

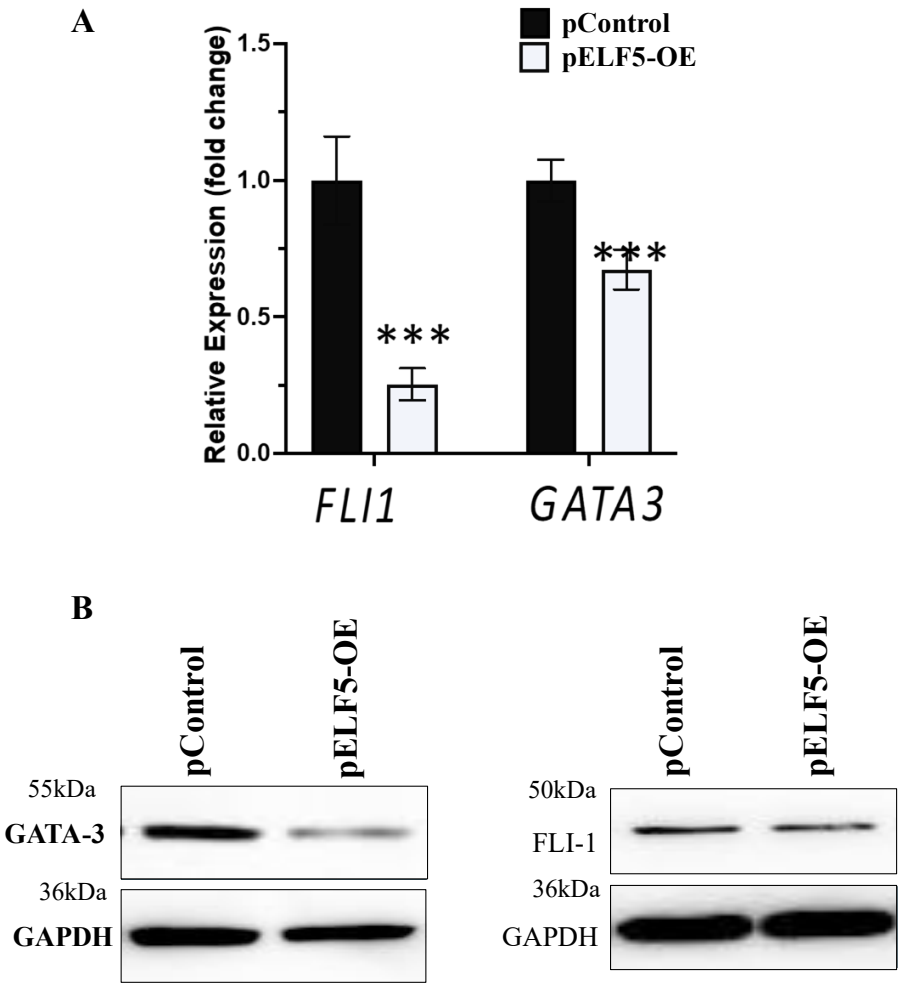

Figure 3.17: GATA-3 and FLI-1 are direct targets of ELF5 in keratinocytes.

A. *RT-qPCR analysis overexpression of pELF5-OE (overexpression) leads to a significant reduction in expression of FLI-1 and GATA-3 compared to their corresponding controls (pControl).* ***B.*** *Protein analysis of both FLI-1 and GATA-3 showed decreased expression in pELF5-OE (overexpression) cells compared to pControl cells. Data are reexpressed as mean ± SEM values from three experimental repeats per group. ***p<0.001. WB Images are illustrative of n=3 technical repeats per treatment.*

3.3.6 IDENTIFICATION OF FLI-1 AND GATA-3 AS DIRECT TARGETS OF ELF5 BY LUCIFERASE REPORTER ASSAY

To confirm that FLI-1 and GATA-3 are indeed direct targets of ELF5, we utilized a dual luciferase reporter assay. Reporter constructs containing ELF5 binding sites in the promoter regions of GATA-3 and FLI-1 were cloned into pGL3 basic plasmid and transfected into HaCaT cells. The data revealed, ELF5 overexpression (pELF5-OE) significantly reduces the activity of both GATA-3 and FLI-1 promoters, as indicated by the reduced luciferase signal (*p<0.01) compared to control groups (Figure 3.18), suggesting that ELF5 does indeed directly regulates both GATA-3 and FLI-1 activities in keratinocytes.

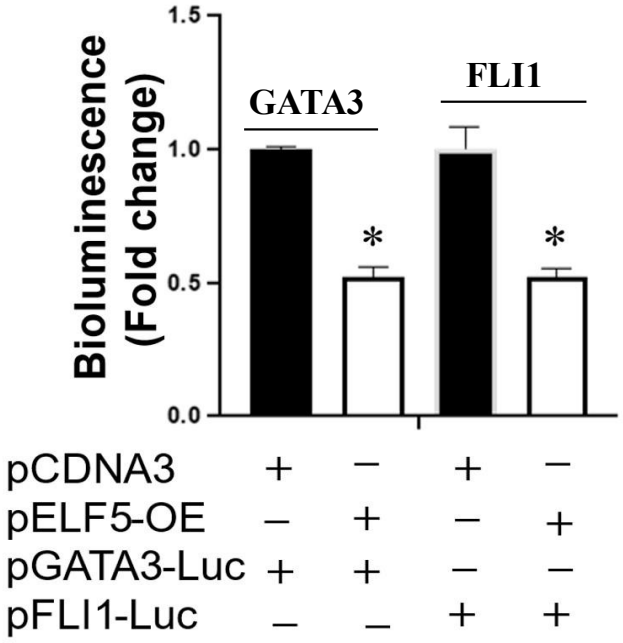

Figure 3.18: Luciferase Reporter Assay.

HaCaT cells were co-transfected with FLI-1 and GATA-3 promoter reporter constructs and either a pGL3-based reporter vector or the pCDNA3 empty control. Significant decrease in the pGATA-3-Luc or pFLI-1-Luc activities was observed in presence of ELF5-ovexpression (pELF5-OE) compared to control groups (pCDNA3). Bioluminescence was measured as an indicator of transcriptional activity,

*Data are expressed as mean ± SEM values from three experimental repeats: *p<0.01, unpaired Student's t-test.*

3.4. GATA-3 AND FLI-1 NOVEL TARGETS OF KERATINOCYTES

AIM: To isolate, characterize and validate GATA-3 and FLI-1 as novel transcriptional targets of ELF5 using fluorescence-activated cell sorting (FACS) and functional assays.

3.4.1 WORKFLOW DEPICTING FACS SORTING OF KERATINOCYTES

To determine if the effects observed in ELF5-KO cell are in part due to deregulation of GATA-3 and FLI-1 gene expressions in keratinocytes, we subsequent performed rescue and knockdown experiments where GATA-3 was re-expressed and FLI-1 was knockdown in ELF5-KO cells. We first transduced our ELF5 knockout (ELF5-KO) cells using lentivirals with each construct containing a fluorescent reporter (e.g., GFP/RFP) to facilitate selection and downstream tracking. Three constructs were introduced to our ELF5-KO cells: GATA-3 overexpression (GATA-OE-GFP+), short-hairpin RNA-mediated knockdown of FLI-1 (shFLI-1-GFP+) and Control RFP+ (Figure 3.19A). Following expansion and confirmation of transduction, fluorescence-activated cell sorting (FACS) was carried out using the BD FACS Melody™ Cell Sorter, a high-precision benchtop instrument designed for sorting and isolating live cells based on fluorescence intensity (Figure 3.19B). Sorted cells expressing the fluorescent marker were then immediately plated into fresh culture and monitored for growth and behaviour using the Incucyte® Live-Cell Imaging System. The presence of fluorescent signal in culture post-sorting three days confirmed successful enrichment of transduced cells (Figure 3.19C).

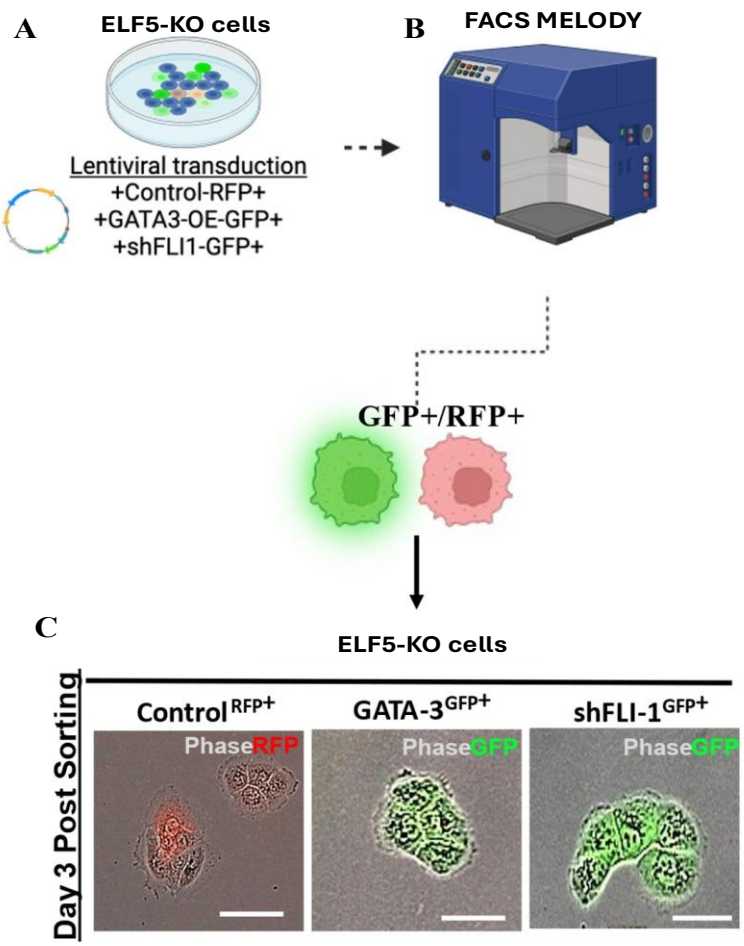

Figure 3.19: FACS Isolation.

A. *Keratinocytes were transduced with lentiviral tagged control RFP+, GATA3-OE-GFP+ and shFLI1-GFP+ for ELF5-KO and ELF5-Controls respectively.* ***B.*** *Keratinocytes tagged GFP+/RFP+ were sorted with FACS Melody and expanded.* ***C.*** *Illustrative micrographs of the corresponding tagged keratinocytes three days post sorting, cells are still positive for RFP and GFP signals in culture (captured in Incucyte). Scale bar 50 µm.*

3.4.2 VALIDATION OF FACS SORTED KERATINOCYTES

While fluorescence-activated cell sorting (FACS) enables precise isolation based on specific markers, it is crucial to validate the sorted cells at both transcript and protein levels to confirm successful enrichment. In this study, we performed RT-qPCR and Western blotting to assess the expression of target genes GATA-3 and FLI-1 in two experimental conditions GATA-3

overexpression (GATA-3 OE) and FLI-1 knockdown (shFLI-1)- relative to ELF5 knockout (ELF5 KO) controls. In this study, we performed both RT-qPCR and immunoblotting to confirm the gene and protein expression profiles of the sorted populations. RT-qPCR analysis revealed a highly significant (***$p < 0.001$) upregulation of ELF5-KO-GATA-3-OE^{GFP+} in the GATA-3 OE group, and a similarly significant (***$p < 0.001$) downregulation of ELF5-KO-shFLI-1^{GFP+} in the shFLI-1 group (Figure 3.20A). These findings were further supported by Western blot analysis, which confirmed corresponding changes at the protein level (Figure 3.20B). This dual-layered validation confirms the efficiency of the genetic manipulations and the integrity of the sorted populations. Together, these results underscore the importance of molecular validation post-FACS sorting to ensure the biological relevance and integrity of the experimental cell populations.

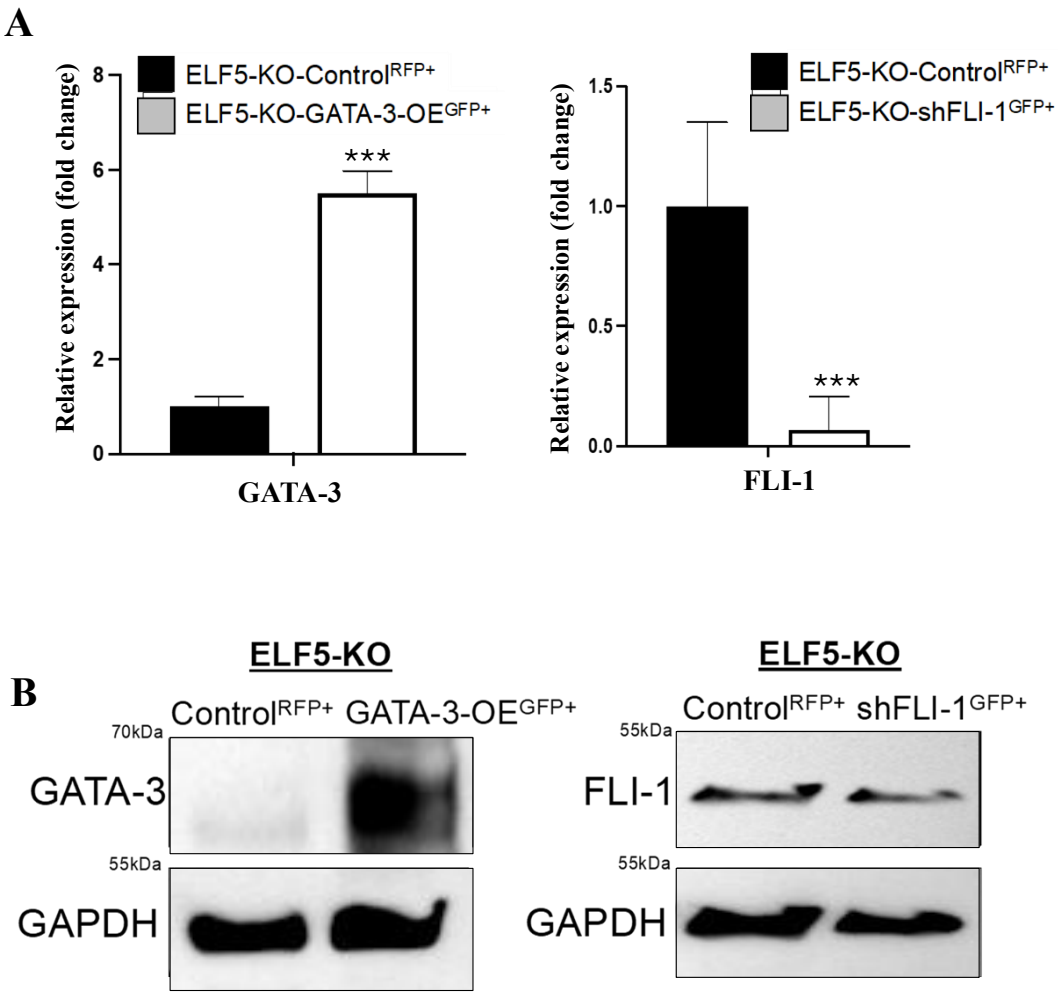

Figure 3.20: Validation of FACs sorted keratinocytes.

A. *RT-qPCR analysis for ELF5-KO-Control RFP+ compared to ELF5-KO-GATA-3-OE-GFP+ overexpression shows increased expression for GATA-3 OE compared to controls, whereas ELF5-KO-shFLI1-GFP+ shows significantly reduced expression for shFLI-1.* ***B.*** *Western blotting analysis of GFP+/RFP+ GATA-3 OE and control shows strong expression for GATA-3 OE protein compared to control, whereas FLI-1 shows reduced expression compared to controls. RT-qPCR data are expressed as mean ± SEM values from n=3 technical experimental repeats per group. Western blot data shown are from a single illustrative experiment from three independent experiments. ***p<0.001.*

3.4.3 OVEREXPRESSION OF GATA-3 EXPRESSION RESCUES POTENTIAL OF KERATINOCYTES TO UNDERGO DIFFERENTIATION

Next, we assessed the ability of ELF5-KO-GATA-3-OE^{GFP+}to differentiate after the re-expression of GATA-3 during calcium induced keratinocyte differentiation, *in vitro* via RT-qPCR and western blotting. In RT-qPCR we observed that ELF5-KO-GATA-3-OE^{GFP+} cells were able to re-differentiate as seen by elevated transcript expression of differentiation markers *CYTOKERATIN 1 (KRT1), CYTOKERATIN 10 (KRT10) and INVOLUCRIN (INVOL)(*p* value <0.01; ***p* value <0.01; ****p* value <0.001) (Figure 3.21A). The data from the western blot revealed a progressive increase in protein expression of *CYTOKERATIN (KRT1)* overtime under both low and high calcium conditions overtime. At 24 and 48 hours, expression levels were reduced compared to low calcium treated ELF5-KO-GATA-3-OE^{GFP+} however at 72 hours the protein expression levels were generally more pronounced in both calcium conditions, indicating that calcium concentrations overtime may enhance the transcriptional or post-translational regulation during differentiation (Figure 3.21B).

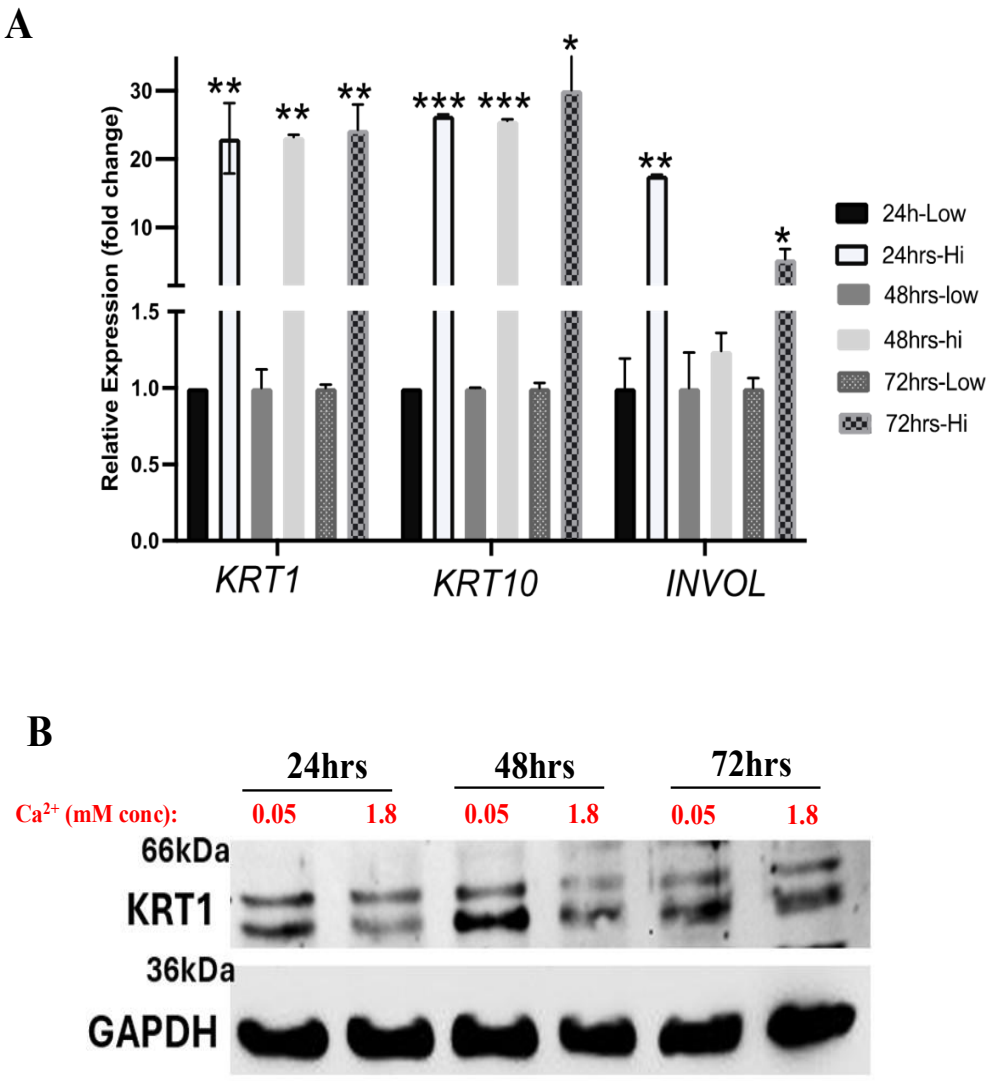

Figure 3.21: Modulation of GATA-3 and FLI-1 in ELF5-KO keratinocyte differentiation.

A. *RT-qPCR analysis in ELF5-KO-GATA-3-OE^{GFP+} show significant expression of CYTOKERATIN 1 (KRT1), KRT10 and INVOLUCRIN (INVOL), during the differentiation process.* ***B****. Western blot analysis of ELF5-KO-GATA-3-OE^{GFP+} cells during calcium induced keratinocyte differentiation (low: 0.05mM; high: 1.8mM); increase in GATA-3 expression rescues the ability of ELF5-KO cells to re-differentiate as seen by re-expression of CYTOKERATIN 1 (KRT1) differentiation marker. RT-qPCR data are reexpressed as mean ± SEM values from three experimental repeats per group. WB data shown are from a single illustrative experiment from three independent experiments, n=3 technical replicates, *p<0.01, **p<0.005, ***p<0.001.*

3.4.4 CELL MIGRATION ANALYSIS OF ELF5-KO KERATINOCYTES AFTER MODULATION OF GATA-3 AND FLI-1

We then assessed the migratory abilities of ELF5-KO-GATA-3-OE^{GFP+} and ELF5-KO-shFLI-1^{GFP+} cells. We observed that both loss of FLI-1 and overexpression of GATA-3, significantly inhibited the migratory abilities of cells compared to ELF5-KO cells overtime (**p value <0.01; ***p value <0.001). Cells subjected to the ELF5-KO-Control^{RFP+} condition exhibited accelerated migration (Figure 3.22). A significant reduction in wound width was documented overtime, signifying a pronounced intrinsic migratory capacity.

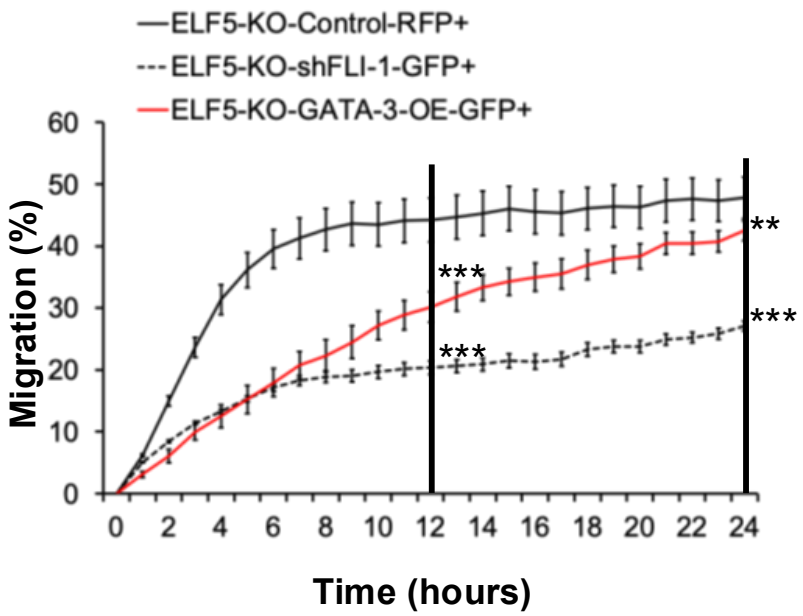

Figure 3.22: Modulation of GATA3 and FLI1 expression inhibits migration of keratinocytes.

*2D Scratch assay analysis of lentiviral transduced ELF5-KO-GATA-3-OE^{GFP+}, ELF5-KO-shFLI-1^{GFP+} compared to ELF5-KO-Control^{RFP+} cells showed significantly reduced migration compared to ELF5-KO-Control^{RFP+} cells over the period of 24 hours. n= 5 technical experimental groups per treatment, unpaired Student t-test; *p<0.01.*

3.4.5 INVASION ABILITIES OF KERATINOCYTES AFTER LOSING ELF5

Next, we assessed the invasion capabilities of ELF5-KO cells. We observed that a significant number of cells were able to invade in ELF5-KO cells (Figure 3.23B) compared to ELF5-Control cells (Figure 3.23A). The bar graph depicts the significant number of cells were invaded in ELF5-KO keratinocytes (*p value <0.05) (Figure 6.5C)

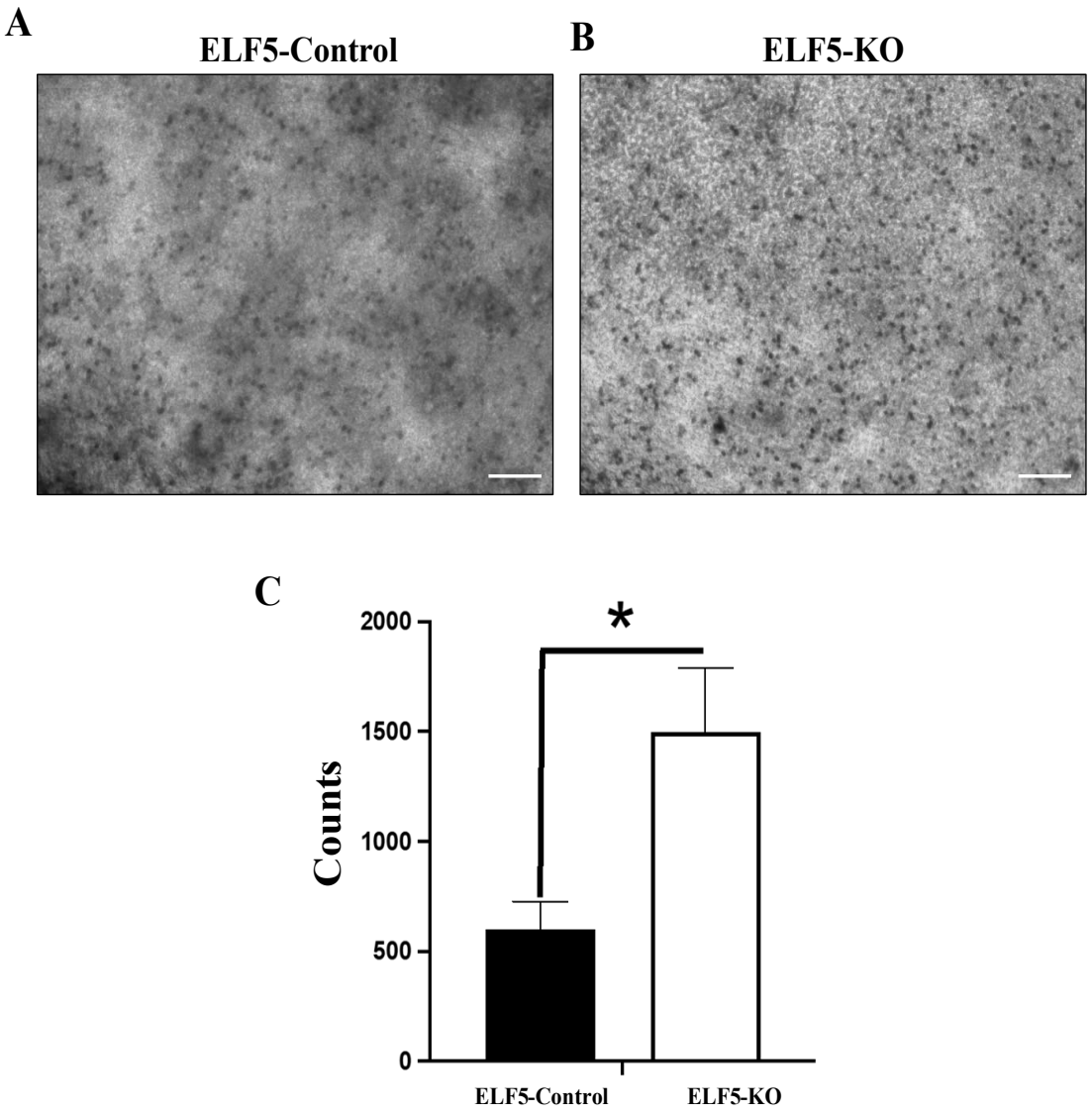

Figure 3.23: Invasion analysis of keratinocytes after loss of *ELF5*.

(A-B). *Illustrative images of ELF5-knockout (ELF5-KO) show a greater number of cells invades compared to ELF5-control cells.* ***C****. Bar graph showing the significant number of cells invading in ELF5-KO compared to ELF5-control wells. Data are reexpressed as mean ± SEM values from n=3 technical repeats per group. *p<0.01. Scale bar 100um.*

3.4.6 INVASION ABILITIES OF KERATINOCYTES AFTER MODULATION OF GATA-3 AND FLI-1

In addition, to further evaluate the effect of GATA-3 overexpression and FLI-1 knockdown on the invasive behaviour of keratinocytes, a Matrigel-based transwell invasion assay was performed. We observed that ELF5-KO-control-RFP+ cells displayed a significantly high number of invading cells, consistent with a more aggressive phenotype (Figure 3.24A). In contrast, both ELF5-KO-GATA-3-OE^{GFP+} and ELF5-KO-shFLI-1^{GFP+} cells showed a significant reduction in invasive capacity (Figure 3.24B-C), indicating that modulation of these transcription factors impairs invasive potential of keratinocytes. (**p* value <0.01; ***p* value <0.01) (Figure 3.24D).

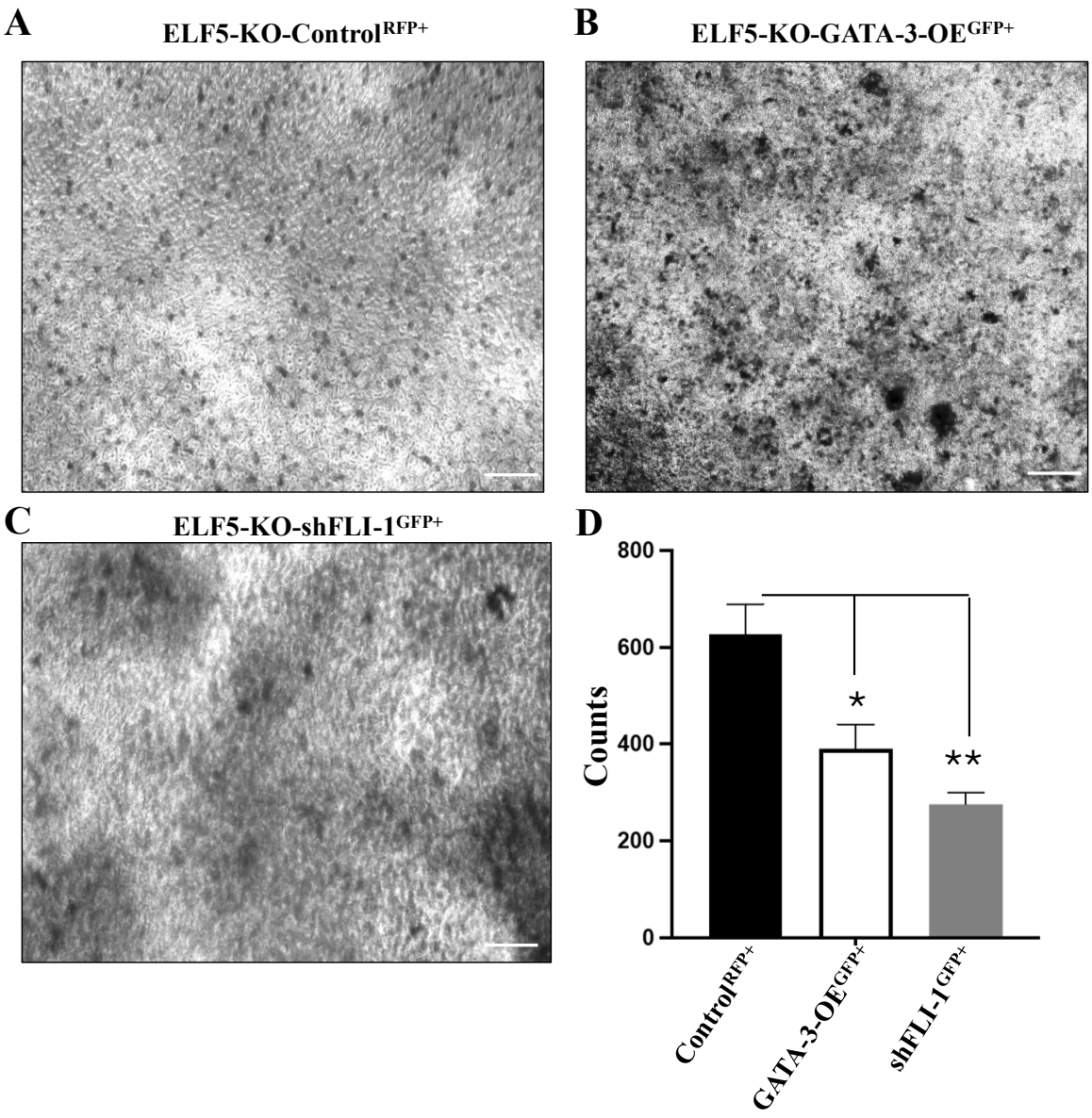

Figure 3.24: Invasion of keratinocytes after modulation of GATA-3 and FLI-1.

(A-C) *Illustrative images of ELF5-KO-GATA-3-OE GFP+ and ELF5-KO-shFLI-1 GFP+ show lower number of cells invading compared to ELF5-KO-control RFP+ cells.* ***D****. Bar graph showing the significant reduced number of cells invading in GATA-3-OE GFP+ and shFLI-1-GFP+ compared to control-RFP+. Data are reexpressed as mean ± SEM values from n=3 technical repeats per group, *p<0.01, **p<0.001). Scale bar 100um.*

3.4.7 MODULATION OF GATA-3 AND FLI-1 IN TUMOURIGENICITY OF KERATINOCYTES

Subsequently, to assess the impact of GATA-3 overexpression and FLI-1 knockdown on the tumourigenic potential of keratinocytes, a soft agar colony formation assay was performed. The ELF5-KO-GATA-3-OE-GFP+ and ELF5-KO-shFLI-1-GFP+ plates exhibited significantly reduced number of colonies ***$p<0.001$ (Figure 3.23B-D). However, ELF5-KO-Control-RFP+, cells formed many colonies, indicating a high capacity for anchorage-independent proliferation (Figure 3.23A). As both GATA-3 overexpressing and shFLI-1 cells exhibited a marked reduction in colony formation, suggests a significant suppression of their tumourigenic potential. These results imply that modulation of GATA-3 and FLI-1 may affect key regulatory pathways involved in transformation, and that restoring GATA-3 expression or reducing FLI-1 levels may counteract pro-tumourigenic features in keratinocytes.

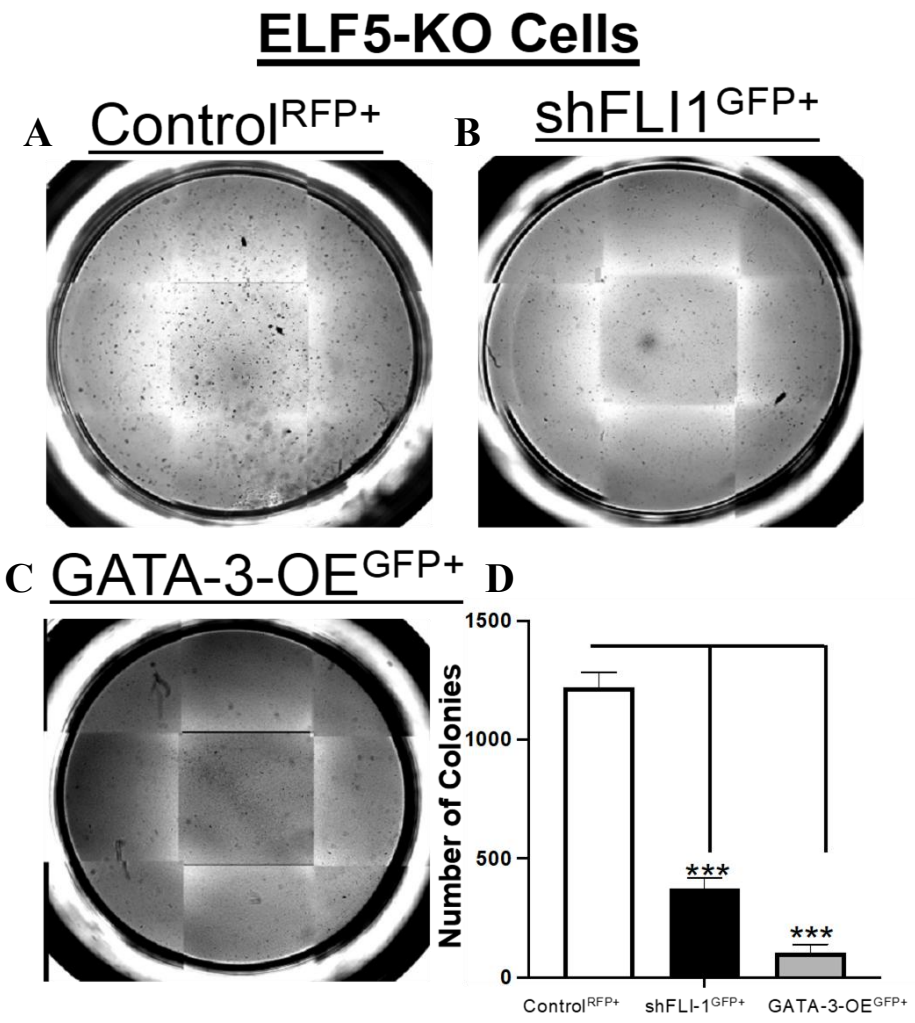

Figure 3.25: Modulation of GATA-3 and FLI-1 expression inhibits tumourigenicity of ELF5-KO cells.

(A-C) *Illustrative images of ELF5-KO-GATA-3-OE GFP+ and ELF5-KO-shFLI-1 GFP+ shows significant reduced number of colonies being formed in culture plates indicating inhibition of tumourigenicity of cells compared to ELF5-KO-control-RFP+ cells.* ***However,*** *the cells looked characteristically similar in each group.* ***D.*** *Bar graph showing the significant reduced number of colonies in GATA-3-OE-GFP+ and shFLI-1-GFP+ compared to control RFP+. Data are reexpressed as mean ± SEM values from n=3 technical repeats per group, ***p<0.001.*

CHAPTER

4.0 DISCUSSION

To date, the function of ELF5 in skin has remained largely unexplored. In this study, our findings on the role of ELF5 as a tumour suppressor in the skin are the first to our knowledge to be reported. In our study, we report a previously uncharacterized involvement of ELF5 in controlling cutaneous carcinogenesis and we have discovered that:

- ELF5 expression is significantly reduced in cSCC tissue samples and in cancerous cell lines (A431 and SCC-9) at both transcript and protein levels compared to healthy skin and cells.
- CRISPR-Cas9 mediated knockout of ELF5 in immortalised human keratinocytes significantly enhances proliferative, migratory, and invasive potential of cells and are more tumourigenic, *in vitro*. Furthermore, loss of ELF5 in keratinocytes, inhibits the ability of these cells to differentiate properly, *in vitro*.
- ELF5 regulates the interplay between keratinocyte expansion and terminal differentiation prevents transformation of keratinocytes in part by directly regulating GATA-3 and FLI-1.

This Discussion integrates the experimental findings presented in Chapters 3.1 to 3.4, including ELF5 expression analyses, functional assays, and transcriptomic target identification, with existing literature to propose a model in which ELF5 safeguards against malignant progression by modulating key downstream targets and cellular programs, and to evaluate the implications of these findings for cutaneous squamous cell carcinoma development.

4.1 LOSS OF ELF5 IS ASSOCIATED WITH CANCER INITIATION

This section draws on ELF5 expression analyses (Chapter 3.1) to evaluate the requirement of ELF5 loss for cancer initiation.

4.1.1 Reduced ELF5 expression in cSCC and epithelial cancers

Examination of endogenous ELF5 expression in healthy human skin reveals strong nuclear localization within both basal and suprabasal layers. However, in cSCC tissue and cancer cell lines, ELF5 expression is reduced (Figure 3.1 and 3.2). These findings indicate that ELF5 may play a key role in regulating genes involved in stem/progenitor cell maintenance, proliferation, and differentiation during skin development and homeostasis. Its loss or downregulation could disrupt these processes, contributing to the progression from precancerous states to cutaneous squamous cell carcinoma (cSCC).

These findings are consistent with ELF5 known role in other epithelial tissues. As ELF5 exhibits an inhibitory effect on the proliferation, migration, and invasion of breast cancer cells through the direct upregulation of *CD24* expression. The authors demonstrated that ELF5 interacts with the promoter region of *CD24*, thereby enhancing its transcriptional activity. Overexpression of ELF5 was found to elevate CD24 levels concurrently attenuating tumour aggressiveness. Conversely, the knockdown of CD24 effectively reversed these outcomes. These observations underscore the ELF5-CD24 axis as a plausible mechanism by which ELF5 exerts its tumour-suppressive effects in breast cancer (Qu et al., 2021) and a potential mechanism which is currently unexplored in skin.

4.1.2 ELF5 can act as a lineage gatekeeper in epithelial tissues

The validity of our findings is further documented by the research conducted by Piggins et al. (2016), who elucidated that the expression of ELF5 is markedly tissue-specific and significantly altered in oncogenic contexts. The study demonstrated that ELF5 expression is

highly tissue-specific, with the highest enrichment observed in epithelial-rich organs, including the mammary gland, salivary gland, and prostate. This pattern supports ELF5's well-established role in epithelial lineage specification and terminal differentiation, where it acts as a gatekeeper maintaining tissue identity by promoting luminal epithelial fate and suppressing mesenchymal or stem-like transitions (Piggins et al., 2016).

Crucially, their study found that ELF5 expression is significantly reduced in multiple cancer types, most notably in basal and luminal B subtypes of breast cancer, where its loss was associated with poor differentiation, higher metastatic potential, and more aggressive clinical behaviour. The authors reported that this downregulation was not merely a bystander effect but was functionally linked to disease progression. Loss of ELF5 was shown to enable lineage plasticity, allowing tumour cells to shift away from their differentiated epithelial identity toward more invasive, mesenchymal-like phenotypes (Piggins et al., 2016).

Within the renal system, ELF5 is typically involved in preserving epithelial identity and differentiation. However, in the context of renal malignancies, this balance is frequently disrupted (loss of ELF5), potentially leads to a loss of epithelial characteristics and the acquisition of pro-tumorigenic attributes (Lapinskas et al., 2011). Such observations imply that dysregulation of ELF5 may have a more extensive role in cancer progression, extending beyond the mammary gland, and may serve as a potential diagnostic or prognostic biomarker in renal cancers.

4.1.3 Functional evidence for ELF5 role as tumour-suppressive activity

In an effort to directly explore the functional implications of ELF5 in renal tumorigenesis, Lapinskas et al. (2011) conducted a series of gain-of-function experiments utilizing the renal carcinoma cell line 786-O renal carcinoma cell line, which characterized by an absence of endogenous ELF5 expression. Upon reintroducing ELF5 into these cells, the authors noted a

significant suppression of their tumorigenic properties of cytokeratin 8. When ELF5 was reintroduced into renal carcinoma cells, specifically the 786-O cell line, there was a significant reduction in their tumorigenic capacity. The study found that re-expression of ELF5 resulted in a 71% decrease in the proportion of cells that formed colonies in soft agar compared to mock-transfected cells, indicating a strong suppression of tumour growth potential. In addition to the reduced number of colonies, the colonies that did form in the ELF5-expressing cells were smaller in size. This suggests that ELF5 not only inhibits the formation of new tumours but also affects the growth characteristics of existing tumour cells (Lapinskas et al., 2011). Specifically, the authors noticed that the re-expression of ELF5 led to a marked reduction in cell proliferation, anchorage-independent growth, and colony formation *in vitro*, thereby indicating an impairment of oncogenic potential (Lapinskas et al., 2011). Moreover, when these ELF5-restored cells were implanted into immunocompromised mice, they exhibited significantly reduced tumour growth *in vivo* compared to control cells devoid of ELF5, thus affirming ELF5's tumour-suppressive function within a physiological context. This functional evidence robustly supports the hypothesis that the loss of ELF5 is not merely a passive byproduct of transformation but rather an active contributor to renal cancer progression. The findings establish ELF5 as a pivotal regulator of epithelial cell homeostasis in the kidney, with its absence potentially facilitating unchecked proliferation and malignant transformation (Lapinskas et al., 2011).

Furthermore, the absence of ELF5 results in heightened epithelial–mesenchymal transition (EMT) characteristics, encompassing increased cell migration and invasion, alongside diminished expression of epithelial markers in Urothelial cells. In contrast, the restoration of ELF5 expression effectively reversed these EMT-related features, thereby highlighting its suppressive role in EMT and tumour progression (Wu et al., 2015).

Miyano et al. (2021) elucidated that diminished expression of ELF5, instigated by promoter methylation, correlates with accelerated biological aging within breast tissue. By constructing breast-specific molecular clocks predicated on ELF5 levels and methylation status, they demonstrated that individuals at high risk, specifically BRCA1/2 mutation carriers, expressed a molecular age approximately two decades older than their chronological age. This observation implies that the impairment of ELF5 function fosters a tissue microenvironment that is increasingly susceptible to transformation (Miyano et al., 2021). The synthesis of these findings reinforces the significance of ELF5 as a pivotal regulator of epithelial cell identity and emphasizes its broader implications in cancer susceptibility.

Chakrabarti et al. (2012) revealed that ELF5 acts as a suppressor of epithelial-mesenchymal transition (EMT) through the direct repression of Snail2 (Slug), a critical transcription factor that induces EMT. The absence of ELF5 was evidenced to precipitate an increase in Snail2 expression, which in turn led to classical EMT-like molecular and phenotypic alterations, particularly, the downregulation of E-cadherin and the upregulation of vimentin. This transition towards a mesenchymal phenotype enhances cellular motility and invasive capabilities. These results indicate that ELF5 plays an indispensable role in curtailing cell migration and invasion, thereby supporting its function as a regulator of epithelial identity and a potential inhibition to tumour progression (Chakrabarti et al., 2012)

In addition, the physiological relevance of ELF5 in mammary gland biology was elucidated through the examination of *Elf5* knockout mouse models during gestation and lactation phases characterized by extensive epithelial proliferation, differentiation, and tissue remodelling (Chakrabarti et al., 2012). In the absence of Elf5, mammary epithelial cells were unable to preserve their epithelial phenotype and instead adopted characteristics indicative of an epithelial-mesenchymal transition (EMT). This EMT-like transition disrupted normal alveolar development and lactation, highlighting ELF5's crucial role in maintaining epithelial identity

during periods of dynamic tissue reorganization. The findings highlight that ELF5 is not only requisite for proper mammary gland morphogenesis but also functions as a molecular constraint against aberrant cellular plasticity, ensuring the preservation of a lineage-restricted, epithelial state even amidst the heightened proliferative and differentiative demands of pregnancy and lactation (Chakrabarti et al., 2012).These developmental insights parallel ELF5's tumour-suppressive role in cancer models, wherein its loss similarly facilitates EMT and contributes to heightened metastatic potential. It has also been demonstrated that ELF5 functions as a tumour suppressor in triple-negative breast cancer by modulating the FBXW7–IFNGR1 signalling axis. The loss of ELF5 results in diminished FBXW7 expression, which culminates in the stabilization of IFNGR1 and the amplification of interferon-γ (IFN-γ) signalling. This aberrant activation fosters tumour growth and metastasis by upregulating PD-L1 and enlisting immunosuppressive neutrophils, thereby enhancing immune evasion. These findings underscore the dual role of ELF5 in restricting both intrinsic tumour progression and immune-mediated escape, suggesting potential therapeutic avenues for targeting IFN-γ or PD-L1 signalling in ELF5-deficient tumours (Singh et al., 2020).

4.1.4 Conservation of ELF5 tumour-suppressive function across epithelial cancers

Taken together, our findings are consistent with the position of ELF5 as a conserved tumour suppressor across multiple epithelial tissues, with its loss repeatedly associated with disrupted differentiation programs and acquisition of oncogenic traits. Studies in breast and mammary gland cancers have shown that ELF5 loss promotes epithelial-to-mesenchymal transition (EMT) and resistance to anti-hormonal therapy, while its restoration suppresses tumour progression and metastatic behaviour. Similarly, in kidney and urothelial cancers, downregulation of ELF5 correlates with aggressive phenotypes and poor prognosis. In alignment with these observations, our current study provides the first evidence of ELF5 loss

contributing to tumorigenic features in cutaneous keratinocytes, including enhanced proliferation, loss of epithelial markers, and increased invasive capacity.

4.2. ELF5 CAN REGULATE CELL PROLIFERATION, MIGRATION, DIFFERENTIATION AND TUMOURIGENICITY OF KERATINOCYTES, *IN VITRO*

This section discusses the functional consequences of ELF5 modulation on keratinocyte proliferation, migration, differentiation, and tumorigenic potential, drawing directly on the *in vitro* assays presented in Chapter 3.2 and 3.4.

Our functional analysis has shown that ELF5 can regulate important cellular processes such as proliferation, differentiation, migration and tumorigenicity (Figures 3.6, 3.8, 3.10, 3.12, 3.23, 3.25), which is supported by other studies (Lapinskas et al., 2012; Chakrabarti et al., 2012). Furthermore, we observed that overexpression of ELF5 can inhibit these effects in HaCaT and skin cancerous cell lines A431 and SCC-9, *in vitro* (Figures 3.7, 3.8, 3.9, 3.11). This is also consisting with previous studies showing that re-expression of ELF5 led to a marked reduction in cell proliferation and anchorage-independent (Lapinskas et al., 2011; Xiao et al., 2018).

Although no published studies to date have specifically investigated the effects of ELF5 overexpression in HaCaT (healthy), A431 or SCC-9 squamous carcinoma cells, several independent investigations have demonstrated that the overexpression of other tumour-suppressive genes or regulatory RNAs in these models can markedly inhibitory impacts (Chen et al., 2018; Wu et al., 2016; Lin et al., 2017; Kalailingam et al., 2019; Li et al., 2018).

HaCaT cells are widely regarded as non-tumorigenic human keratinocytes, a range of studies have shown that targeted overexpression of specific oncogenes, transcription factors, and non-coding RNAs can significantly alter their cellular processes, leading to phenotypic changes consistent with early malignant transformation. For instance, overexpression of the long non-

coding RNA MALAT1 has been reported to enhance HaCaT cell proliferation, migration, and invasion, largely via activation of the Wnt/β-catenin signalling pathway and was accompanied by upregulation of EMT markers (Chen et al., 2018). Similarly, HOXA13, a developmental transcription factor, when overexpressed in HaCaT cells, promoted anchorage-independent growth, altered cell adhesion, and induced tumour formation in nude mice, marking a clear shift toward tumorigenicity (Wu et al., 2016). These observations were supported by Zhou et al. (2015), who demonstrated that cyclin D1 overexpression accelerated the G1/S transition, significantly increased proliferation, and enabled soft agar colony formation, indicating early transformation capacity (Zhou et al., 2015).

4.2.1 ELF5 can regulates keratinocyte migration and Invasion

Additional evidence comes from studies on EMT and hypoxia signalling. FOXC1 overexpression enhanced HaCaT cell migration and invasion through upregulation of MMP-9, vimentin, and N-cadherin, while reducing E-cadherin, collectively indicating induction of epithelial–mesenchymal transition (Zhang et al., 2019). Likewise, HIF-1α overexpression under hypoxic conditions induced VEGF secretion, anchorage-independent growth, and mesenchymal marker expression, suggesting that hypoxia-responsive genes may push HaCaT cells toward a pro-tumorigenic phenotype (Lin et al., 2017). Furthermore, miR-31 was shown to promote proliferation and suppress apoptosis in HaCaT cells by modulating the Bcl-2/Bax axis, further supporting the role of regulatory RNAs in transforming non-malignant keratinocytes (Yin et al., 2020).

4.2.2 ELF5 can suppresses keratinocyte tumorigenicity

Multiple independent studies have demonstrated that modulating gene expression in A431 and SCC-9 cells significantly affects key oncogenic actions, including proliferation, migration, invasion, and tumorigenicity. These findings are consistent with our own results, where ELF5

overexpression in both A431 and SCC-9 cell lines resulted in marked suppression of proliferative and invasive characteristics, as well as tumour-forming capacity.

Furthermore, Kalailingam et al. (2019) showed that overexpression of CDC42SE1, a downstream effector of CDC42, inhibits A431 cell proliferation via AKT pathway suppression, downregulation of cyclin D1, and increased expression of p27^Kip1, culminating in G1-phase cell cycle arrest (Kalailingam et al., 2019). Similarly, TSLC1 overexpression reduced proliferation and invasion by downregulating MMP-2 and MMP-9, with *in vivo* studies confirming reduced tumour size and mitotic activity (Liu et al., 2013). Finally, Yang et al. (2013) reported that overexpression of DLC1, a RhoGAP protein, suppresses A431 cell proliferation and invasion by downregulating CDK4, cyclin D1, and enhancing apoptotic pathways. DLC1-expressing xenografts showed significantly reduced tumour growth, highlighting its strong antitumor function (Yang et al., 2013).

Similarly, several studies have underscored that targeted overexpression of tumour-suppressive genes or regulatory RNAs in SCC-9 cells—an established model for oral squamous cell carcinoma can markedly impair fundamental malignant processes such as proliferation, migration, invasion, and tumorigenicity. Wu et al. (2021) demonstrated that overexpression of the long non-coding RNA SOX2OT suppressed SCC-9 proliferation and migration via inhibition of the PI3K/AKT pathway, highlighting its role in restraining oncogenic signalling (Wu et al., 2021). A study by Li and colleagues, found that overexpressing Wnt5a in SCC-9 cells inhibited migration and invasion, mediated through reduced expression of MMP-2 and reversion of epithelial–mesenchymal transition (EMT), with elevated E-cadherin and diminished N-cadherin levels (Li et al., 2018). In parallel, Liu et al. (2017) demonstrated that miR-145 overexpression suppressed SCC-9 migration, invasion, and *in vivo* tumorigenicity by targeting the EMT regulator ZEB2 and reducing N-cadherin expression. These findings suggest a critical role for EMT modulation in reducing the metastatic potential of SCC-9 cells (Liu et

al., 2017). Given that SCC-9 cells express similar EMT programs and rely on EMT for invasive behaviour, the observed ELF5-mediated inhibition of migration and invasion likely reflects transcriptional repression of these mesenchymal drivers. The suppression of *in vivo* tumorigenicity observed in other epithelial models further supports the idea that ELF5 re-expression in SCC-9 cells disrupts key regulatory circuits driving oral carcinoma progression (Xiao et al., 2018).

In a recent transcriptomic study of tongue lesions, Zhang et al. (2023) identified *ELF5* as a critical biomarker whose expression decreases progressively from oral potentially malignant disorders (OPMD) to squamous cell carcinoma (SCC). This downregulation was consistently observed across patient-matched lesion and margin samples, highlighting *ELF5*'s potential role in suppressing epithelial-to-mesenchymal transition (EMT) and maintaining epithelial differentiation. Its predictive utility was further validated through logistic regression models, where *ELF5* contributed significantly to distinguishing OPMD from SCC with high diagnostic accuracy. These findings not only support ELF5's role in maintaining epithelial identity but also highlight its clinical potential as a biomarker for early malignant transformation (Zhang et al., 2023)

Our findings are also supported by study carried out by Zhang and colleagues (2019) where functional evidence was provided that ELF5 functions as a suppressor of ovarian cancer metastasis by inhibiting cellular migration and invasion. Employing wound healing and Transwell invasion assays, the researchers illustrated that the overexpression of ELF5 markedly diminished the capacity of ovarian cancer cells to migrate across wound gaps and to invade through extracellular matrix-coated membranes. These *in vitro* models replicate critical stages of metastatic dissemination, including cellular motility and matrix degradation, thereby suggesting that ELF5 plays a direct role in restraining the metastatic behaviour of ovarian cancer cells (Zhang et al., 2019). Our data suggests that ELF5 acts as a molecular switch which

is important for normal keratinocyte differentiation processes and downregulation of ELF5 expression could be an early diagnostic marker to detect precancerous/malignant cell formation before visible lesions.

4.2.3 ELF5 can regulates keratinocyte proliferation

Interestingly, consistent with our previous findings in primary mice epidermal keratinocytes (Hu et al*.,* 2025) that both *CDK16* and *CCNE1,* are significantly up-and downregulated after modulating ELF5 expression in HaCaT and cancerous cells lines (Figures 3.6, 3.7) which are critical regulators of cell cycle progression. Wang et al. (2023) highlighted that *CDK16* is consistently overexpressed across a variety of human malignancies. This pervasive overexpression indicates that *CDK16* may play a conserved and potentially central role in oncogenic processes across diverse tissue types, and it has been indicated that elevated levels of *CDK16* may facilitate tumour cell survival and proliferation by modulating pathways implicated in cell cycle regulation-progression, apoptosis resistance, and oncogenic signalling (Wang et al., 2023)

Furthermore, *CCND1* is significantly elevated in ELF5-KO cells and is downregulated when ELF5 is overexpressed in HaCaT and cancerous cell lines (Figures 3.6). Previous studies have shown that cyclin D1, encoded by the *CCND1* gene, is a key regulator of the G1 phase of the cell cycle, particularly at the restriction point (R-point)-a critical checkpoint beyond which the cell commits to DNA replication and division, regardless of external mitogenic signals. Under standard physiological circumstances, the expression of cyclin D1 is meticulously modulated and stimulated by various growth factors. It associates with CDK4/6 to phosphorylate the retinoblastoma protein (RB), which culminates in the liberation of E2F transcription factors and the activation of genes essential for the entry into the S phase of the cell cycle. In numerous malignancies, this signalling pathway becomes dysregulated. The *CCND1* gene is often subject

to amplification or overexpression, which leads to the persistent activation of CDK4/6, inappropriate phosphorylation of RB, and the premature inactivation of the G1 checkpoint. This phenomenon effectively dissociates cell cycle progression from extrinsic growth signals, thereby permitting cells to proliferate unchecked even in the absence of mitogenic stimuli (Sherr, 1996).

4.2.4 ELF5 can regulates keratinocyte differentiation

Additionally, Nishi et al. (2009) elucidated that the downregulation of cyclin D1 is imperative for the definitive exit from the cell cycle and the commencement of differentiation in keratinocytes under conditions devoid of anchorage. In normal cellular contexts, the loss of cyclin D1 was correlated with G1 arrest and an enhanced expression of differentiation markers, whereas its persistent expression in carcinoma cells obstructed both processes. These observations underscore cyclin D1 as a pivotal regulator that associates the withdrawal from the cell cycle with the initiation of differentiation. This finding aligns with the suggestion that ELF5 may act as a differentiation-inducing factor that is lost during the transition from normal epithelium to carcinoma (Zhang et al, 2023). Therefore, our data suggest (Figures 3.8, 3.9 and 3.12) that ELF5 can act as a switch between proliferation and differentiation of keratinocytes, by balancing and regulating the transition of keratinocytes from proliferation to early differentiation, which if deregulated could potentially lead to malignant transformation of keratinocytes.

4.2.5 Potential downstream mediator-CD24 of ELF5 function

Evidence from breast epithelial systems suggests that CD24 is a key downstream effector of ELF5's tumour-suppressive activity. Qu et al. (2021) showed that ELF5 directly binds to and activates the CD24 promoter, and that CD24 upregulation is required for ELF5-mediated inhibition of proliferation, migration, and invasion. When CD24 was knocked down, these

protective effects were abolished, indicating that CD24 is not merely correlated with ELF5 activity but is mechanistically essential for maintaining epithelial stability.

CD24 is known to regulate cell adhesion, cytoskeletal organisation, and epithelial identity (Kristiansen et al., 2004; Fang et al., 2010). Loss of CD24 has been widely linked to increased EMT, enhanced motility, and acquisition of stem-like features across multiple epithelial cancers (Lee et al., 2011; Chen et al., 2018). These behaviours closely mirror the phenotypes observed in ELF5-deficient keratinocytes in this study, suggesting that ELF5 loss may drive a CD24-low, EMT-permissive state that facilitates early stages of cSCC initiation.

Although CD24 was not directly investigated in the present work, the convergence between ELF5 KO phenotypes and established consequences of CD24 downregulation in epithelial cells supports the hypothesis that disruption of the ELF5-CD24 axis may be an early molecular event contributing to keratinocyte transformation. Future studies assessing CD24 levels following ELF5 manipulation and confirming promoter binding using ChIP-qPCR would help define the relevance of this pathway in human skin.

4.2.6 Integration of ELF5 function with epidermal signalling pathways

The phenotypes observed following loss of ELF5 (ELF5-KO) by CRISPR/Cas9 editing, enhanced proliferation, impaired differentiation, and increased motility are consistent with disruption of the core signalling pathways controlling epidermal homeostasis (Figure 3.6, 3.10, 3.12). BMP signalling promotes keratinocyte differentiation (Botchkarev & Sharov, 2004; Cui & Schlessinger, 2006), and the reduced expression of GATA3 and differentiation markers in ELF5-KO cells aligns with attenuation of BMP-driven differentiation programs (Rácz et al., 2011). Conversely, the increased proliferation and Cyclin D1/2 and Cyclin E1 expression mirror outcomes of aberrant WNT/β-catenin activation (Lim et al., 2013; Watt, 2014). The role of ELF5 as a lineage determinant downstream of FGF signalling (Oakes et al., 2008) further

supports the interpretation that ELF5 coordinates FGF-dependent epithelial identity cues, and its loss may release keratinocytes toward a more plastic, invasive state (Kurek et al., 2007). Together, these findings position ELF5 as a transcriptional integrator of BMP, WNT, and FGF pathways essential for preserving epidermal stability, with its loss contributing to cSCC initiation and progression (Blanpain et al., 2006; Dotto, 2009).

4.3. INTERPLAY OF ELF5 WITH GATA-3 AND FLI-1 REGULATES KERATINOCYTE TUMOURIGENICITY

Transcriptomic analysis identified GATA3 and FLI1 as ELF5-dependent targets (Chapter 3.3), which were subsequently validated and functionally characterised in HaCaT keratinocytes (Chapter 3.4).

4.3.1 GATA3 as a direct downstream target of ELF5 in keratinocytes

In this study, we have also identified GATA-3 and FLI-1 as direct targets of ELF5 in keratinocytes (Figures 3.13 and 3.17). Of note, GATA-3 has been shown to serve as a fundamental transcriptional regulator of epidermal homeostasis, functioning to equilibrate keratinocyte proliferation and differentiation within the human interfollicular epidermis. Their investigation revealed that the ablation of GATA-3 expression led to a pronounced increase in keratinocyte proliferation (Masse et al., 2014). These insights suggest that GATA-3 is not simply a passive marker of differentiation, but rather a functional gatekeeper that actively inhibits proliferation while facilitating the keratinocyte transition through the differentiation cascade. This duality positions GATA-3 at the nexus of interfollicular epidermal renewal, where the synchronization of self-renewal and differentiation is vital for barrier maintenance and cutaneous integrity (Masse et al., 2014). GATA-3 was also observed to be robustly expressed in the nuclei of keratinocytes, particularly within the epidermal layer and adnexal structures such as hair follicles and sebaceous glands. This distribution corresponds with

GATA-3's established role as a transcription factor integral to epithelial differentiation and homeostasis (Mertens et al., 2015).

4.3.2 ELF5-dependent regulation of GATA3 is required for keratinocyte differentiation

Consistent with previous findings (Masse *et al*, 2014 and Mertens et al., 2015), we observed GATA-3 expression is reduced in cSCC tissues and after loss of ELF5 in keratinocytes (Figure 3.16). GATA-3 is integral to the development of the skin barrier, particularly through its role in epidermal keratinocytes. By employing a mouse model with epidermal-specific deletion of GATA-3, the researchers were able to examine the consequences of GATA-3 loss in the skin while maintaining its function in other tissues. These knockout mice appeared morphologically typical at birth but displayed rapid and excessive transepidermal water loss (TEWL), resulting in severe dehydration and neonatal mortality within hours postpartum (*de* Guzman et al., 2006). To investigate the repercussions of GATA-3 loss in adult skin, histological examination of the grafted skin revealed marked epidermal abnormalities: the mutant epidermis was significantly thicker, comprising approximately ten cell layers in contrast to the standard three to four layers observed in control grafts (*de* Guzman et al., 2006).

It also has been investigated the long-term implications of epidermal-specific GATA-3 deletion in murine models demonstrated that GATA-3 is crucial not only for the proper morphogenesis of hair follicles but also for the preservation and regulation of the adult epidermal compartment (Kurek et al., 2007). In human skin, GATA-3 has a critical role in epidermal differentiation and immune regulation, specifically within the context of psoriasis, a chronic inflammatory dermatological condition marked by keratinocyte hyperproliferation and impaired differentiation (Rácz et al., 2011). These findings support the hypothesis that GATA-3 is essential for maintaining epidermal homeostasis. The reduced expression of GATA-3 in lesional skin is likely to impair keratinocyte differentiation, thereby contributing to epidermal

hyperplasia, increased cellular proliferation, and the pro-inflammatory microenvironment characteristic of psoriasis and silencing of GATA-3 during differentiation of human primary keratinocytes decreased the expression of several differentiation markers, signifying that GATA-3 is key regulator of keratinocyte differentiation (Masse et al., 2014). These studies are consistent with our findings when CRISPR-mediated loss of ELF5 in HaCaT cells leads to the inability of cells to differentiation properly as observed with a significant reduction of keratinocyte differentiation associated markers as well as reduced GATA-3 expression (Figure 3.12). These findings were further supported by our observations after overexpression of GATA-3 in ELF5-KO cells rescues the keratinocytes' ability to differentiation again (Figure 3.21). Our data suggests that ELF5 regulation of keratinocytes differentiation is in part due to regulation and maintenance of GATA-3 expression and deregulation of this mechanism could be a prerequisite for precancerous cell and dysplastic skin formation.

4.3.3 FLI1 is negatively regulated by ELF5 and promotes a proliferative state

Conversely, we found that FLI-1 was significantly upregulated after loss of ELF5 and cSCC tissue biopsies (Figure 3.16). These results align with prior research in which FLI-1 was identified as a prevalent integration site of the Friend murine leukaemia virus (F-MuLV), resulting in its overexpression and facilitating the development of erythroleukemia (Ben-David et al., 1990; 1991). These investigations elucidated that FLI-1- an ETS transcription factor family, can function as an oncogenic driver by perturbing normal hematopoietic differentiation pathways when aberrantly activated (Ben-David et al., 1990; 1991). The recurrent upregulation of FLI-1 indicates a conserved role in promoting proliferation or lineage specification, potentially contributing to phenotypes relevant to disease. Considering FLI-1's established regulatory influence on genes implicated in cellular proliferation, differentiation, and survival, its elevated expression may represent a crucial regulatory node within our system and necessitates further functional validation (Athanasiou et al., 2000; Pereira et al., 199). While

FLI-1 has primarily been the subject of investigation in hematopoietic malignancies, emerging evidence suggests that ETS factors, including FLI-1, can be aberrantly activated in non-hematopoietic contexts, where they may influence altered cell fate or invasive potential. Moreover, FLI-1 was recognised as one of the most significantly elevated transcription factors in this RNA-seq analysis, indicating its involvement in the modulation of proliferation and cellular plasticity within keratinocytes (Pereira et al., 1999; Athanasiou et al., 2000). The observed upregulation of FLI-1 in our experimental system may reflect its crucial role in obstructing differentiation and promoting proliferation

Also, it has been demonstrated that FLI-1 inhibits the expression of both Rb and GATA-1, which are critical for erythroid differentiation (Tamir et al., 1999). By repressing these genes, FLI-1 facilitates the maintenance of cells in a less differentiated, more proliferative state. Although our experimental keratinocytes do not pertain to erythroid lineage, FLI-1 may similarly assist in sustaining an undifferentiated state by obstructing the activation of lineage-specific programs. (Tamir et al., 1999). FLI-1 upregulation in the context of our study may signify a more extensive transcriptional role in sustaining an undifferentiated, pro-survival state, which could contribute to dysregulated tissue homeostasis or tumour progression.

The upregulation of anti-apoptotic genes such as BCL-2 and MDM2, attributed to FLI-1, has been correlated with enhanced cellular survival and resistance to apoptotic stimuli. Lesault et al. (2002) provided direct evidence that FLI-1 interacts with and activates the BCL-2 promoter, establishing a transcriptional mechanism through which FLI-1 sustains the viability of transformed erythroblasts. This supports the assertion that FLI-1-driven enhancement of survival pathways, including BCL-2 and potentially MDM2, may contribute to apoptotic resistance (Lesault et al., 2002) Furthermore, FLI-1 plays a critical role in regulating genes involved in haematopoiesis and vascular development, by maintaining the balance between proliferation and differentiation of hematopoietic stem and progenitor cells. Its abnormal

expression has been associated with various cancers, including Friend virus-induced erythroleukemia and Ewing's sarcoma, where chromosomal translocations involving FLI-1 drive tumorigenesis. Moreover, FLI-1 is implicated in autoimmune disorders such as systemic lupus erythematosus and systemic sclerosis, where its altered expression contributes to dysregulated inflammatory responses. Notably, during erythropoietin (Epo)-stimulated terminal differentiation of erythroblasts, a natural decline in FLI-1 levels is observed, indicating its role in erythroid maturation (Li et al., 2022). Conversely, when FLI-1 was expressed in a constitutive manner, erythroid cells were unable to undergo differentiation and instead persisted in a proliferative, undifferentiated phenotype. This obstruction to differentiation was evidenced through direct repression of transcription of the retinoblastoma gene, which is recognized as a pivotal regulator of cell cycle exit and differentiation (Tamir et al., 1999).

Cui and colleagues (2009) elucidated that persistent expression of FLI-1 is requisite for the preservation of the proliferative and undifferentiated phenotype of both murine and human erythroleukemia cells. Their findings indicated that shRNA-mediated knockdown of FLI-1 led to marked reduction in cellular proliferation and initiated erythroid differentiation, as demonstrated by the augmented expression of alpha-globin (Cui et al., 2009). Mechanistically, this phenomenon was linked to the upregulation of *GATA-1*, a crucial erythroid differentiation factor that is repressed by FLI-1, alongside the downregulation of *BCL-2*, which is a key target gene of FLI-1 that fosters cellular survival. Consequently, the assertion that FLI-1 knockdown attenuates proliferation and stimulates differentiation through GATA-1 and BCL-2 is robustly corroborated by the experimental results of this investigation, thereby emphasizing the role of FLI-1 as a transcriptional regulator that obstructs differentiation and enhances leukemic cell viability (Cui et al., 2009).This indicates that ELF5 suppression of FLI-1 in keratinocytes is

important to maintain the ability of keratinocytes to differentiation and to prevent precancerous cell formation.

4.3.4 Co-ordinated regulation of GATA3 and FLI1 by ELF5 maintains keratinocyte homeostasis

Our data show that loss of ELF5 inhibited the ability of keratinocytes to differentiation properly (Figure 3.12) in part by reduced GATA-3 expression and potentially due to elevated FLI-1 expression in keratinocytes (Figure 3.21). This suggests that ELF5 regulation of GATA-3 and FLI-1 is required to prevent the disruption to the differentiation program in keratinocytes leading to the malignant transformation of keratinocytes and loss of ELF5 can cause keratinocytes to fail to complete the differentiation process, leading to precancerous cell formation and dysplastic epithelium in skin. Collectively, our data has identified ELF5 an important regulator of both GATA-3 and FLI-1, which are required to maintain keratinocyte homeostasis and if deregulated can lead to cancer initiation and formation.

5.0 CONCLUSION

This study has shown a peculiar representation of ELF5 into keratinocyte transformation, which will have wide range of significance for dermatological and cancer research. In conclusion, this data reveals that ELF5 is required to regulate in preventing malignant transformation of keratinocytes in part by regulating GATA-3 and FLI-1 expression (Figure 5.1). GATA-3 is required for differentiation and SC maintenance (Miyano et al., 2021; Zhang et al., 2019). FLI-1 expression levels dictate if differentiation takes place (FLI-1^{Low}) or tumorigenesis (FLI-1^{High}). Our data highlights the intricate interplay between ELF5 and its gene targets GATA-3 and FLI-1 in keratinocytes, which further adds to the complexity to keratinocyte cell fate determination. Our results strongly suggest that ELF5 holds significant promise as an important remedial target, warranting more in-depth investigation. Additionally, these results lay a crucial groundwork for future studies into ELF5's function as a regulator of signalling pathways in broader research contexts, such as regenerative medicine, ageing and stem cell biology.

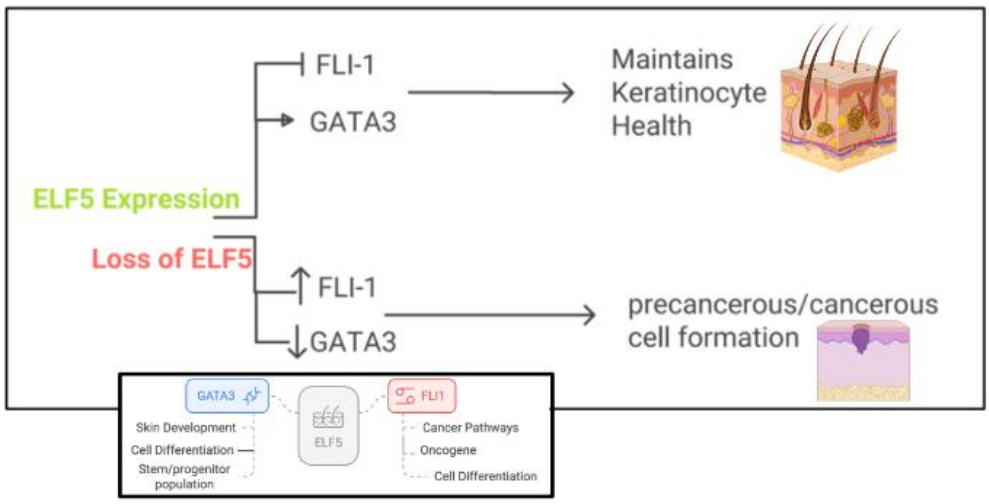

Figure 5.1: Working model illustrating the role of ELF5 in regulating homeostasis along with tumorigenic potential through GATA-3 and FLI-1.

When ELF5 is expressed, it exerts a positive regulatory effect on GATA-3 (indicated by a right-pointing arrow), promoting epithelial differentiation, stem/progenitor population and suppressing tumorigenic features. Simultaneously, ELF5 inhibits FLI-1 expression (reexpressed by an inhibition symbol), thereby restricting pro-invasive and proliferative signalling. Loss of ELF5 disrupts this regulatory balance, leading to downregulation of GATA-3 (downward arrow) and upregulation of FLI-1 (upward arrow), which collectively contribute to aberrant keratinocyte behaviour, loss of homeostasis, and progression toward tumorigenicity. This model highlights ELF5 as a critical modulator in skin epithelial biology and a potential suppressor of cutaneous squamous cell carcinoma development.

6.1 LIMITATIONS

Although RNA-seq, differential expression analysis, luciferase reporter assays, and functional rescue experiments collectively demonstrate that ELF5 regulates GATA3 and FLI1 expression, this study did not directly assess whether ELF5 can directly bind to the promoter regions of target genes identified in our study (GATA-3 and FLI-1). We highlight below some reason as to why we did not perform ChIP-seq or ChIP-qPCR in this study:

- **Technical constraints of keratinocyte chromatin:** Keratinocytes exhibit dense chromatin organisation, requiring extensive optimisation for ChIP workflows, which was not feasible within the project timeframe.
- **Scope and feasibility:** ChIP-seq requires deep sequencing, multiple biological replicates, and high optimisation. One of the primary aim of my study was to evaluate the functional consequences of ELF5 loss, these resources were allocated to luciferase promoter assays with direct mechanistic output, which is widely accepted method of identify gene target regulation, *in vitro* (Wood,1995).
- **Alternative functional evidence was strong:** Promoter-reporter assays and transcriptomics shifts already indicated transcriptional regulation, making ChIP a valuable future direction and plan to do it in near future.

6.2 FUTURE PERSPECTIVES

The findings of this research establish ELF5 as a central transcriptional regulator of keratinocyte homeostasis, with downstream effects on both GATA-3 and FLI-1, influencing cell differentiation, proliferation, and tumorigenic potential. Building on this foundation, several future directions can be envisioned to deepen mechanistic understanding and explore therapeutic potential.

1. Mechanistic dissection of ELF5 regulatory networks:
   While this study highlights ELF5 as a regulator of GATA-3 and FLI-1, the broader transcriptional network governed by ELF5 in keratinocytes remains to be fully characterized. Future studies using chip-seq or CUT&RUN could identify direct ELF5 binding sites and downstream gene targets. Additionally, RNA-seq of ELF5-deficient versus reconstituted cells may uncover further pathways contributing to carcinogenesis.

2. Interrogation of ELF5 in human SCC samples:
   Translating these findings to the clinical context will require examining ELF5, GATA-3, and FLI-1 expression patterns in human carcinoma tissues such as cSCC across different grades and stages. Correlation of expression levels with patient outcomes could validate the use of ELF5 or its downstream targets as diagnostic or prognostic biomarkers.

3. Functional Role of FLI-1 as an oncogenic driver:
   Given the pro-invasive phenotype associated with FLI-1 upregulation, it would be valuable to investigate its role in epithelial to mesenchymal transition and metastasis. Identifying FLI-1 target genes using transcriptomic profiling could provide insight into its prospective role as a remedial target in SCC and possibly in different epithelial cancers.

4. 3D Skin Models and *In Vivo* validation:
   Future experiments should incorporate 3D organotypic skin models and *in vivo* xenograft models to validate the impact of ELF5, GATA-3, and FLI-1 modulation in a more physiologically relevant environment. These models would allow for the assessment of tissue architecture, invasion, and tumour progression in response to gene perturbations.

5. Crosstalk with the tumour microenvironment:
   Finally, the interaction between ELF5-driven keratinocyte behaviour and the surrounding stromal and immune cells warrants further study. Given the dynamic interplay between epithelial cells and their microenvironment in cancer, co-culture systems or spatial transcriptomics could provide insight into how ELF5 loss reshapes local signalling landscapes.

6. Restoration of ELF5 function as a therapeutic potential:
   Based on our data the developing a suitable administering system for introducing ELF5 into cancer cell lines and overexpress ELF5 may have remedial potential. Elevated FLI-1 has depicted to have a critical function in cell survival and cell growth of angiogenic cells (Li et al., 2015). Thus, by targeting ELF5, may not only inhibit expression of FLI-1 but also inhibit proliferation in tumours, as well as cut off their blood supply. Our data underscores the possible high potency of ELF5 as a promising therapeutic goal for preventing cSCC formation and/or restoring homeostatic mechanisms in the skin. However, additional analysis is required to dictate whether the loss of ELF5 is the main driving force for malignancies or if other factors need to be considered. Furthermore, restoring ELF5 may have benefits beyond proliferation and differentiation regulation. Overall, our data demonstrating that ELF5 as a compelling upstream regulator whose restoration could inhibit cSCC development at very early stages. Understanding how

ELF5 regulate gene expression and cellular function could ultimately benefit patients, particularly those with precancerous lesions progressing toward cSCC by informing targeted therapeutic strategies in the long run.

7.0 APPENDIX

7.1. LIST OF REAGENTS

NAME OF REAGENTS	CATALOGUE ID	SOURCE
0.25% Trypsin-EDTA	25200-072	ThermoFisher
0.45µm nitrocellulose membrane	1620115	BIO-RAD
2-Mercaptoethanol	125470010	ThermoFisher
30% Acrylamide/Bis solution (37.5:1)	1610158	BIO-RAD
Acetic acid	10171460	ThermoFisher
Acetic anhydride	320102	Merck
Agarose	11496950	ThermoFisher
Ammonium persulfate (APS)	161-0700	BIO-RAD
Ampicillin Sodium Salt BP1760	Fisher	Scientific
Blocking reagent	11096176001	Roche
BM Purple AP substrate	11442074001	Roche
Bovine serum albumin (BSA) BP9702	Fisher	Scientific
BT chelex 100 resin	143-2832	BIO-RAD
Calcium chloride (CaCl2) 0.5M C/1400/60	Fisher	Scientific
Chondroitin sulfate sodium salt from shark cartilage (CSC)	C4384	Merck
cOmplete ULTRA Protease inhibitor cocktail tablets, Mini EDT4A90-6fr8e3e7	001	Merck
DAPI	D9542	Merck
DMEM media (+4.5g/L Dglucose, -L-glut, -pyruvate)	11960-044	ThermoFisher
DMEM/F-12 Ham (3:1) High Glucose (+Lglutamine, -CaCl2, -DS8o4d3iu7m	bicarbonate)	Sigma-Aldrich
DPX mounting medium	6522	Merck
EDTA UltrPure 0.5M, pH8.0	15575-020	ThermoFisher

Ethanol BP8202	Fisher	Scientific
Filter paper, 5-13µm pore size	11445248	ThermoFisher
Formamide	F9037	Merck
Glycerol G/0650/17	Fisher	Scientific
Heat-inactivated Fetal bovine serum 11550356	Fisher	Scientific
Hematoxylin BP2424	Fisher	Scientific
Hydrocortisone	H0888	Merck
Isopropanol BP2618	Fisher	Scientific
Kanamycin Sulfate BP906-5	Fisher	Scientific
L-Glutamine (200mM)	25030-081	ThermoFisher
Lipofectamine 3000	L3000001	ThermoFisher
MEM non-essential amino acid solution 100X	M7145	Merck
Milk	powder	Marvel
Mitomycin C (MMC)	BP2531	ThermoFisher
Normal Donkey Serum	S30	Merck
Normal Goat Serum 191356	MP	Biomedicals
OCT medium	KMA-0100-00A	ThermoFisher
Pageruler plus prestained protein ladder	26619	ThermoFisher
Paraformaldehyde P/0840/53	Fisher	Scientific
PCRBIO DNA ladder IV PB40.14-01	PCR	Biosystems
Penicillin/Streptomycin (10,000U/ml)	15140122	ThermoFisher
Polybrene	TR-1003-G	Merck
Ponceau S	10454915	ThermoFisher
Propidium Iodide	P1304MP	ThermoFisher
qPCRBIO SyGreen High ROX PB089618-041-6	PCR	Biosystems
Reduced serum OptiMEM	31985070	ThermoFisher
RiboRuler High Range RNA ladder	SM1821	ThermoFisher
RNase A	10109169001	Roche
Sheep Serum	16070096	ThermoFisher
SOC outgrowth medium B9020S New	England	Biolabs
Sodium Chloride (NaCl) 10316943	Fisher	Scientific

Sodium dodecyl sulphate (SDS) BP1311-1	Fisher	Scientific
Sodium nitrite	G7398	Merck
Subcloning Efficiency DH5α Competent Cells	18265017	ThermoFisher
SybrSafe	533102	ThermoFisher
T4 DNA ligase M0202 New	England	Biolabs
TEMED	161-0800	BIO-RAD
Tris Base BP152	Fisher	Scientific
Tris-HCl BP1758	Fisher	Scientific
Triton X-100 BP151-500	Fisher	Scientific
TRIzol	R050-1-50	Zymo-Research
Tween-20 BP337-500	Fisher	Scientific
Vectashield antifade mounting medium with DAPI H-1200	Vector	Labs
Versene	15040-033	ThermoFisher
Xylene 534056	Fisher	Scientific

7.2. LIST OF INSTRUMENTS

NAME OF INSTRUMENTS	CATALOGUE ID	SOURCE
Automated cell counter	TC20	BIO-RAD
Avanti Ultra centrifuge	JXN-26	Beckman coulter
CLARIOStar plus plate reader	-	BMG-Labtech
Compact orbital shaker (Incubator)	ES20	Grant Instruments
Cryostat	CM1860	Leica
DM1500 microscope with EC4 camera	-	Leica
FACS Melody	-	Cytek Aurora
Flow Cytometer	-	Cytek Aurora
Hula sample mixer	10548425	ThermoFisher
iBrightFL1000 Imaging system	A32752	Thermofisher
IncyCyte S3 live cell analysis instrument	-	Sartorius
Leica Thunder 3D cell culture imaging system	-	Leica
Nanodrop 8000	ND-8000	ThermoFisher
QuantStudio 5 Real-Time PCR system	A34322	ThermoFisher
Refrigerated Microcentrifuge	75002543	ThermoFisher
Thermocycler	T-100	BIO-RAD
Transilluninator-Blue light	13193102	ThermoFisher
Universal Oven	UN110	Memmert

7.3. LIST OF PLASTICWARES

NAME OF ITEMS	CATALOGUE ID	SOURCE
1.5ml microcentrifuge tubes	72.690.001	Sarstedt
12-well plate	CC7682-7512	StarLab
15ml sterile tubes	62.554.503	Sarstedt
2.0ml microcentrifuge tubes	72.695.500	Sarstedt
24-well plate	CC7682-7524	StarLab
40µm cell strainer	22-363-547	ThermoFisher
50ml sterile tubes	62.547.254	Sarstedt
60mm dish	CC7682-3359	ThermoFisher
6-well plate	CC7682-7506	StarLab
70µm cell strainer	1-800-766-7000	ThermoFisher
96 well semi-skirted PCR plates	E1403-6200	StarLab
96-well plate	83.3924	Sarstedt
Cell Scraper	08100241	ThermoFisher
Glass coverslips	12323148	ThermoFisher
Haemocytometer	145-0011	BIO-RAD
Petri-dishes	12654785	ThermoFisher
Polyolefin sealing film for qPCR, Self-adhesive	E2796-9895	StarLab
Serological pipettes, 10ml	86.1254.001	Sarstedt
Slide mailers	HEA15986	HeathrowScientific
SuperFrost plus microscope slides	631-0108	VWR
T25	83.3910.002	Sarstedt

7.4 LIST OF ANTIBODIES

NAME OF ANTIBODIES	HOSTS	DILUTION USED	CATALOGUE ID	SOURCE
ELF5	Rabbit	WB: 1:1000	E-AB-19199	Elabscience
ELF5	Rabbit	IHC/ICC: 1:1000	A7181	2B scientific/ABClonal
GAPDH	Mouse	WB: 1:10,000	Ab8245	Abcam
Anti-mouse IgG-HRP	Mouse	WB: 1:3000	7076S	Cell signalling
Anti-rabbit IgG-HRP	Rabbit	WB: 1:3000	7074S	Cell signalling
Donkey anti-rabbit A488	Rabbit	ICC: 1:200	21206	Invitrogen
Donkey anti-rabbit A555	Rabbit	ICC: 1:200	31572	Invitrogen
Cytokeartin 1 (Krt1)	Rabbit	WB: 1:10,000	Ab93652	Abcam
Cytokeratin 15 (Krt15)	Guinea pig	IHC: 1:100	BP5077	Origene/Insight Biotechnology
GATA3	Mouse	WB: 1:3000	66400-1-ig	Proteintech
FLI1	Mouse	WB: 1:500	MA1-196	Invitrogen

7.5. LIST OF PRIMERS

SYMBOLS OF GENES	NAME OF GENES	ACCESSION ID	SENSE SEQUENCES	ANTI-SENSE SEQUENCES
ACTB	Actin, beta	NM_001101.5	cccagcacaatgagatcaa	acatctgctggaaggtggac
CCNB1	Cyclin B1	NM_001354844.2	acaccaactctacaacattacct	ttagcatgcttcgatgtggc
CCNB2	Cyclin B2	NM_004701.4	tgaacagcacactttagcca	tgtgctgcatgacttccaat
CCND1	Cyclin D1	NM_053056.3	cttcctgtcctactaccgcc	ctcctcctcttcctcctcct
CCND2	Cyclin D2	NM_001759.4	aggatgaggaagtgagctcg	ctcctggcaagctttgagac
CCNE1	Cyclin E1	NM_001238.4	cgctgatgaagatgcacaca	acatggctttctttgctcgg
CDK1	Cyclin dependent kinase 1	NM_001170406.1	agcctagcatcccatgtcaa	tcagtgccattttgccagaa
CDK16	Cyclin dependent kinase 16	NM_001170460.2	tcagctacaaaaggaggcca	tgtggcttagaactcggtgt
ELF5	E74-like factor 5	NM_001243080.2	tgcttgaaaacaagtggcatc	agggcttccgatttaaccacc
IVL	Involucrin	NM_005547.4	gcactccaccaaagcctct	tggaggaggaacagtcttgag
KRT1	Keratin 1	NM_006121.4	tttctctaagtcaacatga	cttgaaaatctcccacca
KRT10	Keratin 10	NM_000421.5	gatcttccagtgggatctgtgtcca	gcagtttaatagtagtgtttct
KRT14	Keratin 14	NM_000526.5	ccagttctcctctggatcgcag	gatcttccagtgggatctgtgtcca
GATA3	GATA binding protein 3	NM_001002295.2	gtcctgtgcgaactgtcaga	cgagctgttcttggggaagt
FLI1	FLI1 proto-oncogene ETS transcription factor	NM_001167681.3	acggaagtgctgttgtcacacc	caagctcctcttctgactgagtc

7.6. LIST OF KITS

NAME OF KITS	CATALOGUE ID	SOURCE
Direct-zol RNA MiniPrep Kit	R2050	Zymo-Research
Lenti-vpak Packaging Kit	TR30037	OriGene
Micro BCA Protein Assay Kit	23235	ThermoFisher
Mini Trans-Blot Electrophoretic Transfer Cell	1703930	BIO-RAD
Nucleospin Gel and PCR Clean-up	740609.50	Machery-Nage
Nucleospin Plasmid Mini kit for Plasmid DNA	740588.250	Machery-Nagel
Phusion Flash HighFidelity PCR Master Mix	F548S	ThermoFisher
qPCR Lentivirus Complete Titration Kit	LV900	Abm
qPCRBIO cDNA Synthesis Kit	PB30.11-02	PCR Biosystems
Quick-DNA Miniprep Plus Kit	D4068S	Zymo-Research
SuperSignal West Pico PLUS Chemiluminescent Substate	34577	ThermoFisher
Zero Blunt PCR Cloning Kit	K270020	ThermoFisher

7.7. LIST OF VECTORS

NAME OF VECTORS	CATALOGUE/CLONE ID	SOURCE
pAIOsgRNA mCMV (ELF5)	GSGH11935-247741627/VSGHSOM_28723476	Horizon
Lentiviral mCMV non-targeting control	GSGC11953/SVC18050201	Horizon
pLenti-C-mGFP (PS100071) (GATA-3)	RC211904L2	Origene
Lentiviral Human FLI1 hCMV-turboGFP shRNA (FLI-1)	V3SVHS00_7673437	Horizon
Precision LentiORF turboRFP control	10HS5832	Horizon

7.8. CLONING PRIMERS USED FOR LUCIFERASE REPORTER ASSAY

PRIMER NAME F	FORWARD (LOWERCASE LETTERS = KPNI RESTRICTION SITES)	PRIMER NAME R	REVERSE (LOWERCASE LETTERS = XHOI RESTRICTION SITES)	PCR PRODUCT SIZE
h_FLI1_F_Luc_KpnI-BS-1 (binding region)	ttttggtaccCCTGCTGACTGTCCTAGAGG	h_FLI1_R_Luc_XhoI-BS-1 (binding region)	aaaactcgagGCATCTTCTCGAGCCAAACC	137bp
h_FLI1_F_Luc_KpnI-BS-2 (binding region)	ttttggtaccCGCCTCAGGAAAAGCAAAGA	h_FLI1_R_Luc_XhoI-BS-2 (binding region)	aaaactcgagAAGAGCTAGCCGGGAACAAT	136bp
h_FLI1_F_Luc_KpnI-NB (non-binding region)	ttttggtaccAGGCTGGGTAGGGAGGAC	h_FLI1_R_Luc_XhoI-NB (non-binding region)	aaaactcgagTCTAGGACAGTCAGCAGGTC	117bp
h_GATA3_F_Luc_KpnI-BS-1 (binding region)	ttttggtaccGGTTGGGGTCGGTGCAGA	h_GATA3_R_Luc_XhoI-BS-1 (binding region)	aaaactcgagACGCTCAGTGTAGACGGAC	162bp
h_GATA3_F_Luc_KpnI-BS-2 (binding region)	tttggtaccGACAACAAAATTGACGCGGAC	h_GATA3_R_Luc_XhoI-BS-2 (binding region)	aaaactcgagCATCGATGTGGGGAAACGTG	162bp
h_GATA3_F_Luc_KpnI-BS-3 (binding region)	ttttggtaccCAAACACCCTGCATTAGATCCT	h_GATA3_R_Luc_XhoI-BS-3 (binding region)	aaaactcgag CTCCTGCCAATTCATTCGGG	158bp
h_GATA3_F_Luc_KpnI-NB (non-binding region)	ttttggtacc ACCGAGTTCTTTCTGTCCGT	h_GATA3_R_Luc_XhoI-NB (non-binding region)	aaaaactcgag CGTCCGCGTCAATTTTGTTG	241p

7.9 RNA SEQUENCING TOOLS

TOOLS (VERSION)	DESCRIPTION	REFERENCES
FastQC (v0.12.1)	Assessment of raw RNA-seq read quality, including base quality scores, GC content, and detection of adapter contamination and low-quality reads.	Andrews, S. (2010). *FastQC: A quality control tool for high throughput sequence data*. Babraham Institute.
STAR (v2.7.10b)	Splice-aware alignment of RNA-seq reads to the human reference genome GRCh38.p14.	Dobin, A., et al. (2013). *Bioinformatics*, 29(1), 15–21.
FeatureCounts / Subread (v2.0.1)	Quantification of gene-level read counts from aligned BAM files.	Liao, Y., Smyth, G. K., & Shi, W. (2014). *Bioinformatics*, 30(7), 923–930.
R / RStudio (v4.2.2)	Statistical computing environment used for downstream data processing, analysis, and visualization.	R Core Team (2022). *R: A language and environment for statistical computing*.
edgeR (v3.38.4)	Library size normalization and differential gene expression analysis using negative binomial models.	Robinson, M. D., McCarthy, D. J., & Smyth, G. K. (2010). *Bioinformatics*, 26(1), 139-140.
Benjamini-Hochberg method	Adjustment for multiple hypothesis testing to control the false discovery rate (FDR < 0.05).	Benjamini, Y., & Hochberg, Y. (1995). *Journal of the Royal Statistical Society B*, 57(1), 289-300.
pheatmap (v1.0.12)	Generation of heatmaps using normalized gene expression values.	Kolde, R. (2019). *pheatmap: Pretty Heatmaps*.

EnhancedVolcano (v1.14.0)	Visualization of differentially expressed genes based on fold change and statistical significance.	Blighe, K., Rana, S., & Lewis, M. (2021). *EnhancedVolcano*.
clusterProfiler (v4.4.4)	Gene Ontology enrichment analysis of differentially expressed genes.	Yu, G., et al. (2012). *OMICS*, 16(5), 284-287.
org.Hs.eg.db (v3.15.0)	Annotation of human gene identifiers for enrichment analyses.	Carlson, M. (2022). *org.Hs.eg.db*.
fgsea (v1.24.0)	Fast preranked gene set enrichment analysis and calculation of normalized enrichment scores.	Korotkevich, G., et al. (2021). *Bioinformatics*, 37(21), 3733-3735.
PCAtools (v2.14.0)	Principal component analysis for dimensionality reduction and sample clustering.	Blighe, K., & Lun, A. (2022). *PCAtools*.

8.0 REFERENCES

ABDALLAH, B.M., 2017. Marrow adipocytes inhibit the differentiation of mesenchymal stem cells into osteoblasts via suppressing BMP-signalling. *Journal of Biomedical Science,* 24, 1–10.

ABDALLAH, F., et al., 2017. Skin immune landscape: inside and outside the organism. *Mediators of Inflammation*, 2017, pp.5095293–5095317. https://doi.org/10.1155/2017/5095293

ABRAHAM, J. and MATHEW, S., 2019. Merkel cells: A collective review of current concepts. *International Journal of Applied and Basic Medical Research*, 9, pp.9–13.

AFGAN, E., BAKER, D., BATUT, B., et al., 2018. The Galaxy platform for accessible, reproducible and collaborative biomedical analyses. *Nucleic Acids Research*, 46(W1), pp. W537–W544. https://doi.org/10.1093/nar/gky379

AGOSTINI, M., et al., 2022. Long non-coding RNAs affecting cell metabolism in cancer. *Biology Direct*, 17(1), p.26.

AHMED, M.I., et al., 2016. The transcriptional repressor Blimp1 is expressed in rare luminal progenitors and is essential for mammary gland development. *Development,* 143 (10), 1663–1673.

ALAM, J. and COOK, J.L., 1990. Reporter genes: applications to the study of mammalian gene transcription. *Analytical Biochemistry*, 188(2), pp. 245–254. https://doi.org/10.1016/0003-2697(90)90297-3

ALAM, M. and RATNER, D., 2001. Cutaneous squamous-cell carcinoma. *New England Journal of Medicine*, 344, pp.975–983.

AMELIO, I., et al., 2021. Emerging roles of long non-coding RNAs in breast cancer biology and management. *Seminars in Cancer Biology*, 72, pp.36–45.

AMIN, N. and VINCAN, E., 2012. The Wnt signalling pathways and cell adhesion. *Front Biosci (Landmark Ed),* 17 (2), 784–804.

AMISTEN, S., et al., 2015. An atlas of G-protein coupled receptor expression and function in human subcutaneous adipose tissue. *Pharmacology & Therapeutics,* 146, 61–93.

ANDL, T., et al., 2002. WNT signals are required for the initiation of hair follicle development. *Developmental Cell,* 2 (5), 643–653.

ANDREWS, S., 2010. *FastQC: A quality control tool for high throughput sequence data*. Babraham Institute, Cambridge, UK.

ASHTON, K., et al., 2005. Cytogenetic alterations in nonmelanoma skin cancer: A review. *Genes, Chromosomes and Cancer*, 43, pp.239–248.

ASNAGLI, H., et al., 2002. Cutting Edge: Identification of an Alternative GATA-3 Promoter Directing Tissue-Specific Gene Expression in Mouse and Human. *The Journal of Immunology,* 168 (9), 4268.

ASSELIN-LABAT, M., et al., 2007. Gata-3 is an essential regulator of mammary-gland morphogenesis and luminal-cell differentiation. *Nature Cell Biology,* 9 (2), 201–209.

ATHANASIOU, M., et al., 2000. FLI-1 is a suppressor of erythroid differentiation in human hematopoietic cells. *Leukaemia,* 14 (3), 439–445.

BAE, Y., et al., 2012. The role of FGF signalling in guiding coordinate movement of cell groups: guidance cue and cell adhesion regulator? *Cell Adhesion & Migration,* 6 (5), 397–403.

BARBIERI, J. et al., 2014. Skin: Basic structure and function. In: McManus, L.M. & Mitchell, R.N.B.T.-P., eds. *Pathobiology of Human Disease*. Cambridge, MA: Academic Press, pp.1134–1144.

BARBIERI, J.S., et al., 2019. Approaches to limit systemic antibiotic use in acne: systemic alternatives, emerging topical therapies, dietary modification, and laser and light-based treatments. *Journal of the American Academy of Dermatology,* 80 (2), 538–549.

BARRANGOU, R., et al., 2007. CRISPR provides acquired resistance against viruses in prokaryotes. *Science,* 315 (5819), 1709–1712.

BEN-DAVID, Y., et al., 1990. Identification and mapping of a common proviral integration site Fli-1 in erythroleukemia cells induced by Friend murine leukaemia virus. *Proceedings of the National Academy of Sciences,* 87 (4), 1332–1336.

BEN-DAVID, Y., et al., 1991. Erythroleukemia induction by Friend murine leukaemia virus: insertional activation of a new member of the ets gene family, Fli-1, closely linked to c-ets-1. *Genes & Development,* 5 (6), 908–918.

BEN-DAVID, Y., et al., 2022. Current insights into the role of Fli-1 in haematopoiesis and malignant transformation. *Cellular and Molecular Life Sciences,* 79 (3), 163.

BENJAMINI, Y. and HOCHBERG, Y., 1995. Controlling the false discovery rate: a practical and powerful approach to multiple testing. *Journal of the Royal Statistical Society: Series B*, 57(1), pp. 289–300.

BERG, D. and OTLEY, C., 2002. Skin cancer in organ transplant recipients: Epidemiology, pathogenesis, and management. *Journal of the American Academy of Dermatology*, 47, pp.1–17.

BERG, R., et al., 1996. Early p53 alterations in mouse skin carcinogenesis by UVB radiation: Immunohistochemical detection of mutant p53 protein in clusters of preneoplastic epidermal cells. *Proceedings of the National Academy of Sciences of the USA*, 93, pp.274–278.

BERNARD, A.M. and BERNARD, G.R., 2012. The immune response: targets for the treatment of severe sepsis. *International Journal of Inflammation,* 2012 (1), 697592.

BERNARD, J., et al., 2012. Ultraviolet radiation damages self-noncoding RNA and is detected by TLR3. *Nature Medicine*, 18, pp.1286–1290. https://doi.org/10.1038/nm.2861

BERNAT-PEGUERA, A., et al., 2019. PDGFR-induced autocrine SDF-1 signalling in cancer cells promotes metastasis in advanced skin carcinoma. *Oncogene*, 38, pp.5021–5037.

BERONJA, S., et al., 2013. RNAi screens in mice identify physiological regulators of oncogenic growth. *Nature,* 501 (7466), 185–190.

BLANPAIN, C., et al., 2004. Self-renewal, multipotency, and the existence of two cell populations within an epithelial stem cell niche. *Cell,* 118 (5), 635–648.

BLANPAIN, C., et al., 2006. Self-renewal, multipotency, and the existence of two cell populations within an epithelial stem cell niche. *Cell*, 118(5), pp. 635–648.

BLIGHE, K. and LUN, A., 2022. *PCAtools: Everything principal components analysis*. R package version 2.14.0.

BLIGHE, K., RANA, S. and LEWIS, M., 2021. *EnhancedVolcano: Publication-ready volcano plots with enhanced colouring and labeling*. R package version 1.14.0.

BOCHERT, M.A., et al., 1998. Molecular Cloning and Expression of Ehf, a New Member of the ets Transcription Factor/Oncoprotein Gene Family. *Biochemical and Biophysical Research Communications,* 246 (1), 176–181.

BOELSMA, E., et al., 2003. Human skin condition and its associations with nutrient concentrations in serum and diet. *The American Journal of Clinical Nutrition,* 77 (2), 348–355.

BOIREAU-ADAMEZYK, E, et al., 2014. Age-dependent changes in stratum corneum barrier function. *Skin Research and Technology,* 20 (4), 409–415.

BORKOWSKI, A. and GALLO, L., 2014. UVB radiation illuminates the role of TLR3 in the epidermis. *Journal of Investigative Dermatology*, 134, pp.2315–2320. https://doi.org/10.1038/JID.2014.167

BOROWICZ, S., et al., 2014. The soft agar colony formation assay. *Journal of Visualized Experiments*, (92), p.e51998.

BOTCHKAREV, V.A. and KISHIMOTO, J., 2003. Molecular control of epithelial–mesenchymal interactions during hair follicle cycling. *In: Journal of Investigative Dermatology Symposium Proceedings,* Elsevier, pp. 46–55.

BOTCHKAREV, V.A. and SHAROV, A.A., 2004. BMP signalling in the control of skin development and hair follicle growth. *Differentiation*, 72(9–10), pp. 512–526.

BOTTOMLEY, M., et al., 2019. The role of the immune system in cutaneous squamous cell carcinoma. *International Journal of Molecular Sciences*, 20, p.2009.

BOUKAMP, P., et al., 1988. Normal keratinization in a spontaneously immortalized aneuploid human keratinocyte cell line. *Journal of Cell Biology*, 106(3), pp. 761–771.

BOYDEN, S., 1962. The chemotactic effect of mixtures of antibody and antigen on polymorphonuclear leucocytes. *The Journal of Experimental Medicine*, 115, pp. 453–466. https://doi.org/10.1084/jem.115.3.453

BRAND, R. et al., 2018. Targeting mitochondrial oxidative stress to mitigate UV-induced skin damage. *Frontiers in Pharmacology*, 9, p.920. https://doi.org/10.3389/fphar.2018.00920

BRASH, D. et al., 1991. A role for sunlight in skin cancer: UV-induced p53 mutations in squamous cell carcinoma. *Proceedings of the National Academy of Sciences of the United States of America*, 88, pp.10124–10128.

BRASH, D., et al., 1996. Sunlight and sunburn in human skin cancer: P53, apoptosis, and tumour promotion. *Journal of Investigative Dermatology Symposium Proceedings*, 1, pp.136–142.

BRASIER, A.R. and RON, D., 1992. Luciferase reporter gene assays in mammalian cells. *Methods in Enzymology*, 216, pp. 386–397. https://doi.org/10.1016/0076-6879(92)16036-J

BROUGHAM, N. and TAN, S., 2014. The incidence and risk factors of metastasis for cutaneous squamous cell carcinoma—Implications on the T-classification system. *Journal of Surgical Oncology*, 110, pp.876–882.

BROWN, V., et al., 2004. p16INK4a and p14ARF tumour suppressor genes are commonly inactivated in cutaneous squamous cell carcinoma. *Journal of Investigative Dermatology*, 122, pp.1284–1292.

BUDU-AGGREY, A., et al., 2019. Evidence of a causal relationship between body mass index and psoriasis: A mendelian randomization study. *PLoS Medicine,* 16 (1), e1002739.

BURN, S.F., et al., 2011. Calcium/NFAT signalling promotes early nephrogenesis. *Developmental Biology,* 352 (2), 288–298.

BUXMAN, M. and WUEPPER, K., 1978. Cellular localization of epidermal transglutaminase: a histochemical and immunochemical study. *Journal of Histochemistry & Cytochemistry*, 26, pp.340–348.

BYRD, A.L., et al., 2018a. The human skin microbiome. *Nature Reviews Microbiology,* 16 (3), 143–155.

CADIGAN, K.M. and NUSSE, R., 1997. Wnt signalling: a common theme in animal development. *Genes & Development,* 11 (24), 3286–3305.

CAI, T., et al., 2013. Fibroblast growth factor 2 induces mesenchymal stem cells to differentiate into tenocytes through the MAPK pathway. *Molecular Medicine Reports,* 8 (5), 1323–1328.

CAMPIONE, E., et al., 2020. Skin immunity and its dysregulation in atopic dermatitis, hidradenitis suppurativa and vitiligo. *Cell Cycle,* 19 (3), 257–267.

Cancer Research UK. (2024). *Non-melanoma skin cancer statistics*. https://www.cancerresearchuk.org/health-professional/cancer-statistics/non-melanoma-skin-cancer

CAÑUETO, J., et al., 2017. Epidermal growth factor receptor expression is associated with poor outcome in cutaneous squamous cell carcinoma. *British Journal of Dermatology,* 176 (5), 1279–1287.

CAPONE, K.A., et al., 2011. Diversity of the human skin microbiome early in life. *Journal of Investigative Dermatology,* 131 (10), 2026–2032.

CARLSON, M., 2022. *org.Hs.eg.db: Genome-wide annotation for Human*. R package version 3.15.0.

CHAKRABARTI, R., et al., 2012. Elf5 inhibits the epithelial–mesenchymal transition in mammary gland development and breast cancer metastasis by transcriptionally repressing Snail2. *Nature Cell Biology,* 14 (11), 1212–1222.

CHAKRABARTI, R., et al., 2012. Elf5 regulates mammary gland stem/progenitor cell fate by influencing notch signalling. *Stem Cells,* 30 (7), 1496–1508.

CHAN, J., et al., 2018. Targeting nuclear receptors in cancer-associated fibroblasts as concurrent therapy to inhibit development of chemo resistant tumours. *Oncogene*, 37, pp.160–173.

CHEN, N., et al., 2018. A novel FLI1 exonic circular RNA promotes metastasis in breast cancer by co-ordinately regulating TET1 and DNMT1. *Genome Biology,* 19, 1–14.

CHERMNYKH, E., et al., 2018. Extracellular matrix as a regulator of epidermal stem cell fate. *International Journal of Molecular Sciences*, 19, p.1003.

CHIKH, A., et al., 2007. Expression of GATA-3 in epidermis and hair follicle: relationship to p63. *Biochemical and Biophysical Research Communications,* 361 (1), 1–6.

CHOI, S., et al., 1998. A novel ets-related transcription factor, ERT/ESX/ESE-1, regulates expression of the transforming growth factor-β type II receptor. *Journal of Biological Chemistry,* 273 (1), 110–117.

CHOU, J., et al., 2010. GATA3 in development and cancer differentiation: cells GATA have it! *Journal of Cellular Physiology,* 222 (1), 42–49.

CHUA, A.W.C., et al., 2011. Keloid fibroblasts are more sensitive to Wnt3a treatment in terms of elevated cellular growth and fibronectin expression. *Journal of Dermatological Science,* 64 (3), 199–209.

CIBRIAN, D, et al., 2020. Metabolic pathways that control skin homeostasis and inflammation. *Trends in Molecular Medicine,* 26 (11), 975–986.

CICHOREK, M., et al., 2013. Skin melanocytes: Biology and development. *Postępy Dermatologii i Alergologii*, 30, pp.30–41.

CLEVERS, H, et al., 2014. An integral program for tissue renewal and regeneration: Wnt signalling and stem cell control. *Science,* 346 (6205), 1248012.

CLEVERS, H., 2006. Wnt/β-catenin signalling in development and disease. *Cell,* 127 (3), 469–480.

CODERCH, L., et al., 2003. Ceramides and skin function. *American Journal of Clinical Dermatology,* 4, 107–129.

COLOMBO, I., et al., 2017. HaCaT cells as a reliable in vitro differentiation model to dissect the inflammatory/repair response of human keratinocytes. *Mediators of Inflammation*, 2017, Article ID 7435621.

CUI, C.-Y. and SCHLESSINGER, D., 2006. Ectodermal dysplasia: regulation and function of bone morphogenetic protein signalling. *Endocrine Reviews*, 27(4), pp. 427–449.

CUI, J.W., et al., 2009. Continuous Fli-1 expression plays an essential role in the proliferation and survival of F-MuLV-induced erythroleukemia and human erythroleukemia. *Leukaemia,* 23 (7), 1311–1319.

DAMANTE, G., et al., 1994. Sequence-specific DNA recognition by the thyroid transcription factor-1 homeodomain. *Nucleic Acids Research,* 22 (15), 3075–3083.

DANG, C., et al., 2006. E6/E7 expression of human papillomavirus types in cutaneous squamous cell dysplasia and carcinoma in immunosuppressed organ transplant recipients. *British Journal of Dermatology*, 155, pp.129–136.

DARZYNKIEWICZ, Z., JUAN, G. and BEDNER, E., 2004. Determining cell cycle stages by flow cytometry. *Current Protocols in Cell Biology*, Chapter 8, Unit 8.4. https://doi.org/10.1002/0471143030.cb0804s01

DASGUPTA, R. and FUCHS, E., 1999. Multiple roles for activated LEF/TCF transcription complexes during hair follicle development and differentiation. *Development,* 126 (20), 4557–4568.

DAVIES, J. and DAVIES, D., 2010. Origins and evolution of antibiotic resistance. *Microbiology and Molecular Biology Reviews*, 74(3), pp. 417–433. https://doi.org/10.1128/MMBR.00016-10

De GRUIJL, F., et al., 2010. Early and late effects of the immunosuppressants rapamycin and mycophenolate mofetil on UV carcinogenesis. *International Journal of Cancer*, 127, pp.796–804.

DE GUZMAN STRONG, C., et al., 2006. Lipid defect underlies selective skin barrier impairment of an epidermal-specific deletion of Gata-3. *The Journal of Cell Biology,* 175 (4), 661–670.

DE VAL, S. and BLACK, B.L., 2009. Transcriptional control of endothelial cell development. *Developmental Cell,* 16 (2), 180–195.

DEMEHRI, S., et al., 2009. Epidermal Notch1 loss promotes skin tumorigenesis by impacting the stromal microenvironment. *Cancer Cell*, 16, pp.55–66.

DERYNCK, R. and AKHURST, R.J., 2007. Differentiation plasticity regulated by TGF-β family proteins. *Nature Cell Biology*, 9(9), pp. 1000–1004.

DEVEAU, H., et al., 2008. Phage response to CRISPR-encoded resistance in Streptococcus thermophilus. *Journal of Bacteriology,* 190 (4), 1390–1400.

DEVGAN, V., et al., 2005. p21WAF1/Cip1 is a negative transcriptional regulator of Wnt4 expression downstream of Notch1 activation. *Genes & Development*, 19, pp.1485–1495.

DHILLON, A.S., et al., 2007. MAP kinase signalling pathways in cancer. *Oncogene*, 26(22), pp. 3279–3290.

DOBIN, A., et al., 2013. STAR: ultrafast universal RNA-seq aligner. *Bioinformatics*, 29(1), pp. 15–21.

DOPYTALSKA, K., et al., 2021. The role of epigenetic factors in psoriasis. *International Journal of Molecular Sciences*, 22(17), p.9294.

DOTTO, G., et al., 1988. Malignant transformation of mouse primary keratinocytes by Harvey sarcoma virus and its modulation by surrounding normal cells. *Proceedings of the National Academy of Sciences of the USA*, 85, pp.6389–6393.

DOTTO, G.P., 2009. Notch tumor suppressor function. *Oncogene*, 27(38), pp. 5115–5123.

DOUDNA, J.A. and CHARPENTIER, E., 2014. Genome editing: the new frontier of genome engineering with CRISPR-Cas9. *Science*, 346(6213), p. 1258096. https://doi.org/10.1126/science.1258096

DUFFILL, M., et al., 1976. The cell proliferation kinetics of psoriasis examined by three in vivo techniques. *British Journal of Dermatology*, 94, pp.355–362.

DUPERRET, E.K., 2015. *The role of αv integrins in human skin tissue homeostasis, wound healing and squamous cell carcinoma.* University of Pennsylvania.

DUSENDANG, J.R., et al., 2022. Cohort and nested case-control study of cutaneous squamous cell carcinoma in solid organ transplant recipients, by medication. *Journal of the American Academy of Dermatology,* 86 (3), 598–606.

ELIAS, P., et al., 2014. Formation and functions of the corneocyte lipid envelope (CLE). *Biochimica et Biophysica Acta*, 1841, pp.314–318.

ELIAS, P.M., 2005. Stratum corneum defensive functions: an integrated view. *Journal of Investigative Dermatology,* 125 (2), 183–200.

FAN, C., et al., 2017. Role of long non-coding RNAs in glucose metabolism in cancer. *Molecular Cancer*, 16, p.1.

FARAGE, M.A., et al., 2008. Intrinsic and extrinsic factors in skin ageing: a review. *International Journal of Cosmetic Science,* 30 (2), 87–95.

FELDMAN, R.J., et al., 2003. The epithelial-specific Ets factors occupy a unique position in defining epithelial proliferation, differentiation and carcinogenesis. *Anticancer Research,* 23 (3), 2125–2132.

FJELDBORG, K., et al., 2014. Human adipose tissue macrophages are enhanced but changed to an anti-inflammatory profile in obesity. *Journal of Immunology Research,* 2014 (1), 309548.

FLOURIS, A.D., 2011. Functional architecture of behavioural thermoregulation. *European Journal of Applied Physiology,* 111 (1), 1–8.

FONG, A.P. and TAPSCOTT, S.J., 2013. Skeletal muscle programming and re-programming. *Current Opinion in Genetics & Development,* 23 (5), 568–573.

FOULQUIER, S., et al., 2018. WNT signalling in cardiac and vascular disease. *Pharmacological Reviews,* 70 (1), 68–141.

FRESHNEY, R.I., 2010. *Culture of Animal Cells: A Manual of Basic Technique and Specialized Applications*. 6th ed. Oxford: Wiley-Blackwell.

FU, P., et al., 2021. CRISPR/Cas9-based generation of a recombinant double-reporter pseudorabies virus and its characterization in vitro and in vivo. *Veterinary Research,* 52 (1), 95.

FUCHS, E., 2007. Scratching the surface of skin development. *Nature,* 445 (7130), 834–842.

FULTON, D.L., et al., 2009. TFCat: the curated catalog of mouse and human transcription factors. *Genome Biology,* 10, 1–14.

GAJOS-MICHNIEWICZ, A. and CZYZ, M., 2020. WNT signalling in melanoma. *International Journal of Molecular Sciences,* 21 (14), 4852.

GARCIA-SANCHA, N., et al., 2019. MicroRNA dysregulation in cutaneous squamous cell carcinoma. *International Journal of Molecular Sciences*, 20, p.2181.

GARCOVICH, S., et al., 2017. Skin cancer epidemics in the elderly as an emerging issue in geriatric oncology. *Aging and Disease*, 8, pp.643–661.

GAUR, M., et al., 2017. Mesenchymal stem cells from adipose tissue in clinical applications for dermatological indications and skin aging. *International Journal of Molecular Sciences,* 18 (1), 208.

GELFAND, J.M., et al., 2006. Risk of myocardial infarction in patients with psoriasis. *Jama,* 296 (14), 1735–1741.

GHOSH, D., et al., 2023. Emerging roles of non-coding RNAs in psoriasis pathogenesis. *Functional & Integrative Genomics*, 23, p.129.

GLOSTER JR, H.M. and NEAL, K., 2006. Skin cancer in skin of color. *Journal of the American Academy of Dermatology,* 55 (5), 741–760.

GORDON, M.D. and NUSSE, R., 2006. Wnt signalling multiple pathways, multiple receptors, and multiple transcription factors. *Journal of Biological Chemistry,* 281 (32), 22429–22433.

GRASSMEYER, J., et al., 2017. Elf5 is a principal cell lineage specific transcription factor in the kidney that contributes to Aqp2 and Avpr2 gene expression. *Developmental Biology,* 424 (1), 77–89.

GREEN, M.R. and SAMBROOK, J., 2012. *Molecular Cloning: A Laboratory Manual*. 4th ed. Cold Spring Harbor, NY: Cold Spring Harbor Laboratory Press.

GRICE, E.A. and SEGRE, J.A., 2011. The skin microbiome. *Nature Reviews Microbiology,* 9 (4), 244–253.

GRIFFITHS, C, et al., 2021. Barker JNWN. Psoriasis. *Lancet,* 397 (10281), 1301–1315.

GRIVENNIKOV, et al., 2010. Immunity, inflammation, and cancer. *Cell*, 140, pp.883–899.

GROTE, D., et al., 2008. Gata3 acts downstream of β-catenin signalling to prevent ectopic metanephric kidney induction. *PLoS Genetics,* 4 (12), e1000316.

GUAN, Y., et al., 2021. Transcriptional and signalling regulation of skin epithelial stem cells in homeostasis, wounds and cancer. *Experimental Dermatology,* 30 (4), 529–545.

GUIMBERTEAU, J.C., et al., 2010. The microvacuolar system: how connective tissue sliding works. *Journal of Hand Surgery (European Volume),* 35 (8), 614–622.

GULBINAS, A., et al., Aberrant Gata-3 Expression in Human Pancreatic Cancer.

GUTTMAN, M. and RINN, J., 2012. Modular regulatory principles of large non-coding RNAs. *Nature*, 482(7385), pp.339–346.

HAFNER, M., NIEPEL, M., CHUNG, M. and SORGER, P.K., 2016. Growth rate inhibition metrics correct for confounders in measuring sensitivity to cancer drugs. *Nature Methods*, 13, pp. 521–527. https://doi.org/10.1038/nmeth.3853

HAFT, D.H., et al., 2005. A guild of 45 CRISPR-associated (Cas) protein families and multiple CRISPR/Cas subtypes exist in prokaryotic genomes. *PLoS Computational Biology,* 1 (6), e60.

HALL, P. and WATT, F.., 1989. Stem cells: the generation and maintenance of cellular diversity. *Development*, 106, pp.619–633.

HAMANAKA, R. and CHANDEL, N., 2013. Mitochondrial metabolism as a regulator of keratinocyte differentiation. *Cell Logistics*, 3, e25456. https://doi.org/10.4161/cl.25456

HAMBURGER, A.W. and SALMON, S.E., 1977. Primary bioassay of human tumour stem cells. *Science*, 197(4302), pp. 461–463. https://doi.org/10.1126/science.560061

HAN, W., et al., 2010. Immunosuppressive cyclosporin A activates AKT in keratinocytes through PTEN suppression: Implications in skin carcinogenesis. *Journal of Biological Chemistry*, 285, pp.11369–11377.

HAN, W., et al., 2012. Deregulation of XPC and CypA by cyclosporin A: An immunosuppression-independent mechanism of skin carcinogenesis. *Cancer Prevention Research (Philadelphia)*, 5, pp.1155–1162.

HANAHAN, D. and COUSSENS, M., 2012. Accessories to the crime: Functions of cells recruited to the tumour microenvironment. *Cancer Cell*, 21, pp.309–322.

HARKNESS, R., et al., 2020. Primary ovarian high-grade neuroendocrine carcinoma with Merkel cell–like immunophenotype arising in a teratoma. *International Journal of Gynaecological Pathology,* 39 (5), 478–484.

HASSAN, S., et al., 2019. A unique panel of patient-derived cutaneous squamous cell carcinoma cell lines provides a preclinical pathway for therapeutic testing. *International Journal of Molecular Sciences*, 20, p.3428.

HE, X., et al., 2004. LDL receptor-related proteins 5 and 6 in Wnt/β-catenin signalling: arrows point the way.

HEMIDA, A.S. and HOLAH, N.S., 2022. Expression of Friend Leukaemia Integration-1 (Fli-1) and the Apoptosis Regulator B Cell Lymphoma-2 (BCL-2) in Gastric Carcinoma; an Immunohistochemical Study. *Journal of Immunoassay and Immunochemistry,* 43 (1), 1954948.

HENNINGS, H., MICHAEL, D., CHENG, C., et al., 1980. Calcium regulation of growth and differentiation of mouse epidermal cells in culture. *Cell*, 19(1), pp. 245–254. https://doi.org/10.1016/0092-8674(80)90406-7

HILL, D.S., et al., 2015. A novel fully humanized 3D skin equivalent to model early melanoma invasion. *Molecular Cancer Therapeutics,* 14 (11), 2665–2673.

HO, I., et al., 2009. GATA3 and the T-cell lineage: essential functions before and after T-helper-2-cell differentiation. *Nature Reviews Immunology,* 9 (2), 125–135.

HO, I.C., et al., 1991. Human GATA-3: a lineage-restricted transcription factor that regulates the expression of the T cell receptor alpha gene. *The EMBO Journal,* 10 (5), 1187.

HOCH, R.V., et al., 1999. GATA-3 is expressed in association with estrogen receptor in breast cancer. *International Journal of Cancer,* 84 (2), 122–128.

HOFMANN, E., et al., 2023. Modelling the complexity of human skin in vitro. *Biomedicines*, 11, p.794. https://doi.org/10.3390/biomedicines11030794

HOLBROOK, K.A., 1979. Human epidermal embryogenesis. *International Journal of Dermatology,* 18 (1).

HOLICK, M.F., 2007. Vitamin D Deficiency New England Journal of Medicine 357 (3) 266–281. doi: 10.1056. *NEJMra070553.*

HOLSTEIN, T.W., 2012. The evolution of the Wnt pathway. *Cold Spring Harbor Perspectives in Biology,* 4 (7), a007922.

HORST, A.K, et al., 2019. Contribution of macrophage efferocytosis to liver homeostasis and disease. *Frontiers in Immunology,* 10, 2670.

HOUBEN, E, et al., 2007. A keratinocyte's course of life. *Skin Pharmacology and Physiology,* 20 (3), 122–132.

HOUBEN, E., et al., 2007. A keratinocyte's course of life. *Skin Pharmacology and Physiology*, 20, pp.122–132.

HOUSCHYAR, K.S., et al., 2019. Wnt pathway in bone repair and regeneration–what do we know so far. *Frontiers in Cell and Developmental Biology,* 6, 170.

HSU, P.D, et al., 2014. Development and applications of CRISPR-Cas9 for genome engineering. *Cell,* 157 (6), 1262–1278.

HU, A., et al., 2025. The involvement of Elf5 in regulating keratinocyte proliferation and differentiation processes in skin. *PloS One,* 20 (1), e0316134.

HU, M.S., et al., 2018. Embryonic skin development and repair. *Organogenesis,* 14 (1), 46–63.

HUELSKEN, J., et al., 2001. β-Catenin controls hair follicle morphogenesis and stem cell differentiation in the skin. *Cell,* 105 (4), 533–545.

INMAN, G., et al., 2018. The genomic landscape of cutaneous SCC reveals drivers, and a novel azathioprine associated mutational signature. *Nature Communications*, 9, p.3667.

ISHIGURO, S., et al., 2009. Basic fibroblast growth factor induces down-regulation of α-smooth muscle actin and reduction of myofibroblast areas in open skin wounds. *Wound Repair and Regeneration,* 17 (4), 617–625.

ITO, N., et al., 2005. Human hair follicles display a functional equivalent of the hypothalamic-pituitary-adrenal (HPA) axis and synthesize cortisol. *The FASEB Journal,* 19 (10), 1332–1334.

JACKSON, B., et al., 2005. Late cornified envelope family in differentiating epithelia—response to calcium and ultraviolet irradiation. *Journal of Investigative Dermatology*, 124, pp.1062–1070.

JANDA, C.Y., et al., 2017. Surrogate Wnt agonists that phenocopy canonical Wnt and β-catenin signalling. *Nature,* 545 (7653), 234–237.

JENSEN, P., et al., 2000. Skin cancer in kidney and heart transplant recipients and different long-term immunosuppressive therapy regimens. *Journal of the American Academy of Dermatology*, 42, p.307.

JENSEN, T.J., et al., 2009. Epigenetic mediated transcriptional activation of WNT5A participates in arsenical-associated malignant transformation. *Toxicology and Applied Pharmacology,* 235 (1), 39–46.

JENSEN, U.B. and WATT, F.M., 2006. Single-cell expression profiling of human epidermal stem and transit-amplifying cells. *Proceedings of the National Academy of Sciences of the USA*, 103(32), pp. 11958–11963.

JIANG, F., et al., 2020. Functional classification of prostate cancer-associated miRNAs through CRISPR/Cas9-mediated gene knockout. *Molecular Medicine Reports,* 22 (5), 3777–3784.

JONKER, D., et al., 2007. Cetuximab for the treatment of colorectal cancer. *New England Journal of Medicine*, 357, pp.2040–2048.

JOST, M., et al., 2000. The EGF receptor—an essential regulator of multiple epidermal functions. *European Journal of Dermatology*, 10, pp.505–510.

JUNTTILA, M. and de SAUVAGE, F., 2013. Influence of tumour micro-environment heterogeneity on therapeutic response. *Nature*, 501, pp.346–354.

KALAILINGAM, P., et al., 2019. Overexpression of CDC42SE1 in A431 cells reduced cell proliferation by inhibiting the Akt pathway. *Cells,* 8 (2), 117.

KALYUGA, M., et al., 2012. ELF5 suppresses estrogen sensitivity and underpins the acquisition of antiestrogen resistance in luminal breast cancer. *PLoS Biology,* 10 (12), e1001461.

KAUFFMAN, H., et al., 2006. Post-transplant de novo malignancies in renal transplant recipients: The past and present. *Transplant International*, 19, pp.607–620.

KAUFMAN, C.K., et al., 2003. GATA-3: an unexpected regulator of cell lineage determination in skin. *Genes & Development,* 17 (17), 2108–2122.

KIM, K.H., et al., 2015. Assaying cell cycle status using flow cytometry. *Methods in Molecular Biology*, 1239, pp. 157–166.

KIM, T.K. and EBERWINE, J.H., 2010. Mammalian cell transfection: the present and the future. *Analytical and Bioanalytical Chemistry*, 397, pp. 3173–3178. https://doi.org/10.1007/s00216-010-3821-6

KIM, Y., et al., 2020. Senescent fibroblast–derived GDF15 induces skin pigmentation. *Journal of Investigative Dermatology*, 140, pp.2478–2486. https://doi.org/10.1016/j.jid.2020.04.016

KISHI, C., et al., 2015. Hypo-osmotic shock-induced subclinical inflammation of skin in a rat model of disrupted skin barrier function. *Biological Research for Nursing,* 17 (2), 135–141.

KLEIN, S.L. and FLANAGAN, K.L., 2016. Sex differences in immune responses. *Nature Reviews Immunology,* 16 (10), 626–638.

KOBIELAK, K., et al., 2007. Loss of a quiescent niche but not follicle stem cells in the absence of bone morphogenetic protein signaling. *Proceedings of the National Academy of Sciences,* 104 (24), 10063–10068.

KOLARSICK, P.A., et al., 2011. Anatomy and physiology of the skin. *Journal of the Dermatology Nurses' Association,* 3 (4), 203–213.

KOLDE, R., 2019. *pheatmap: Pretty heatmaps*. R package version 1.0.12.

KOMIYA, Y. and HABAS, R., 2008. Wnt signal transduction pathways. *Organogenesis,* 4 (2), 68–75.

KONG, H.H. and SEGRE, J.A., 2017. The molecular revolution in cutaneous biology: investigating the skin microbiome. *Journal of Investigative Dermatology,* 137 (5), e119–e122.

KOROTKEVICH, G., et al., 2021. Fast gene set enrichment analysis. *Bioinformatics*, 37(21), pp. 3733–3735.

KOUROS-MEHR, H., et al., 2006. GATA-3 maintains the differentiation of the luminal cell fate in the mammary gland. *Cell,* 127 (5), 1041–1055.

KRETZ, M., et al., 2012. Suppression of progenitor differentiation requires the long noncoding RNA ANCR. *Genes & Development*, 26, pp.338–343.

KRETZ, M., et al., 2013. Control of somatic tissue differentiation by the long non-coding RNA TINCR. *Nature*, 493, pp.231–235.

KUBO, Y., et al., 1994. p53 gene mutations in human skin cancers and precancerous lesions: Comparison with immunohistochemical analysis. *Journal of Investigative Dermatology*, 102, pp.440–444.

KUREK, D., et al., 2007. FGF signalling regulates self-renewal and differentiation of adult epidermal stem cells. *Development*, 134(4), pp. 673–683.

KUREK, D., et al., 2007. Transcriptome and phenotypic analysis reveal Gata3-dependent signalling pathways in murine hair follicles.

KURIEN, B.T. and SCOFIELD, R.H., 2015. Protein extraction methods for western blotting. *Methods in Molecular Biology*, 1312, pp. 15–26. https://doi.org/10.1007/978-1-4939-2694-7_2

LANDRUM, M.J., et al., 2016. ClinVar: public archive of interpretations of clinically relevant variants. *Nucleic Acids Research,* 44 (D1), D862–D868.

LANNA, C., et al., 2019. Skin immunity and its dysregulation in psoriasis. *Cell Cycle,* 18 (20), 2581–2589.

LAPINSKAS, E.J., et al., 2011. The Ets transcription factor ELF5 functions as a tumour suppressor in the kidney. *Twin Research and Human Genetics,* 14 (4), 316–322.

LAVKER, R. and MATOLTSY, A., 1971. Substructure of keratohyalin granules of the epidermis as revealed by high resolution electron microscopy. *Journal of Ultrastructure Research*, 35, pp.575–581.

LAZAROV, M., et al., 2002. CDK4 coexpression with Ras generates malignant human epidermal tumorigenesis. *Nature Medicine*, 8, pp.1105–1114.

LEE, D.H, et al., 2016. Glycosaminoglycan and proteoglycan in skin aging. *Journal of Dermatological Science,* 83 (3), 174–181.

LEE, S.D. and TONTONOZ, P., 2014. Eosinophils in fat: pink is the new brown. *Cell,* 157 (6), 1249–1250.

LEE, T.I. and YOUNG, R.A., 2013. Transcriptional regulation and its mis regulation in disease. *Cell,* 152 (6), 1237–1251.

LEFORT, K. and DOTTO, G., 2004. Notch signalling in the integrated control of keratinocyte growth/differentiation and tumour suppression. *Seminars in Cancer Biology*, 14, pp.374–386.

LEFORT, K., et al., 2007. Notch1 is a p53 target gene involved in human keratinocyte tumour suppression through negative regulation of ROCK1/2 and MRCK alpha kinases. *Genes & Development*, 21, pp.562–577.

LEITER, U., et al., 2017. Incidence, mortality, and trends of nonmelanoma skin cancer in Germany. *Journal of Investigative Dermatology*, 137, pp.1860–1867.

LESAULT, I., et al., 2002. Direct regulation of BCL-2 by FLI-1 is involved in the survival of FLI-1-transformed erythroblasts. *The EMBO Journal.*

LESAULT, I., et al., 2002. FLI1 regulates transcription of BCL2 and MDM2. *Oncogene*, 21(37), pp. 5586–5595.

LEUSHACKE, M. and BARKER, N., 2012. Lgr5 and Lgr6 as markers to study adult stem cell roles in self-renewal and cancer. *Oncogene,* 31 (25), 3009–3022.

LI, C., et al., 2021. DNA damage-triggered activation of cGAS-STING pathway induces apoptosis in human keratinocyte HaCaT cells. *Molecular Immunology*, 131, pp.180–190. https://doi.org/10.1016/J.MOLIMM.2020.12.037

LI, D., et al., 2013. Crucial role for early growth response-1 in the transcriptional regulation of miR-20b in breast cancer. *Oncotarget,* 4 (9), 1373.

LI, G., et al., 1998. Induction of squamous cell carcinoma in p53-deficient mice after ultraviolet irradiation. *Journal of Investigative Dermatology*, 110, pp.72–75.

LI, L., et al., 2022. Transcription factor Fli-1 as a new target for antitumor drug development. *International Journal of Biological Macromolecules,* 209, 1155–1168.

LI, M., et al., 2021. UV-induced reduction in Polycomb repression promotes epidermal pigmentation. *Developmental Cell,* 56 (18), 2547–2561. e8.

LI, T., et al., 2023. CRISPR/Cas9 therapeutics: progress and prospects. *Signal Transduction and Targeted Therapy,* 8 (1), 36.

LI, Y., et al., 2015. Genomic analysis of metastatic cutaneous squamous cell carcinoma. *Clinical Cancer Research*, 21, pp.1447–1456.

LI, Y., et al., 2015. The ets transcription factor Fli-1 in development, cancer and disease. *Oncogene,* 34 (16), 2022–2031.

LIANG, C.C., PARK, A.Y. and GUAN, J.L., 2007. In vitro scratch assay: a convenient and inexpensive method for analysis of cell migration. *Nature Protocols*, 2, pp. 329–333. https://doi.org/10.1038/nprot.2007.30

LIAO, Y., et al., 2014. featureCounts: an efficient general-purpose program for assigning sequence reads to genomic features. *Bioinformatics*, 30(7), pp. 923–930.

LIM, K., et al., 2000. Gata3 loss leads to embryonic lethality due to noradrenaline deficiency of the sympathetic nervous system. *Nature Genetics,* 25 (2), 209–212.

LIM, X. and NUSSE, R., 2013a. Wnt signalling in skin development, homeostasis, and disease. *Cold Spring Harbor Perspectives in Biology,* 5 (2), a008029.

LIM, X., et al., 2013. Interfollicular epidermal stem cells self-renew via autocrine Wnt signalling. *Science*, 342(6163), pp. 1226–1230.

LINDELOF, B., et al., 2000. Incidence of skin cancer in 5356 patients following organ transplantation. *British Journal of Dermatology*, 143, pp.513–519.

LIU, D., et al., 2013. Tumor suppressor in lung cancer 1 (TSLC1), a novel tumor suppressor gene, is implicated in the regulation of proliferation, invasion, cell cycle, apoptosis, and tumorigenicity in cutaneous squamous cell carcinoma. *Tumor Biology,* 34 (6), 3773–3783.

LIU, H., et al., 2012a. Immunohistochemical Evaluation of GATA3 Expression in Tumours and Normal Tissues. *American Journal of Clinical Pathology,* 138 (1), 57.

LIVAK, K.J. and SCHMITTGEN, T.D., 2001. Analysis of relative gene expression data using real-time quantitative PCR. *Methods*, 25(4), pp. 402–408. https://doi.org/10.1006/meth.2001.1262

LOGAN, C.Y. and NUSSE, R., 2004. The Wnt signalling pathway in development and disease. *Annu.Rev.Cell Dev.Biol.,* 20 (1), 781–810.

LYLE, S., et al., 1998. The C8/144B monoclonal antibody recognizes cytokeratin 15 and defines a population of hair follicle stem cells. *Journal of Cell Science*, 111(21), pp. 3179–3188.

LYNLEY, A. and DALE, B., 1983. The characterisation of human epidermal filaggrin, a histidine-rich keratin filament-aggregating protein. *Biochimica et Biophysica Acta*, 744, pp.28–35.

M'BONEKO, V. and MERKER, H., 1988. Development and morphology of the periderm of mouse embryos (days 9–12 of gestation). *Cells Tissues Organs,* 133 (4), 325–336.

MADISON, K.C., 2003. Barrier function of the skin:“la raison d'etre” of the epidermis. *Journal of investigative dermatology*, *121*(2), pp.231-241.

MAHMOOD, T. and YANG, P.C., 2012. Western blot: technique, theory, and troubleshooting. *North American Journal of Medical Sciences*, 4(9), pp. 429–434. https://doi.org/10.4103/1947-2714.100998

MAKAROVA, K.S., et al., 2011. Evolution and classification of the CRISPR–Cas systems. *Nature Reviews Microbiology,* 9 (6), 467–477.

MAKAROVA, K.S., et al., 2015. An updated evolutionary classification of CRISPR–Cas systems. *Nature Reviews Microbiology,* 13 (11), 722–736.

MANCUSO, P. and BOUCHARD, B., 2019. The impact of aging on adipose function and adipokine synthesis. *Frontiers in Endocrinology*, 10, p.137. https://doi.org/10.3389/fendo.2019.00137

MAO, J., et al., 2001. Low-density lipoprotein receptor-related protein-5 binds to Axin and regulates the canonical Wnt signalling pathway. *Molecular Cell,* 7 (4), 801–809.

MARDARYEV, A.N., et al., 2011. Lhx2 differentially regulates Sox9, Tcf4 and Lgr5 in hair follicle stem cells to promote epidermal regeneration after injury. *Development*, 138(22), pp.4843–4852.

MASSE, I., et al., 2014. GATA3 inhibits proliferation and induces expression of both early and late differentiation markers in keratinocytes of the human epidermis. *Archives of Dermatological Research,* 306, 201–208.

MATSUYAMA, M., et al., 2014. Secreted Frizzled-related protein 1 (Sfrp1) regulates the progression of renal fibrosis in a mouse model of obstructive nephropathy. *Journal of Biological Chemistry,* 289 (45), 31526–31533.

MAURICE, M.M. and ANGERS, S., 2025. Mechanistic insights into Wnt–β-catenin pathway activation and signal transduction. *Nature Reviews Molecular Cell Biology,* 1–18.

MAZZOTTA, C., et al., 2021. FLI1 and ERG protein degradation is regulated via Cathepsin B lysosomal pathway in human dermal microvascular endothelial cells. *Microcirculation,* 28 (1), e12660.

MCGRATH, J., et al., 2004. Anatomy and organization of human skin. In: Burns, T., Breathnach, S., Cox, N. & Griffiths, C. (eds.) *Rook's Textbook of Dermatology*. 7th ed. Oxford: Blackwell Publishing, Vol. 1, pp.3.1–3.62.

MCGRATH, J.A. and UITTO, J., 2023. Structure and function of the skin. *Rook's Textbook of Dermatology,* 1–50.

MCKINLEY, K.L., 2018, Employing CRISPR/Cas9 genome engineering to dissect the molecular requirements for mitosis. *In:* Employing CRISPR/Cas9 genome engineering to dissect the molecular requirements for mitosis *Methods in Cell Biology.* Elsevier, 2018, pp. 75–105.

MEDICATIONS AND SQUAMOUS CELL SKIN CARCINOMA: nested case-control study within the skin cancer after organ transplant (scot) cohort, 2016. *American journal of transplantation*, 16, pp.565–573.

MEHRA, R., et al., 2005. Identification of GATA3 as a breast cancer prognostic marker by global gene expression meta-analysis. *Cancer Research,* 65 (24), 11259–11264.

MEHRANY, K., et al., 2005. High recurrence rates of squamous cell carcinoma after Mohs' surgery in patients with chronic lymphocytic leukaemia. *Dermatologic Surgery*, 31, pp.38–42.

MENON, G.K. and KLIGMAN, A.M., 2009. Barrier functions of human skin: a holistic view. *Skin Pharmacology and Physiology,* 22 (4), 178–189.

MERTENS, R.B., et al., 2015. GATA3 expression in normal skin and in benign and malignant epidermal and cutaneous adnexal neoplasms. *The American Journal of Dermatopathology,* 37 (12), 885–891.

METZGER, D.E, et al., 2008. Misexpression of ELF5 disrupts lung branching and inhibits epithelial differentiation. *Developmental Biology,* 320 (1), 149–160.

MIAO, B., et al., 2020. The transcription factor FLI1 promotes cancer progression by affecting cell cycle regulation. *International Journal of Cancer,* 147 (1), 189–201.

MILLER, C.S, et al., 1994. Detection of HPV DNA in oral carcinoma using polymerase chain reaction together with in situ hybridization. *Oral Surgery, Oral Medicine, Oral Pathology,* 77 (5), 480–486.

MILLER, L. and WEINSTOCK, M., 1994. Nonmelanoma skin cancer in the United States: Incidence. *Journal of the American Academy of Dermatology*, 30, pp.774–778.

MING K, K., et al., 2004. Essential roles of BMPR-IA signalling in differentiation and growth of hair follicles and in skin tumorigenesis. *Genesis,* 39 (1), 10–25.

MIYANO, M., et al., 2021. Breast-specific molecular clocks comprised of ELF5 expression and promoter methylation identify individuals susceptible to cancer initiation. *Cancer Prevention Research,* 14 (8), 779–794.

MORRIS, R.J., et al., 2004. Capturing and profiling adult hair follicle stem cells. *Nature Biotechnology*, 22(4), pp. 411–417.

MORTIMER, P., et al., 1983. Hypertrichosis and multiple cutaneous squamous cell carcinomas in association with cyclosporin A therapy. *Journal of the Royal Society of Medicine*, 76, pp.786–787.

MOUSSAI, D., et al., 2011. The human cutaneous squamous cell carcinoma microenvironment is characterized by increased lymphatic density and enhanced expression of macrophage-derived VEGF-C. *Journal of Investigative Dermatology*, 131, pp.229–236.

MURAO, K., et al., 2006. Epigenetic abnormalities in cutaneous squamous cell carcinomas: Frequent inactivation of the RB1/p16 and p53 pathways. *British Journal of Dermatology*, 155, pp.999–1005.

NADHAN, K.S., et al., 2019. Risk factors for keratinocyte carcinoma skin cancer in nonwhite individuals: a retrospective analysis. *Journal of the American Academy of Dermatology,* 81 (2), 373–378.

NAKAMURA, T., et al., 1998. Axin, an inhibitor of the Wnt signalling pathway, interacts with β-catenin, GSK-3β and APC and reduces the β-catenin level. *Genes to Cells,* 3 (6), 395–403.

NALDINI, L., 2015. Gene therapy returns to centre stage. *Nature*, 526, pp. 351–360. https://doi.org/10.1038/nature15818

NELSON, M. et al., 1994. Analysis of the p53 gene in human precancerous actinic keratosis lesions and squamous cell cancers. *Cancer Letters*, 85, pp.23–29.

NEMES, Z. and STEINERT, M., 1999. Bricks and mortar of the epidermal barrier. *Experimental and Molecular Medicine*, 31, pp.5–19.

NESTLE, F.O., et al., 2009. Skin immune sentinels in health and disease. *Nature Reviews Immunology,* 9 (10), 679–691.

NEVE, R., et al., 1998. The epithelium-specific ets transcription factor ESX is associated with mammary gland development and involution. *The FASEB Journal,* 12 (14), 1541–1550.

NI, X. and LAI, Y., 2020. Keratinocyte: A trigger or an executor of psoriasis? *Journal of Leucocyte Biology,* 108 (2), 485–491.

NICOLAS, M., et al., 2003. Notch1 functions as a tumour suppressor in mouse skin. *Nature Genetics*, 33, pp.416–421.

NISHI, K., et al., 2009. Cyclin D1 downregulation is important for permanent cell cycle exit and initiation of differentiation induced by anchorage-deprivation in human keratinocytes. *Journal of Cellular Biochemistry,* 106 (1), 63–72.

NISHIMASU, H., et al., 2014. Crystal structure of Cas9 in complex with guide RNA and target DNA. *Cell,* 156 (5), 935–949.

NUSSE, R. and CLEVERS, H., 2017. Wnt/β-catenin signalling, disease, and emerging therapeutic modalities. *Cell,* 169 (6), 985–999.

OAKES, S.R., et al., 2008. The alveolar switch: coordinating the proliferative cues and cell fate decisions that drive mammary gland development. *Breast Cancer Research*, 10(2), p. 207.

OAKES, S.R., et al., 2008. The Ets transcription factor Elf5 specifies mammary alveolar cell fate. *Genes & Development,* 22 (5), 581–586.

OAKES, S.R., et al., 2006. The alveolar switch: coordinating the proliferative cues and cell fate decisions that drive mammary gland development. *Breast Cancer Research*, 10(2), p. 207.

OBERYSZYN, T., 2008. Non-melanoma skin cancer: Importance of gender, immunosuppressive status and vitamin D. *Cancer Letters*, 261, pp.127–136.

ODA, K., et al., 2005. A comprehensive pathway map of epidermal growth factor receptor signalling. *Molecular Systems Biology*, 1, p.10.

ODLAND, G., 1991. Structure of the skin. In: Goldsmith, L.A. (ed.) *Physiology, Biochemistry, and Molecular Biology of the Skin*. New York: Oxford University Press, pp.3–62.

OETTGEN, P., et al., 1997. Isolation and characterization of a novel epithelium-specific transcription factor, ESE-1, a member of the ets family. *Molecular and Cellular Biology,* 17 (8), 4419–4433.

OETTGEN, P., et al., 1999. Genomic organization of the human ELF3 (ESE-1/ESX) gene, a member of the Ets transcription factor family, and identification of a functional promoter. *Genomics,* 55 (3), 358–362.

OETTGEN, P., et al., 2000. PDEF, a novel prostate epithelium-specific ets transcription factor, interacts with the androgen receptor and activates prostate-specific antigen gene expression. *Journal of Biological Chemistry,* 275 (2), 1216–1225.

ORNITZ, D.M. and MARIE, P.J., 2019. Fibroblast growth factors in skeletal development. *Current Topics in Developmental Biology,* 133, 195–234.

PAI, S.G., et al., 2017. Wnt/beta-catenin pathway: modulating anticancer immune response. *Journal of Haematology & Oncology,* 10, 1–12.

PALMER, C.N., et al., 2006. Common loss-of-function variants of the epidermal barrier protein filaggrin are a major predisposing factor for atopic dermatitis. *Nature Genetics,* 38 (4), 441–446.

PAPPAS, A., et al., 2018. Seasonal changes in epidermal ceramides are linked to impaired barrier function in acne patients. *Experimental Dermatology,* 27 (8), 833–836.

PARISI, R., et al., 2020. National, regional, and worldwide epidemiology of psoriasis: systematic analysis and modelling study. *Bmj,* 369.

PARK, P.J., 2009. ChIP–seq: advantages and challenges of a maturing technology. *Nature Reviews Genetics*, 10(10), pp. 669–680.

PASPARAKIS, et al., 2014a. Mechanisms regulating skin immunity and inflammation. *Nature Reviews Immunology,* 14 (5), 289–301.

PATIENT, R.K. and MCGHEE, J.D., 2002. The GATA family (vertebrates and invertebrates). *Current Opinion in Genetics & Development,* 12 (4), 416–422.

PEREIRA, R., et al., 1999. FLI-1 inhibits differentiation and induces proliferation of primary erythroblasts. *Oncogene,* 18 (8), 1597–1608.

PICKERING, C., et al., 2014. Mutational landscape of aggressive cutaneous squamous cell carcinoma. *Clinical Cancer Research*, 20, pp.6582–6592.

PICKUP, M.E., et al., 2023. MicroRNA-148a controls epidermal and hair follicle stem/progenitor cells by modulating the activities of ROCK1 and ELF5. *Journal of Investigative Dermatology,* 143 (3), 480–491. e5.

PIERCEALL, W., et al., 1991. Ras gene mutation and amplification in human nonmelanoma skin cancers. *Molecular Carcinogenesis*, 4, pp.196–202.

PIGGIN, C.L., et al., 2016. ELF5 isoform expression is tissue-specific and significantly altered in cancer. *Breast Cancer Research,* 18, 1–18.

PLIKUS, M.V., et al., 2008. Cyclic dermal BMP signalling regulates stem cell activation during hair regeneration. *Nature,* 451 (7176), 340–344.

PRGOMET, Z., et al., 2015. Migration and invasion of oral squamous carcinoma cells is promoted by WNT 5A, a regulator of cancer progression. *Journal of Oral Pathology & Medicine,* 44 (10), 776–784.

PRICE, M., et al., 1985. Skin cancer and cyclosporine therapy. *New England Journal of Medicine*, 313, p.1420.

PROKSCH, E, et al., 2008. The skin: an indispensable barrier. *Experimental Dermatology,* 17 (12), 1063–1072.

PROWELLER, A., et al., 2006. Impaired notch signalling promotes de novo squamous cell carcinoma formation. *Cancer Research*, 66, pp.7438–7444.

PTASHNE, M., 2011. Principles of a switch. *Nature Chemical Biology,* 7 (8), 484–487.

QIAO, Y., et al., 2012. AP2γ regulates neural and epidermal development downstream of the BMP pathway at early stages of ectodermal patterning. *Cell Research,* 22 (11), 1546–1561.

QU, X., et al., 2021. ELF5 inhibits the proliferation and invasion of breast cancer cells by regulating CD24. *Molecular Biology Reports,* 48 (6), 5023–5032.

QUE, S. et al., 2018. Cutaneous squamous cell carcinoma: Incidence, risk factors, diagnosis, and staging. *Journal of the American Academy of Dermatology*, 78, pp.237–247.

QURESHI, A.A., et al., 2008. Geographic variation and risk of skin cancer in US women: differences between melanoma, squamous cell carcinoma, and basal cell carcinoma. *Archives of Internal Medicine,* 168 (5), 501–507.

R CORE TEAM, 2022. *R: A language and environment for statistical computing*. Vienna: R Foundation for Statistical Computing.

RÁCZ, E., et al., 2011. GATA3 expression is decreased in psoriasis and atopic dermatitis. *Journal of Investigative Dermatology*, 131(6), pp. 1188–1195.

RAN, F.A., et al., 2013. Genome engineering using the CRISPR-Cas9 system. *Nature Protocols,* 8 (11), 2281–2308.

RATUSHNY, V., et al., 2012. From keratinocyte to cancer: The pathogenesis and modelling of cutaneous squamous cell carcinoma. *Journal of Clinical Investigation*, 122, pp.464–472.

REIHSNER, R., et al., 1995. Two-dimensional elastic properties of human skin in terms of an incremental model at the in vivo configuration. *Medical Engineering & Physics*, 17, pp.304–313.

REN, Q., et al., 2006. Malignant transformation of immortalized HaCaT keratinocytes through deregulated nuclear factor κB signalling. *Cancer Research*, 66(10), pp.5209–5215.

RENDL, M, et al., 2008. BMP signaling in dermal papilla cells is required for their hair follicle-inductive properties. *Genes & Development,* 22 (4), 543–557.

RENDON, A. and SCHÄKEL, K., 2019. Psoriasis pathogenesis and treatment. *International Journal of Molecular Sciences,* 20 (6), 1475.

RICE, R. and GREEN, H., 1977. The cornified envelope of terminally differentiated human epidermal keratinocytes consists of cross-linked protein. *Cell*, 11, pp.417–422.

RIO, D.C., et al., 2010. Purification of RNA using TRIzol. *Cold Spring Harbor Protocols*, 2010(6), prot5439. https://doi.org/10.1101/pdb.prot5439

RITCHIE, M.E., et al., 2015. limma powers differential expression analyses for RNA-sequencing and microarray studies. *Nucleic Acids Research*, 43(7), e47.

RITTIÉ, L. and FISHER, G.J., 2002. UV-light-induced signal cascades and skin aging. *Ageing Research Reviews,* 1 (4), 705–720.

RITTIÉ, L. and FISHER, G.J., 2015. Isolation and culture of skin fibroblasts. *Methods in Molecular Biology*, 1172, pp. 83–98. https://doi.org/10.1385/1-59259-940-0:083

ROBINSON, M.D., et al., 2010. edgeR: a Bioconductor package for differential expression analysis of digital gene expression data. *Bioinformatics*, 26(1), pp. 139–140.

ROBINSON, M.D., et al., 2010. edgeR: a Bioconductor package for differential expression analysis of digital gene expression data. *Bioinformatics*, 26(1), pp. 139–140.

RODRIGUEZ-PAREDES, M., et al., 2018. Methylation profiling identifies two subclasses of squamous cell carcinoma related to distinct cells of origin. *Nature Communications*, 9, p.577.

RONCA, R., et al., 2015. The potential of fibroblast growth factor/fibroblast growth factor receptor signaling as a therapeutic target in tumor angiogenesis. *Expert Opinion on Therapeutic Targets,* 19 (10), 1361–1377.

ROUSSELLE, P, et al., 2019. The involvement of extracellular matrix proteins in the re-epithelialization of skin wounds. *Matrix Biology,* 75, 12–26.

ROUSSELLE, P., et al., 2019. Re-epithelialization of adult skin wounds: Cellular mechanisms and therapeutic strategies. *Advanced Drug Delivery Reviews*, 146, pp.344–365.

SAKURAI, T., et al., 2007. Functional roles of Fli-1, a member of the Ets family of transcription factors, in human breast malignancy. *Cancer Science,* 98 (11), 1775–1784.

SAMBROOK, J. and RUSSELL, D.W., 2001. *Molecular Cloning: A Laboratory Manual*. 3rd ed. Cold Spring Harbor, NY: Cold Spring Harbor Laboratory Press.

SASAKI, K., et al., 2018. Analysis of cancer-associated fibroblasts and the epithelial-mesenchymal transition in cutaneous basal cell carcinoma, squamous cell carcinoma, and malignant melanoma. *Human Pathology*, 79, pp.1–8.

SCHÄBITZ, A., et al., 2022. Spatial transcriptomics landscape of lesions from non-communicable inflammatory skin diseases. *Nature Communications,* 13 (1), 7729.

SCHARSCHMIDT, T.C., et al., 2017. Commensal microbes and hair follicle morphogenesis coordinately drive Treg migration into neonatal skin. *Cell Host & Microbe,* 21 (4), 467–477. e5.

SCHEIBER, M.N., et al., 2014. FLI1 expression is correlated with breast cancer cellular growth, migration, and invasion and altered gene expression. *Neoplasia,* 16 (10), 801–813.

SCHLESSINGER, K., HALL, A. and TOLWINSKI, N., 2009. Wnt signalling pathways meet Rho GTPases. *Genes & Development,* 23 (3), 265–277.

SCHMULTS, C. et al., 2013. Factors predictive of recurrence and death from cutaneous squamous cell carcinoma: A 10-year, single-institution cohort study. *JAMA Dermatology*, 149, pp.541–547.

SCHRÖDER, S., et al., 2008. Quantitative gel electrophoresis: sources of variation. *Journal of Proteome Research*, 7(3), pp.1226–1234.

SEGRE, J.A., 2006. Epidermal barrier formation and recovery in skin disorders. *The Journal of Clinical Investigation,* 116 (5), 1150–1158.

SELLERI, L., et al., 1994. Cloning of the entire FL11 gene, disrupted by the Ewing's Sarcoma translocation breakpoint on 11q24, in a yeast artificial chromosome. *Cytogenetic and Genome Research,* 67 (2), 129–136.

SEMENTCHENKO, V.I. and WATSON, D.K., 2000. Ets target genes: past, present and future. *Oncogene,* 19 (55), 6533–6548.

Sergi, C.M. (2020). Skin. In: Pathology of Childhood and Adolescence. Springer, Berlin, Heidelberg. https://doi.org/10.1007/978-3-662-59169-7_17

SERRANO, M., et al., 1993. A new regulatory motif in cell-cycle control causing specific inhibition of cyclin D/CDK4. *Nature*, 366, pp.704–707.

SHAPIRO, H.M., 2005. *Practical Flow Cytometry*. 4th ed. Hoboken, NJ: Wiley-Liss.

SHAROV, A.A., et al., 2006. Bone morphogenetic protein signalling regulates the size of hair follicles and modulates the expression of cell cycle-associated genes. *Proceedings of the National Academy of Sciences,* 103 (48), 18166–18171.

SHARROCKS, A.D., 2001. The ETS-domain transcription factor family. *Nature Reviews Molecular Cell Biology,* 2 (11), 827–837.

SHARROCKS, A.D., et al., 1997. The ETS-domain transcription factor family. *The International Journal of Biochemistry & Cell Biology,* 29 (12), 1371–1387.

SHEPHERD, F., et al., 2005. Erlotinib in previously treated non-small-cell lung cancer. *New England Journal of Medicine*, 353, pp.123–132.

SHERR, C.J., 1996. Cancer cell cycles. *Science,* 274 (5293), 1672–1677.

SHIMIZU, T., et al., 2001. Epidermal growth factor receptor overexpression and genetic aberrations in metastatic squamous-cell carcinoma of the skin. *Dermatology*, 202, pp.203–206.

SHPICHKA, A., et al., 2019. Skin tissue regeneration for burn injury. *Stem Cell Research & Therapy*, 10, p.94.

SIEGEL, R.L, et al., 2024. Cancer statistics, 2024. *CA: A Cancer Journal for Clinicians,* 74 (1), 12–49.

SINGH, M.V., et al., 2014. The immune system and hypertension. *Immunologic Research,* 59, 243–253.

SINGH, S., et al., 2020. Loss of ELF5–FBXW7 stabilizes IFNGR1 to promote the growth and metastasis of triple-negative breast cancer through interferon-γ signalling. *Nature Cell Biology,* 22 (5), 591–602.

Skin Cancer Foundation. (2024). *Skin Cancer Facts & Statistics*. https://www.skincancer.org/skin-cancer-information/skin-cancer-facts/

SLACK, J.M. and DALE, L., 2021. *Essential developmental biology.* John Wiley & Sons.

SLOMINSKI, A. and WORTSMAN, J., 2000. Neuroendocrinology of the skin. *Endocrine Reviews,* 21 (5), 457–487.

SLOMINSKI, A.T., et al., 2012. Biogenic amines in the skin. *Sensing the Environment: Regulation of Local and Global Homeostasis by the Skin's Neuroendocrine System,* , 7–26.

SNIPPERT, H.J., et al., 2010. Intestinal crypt homeostasis results from neutral competition between symmetrically dividing Lgr5 stem cells. *Cell,* 143 (1), 134–144.

SOKOL, S.Y., 2015. Spatial and temporal aspects of Wnt signalling and planar cell polarity during vertebrate embryonic development. *In: Seminars in cell & developmental biology,* Elsevier, pp. 78–85.

SOLUS, J.F., et al., 2016. Cutaneous squamous cell carcinoma progression is associated with decreased GATA-3 immunohistochemical staining. *Journal of Cutaneous Pathology,* 43 (4), 347–353.

SONG, J., et al., 2021. An update on the role of long non-coding RNAs in psoriasis. *Chinese Medical Journal*, 134(4), pp.379–389.

SOUTH, A., et al., 2014. NOTCH1 mutations occur early during cutaneous squamous cell carcinogenesis. *Journal of Investigative Dermatology*, 134, pp.2630–2638.

SPALDING, J., et al., 1993. Chemically induced skin carcinogenesis in a transgenic mouse line (TG.AC) carrying a v-Ha-ras gene. *Carcinogenesis*, 14, pp.1335–1341.

SRIVASTAVA, A, et al., 2025. Sensory nerve-secreted factors regulate basal keratinocyte function in vitro. *Integrative Organismal Biology,* 7 (1), obaf009.

SRIVASTAVA, S. et al., 2018. Keratin 5/14-mediated cell differentiation and transformation are regulated by TAp63 and Notch-1 in oral squamous cell carcinoma-derived cells. *Oncology Reports*, 39, pp.2393–2401.

STAMATAS, G.N., et al., 2011. Infant skin physiology and development during the first years of life: a review of recent findings based on in vivo studies. *International Journal of Cosmetic Science,* 33 (1), 17–24.

STEPHEN, N., et al., 2021. Neuroectodermal tumours of the sino-nasal tract: a clinicopathological study of 18 cases with a newly proposed revised classification and a brief review of literature. *European Archives of Oto-Rhino-Laryngology,* 1–11.

STIENSTRA, R., et al., 2014. Mannose-binding lectin is required for the effective clearance of apoptotic cells by adipose tissue macrophages during obesity. *Diabetes,* 63 (12), 4143–4153.

STOKER, M., et al., 1968. Anchorage and growth regulation in normal and virus-transformed cells. *International Journal of Cancer*, 3(5), pp.683–693.

STOTT, F., et al., 1998. The alternative product from the human CDKN2A locus, p14(ARF), participates in a regulatory feedback loop with p53 and MDM2. *EMBO Journal*, 17, pp.5001–5014.

SU, F., et al., 2012. RAS mutations in cutaneous squamous-cell carcinomas in patients treated with BRAF inhibitors. *New England Journal of Medicine*, 366, pp.207–215.

TAKAHASHI, K. and YAMANAKA, S., 2016. A decade of transcription factor-mediated reprogramming to pluripotency. *Nature Reviews Molecular Cell Biology,* 17 (3), 183–193.

TAMIR, A., et al., 1999. Fli-1, an Ets-related transcription factor, regulates erythropoietin-induced erythroid proliferation and differentiation: evidence for direct transcriptional repression of the Rb gene during differentiation. *Molecular and Cellular Biology,* 19 (6), 4452–4464.

TANG, L., et al., 2020. Long non-coding RNAs in cutaneous biology and proliferative skin diseases: advances and perspectives. *Cell Proliferation*, 53, e12698.

TAYLOR, C.R. and LEVENSON, R.M., 2006. Quantification of immunohistochemistry issues concerning methods, utility and semiquantitative assessment. *Histopathology*, 49(4), pp. 411–424. https://doi.org/10.1111/j.1365-2559.2006.02513.x

TELERMAN, S.B., et al., 2017. Dermal Blimp1 acts downstream of epidermal TGFβ and Wnt/β-catenin to regulate hair follicle formation and growth. *Journal of Investigative Dermatology,* 137 (11), 2270–2281.

TERATANI, T., et al., 2018. Aortic carboxypeptidase–like protein, a WNT ligand, exacerbates non-alcoholic steatohepatitis. *The Journal of Clinical Investigation,* 128 (4), 1581–1596.

THOMAS, K.A., 1987. Fibroblast growth factors. *The FASEB Journal,* 1 (6), 434–440.

THOMAS-AHNER, J. et al., 2007. Gender differences in UVB-induced skin carcinogenesis, inflammation, and DNA damage. *Cancer Research*, 67, pp.3468–3474.

THOMMEN, D. and SCHUMACHER, T., 2018. T cell dysfunction in cancer. *Cancer Cell*, 33, pp.547–562.

TOLL, A., et al., 2010. Epidermal growth factor receptor gene numerical aberrations are frequent events in actinic keratoses and invasive cutaneous squamous cell carcinomas. *Experimental Dermatology*, 19, pp.151–153.

TONG, L., et al., 2006. Expression and regulation of cornified envelope proteins in human corneal epithelium. *Investigative Ophthalmology & Visual Science*, 47, pp.1938–1946.

TREVOR, L. et al., 2020. Adipose tissue: a source of stem cells with potential for regenerative therapies for wound healing. *Journal of Clinical Medicine*, 9, p.2161. https://doi.org/10.3390/jcm9072161

TRUONG, A.H. and BEN-DAVID, Y., 2000. The role of Fli-1 in normal cell function and malignant transformation. *Oncogene,* 19 (55), 6482–6489.

TSOI, L., et al., 2015. Analysis of long non-coding RNAs highlights tissue-specific expression patterns and epigenetic profiles in normal and psoriatic skin. *Genome Biology*, 16, p.24.

TUMMALA, R. and SINHA, S., 2006. Differentiation-specific transcriptional regulation of the ESE-2 gene by a novel keratinocyte-restricted factor. *Journal of Cellular Biochemistry,* 97 (4), 766–781.

VAN MATER, D., et al., 2003. Transient activation of β-catenin signalling in cutaneous keratinocytes is sufficient to trigger the active growth phase of the hair cycle in mice. *Genes & Development,* 17 (10), 1219–1224.

VARRA, V., et al., 2018. Suboptimal outcomes in cutaneous squamous cell cancer of the head and neck with nodal metastases. *Anticancer Research*, 38, pp.5825–5830.

VECCHIARELLI-FEDERICO, L.M., et al., 2017a. Fli-1 overexpression in erythroleukemic cells promotes erythroid de-differentiation while Spi-1/PU. 1 exerts the opposite effect. *International Journal of Oncology,* 51 (2), 456–466.

VELTRI, A., et al., 2018. Concise review: Wnt signalling pathways in skin development and epidermal stem cells. *Stem Cells,* 36 (1), 22–35.

VIERKÖTTER, A, et al., 2017, Ambient particulate matter and skin. *In:* Ambient particulate matter and skin *Environment and Skin.* Springer, 2017, pp. 105–111.

VIERKÖTTER, A. and KRUTMANN, J., 2012. Environmental influences on skin aging and ethnic-specific manifestations. *Dermato-Endocrinology,* 4 (3), 227–231.

VITALE, I., et al., 2023. Apoptotic cell death in disease Current understanding of the NCCD 2023. *Cell Death & Differentiation,* 30 (5), 1097–1154.

VUJEVICH, J.J. and MANCINI, A.J., 2004. The epidermal nevus syndromes: multisystem disorders. *Journal of the American Academy of Dermatology,* 50 (6), 957–961.

WALKER, M., 2022. Human skin through the ages. *International Journal of Pharmaceutics,* 622, 121850.

WALLINGFORD, J.B. and HABAS, R., 2005. The developmental biology of Dishevelled: an enigmatic protein governing cell fate and cell polarity.

WALSH, S., et al., 2011. Cyclosporine A mediates pathogenesis of aggressive cutaneous squamous cell carcinoma by augmenting epithelial-mesenchymal transition: Role of TGFβ signalling pathway. *Molecular Carcinogenesis*, 50, pp.516–527.

WANG, H., et al., 2018. Fli-1 promotes metastasis by regulating MMP2 signalling in hepatocellular carcinoma. *Molecular Medicine Reports,* 17 (1), 1986–1992.

WANG, H., et al., 2020. CO2 lattice laser reverses skin aging caused by UVB. *Aging (Albany NY)*, 12, pp.7056–7065. https://doi.org/10.18632/aging.103063

WANG, N., et al., 2011. Loss-of-function mutations in Notch receptors in cutaneous and lung squamous cell carcinoma. *Proceedings of the National Academy of Sciences of the USA*, 108, pp.17761–17766.

WANG, X., et al., 2021. Expression of GM-CSF is regulated by Fli-1 transcription factor, a potential drug target. *The Journal of Immunology,* 206 (1), 59–66.

WASEEM, A. and LANE, E.B., 1990. Expression of keratins 15 and 19 in stratified epithelia and their relationship to the cell cycle. *Journal of Cell Biology*, 111(1), pp. 85–94.

WATT, F., 2001. Stem cell fate and patterning in mammalian epidermis. *Current Opinion in Genetics & Development*, 11, pp.410–417.

WATT, F.M., 1989. Terminal differentiation of epidermal keratinocytes. *Current Opinion in Cell Biology*, 1(6), pp. 1107–1115. https://doi.org/10.1016/S0955-0674(89)80058-4

WATT, F.M., 2014. Mammalian skin cell biology: at the interface between laboratory and clinic. *Science*, 346(6212), pp. 937–940.

WEBSTER, A., et al., 2005. Tacrolimus versus ciclosporin as primary immunosuppression for kidney transplant recipients: Meta-analysis and meta-regression of randomised trial data. *BMJ*, 331, p.810.

WEI, W., et al., 2022. Upregulation of long noncoding RNA linc02544 and its association with overall survival rate and the influence on cell proliferation and migration in lung squamous cell carcinoma. *Discover Oncology*, 13, p.41.

WENG, T., et al., 2020. Regeneration of skin appendages and nerves: Current status and further challenges. *Journal of Translational Medicine*, 18, p.53.

WERNER, R. et al., 2013. The natural history of actinic keratosis: A systematic review. *British Journal of Dermatology*, 169, pp.502–518.

WERNER, S. and GROSE, R., 2003. Regulation of wound healing by growth factors and cytokines. *Physiological Reviews,* 83 (3), 835–870.

WERTZ, P.W., 2013. Current understanding of skin biology pertinent to skin penetration: skin biochemistry. *Skin Pharmacology and Physiology,* 26 (4-6), 217–226.

WHYTE, J.L., et al., 2013. Augmenting endogenous Wnt signalling improves skin wound healing. *PloS One,* 8 (10), e76883.

WIDELITZ, R.B., 2008. Wnt signalling in skin organogenesis. *Organogenesis,* 4 (2), 123–133.

WIEDUWILT, M. and MOASSER, M., 2008. The epidermal growth factor receptor family: Biology driving targeted therapeutics. *Cellular and Molecular Life Sciences*, 65, pp.1566–1584.

WIKONKAL, N. and BRASH, D., 1999. Ultraviolet radiation induced signature mutations in photo carcinogenesis. *Journal of Investigative Dermatology Symposium Proceedings*, 4, pp.6–10.

WILSON, S., et al., 2001. The status of Wnt signalling regulates neural and epidermal fates in the chick embryo. *Nature,* 411 (6835), 325–330.

WILSON, V.G., 2014. Growth and differentiation of HaCaT keratinocytes. *Methods in Molecular Biology*, 1195, pp. 33–41.

WILSON, V.G., 2014. Growth and differentiation of HaCaT keratinocytes. *Methods in Molecular Biology*, 1195, pp. 33–41.

WINGE, M.C., et al., 2023. Advances in cutaneous squamous cell carcinoma. *Nature Reviews Cancer,* 23 (7), 430–449.

WODARZ, A. and NUSSE, R., 1998. Mechanisms of Wnt signalling in development. *Annual Review of Cell and Developmental Biology,* 14 (1), 59–88.

WONG, C., et al., 2013. Inflammation and Hras signalling control epithelial-mesenchymal transition during skin tumour progression. *Genes & Development*, 27, pp.670–682.

WONG, K.S., et al., 1999. Loss of p53 in F-MuLV induced-erythroleukemias accelerates the acquisition of mutational events that confers immortality and growth factor independence. *Oncogene,* 18 (40), 5525–5534.

WONG, R., et al., 2016. The dynamic anatomy and patterning of skin. *Experimental Dermatology*, 25, pp.92–98.

WOOD, K.V., 1995. Marker proteins for gene expression. *Current Opinion in Biotechnology*, 6(1), pp. 50–58.

WORK, G., et al., 2018. Guidelines of care for the management of cutaneous squamous cell carcinoma. *Journal of the American Academy of Dermatology*, 78, pp.560–578.

WRIGHT, A.V., et al., 2016. Biology and applications of CRISPR systems: harnessing nature's toolbox for genome engineering. *Cell,* 164 (1), 29–44.

WU, B., et al., 2015. Epigenetic regulation of Elf5 is associated with epithelial-mesenchymal transition in urothelial cancer. *PloS One,* 10 (1), e0117510.

WU, J., et al., 2025. CRISPR-Cas System-Mediated Genetic Modification in Bacillus spp.: Current Status and Future. *Journal of Agricultural and Food Chemistry,* .

WU, X., et al., 2010. Opposing roles for calcineurin and ATF3 in squamous skin cancer. *Nature*, 465, pp.368–372.

XUE, C., et al., 2025. Wnt signalling pathways in biology and disease: mechanisms and therapeutic advances. *Signal Transduction and Targeted Therapy,* 10 (1), 106.

YAN, X., et al., 2018. Friend leukaemia virus integration 1 is a predictor of poor prognosis of breast cancer and promotes metastasis and cancer stem cell properties of breast cancer cells. *Cancer Medicine,* 7 (8), 3548–3560.

YANG, C., et al., 2013. DLC1 as a regulator of proliferation, invasion, cell cycle, and apoptosis in cutaneous squamous cell carcinoma. *Tumour Biology,* 34 (5), 2633–2643.

YANG, J., et al., 2021. The role of GATA3 in breast cancer: an updated review. *Current Chinese Science,* 1 (6), 608–615.

YANG, Y. and MLODZIK, M., 2015. Wnt-Frizzled/planar cell polarity signalling: cellular orientation by facing the wind (Wnt). *Annual Review of Cell and Developmental Biology,* 31 (1), 623–646.

YAO, B., et al., 2015. Elf5 inhibits TGF-β-driven epithelial-mesenchymal transition in prostate cancer by repressing SMAD3 activation. *The Prostate,* 75 (8), 872–882.

YAROSH, D. et al., 2005. Calcineurin inhibitors decrease DNA repair and apoptosis in human keratinocytes following ultraviolet B irradiation. *Journal of Investigative Dermatology*, 125, pp.1020–1025.

YASMIN, N., et al., 2013. Identification of bone morphogenetic protein 7 (BMP7) as an instructive factor for human epidermal Langerhans cell differentiation. *Journal of Experimental Medicine,* 210 (12), 2597–2610.

YONEDA, M., et al., 1995. Oxygen stress induces an apoptotic cell death associated with fragmentation of mitochondrial genome. *Biochemical and Biophysical Research Communications,* 209 (2), 723–729.

YOSHIDA, N., et al., 2000. Ets family transcription factor ESE-1 is expressed in corneal epithelial cells and is involved in their differentiation. *Mechanisms of Development,* 97 (1-2), 27–34.

YOUNG, L., et al., 2010. Detection of mycoplasma in cell cultures. *Nature Protocols*, 5, pp. 929–934. https://doi.org/10.1038/nprot.2010.43

YOUSEF, et al., 2017. Anatomy, skin (integument), epidermis.

YOUSEF, H., et al., 2022. Anatomy, skin (integument), epidermis. In: *StatPearls [Internet]*. Treasure Island, FL: StatPearls.

YU, G., et al., 2012. clusterProfiler: an R package for comparing biological themes among gene clusters. *OMICS*, 16(5), pp. 284–287.

YUN, Y., et al., 2010. Fibroblast growth factors: biology, function, and application for tissue regeneration. *Journal of Tissue Engineering,* 1 (1), 218142.

ZEITVOGEL, J., et al., 2017. GATA3 regulates FLG and FLG2 expression in human primary keratinocytes. *Scientific Reports,* 7 (1), 11847.

ZENG, J., et al., 2019. Cytokinin inhibits cotton fiber initiation by disrupting PIN3a-mediated asymmetric accumulation of auxin in the ovule epidermis. *Journal of Experimental Botany,* 70 (12), 3139–3151.

ZENG, Q., et al., 2017. 6.20 Skin tissue engineering. In: Ducheyne, P., ed. *Comprehensive Biomaterials II*. Oxford: Elsevier, pp.334–382.

ZENG, X., et al., 2008. Initiation of Wnt signalling control of Wnt coreceptor Lrp6 phosphorylation/activation via frizzled, dishevelled and axin functions.

ZHANG, L., et al., 2022. Overexpression of Activating Transcription Factor-2 (ATF-2) Activates Wnt/Ca2 Signalling Pathways and Promotes Proliferation and Invasion in Non-Small-Cell Lung Cancer. *Disease Markers,* 2022 (1), 5772089.

ZHANG, M., et al., 2023. Non-canonical pathway for Rb inactivation and external signalling coordinate cell-cycle entry without CDK4/6 activity. *Nature Communications,* 14 (1), 7847.

ZHANG, T., et al., 2023. Transcriptomic analysis predicts the risk of progression of premalignant lesions in human tongue. *Discover Oncology,* 14 (1), 24.

ZHANG, X., et al., 2019. Overexpression of E74-like factor 5 (ELF5) inhibits migration and invasion of ovarian cancer cells. *Medical Science Monitor: International Medical Journal of Experimental and Clinical Research,* 25, 856.

ZHANG, Y., et al., 2009. Inhibition of Wnt signaling by Dishevelled PDZ peptides. *Nature Chemical Biology,* 5 (4), 217–219.

ZHANG, Z. and MICHNIAK-KOHN, B., 2012. Tissue engineered human skin equivalents. *Pharmaceutics*, 4, pp.26–41. https://doi.org/10.3390/pharmaceutics4010026

ZHAO, H., et al., 2018. FLI1 and PKC co-activation promote highly efficient differentiation of human embryonic stem cells into endothelial-like cells. *Cell Death & Disease,* 9 (2), 131.

ZHENG, R. and BLOBEL, G.A., 2010. GATA Transcription Factors and Cancer. *Genes &Amp; Cancer,* 1 (12), 1178.

ZHOU, J., et al., 1998. A novel transcription factor, ELF5, belongs to the ELF subfamily of ETS genes and maps to human chromosome 11p13–15, a region subject to LOH and rearrangement in human carcinoma cell lines. *Oncogene,* 17 (21), 2719–2732.

ZHOU, J., et al., 2005. Elf5 is essential for early embryogenesis and mammary gland development during pregnancy and lactation. *The EMBO Journal,* 24 (3), 635–644.

ZHOU, X., et al., 2022. Advances in the pathogenesis of psoriasis: from keratinocyte perspective. *Cell Death & Disease,* 13 (1), 81.

ZHU, A.J. and WATT, F.M., 1999. β-catenin signalling modulates proliferative potential of human epidermal keratinocytes independently of intercellular adhesion. *Development,* 126 (10), 2285–2298.

ZHU, Y., et al., 2014. Activation of RhoA-ROCK-BMP signalling reprograms adult human corneal endothelial cells. *Journal of Cell Biology,* 206 (6), 799–811.

ZIEGLER, A., et al., 1994. Sunburn and p53 in the onset of skin cancer. *Nature*, 372, pp.773–776.